Present and future coastal safety assessment of 'De Slufter' anticipating sea level rise and coastal management changes

Modelling the effects of a natural coastal management strategy on the morphodynamic development and coastal safety of De Slufter on Texel with XBeach Surfbeat

O.P. van der Graaf

Technische Universiteit Delft

Deltares
Enabling Delta Life

hoogheemraadschap
Hollands
Noorderkwartier

TU Delft

Present and future coastal safety assessment of 'De Slufter' anticipating sea level rise and coastal management changes

Modelling the effects of a natural coastal management strategy on the morphodynamic development and coastal safety of De Slufter on Texel with XBeach Surfbeat

by

O.P. van der Graaf

in partial fulfillment of the requirements for the degree of

Master of Science
in Hydraulic Engineering

at the Delft University of Technology,
to be publicly defended on Tuesday January 22nd, 2019 at 15:00

Supervisor:	Prof. dr. ir. S.G.J. Aarninkhof,	Delft University of Technology
Thesis committee:	Dr. ir. S. De Vries,	Delft University of Technology
	Dr. ir. B.C. van Prooijen,	Delft University of Technology
	Ir. P. Goessen,	Hoogheemraadschap Hollands Noorderkwartier
	Dr. ir. A. Van Dongeren,	Deltares
	Ir. C.M. Nederhoff,	Deltares

TU Delft Delft University of Technology

Acknowledgements

There are many people I want to thank. Therefore, to refrain from having to find 20 different synonyms for 'thank you' or 'gratefulness', I will give my thanks in a concise and orderly fashion, like a true engineer.

I want to thank:

My graduation committee, without whom this report would not have been realised.
Petra, for giving me the opportunity to work on this topic and for being so enthusiastic about the world of Hydraulic Engineering. Also, for letting me work at HHNK and experiencing the practical side of working on coastal safety. Ap, for always taking the time to help me when I was stuck on complex issues and for the positive attitude towards some of the bigger mistakes. Also, for letting me do this project at Deltares, which is a fantastic place to work on a master thesis. Sierd, for encouraging Petra and Ap to even let me work on this topic. If you had not put in a good word for me I would probably not have been doing this project. Furthermore, for your enthusiasm and positive mindset and for taking the time in the early morning to discuss my progress and issues with the topic. Your ideas and advice on the report were indispensable. Bram, for critically reading each concept report and for giving such good advice for improvement. Stefan, for agreeing to lead this committee and thus giving me the opportunity to work on this project. And finally, Kees, for not only taking time to help me but also for being so proactive in your supervision. It has been a pleasure to have you as a supervisor as you were very critical towards the technical aspect of the thesis but also towards the writing and structuring aspect. Your comments on each concept have made this report a masterpiece, if I may say so myself. Also, your positive mindset was very welcome when I thought that I had made some fatal mistakes.

Maarten van der Vegt, Anita Engelstad and Maarten Prins, for you valuable data. Without your data a validation might not have been possible. You are thus largely responsible for the fact that I could do a modelling study.

Marco van Middelkoop of Aerophoto-Schiphol, for making such a fantastic aerial photo of De Slufter and for letting me use it for my cover.

My fellow students at Deltares, for making the time at Deltares go by so fast. Without the 'bakkie pauzes' and early lunches a master thesis project would have been a lot more difficult. Furthermore, it is very valuable to have a group of peers with which you can discuss your project and complain about it.

My family and Marein, for your support. Without you, this report would not have been finished.

Onne van der Graaf
Delft, January 2019

Summary

'De Slufter' is a nature conservation area located in the Northwest of the Dutch Wadden island Texel which is inundated with seawater during storm events. A slufter is also a general term to describe "a salt or brackish dune valley which is connected to the sea through an opening in the most seaward dune row". In this opening, a gully is present which is dynamic and migrates alongshore. De Slufter is of ecological importance, evident from its classification as a Natura2000 site. It is, however, also important for the coastal safety of Texel. The landward side of De Slufter is a sand dike which is part of the primary coastal defence ring of the island. The Hoogheemraadschap Hollands Noorderkwartier (HHNK), which is responsible for the coastal safety of Texel, currently relocates the dynamic gully in the slufter mouth every time it reaches one of the dune heads (which is every 5-6 years approximately). It is expected that, if the gully is allowed to migrate uncontrolled, the slufter mouth might widen or migrate north. According to previous studies by Rijkswaterstaat, this could lead to more wave attack on the sand dike and possibly affect the coastal safety of Texel. Even though, the HHNK is planning on ceasing the relocations of the gully to save cost, which will give De Slufter back part of its 'natural character'. The effects of this change in coastal management strategy are, however, still unclear. The goal of this thesis is to assess the effects on the present and future coastal safety of De Slufter. For this purpose, a modelling study is performed with the process-based numerical model XBeach Surfbeat.

A field data analysis was performed on available field observations to analyze the historical migration of the slufter gully and its dominant processes. Three hypotheses were investigated. First, it was investigated if gully migration is dominated by longshore transport. The annual net longshore transport from 1998 to 2017 was calculated using wave, sediment and bathymetry data as input. Next, the results were compared to historical bathymetry measurements. From 1998 to 2013, a general similarity in trends is distinguished between longshore transport and gully migration. From 2013 to 2017 this correlation breaks down however with longshore transport and gully migration in opposing directions. Gully migration can thus not only be dominated by longshore transport.

The second hypothesis was that gully migration is be dominated by storm waves. To that end, the same analysis was performed as for the total wave climate but now only for significant wave heights higher than 4 m. The correlation between longshore transport and gully migration for these waves is even less defined than for the total wave climate.

The third hypotheses involved the process of tide-induced secondary flow in the gully bends during calm conditions. Based on the annually measured location and shape of the gully, a correlation is found between the initial location of the most seaward outer bend of the gully after a relocation and the direction of migration. Therefore, tide-induced secondary flow is deemed a possible driving mechanism for gully migration. Unfortunately, the annual bathymetry measurements of the mouth are too infrequent to further investigate the hypothesis.

To investigate the effect of ceasing relocations of the gully on present and future coastal safety a modelling study was performed with XBeach Surfbeat, a process-based numerical model. For this modelling study 15 scenarios were created to assess the effects of different bathymetry configurations (i.e. the present bathymetry, wider mouths, a second mouth) and of sea level rise and subsequent bed level rise. 3 sea level rise scenarios were modelled to assess future coastal safety: 0.75 m, 1.95 m and 3.17 m sea level rise by 2100. It was either assumed that no bed level rise had occurred or that bed level rise in the valley and on the foreshore was equal to sea level rise.

All scenarios were assessed on two failure mechanisms: 'Grensprofiel', which consists of two aspects. A minimum sand dike volume above storm surge level must be available in every transect alongshore in the sand dike. Also, each post-storm sand dike transect must be large enough to contain a legally defined 'limit profile'. Both requirements must be adhered to to pass as 'safe'. The second mechanism is 'Initiation of flooding', which means that failure occurs when at any point landward of the 'waterstaatswerk' boundary (the outer border of the primary coastal defence) a depth of at least 20 cm is observed. This can either occur due to overtopping of individual waves or large-scale inundation due to an exceedance of the water level compared to the crest level of the dunes.

In all present scenarios no failure occurred for a normative 1/3000 year storm. De Slufter is therefore considered 'safe'. Maximum wave heights did not increase significantly for different bathymetry configurations as a result of the large amount of dissipation that occurs in the slufter valley due to depth-dependent processes such as wave breaking and wave friction. Because of this dissipation, wave attack on the sand dike is governed by the water depth in the valley, not necessarily by the offshore wave height. No overwash or overtopping occurred in any of the modelled scenarios and morphological impact on the sand dike itself was relatively low.

For a scenario with a sea level rise of 0.75 m, no failure occurred either. Based on the model results in this thesis, failure occurred for the 1/3000 year storm with a sea level rise of 1.95 m and 3.17 m. For sea level rise of 3.17 m, failure occurs in the same locations as for 1.95 m, only more extreme. Failure occurs based on the 'Initiation of flooding' and the 'Grensprofiel' criterion. In particular, 'Initiation of flooding' occurs in the southwestern and northeastern parts of the Slufter since water levels in the Slufter rise due to a combination of high offshore water levels and wave setup with a locally low crest level. Furthermore, 'Grensprofiel' failure occurs in the northern part of the sand dike, where the crest height is lowest. However, at that point, 'Initiation of flooding' has already occurred. Failure does not occur in the middle of the sand dike where the majority of the wave attack happens but in the southwestern and northeastern parts. Based on the model results it is expected that the 'tipping point' of De Slufter, which is the sea level rise magnitude beyond which De Slufter does not adhere to safety standards, is at a sea level rise magnitude of 1.70 m.

Contents

List of Figures

List of Tables

Nomenclature

List of symbols

Symbol	*Meaning*	*Unit*
c_{br}	wave propagation speed at the breaker line	$[m/s]$
c_o	offshore wave propagation speed	$[m/s]$
D_{50}	sediment grain diameter	$[m]$
f_w	wave friction factor	$[-]$
H_{m0}	zeroth order spectral wave height	$[m]$
H_s	fignificant wave height	$[m]$
$H_{s,br}$	significant wave height of waves at the breaker line	$[m]$
$H_{s,HF}$	Significant wave height of high frequency waves	$[m]$
$H_{s,LF}$	Significant wave height of low frequency waves	$[m]$
$H_{s,o}$	offshore significant wave height	$[m]$
Hz	frequency	$[1/s]$
K_{swell}	swell factor	$[-]$
n	manning coefficient	$[s/m^{1/3}]$
NTR	Non-tidal residual	$[NAP+m]$
$Q_{t,mass}$	longshore sediment transport volume	$[m^3/year]$
$RMSE$	root-mean-squared-error	$[m]$
RP	storm surge level (NL)	$[NAP+m]$
SCI	scattered interpolant	[%]
SSL	storm surge level (EN)	$[NAP+m]$
$tan(\beta)$	surf zone slope	$[m/m]$
T_{m02}	mean absolute zero-crossing period	$[s]$
T_p	peak period	$[s]$
U_{wind}	wind speed	$[m/s]$
α	calibration coefficient	$[-]$
γ	breaking coefficient	$[-]$
ρ_s	sediment density	$[kg/m^3]$
θ_{br}	wave incidence at the breaker line (location where 5% of waves are breaking)	[°]
θ_o	offshore wave incidence	[°]

List of acronyms

Abbreviation	*Meaning*
1DH	One-dimensional in the horizontal plane
2D	Two-dimensional
2DH	Two-dimensional in the horizontal plane
BLR	Bed Level Rise
CERC	Coastal Engineering Research Center
C-CAP	Coastal Change Analysis Program
DUROS+	Dune eROSion model
ENW	Expertise Netwerk Waterveiligheid
HHNK	Hoogheemraadschap Hollands Noorderkwartier
IPCC	Intergovernmental Panel on Climate Change
NAP	Normaal Amsterdams Peil
RCP	Representative Concentration Pathways
RD	Rijkdriehoekscoordinaten
RWS	Rijkswaterstaat
SLR	Sea Level Rise
XBeach	eXtreme Beach behaviour model
WBI	Wettelijke BeoordelingsInstrumentarium

1 Introduction

1.1. Background

'De Slufter' is a nature conservation area located in the northwest of the Dutch Wadden island Texel (see figure 1.1 (a)) which is inundated with seawater during storms and springtide events (Durieux, 2003). A slufter is also a general term to describe "a salt or brakkish dune valley which is connected to the sea through an opening in the most seaward dune row, in which the following characteristics can be distinguished:

- two times a day in- and outflow of seawater takes place through one gully in the dune row; the tide progresses further into the valley through a branched system of gullies;
- the gully in the dune row has a sill that prevents the gully system in the valley from fully emptying during low tide;
- inundation of the valley (slufter plain) with seawater occurs at least once a year;
- the slufter plain has a predominantly sandy substrate;
- a fresh-salt gradient exists at the edge of the slufter plain, e.g. there is a supply of fresh seepage water to the slufter and a discharge through the slufter mouth to sea; elsewhere, through infiltration of rain water, periodical decrease in salinity can also occur;
- the ecological development is primarily determined by morphological development." (Pedroli and Hoekstra, 1992)

During daily conditions, the slufter valley is dry, except for the gully that extends into the slufter valley.

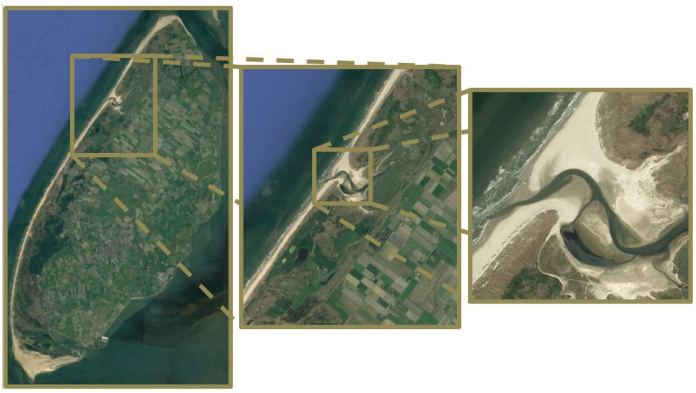

Figure 1.1: Overview of Wadden island Texel with, from left to right: Texel, De Slufter and the slufter mouth (including the gully).

In the Netherlands there are only two areas that match the description above: 't Zwin in Zeeuws-Vlaanderen (on the border with Belgium) and De Slufter on Texel. There are more 'slufter-like' areas that cannot be categorised as a slufter but which do share many of the same characteristics (Pedroli and Hoekstra, 1992). De Slufter is of ecological importance, as is evident from its classification as a Natura2000 site (European Commission, 2017). However, it is also important for coastal safety. The landward side of De Slufter is a sand dike

that is part of the primary coastal defence of Texel (see figure 1.2). The total damage in the event of failure of the primary coastal defence of Texel is estimated at 538 million euro (van der Most, 2011).

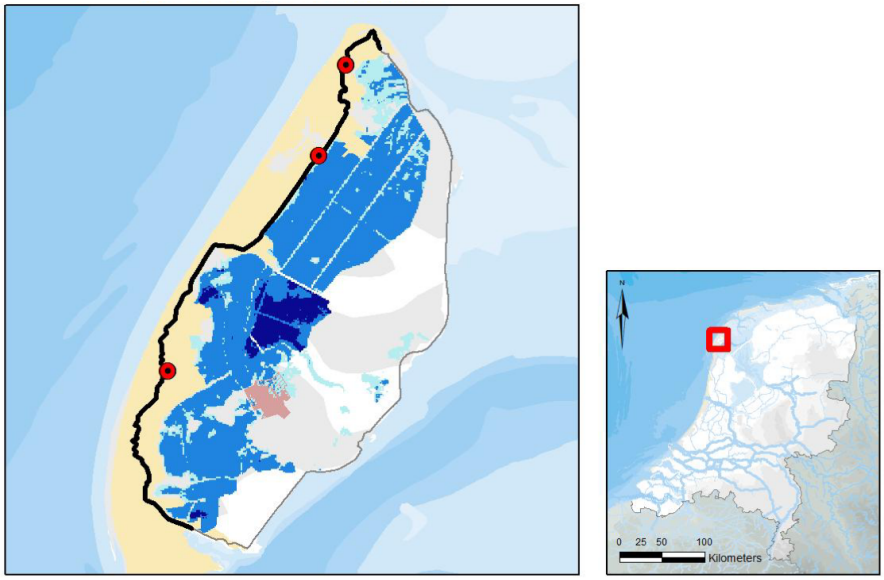

Figure 1.2: Map of Texel present a flooding situation in which the sandy coastal defence (black line) is breached in three locations (red markers) (Slootjes and Wagenaar, 2016). The middle breach is located in the sand dike of De Slufter

The most seaward section of the gully is 'dynamic', meaning it migrates, see figure 1.3. According to a study by Rijkswaterstaat, if the gully is allowed to migrate freely, the mouth of De Slufter, which is the area in between the two dune heads (see figure 1.4), could widen or migrate northwards. Subsequently, migration or widening of the slufter mouth is expected to have a negative effect on the coastal safety of Texel. Particularly, in case of a wider mouth, more wave energy is allowed to penetrate De Slufter during storm and spring tide events, attacking the sand dike. Therefore, the coastal management strategy of the HHNK consists of relocating the gully when it has reached the southern or northern dune head to a location centered between the two dune heads. In practice, this has resulted in relocations every 5-6 years. This has been the coastal management strategy since 1973.

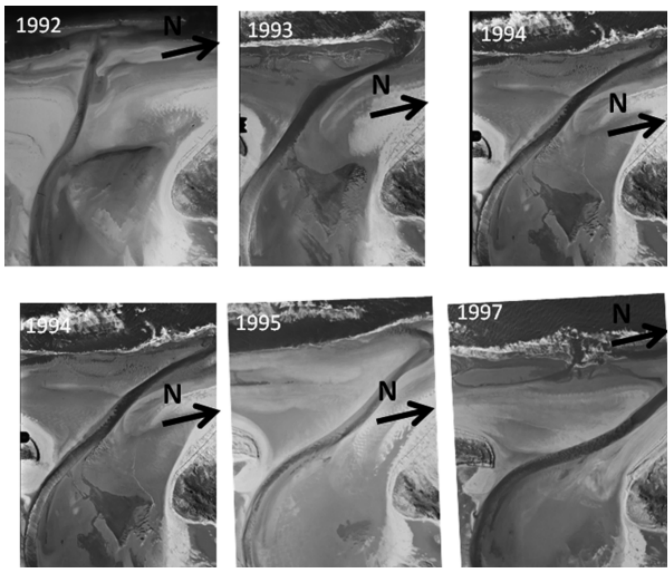

Figure 1.3: Aerial photographs showing the northward migration of the slufter gully from 1992 to 1997 (Van Der Vegt and Hoekstra, 2012). In 1992, the course of the main gully from before the 1991 intervention is still visible.

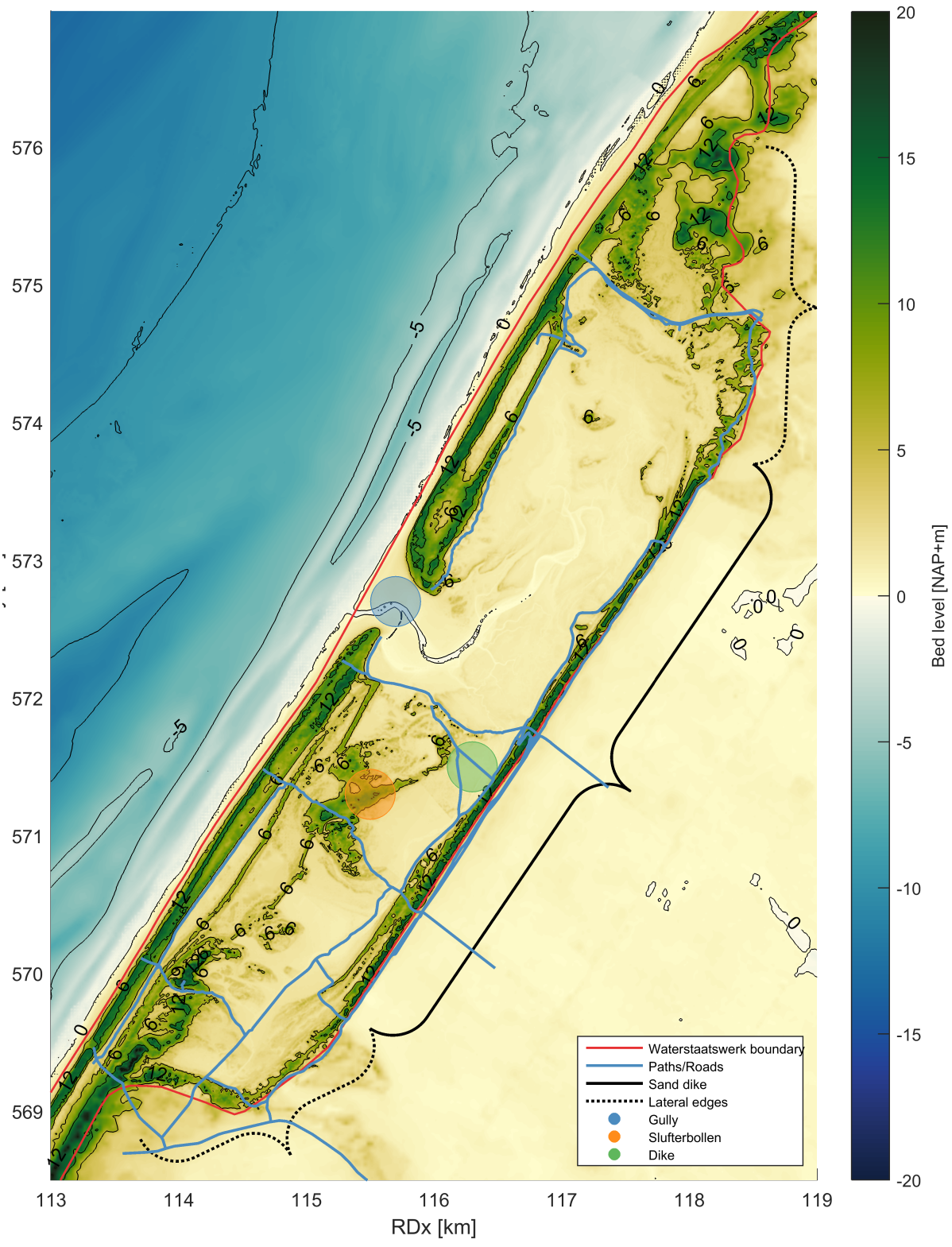

Figure 1.4: Topographic map of De Slufter (2015). The red line indicates the 'Waterstaatswerk' boundary line, which indicates the outer line of the primary water defence. The slufter gully is located in the mouth, which is the area in between the southern and northern dune heads. The location and extent of the sand dike has been indicated with the black curly brace. The 'lateral edges' are the parts of the ridge around the valley which are not part of the sand dike, excluding the front dune row. These have been indicated with the striped black curly braces. The lateral edges and the sand dike together form the 'slufter ridge'. The 'Slufterbollen' is a dune area behind the southern front dune row. The dike is a small NAP+4 m high dike which separates the southern valley from the northern valley. The blue lines indicate all paths and roads that could be discerned on the most recent google earth satellite image (06-01-2017).

1.2. Problem definition

The HHNK's present coastal management strategy for De Slufter is to maintain the present width ($\approx 400m$) and location of the slufter mouth, as this was concluded to be necessary for coastal safety by 'Rijkswaterstaat'. This is done by relocating the slufter gully when it reaches one of the dune heads. In practice, this has resulted in relocations every 5-6 years. However, the HHNK proposes changing this strategy into one where no more relocations are performed (from hereon called the 'proposed coastal management strategy'). This will let De Slufter regain (part of) its natural character. However, there is a limited understanding of the impact this will have on the present and future coastal safety of Texel.

A previous study into the effects of the proposed coastal management strategy on the coastal safety of Texel has been performed by Van Rooijen and Van Thiel de Vries (2014). However, this study has only studied the effects of individual extreme events and has only studied the effects on present coastal safety, thus excluding sea level rise. Dissanayake et al. (2012) found that high sea level rise scenarios lead to drowning of large tidal basin systems. Drowning of De Slufter would mean a year round wave attack on the sand dike which is expected to have significant effects on coastal safety. Furthermore, Van Rooijen and Van Thiel de Vries (2014) concluded that a complete removal of the front dune row of De Slufter would lead to failure. However, it is still unknown for which width this failure occurs.

There are three important aspects that are still not understood:

- **Gully migration:** The gully is relocated because it is believed that the migration of the gully might lead to erosion of the dune heads and consequently, widening of the slufter mouth. It is however not known how the gully will develop in the long term. Furthermore, it is not known whether a sustained migration of the gully will actually lead to widening or migration of the slufter mouth.
- **Wave impact on the sand dike as a result of a wider or more northerly located mouth:** A wider or more northerly located mouth might lead to a larger wave impact on the sand dike. This would likely lead to more erosion of the sand dike. As the sand dike is part of the primary coastal defence of Texel this could thus pose a threat to coastal safety.

  However, the effects of a wider or more northerly located mouth on the wave impact on the sand dike are not fully understood yet. Furthermore, even if the wave impact on the sand dike increases, it is still unclear what the effect would be on dune erosion and consequently, coastal safety.
- **Wave impact on the sand dike as a result of sea level rise:** In addition to the consequences of a different configuration of the slufter mouth, it is also unknown what the effect of sea level rise will be on the future wave impact on the sand dike and the coastal safety of Texel.

In addition to a lack of understanding of consequences, new standards have also been implemented for the assessment of coastal safety (ENW, 2016), affirming the need for a new study. The most important change for De Slufter is that coastal safety is no longer assessed on a 1/4000 year storm but on a 1/3000 year storm.

1.3. Research objective

The main objective of this research is to assess the impacts of the proposed coastal management strategy on the present- and future coastal safety of the Wadden island Texel. For this purpose, the three important aspects discussed in section 1.2 will have to be understood.

First, as concluded by Van Rooijen and Van Thiel de Vries (2014), the location and width of the slufter mouth have a significant effect on the erosion of the sand dike during storm events. The location and width of the mouth are expected to be governed by the migration of the gully. The processes dominating gully migration will therefore have to be investigated.

Second, the effect of a different location or width of the slufter mouth on the wave impact on the sand dike will have to be investigated. Furthermore, the magnitude of storm wave impact on the ulterior sand dike and subsequent erosion will largely be determined by the magnitude of inundation of the slufter valley during storms. This will be largely dependent on future sea level rise scenarios. These will thus also have to be included. XBeach Surfbeat (Roelvink et al., 2009) will be used as a modelling tool for this purpose.

1.4. Research questions

Based on the research objective, the main research question is:

"What will be the effect of ceasing human interventions into the mouth of the slufter gully on the present and future coastal safety of the Wadden island Texel?"

The following subquestions were formulated to answer this research question:

1. "Which processes govern the direction and magnitude of migration of the slufter gully?"
2. "How will the proposed coastal management strategy affect the present coastal safety of Texel?"
3. "How will the proposed coastal management strategy and sea level rise affect the future coastal safety of Texel?"

1.5. Research approach and thesis outline

- **Literature study**
  In chapter 2, the necessary theory and background for this study are given. The morpho- and hydrodynamic processes that are relevant for De Slufter are elaborated on here. Apart from short-term processes such as dune erosion, sea level rise measurements and projections are also discussed, as well as the expected dominant processes for the migration of the slufter gully. The definition of dune failure and the method of assessing flood safety for the primary coastal defence in the Netherlands is also discussed, as well as corresponding modelling programs.

- **Field data analysis**
  In chapter 3, a field data analysis on hydrodynamic, sediment and bathymetric data is performed to study the historical migration of the slufter gully. The hydrodynamic data is analysed to assess the historical forcing of waves and water levels on the slufter gully. This data is also used for the determination of hydraulic boundary conditions for the modelling study. Combined with the sediment data, the annual historical longshore transport rates are calculated. The bathymetric data is studied to determine the historical migration of the slufter gully. Together this is expected to shed light on the dominant processes in the slufter mouth migration and on the expected future migration. This will answer research subquestion 1.

- **Modelling study**
  In chapter 4 the model setup is discussed. The modelling study comprises of a collection of possible scenarios. It is thus a study on a range of possible scenarios. No assumption is made on the probability of a scenario. For all scenarios, the occurrence of failure is assessed.

  The model scenarios that have been formulated for this study can be divided into *present* and *future* scenarios (in the year 2100). Current scenarios exclude sea level rise (from here on called SLR) and bed level rise (from here on called BLR) and will differ only in storm magnitude and width and location of the slufter mouth. Taking note of the recommendations by Van Rooijen and Van Thiel de Vries (2014), the effects of a serie of storms has also been studied. Future scenarios will include different SLR and BLR scenarios. To model both BLR extremes it is either assumed that BLR is equal to SLR or that there has been no BLR at all.

  In chapter 5 the model validation process is covered. The validation is divided into a hydrodynamic part and a morphological part. In chapter 6 the results of the model simulations are discussed and studied.

- **Discussion**
  In chapter 7 the assumptions and model settings, as well as the validity of the results are critically reflected on.

- **Conclusions and recommendations**
  Lastly, the conclusions and recommendations that have resulted from the study are presented and explained.

2

Literature study

In this literature study, 3 general aspects are discussed: in Section 2.1, **processes** that are relevant for understanding and answering the research questions; in Section 2.2, **models** that are used in the field to model dune erosion and other relevant processes; in Section 2.3, different **dune failure assessment methods** that are currently in use in the field.

2.1. Relevant processes

The migration of the gully is expected to affect the width of the mouth. Processes that are of importance for the understanding of the gully migration are thus discussed first in section 2.1.1 The primary coastal defence on the North Sea side of Texel consists of dunes. Furthermore, the sand dike can also be characterised as a dune. To analyze the coastal safety of Texel it is therefore important to understand the processes involved in dune erosion. These are treated in subsection 2.1.2. Sea level rise will have a large influence on tidal asymmetry and dune erosion. Therefore, in subsection 2.1.3, the latest projections for sea level rise in 2100 will be given.

2.1.1. Gully migration

Three processes are expected to play a role in the migration of the slufter gully: wave induced longshore transport, overwash during storms (Van Der Vegt and Hoekstra, 2012) and secondary flow in the gully (Durieux, 2003). All three processes will be described here.

Wave induced longshore transport

"Longshore sediment transport is the net movement of sediment particles through a fixed vertical plane perpendicular to the shoreline" (Bosboom and Stive, 2012). The direction of transport is thus parallel to the shoreline, see figure 2.1. Wave-induced longshore transport is mainly governed by the hydrodynamics in the breaker zone and the sediment characteristics at the coast. The generation of wave-induced longshore transport consists of two main components.

- **Sediment upstirring**
  Due to the orbital motion of waves sediment is mobilized and brought into suspension. The entrainment peaks twice per wave cycle when bed shear stress is maximal. Also, during wave breaking turbulence increases in the water column which brings suspended sediment to the upper part of the flow. This is mainly a cross-shore component.
- **Wave-induced longshore current**
  The longshore component is called the longshore current which is induced by obliquely incident breaking waves and is concentrated in the surfzone. The current transports upstirred sediment alongshore.

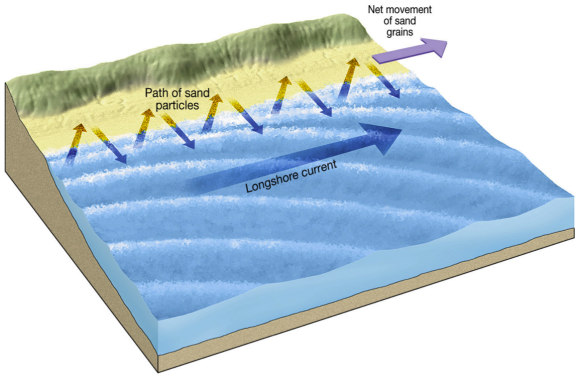

Figure 2.1: Longshore current and sediment transport.

There are two general methods of calculating longshore transport. It is possible to calculate the cross-shore distribution of longshore transport and integrate this over the cross-shore plane. This provides the option of including more processes (e.g. tidal currents or other longshore currents). A more simplistic (but not necessarily less accurate) way is to calculate the bulk longshore transport. This includes only the effect of wave generated longshore currents. One of the most widely used formulas is the CERC formula (CERC, 1984).

The CERC formula has some limitations. First, only wave-induced longshore transport is calculated. Second, the calculated longshore transport is independent of sand properties such as grain size. And third, only sediment transport in the breaker zone is calculated. There are many adaptations of the CERC formula in use. In this study an expression developed by van Rijn (2013) was used. This expression will be discussed in the field data analysis in chapter 3.

Overwash and inundation

Overwash occurs when the runup level of waves exceeds the 'first line of defence' (Sallenger, 2000). In this case the first line of defence is equal to the beach crest. As this happens, waves propagate over the beach flat and will transport sediment from the beach flat into the gully. Inundation occurs when the base of the swash motion is elevated such that the first line of defence is constantly inundated. In De Slufter this occurs during storms and springtide events. Inundation is also accompanied by landward sediment transport (Sallenger, 2000). A schematisation of both regimes is given in figure 2.2.

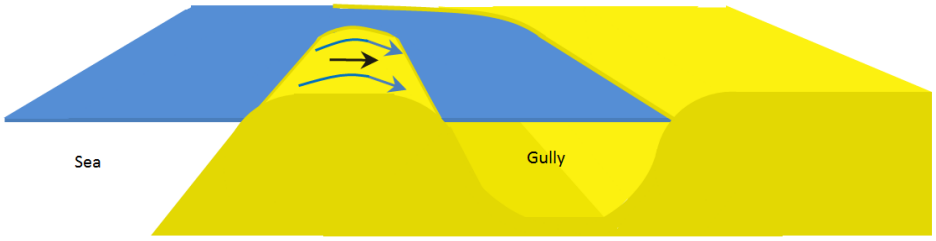

(a) Non-inundated conditions

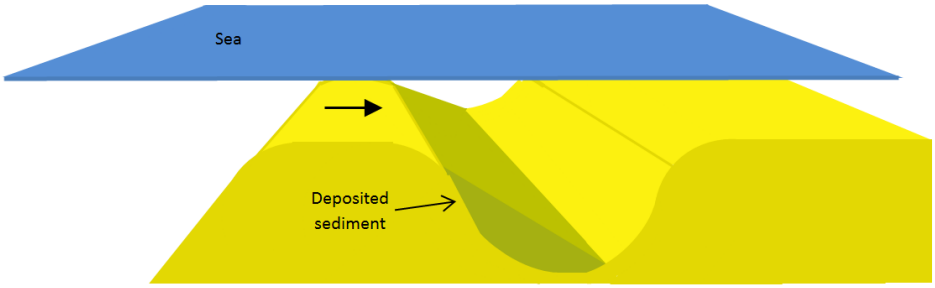

(b) Inundated conditions

Figure 2.2: Schematisation of overwash during storms. The top panel represents calm conditions in which the beach flat is dry. The lower panel represents storm conditions in which the beach flat is inundated and sediment is transported from the beach flat into the gully. The blue arrows indicate overwash of waves. The black arrows indicate the direction in which the sediment is transported.

If not all sediment can be transported along the channel axis the deposition of sediment in the gully will redirect the flow. To maintain a sufficient conveying cross-section erosion will occur at the other side of the gully (cross-channel). The gully shape will thus be altered and migration will occur.

Curvature-induced secondary flow

As in river bends, tidal channels contain curvature-induced secondary flow patterns (Nidzieko et al., 2009; Vennell and Old, 2007). This flow pattern is a result of different depth-distributions of pressure and curvature-induced centrifugal forces. The flow patterns due to curvature induced flow do not change sign when the tidal forcing turns (Bosboom and Stive, 2012). Neglecting stratification and the Coriolis force, which is acceptable for the spatial scale of the study area, leads to the following transversal force balance:

$$-\frac{u^2}{R}+\frac{1}{\rho}\frac{\delta p}{\delta y}-\frac{\delta}{\delta z}\nu_T\frac{\delta v}{\delta z} \tag{2.1}$$

In which:

R	radius of the channel bend (assumed much larger than the channel width)	[m]
u	local velocity along the channel axis	[m/s]
x	lateral coordinate x = $R\theta$	[m]
z	vertical coordinate; bottom: $z=-h$, surface: $z=\eta$	[m]
v	transversal velocity	[m/s]
y	transversal coordinate	[m]
ν_T	eddy viscosity	[m^2/s]

The centrifugal force $-\frac{u^2}{R}$ will lead to a positive water level gradient towards the outer bend. Assuming continuity, this leads to a downwards velocity near the outer bend and, subsequently, a circulation pattern. The tide-averaged transversal circulation erodes the outer channel bend and deposits the eroded sediment on the inner channel bend. This process causes a migration in the (cross-channel) direction of the outer bend and results in a cross-channel profile with a steep outer bend and a shallow inner bend, as seen in figure 2.3.

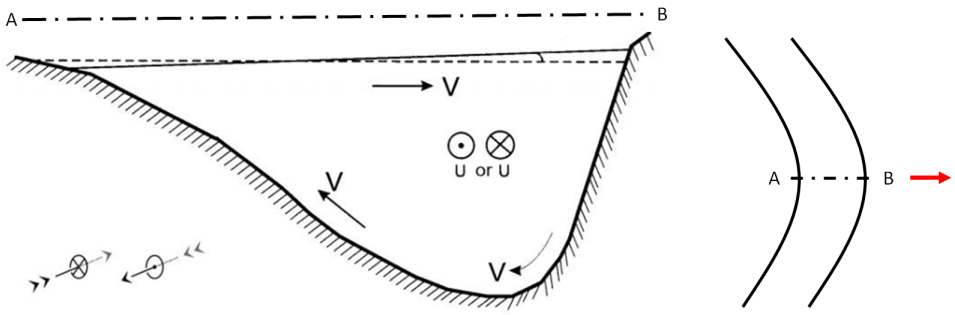

Figure 2.3: Cross-section of a channel bend showing tide-averaged transversal circulation on the left and a top view of the considered channel bend on the right. The red arrow indicates the direction in which the secondary circulation drives the channel migration. The centrifugal force exerts its influence at ebb and flood in the same direction. Adapted from Bosboom and Stive (2012).

2.1.2. Dune erosion

There are 4 main nearshore processes that affect dune erosion (van Rijn, 2009):

- **Wave impact on the dune face.** As waves hit a dune, large quantities of water run up the beach face. This water, called the wave uprush, exerts a force on the duneface which is related to dune erosion (Fisher et al., 1986). The force is caused by the deceleration of the water rushing up the duneface. The beach profile is thus important for the magnitude of this force as mild beaches leads to much less deceleration, and thus a smaller force on the bed, than steep beaches. Consequently, this force is generally higher for the pre-storm duneface as it is for the post-storm duneface, caused by the flattening of beach profiles as storms progress.

- **Turbulence.** Breaking waves, rollers and reflections from the dune and the turbulence they cause lead to sediment upstirring. As compensation for the onshore mass transport by waves and rollers a strong return current (or undertow) is formed which transports the upstirred sediment offshore. Due to this process a new profile is formed with a milder slope (Van Thiel de Vries et al., 2008). This process therefore decreases the contribution of the wave uprush.

- **Sliding/avalanching of the dune face.** Van Thiel de Vries (2009) found that a main contributor to dune erosion is avalanching. Avalanching occurs due to wetting of the duneface. This causes the angle of repose of the soil to decrease and the weight of the duneface to increase. As a result, large quantities of sand are deposited on the beach by sudden slides and transported offshore by the already mentioned undertow. When the deposited sand is transported offshore the process repeats itself.

- **Low frequency wave motions (long waves or infragravity waves).** Assuming a standard beach profile with one dune row (in contrast to the 2 dune rows of De Slufter), short waves start breaking as they approach the shore, reducing in amplitude. Long waves do not break however but grow in amplitude as they approach the shore. Therefore, long wave energy near the duneface can be larger than the short wave energy (Van Thiel de Vries et al., 2008).

2.1.3. Sea level rise

De Slufter's morphology and ecology, as well as the future flood safety of Texel are influenced significantly by sea level rise. Possible effects include: increased dune erosion through higher storm surge levels, dissapearing intertidal basin areas (Van Der Wegen, 2013), salinization of ground water (Oude Essink et al., 2010) and a higher inundation frequency leading to the decrease of or damage to habitats to local fauna (Ecomare, 2018).

Observed sea level rise

In the period 1906-2012 the average sea level rise[1] along the Dutch coast was 17.6 centimeter per century, or 1.76mm/year, based on the linear regression model by Baart et al. (2014) (see black dots in figure 2.4). The measurements during this period show no significant acceleration (Baart et al., 2014).

Projected sea level rise

Projections for local sea level rise along the Dutch coast by Le Bars et al. (2017), which include the expected contribution of Antarctic ice sheet loss (DeConto and Pollard, 2016), range from almost 1 meter sea level rise in 2100 (compared to 1995), to more than 3 meters. The projections are based on the 'Representative Concentration Pathways (RCPs)' (Intergovernmental Panel on Climate Change (IPCC), 2014), which describe four possible 21st century pathways based on greenhouse gas emissions, atmospheric concentrations, air pollutant emissions and land use. Figure 2.4, adapted from the recent Deltares report on the consequences of sea level rise for the Netherlands (Haasnoot et al., 2018), shows the projections by Le Bars et al. (2017), as well as the Deltascenarios and observed sea level rise.

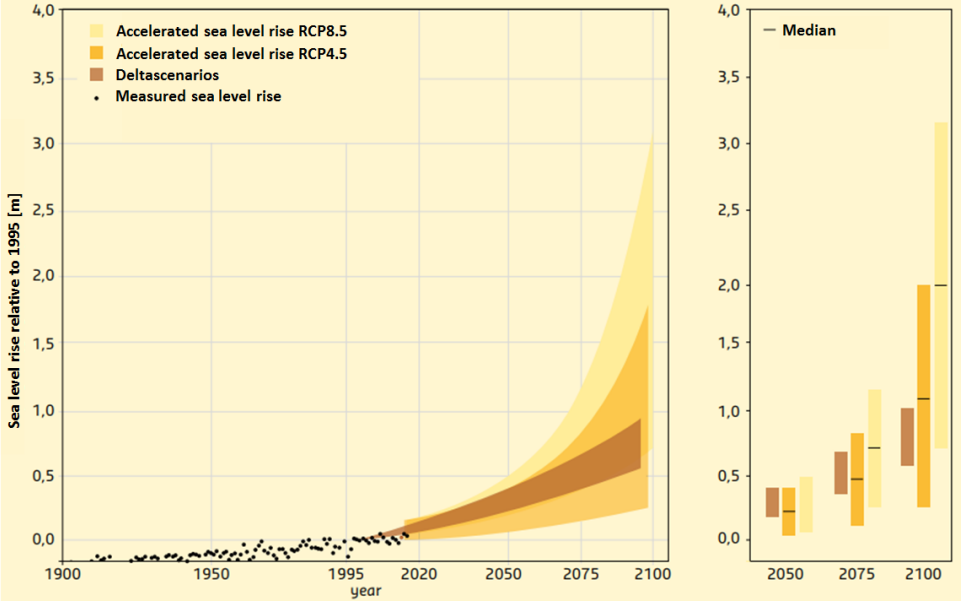

Figure 2.4: Sea level rise scenarios used by KNMI et al. (2014) along with projections by Le Bars et al. (2017) and historical measurements (Baart et al., 2014). Adapted from

Concentration scenario	RCP4.5			RCP8.5		
	Lower boundary	Median	Upper boundary	Lower boundary	Median	Upper boundary
2050	7	24	41	9	29	47
2100	29	108	192	75	195	317

Table 2.1: Overview of sea level rise projections for the Dutch coast in centimeters for 2050 and 2100 compared to 1995 (Le Bars et al., 2017). RCP4.5 and RCP8.5 (Intergovernmental Panel on Climate Change (IPCC), 2014) refer to global concentration scenarios with a 2°C and 4°C global temperature increase, respectively. Adapted from Haasnoot et al. (2018).

[1] Average here means: the average of mean sea level rise over all tidal stations along the Dutch coast.

2.2. Modelling dune erosion

Two different widely used tools for modelling dune erosion are DUROS+ (WL | Delft Hydraulics, 2006) and XBeach Surfbeat (Roelvink et al., 2017 2009). A description of both models is given in this section.

2.2.1. DUROS+

'DUROS+' (Van Gent et al., 2008) is a 1DH, volume based, empirical model which is the prescribed dune erosion model at present for Dutch dune safety assessment (Den Bieman et al., 2014b). Assuming normally incident waves, DUROS+ approximates a post-storm equilibrium dune profile shape (red line in figure 2.5) based on a range of parameters[2]. This profile consists of a dry dune foot, a parabolic post-storm equilibrium beach profile, and a transition slope connecting the pre- and post-storm profile offshore. The cross-shore location of the profile is determined by assuming mass conservation, which means that all sediment eroded from the dune[3] is considered to have been deposited on the beach/foreshore[4]. The profile is then shifted in cross-shore direction such that erosion equals sedimentation.

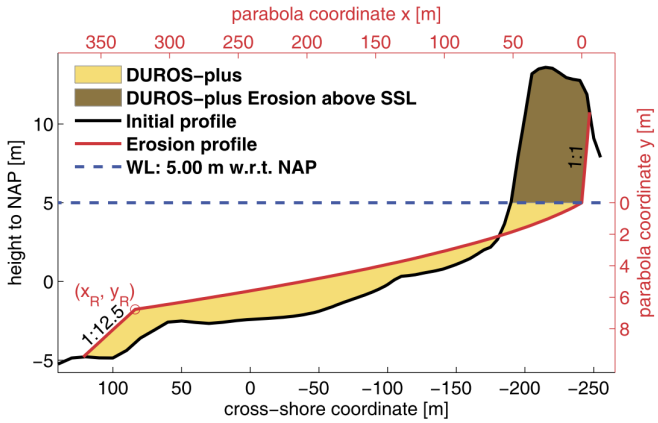

Figure 2.5: Example of DUROS+ calculation consisting of three components: the dry dune foot (1:1 slope), the parabolic post-storm profile, and the transition slope connecting pre- and post-storm profile (1:12.5 slope). Figure taken from Den Heijer (2013).

2.2.2. XBeach Surfbeat

XBeach is a 2DH, process based numerical model which was originally developed to simulate the impact of extreme storms and hurricanes on sandy barrier island systems, including beach and dune erosion, overwash, inland flooding and barrier rollover and breaching (Roelvink et al., 2017 2009). For this purpose, it has been designed such that it resolves all storm regimes defined by Sallenger (2000), i.e. swash, collision, overwash and inundation. The model has been validated by multiple laboratory and field studies (Bolle et al., 2010; Van Dongeren et al., 2009; Van Geer et al., 2015; Van Thiel de Vries, 2009).

XBeach solves coupled 2DH equations for wave propagation, flow, sediment transport and bottom changes, for varying (spectral) wave and flow boundary conditions (Roelvink et al., 2009). In the Surfbeat mode, Xbeach does not resolve individual waves. It resolves the variation of the short-wave envelope on the scale of wave groups. The short-wave envelope variation drives infragravity waves through resulting radiation stresses that exert a force on the water column (Deltares, 2017).

To accurately resolve dune erosion, XBeach incorporates a dune avalanching algorithm which assumes a dry and a wet critical slope. When exceeded, these trigger an avalanching of sediment downwards from the dry duneface to the wet swash (Roelvink et al., 2009). For dissipative beaches, infragravity waves are the main contributor to swash waves that actually hit the dune front (causing dune avalanching due to wave setup) or overtop it (Roelvink et al., 2009). Resolving infragravity waves is thus necessary to accurately assess the storm impact due to dune erosion on the sand dike in De Slufter, as explained in section 2.1.2.

[2] Offshore significant wave height [H_s], peak wave period [T_p], grain size [D_{50}], storm surge level [η], pre-storm dune profile.
[3] Brown and yellow area to the right of the intersection between pre- and post-storm profile in figure 2.5
[4] Yellow area to the left of the intersection between pre- and post-storm profile in figure 2.5.

Apart from the accurate representation of dune erosion processes, XBeach Surfbeat also resolves hydrodynamic processes such as longshore currents, shoaling, refraction (diffraction is not included), bottom dissipation, wave breaking, wave setdown, wave setup and includes a roller model. This renders it very suitable for the modelling of morphological changes on dissipative beaches over time.

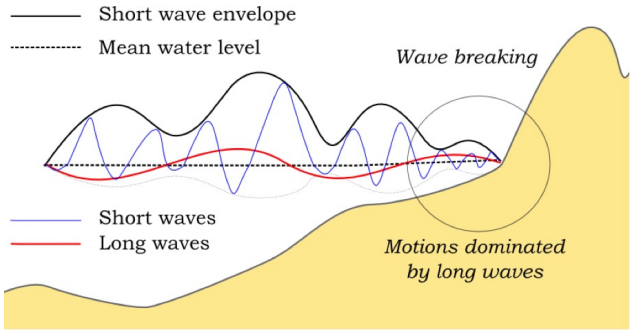

Figure 2.6: Principle sketch of relevant wave processes in XBeach (Deltares, 2017).

2.3. Dune failure assessment

The Statutory Assessment Tools (WBI), which have entered into force in 2017, have led to the assessment of the primary coastal defence system based on new standards (Von Gronau, 2017). Until 2017, the flood safety norm was defined as a water level which had to be safely withstood. This water level ('toetspeil') was equal to the water level belonging to a 'norm frequency', which for Texel was 1/4000 years (Ministerie van Verkeer en Waterstaat, 2007). The old flood safety norm only focussed on the hydraulic loading and did not explicitly include the strength of the barrier.

The new flood safety norm expresses flood safety in terms of flood risk, which refers to both the probability and consequences of failure. These depend on both the hydraulic loading (water levels and waves) and strength (e.g. height, width) of the barrier (ENW, 2016). In the new flood safety norm, 2 norm frequencies are defined, the *ondergrens* (lower boundary) and the *signaleringsnorm* (signalling norm). The lower boundary refers to the minimum probability of failure on which a dune section should be designed. When the signalling norm is exceeded this means that "the dune section will be eligible for reinforcement in the foreseeable future" (Deltares, 2016). For dune section 5-1, which includes De Slufter, the lower boundary is 1/1000 per year and the signalling norm is 1/3000 per year (Slootjes and Wagenaar, 2016).

Dune safety is currently assessed with DUROS+. DUROS+ is only capable of calculating post-storm dune erosion, which renders it unfit for use as an assessment tool under the new law. This requires a new approach to dune safety assessment (Von Gronau, 2017).

At the time of writing, a new method for dune safety assessment has not yet been been legally anchored. However, the limitations of DUROS+ can and likely will be overcome by using XBeach, which can model more processes than DUROS+ (Von Gronau, 2017). In subsection 2.3.1 the old method is discussed. In subsection 2.3.2 a proposed method for dune safety assessment with XBeach Surfbeat is elaborated on.

2.3.1. Current empirical method

After the approximation of the post-storm dune profile with DUROS+, the occurrence of dune failure is assessed by fitting in a 'limit profile' (NL: Grensprofiel). If the limit profile can be fitted into the post-storm dune profile the dune section is 'safe'. If it cannot, it is considered 'failed'. For a visual representation of the limit profile (*NL: Grensprofiel*), see figure 2.7.

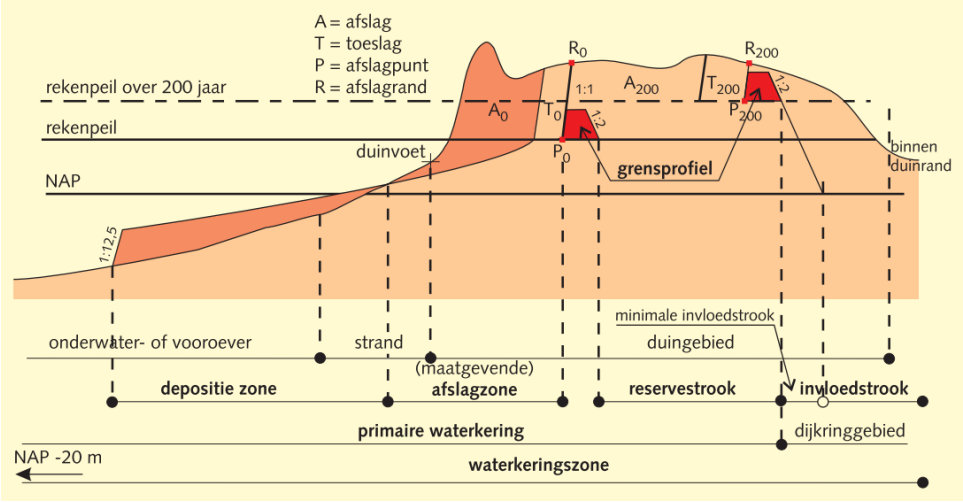

Figure 2.7: Visual representation of the limit profile (NL: 'grensprofiel'). If the limit profile cannot be fitted into the post-storm dune profile, the dune section has failed according to the old method. From Technische Adviescommissie voor de Waterkeringen (2002).

The limit profile in figure 2.7 consists of a 'front slope' of 1:1, a 3 meter wide top and a 'rear slope' of 1:2. The minimum height of the limit profile is determined by formula

$$h_0 = RP + 0.12 T_p * \sqrt{H_{0s}} \tag{2.2}$$

with

- RP = storm surge level
- T_p = Peak wave period
- H_{0s} = Expected value of significant wave height

The use of DUROS+ is subject to 3 important criteria: it can only be used for reasonably straight coastlines, transects without hard structures and pre-storm profiles which range from at least NAP-5m to NAP+5m (Den Heijer et al., 2011). There are some other important limitations to DUROS+ (apart from the fact that it is 1-dimensional and empirical), as mentioned by Den Bieman et al. (2014a); Den Heijer et al. (2011); Hoonhout and Den Heijer (2011); Van Thiel de Vries (2009).

- DUROS+ only calculates dune erosion in the collision regime. Morphological changes during swash, inundation and overwash are not considered.
- DUROS+ can only model profiles with one dune row.
- DUROS+ neglects the storm duration and shape in the calculation of the post-storm profile.
- Wave transformation across the dune profile is not included.
- DUROS+ can only consider shore normal waves.
- The mass conservation assumption is only valid for alongshore uniform coastlines. DUROS+ has an option with which alongshore sediment transport can be included. However, the capability of the model to accurately simulate this process is very limited.
- The calculated post-storm profile shape is independent of the pre-storm profile.

2.3.2. Proposed method

Von Gronau (2017) proposes 5 limit states which can be used to assess dune safety under the new norm:

Erosion failure

- **'Erosion failure':** As soon as any change of the bed can be observed behind the Legger[5], the coast is considered to have failed. In this new definition any form of bed level change behind the 'Legger' is already enough to consider the coast as failed. This situation can happen either due to collision or overtopping.
- **'Grensprofiel':** This definition is closest to the limit state defined for the use of Duros+ and is therefore named accordingly. Failure occurs if the remaining dune volume above the storm surge level (SSL) is less than 20 m2/m which represents more or less the Grensprofiel definition.

Wet failure

- **'Puddles':** Failure due to overtopping has occurred when at any point landward of the Legger a water depth of at least 20 cm can be observed. The definition of 20 cm is derived from the advise of the ENW (2007) with regard to the loss of lives. In this definition the location of failure occurrence is not further defined. It is expected that this type of failure occurs due to wave overtopping where water is collected in a hollow.
- **'Wet feet':** When a water depth at the first house reaches 20 cm more, the flood defence is considered to have failed. This condition is comparable with the previously mentioned limit state but the location of failure is defined at the first house.
- **'Inundation':** The coast is considered as unsafe when in a defined area the average water depth is at least 20 cm. The spatial distribution of the postal code areas in the Netherlands was used as a reference for the size of these areas.

Figure 2.8 presents visual representations of all 5 limit states. The **Wet feet** and **Inundation** failure mechanisms are out of the scope of this study as the landward side of the model domain only includes De Slufter itself (chapter 4). In XBeach, only areas that are inundated are subject to bed level change and inundation will always lead to bed level change, however small it may be. Because of this, the **Erosion** and **Puddles** failure mechanisms are identical.

[5]The Legger is a map which contains the locations of primary coastal defence systems. The utmost landward location of the boundary profile is also stated in the Legger. For this study this boundary is equal to the 'Waterstaatswerk' boundary (the red line in figure 1.4)

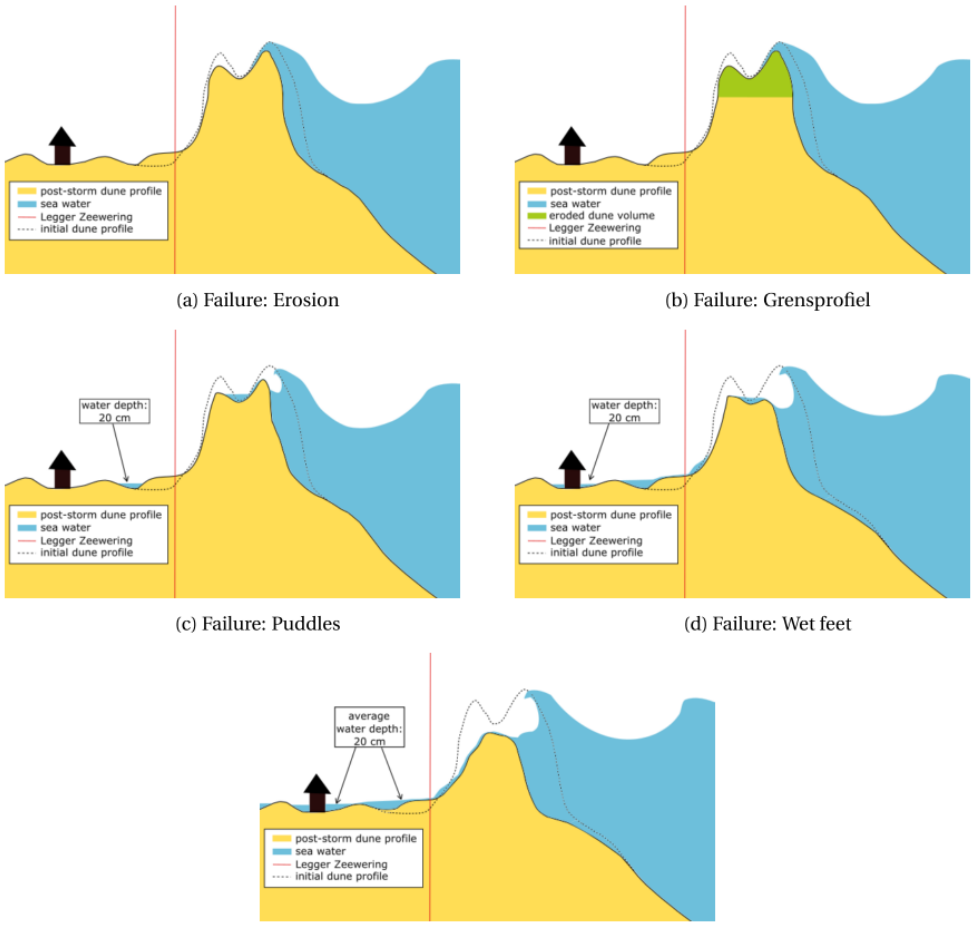

(a) Failure: Erosion

(b) Failure: Grensprofiel

(c) Failure: Puddles

(d) Failure: Wet feet

(e) Failure: Inundation

Figure 2.8: Limit states for dune failure as defined by Von Gronau (2017)

It is important to note that these limit states are propositions which have not been made official and which are thus not legally anchored. However, as there is no official method yet, a part of these limit states will be used in this report because it is currently deemed the most appropriate method in combination with the modelling study with XBeach Surfbeat.

2.4. Conclusion

Theoretical background has been given to three components of this study. First, the processes that are expected to be of importance for the migration of the slufter gully have been discussed. Based on literature, it is expected that gully migration is driven by a combination of curvature-induced secondary flow, wave-induced longshore transport of sediment and overwash during storms.

Second, two methods of modelling dune erosion were discussed: DUROS+, a 1DH volume-based empirical model, and XBeach Surfbeat, a 2DH process-based numerical model. DUROS+ is the presently prescribed dune erosion model for dune safety assessment. It has some limitations however which render it unfit for use as a modelling tool in De Slufter. These limitations can and likely will be overcome by XBeach, which resolves more processes than DUROS+.

Finally, two methods for assessing dune safety have been discussed: the current method in which a 'grensprofiel' is fitted in the post-storm dune profile, and a proposed method which incorporates more failure mechanisms.

3

Field data analysis

To understand what drives the migration of the gully mouth, a study is performed on historical migration and hydrodynamic forcing from 1997 until 2017. In section 3.1, the available historical hydrodynamic, sediment and bathymetric/topographic data is elaborated on. The bathymetric/topographic data consists of the location of the gully over time and shows the historical migration of the gully. With the available hydrodynamic and sediment data an analysis is done in section 3.2 on the historical longshore transport at De Slufter. This is expected to provide insight into what drives the migration of the slufter gully. The analysis of the historical gully migration and its causes are treated in section 3.3. An overview of of the components of this chapter is given in figure 3.1.

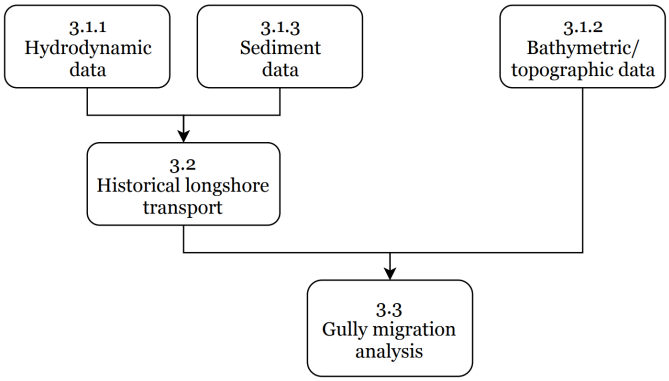

Figure 3.1: Overview of the different components of the field data analysis and their interdependence.

3.1. Data

The hydrodynamics are treated in section 3.1.1. The hydrodynamics are elaborated on as they will also be used later on to determine the boundary conditions for the modelling study. Next, in subsection 3.1.2, the historical topography and bathymetry over time in the area around the slufter mouth are presented. In subsection 3.1.3 the sediment distribution in De Slufter is treated.

3.1.1. Hydrodynamics

The hydrodynamic forcing consists of a **water level**- and a **wave** component. Both components are determined separately and combined afterwards. The wave climate is made up of wave height, period and direction. The timeseries have been derived from two buoys near Texel (see figure 3.2).

Figure 3.2: Wave and water level buoy locations.

Water level

For statistical purposes, the measured water level time series (from here on called total water level) is deconstructed into two components: the tidal water water level and the non-tidal residual (NTR). The tidal water level is the water level solely due to the tide. The NTR is described as 'surge' or 'wind-driven setup' but is in fact all water level fluctuations that cannot be associated with the tidal water level (e.g. due to wind or wave setup). Both the tidal water level and the NTR are later used in the calculation of the boundary conditions for the modelling study. For that purpose it is important to note that the maximum tidal water level is considered a constant. The NTR, however, increases as storms become larger. The total water level thus consists of a constant and a variable component.

The tidal analysis of the total water level is shown in figure 3.3. The top panel represents the total water level as measured at the buoy. The middle panel represents the tidal water level. The lower panel represents the NTR. The tidal water level time series was manually created. First, the tidal components were analysed from the total water level with 'T_TIDE' (Pawlowicz et al., 2002). Next, using these tidal components as input, a water level time series was created for the same period as the measurements, representing the water level solely due to the tide. By subtracting the tidal water level from the total water level, the non-tidal residual (NTR) was calculated.

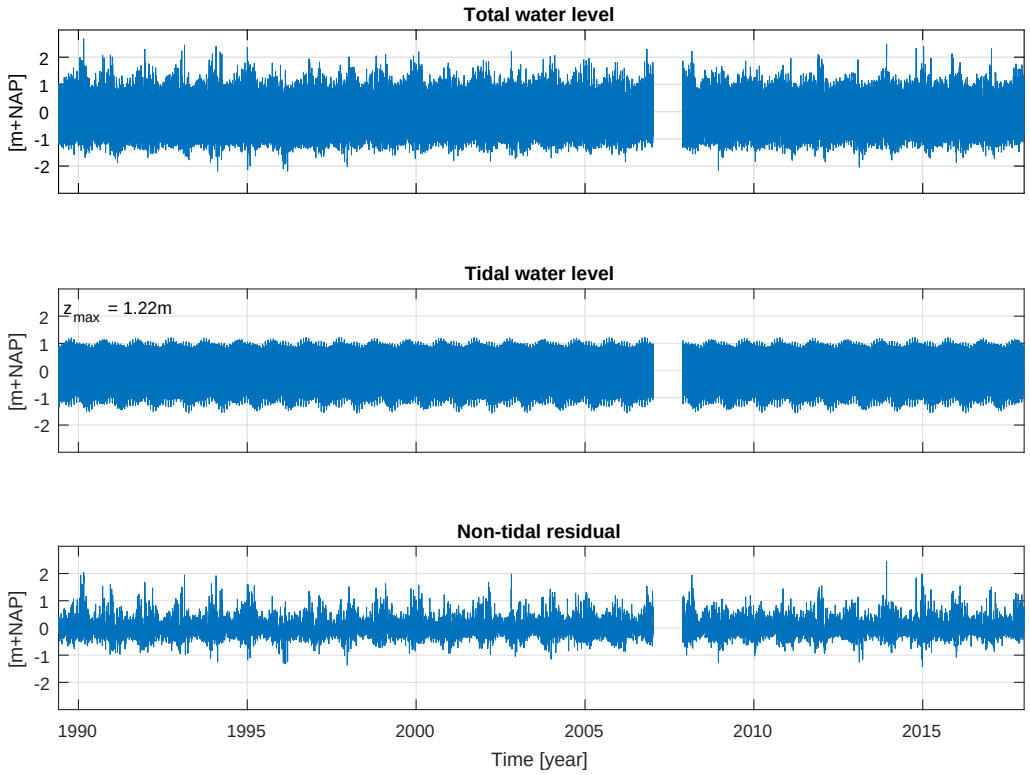

Figure 3.3: Tidal analysis of water level measurements at the 'Texel Noordzee' buoy. The tidal water level, shown in the middle panel, has been manually created. Subtracting the tidal water level from the total water level results in the non-tidal residual, shown in the bottom panel.

Wave

Figure 3.4 presents the zeroth order spectral wave height (top panel) and the mean zero crossing period (bottom panel) over time measured by the 'Eierlandse Gat' buoy. The top panel shows that significant wave height since 1979 has never been higher than 8.2m and seldomly grows higher than 6m. The distribution of historical wave direction is given in figure 3.1, which presents the wave rose of the measurements.

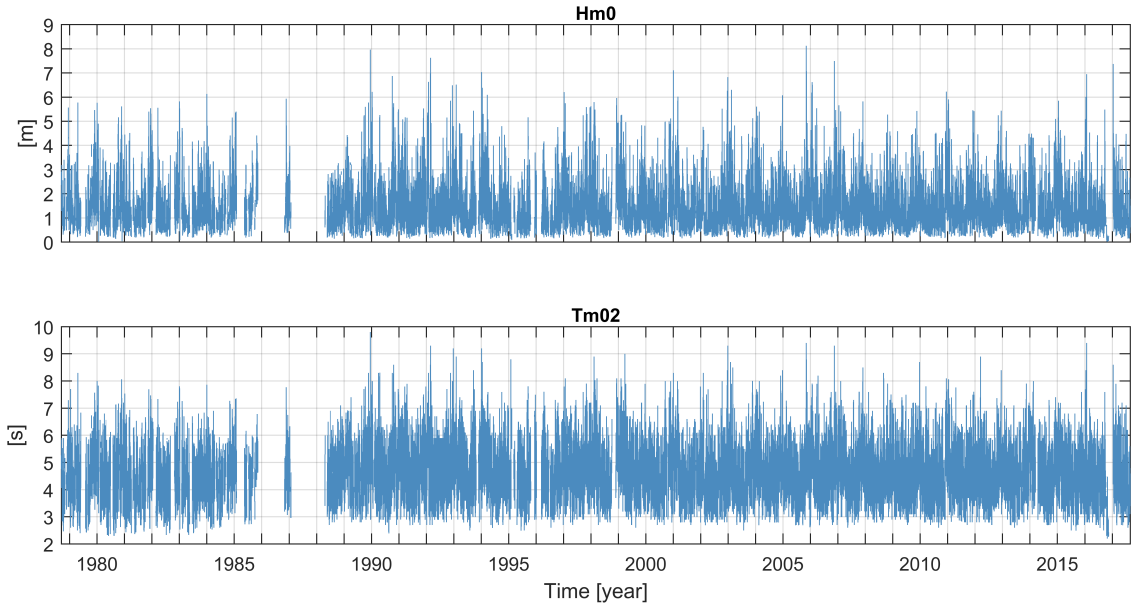

Figure 3.4: Zeroth order spectral wave height (Hm0) and mean zero crossing period (Tm02) measured at the Eierlandse Gat buoy.

The dominant wave directions of the observations are SW, NW and N. This is mainly caused by the location of Great Britain and Scandinavia, which limit wave growth during wind conditions from the West or Northeast, see figure 3.5. Waves from the WNW-WSW cannot attain wave heights higher than 10m according to Bretschneider (1964) However, table 3.1 shows that historically, higher waves come from the West than from the Southwest.

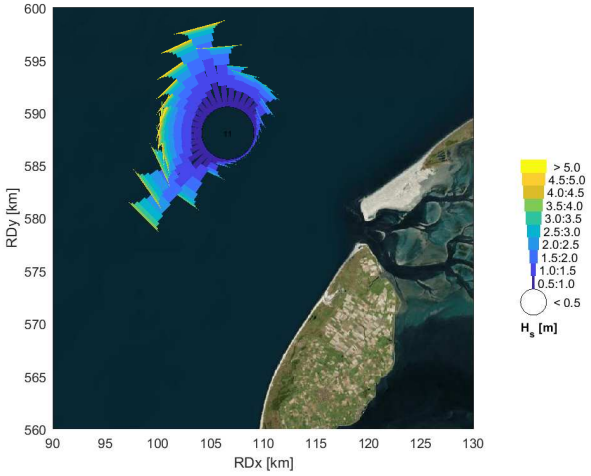

	Boundary		
	Lower [°]	Upper [°]	Occurrence [%]
S	157.5	202.5	2
SW	202.5	247.5	22
W	247.5	292.5	16
NW	292.5	337.5	21
N	337.5	22.5	25
NE	22.5	67.5	12
E	67.5	112.5	2
SE	112.5	157.5	1

Table 3.1: Wave rose of Eierlandse Gat buoy observations along with table of measurements.

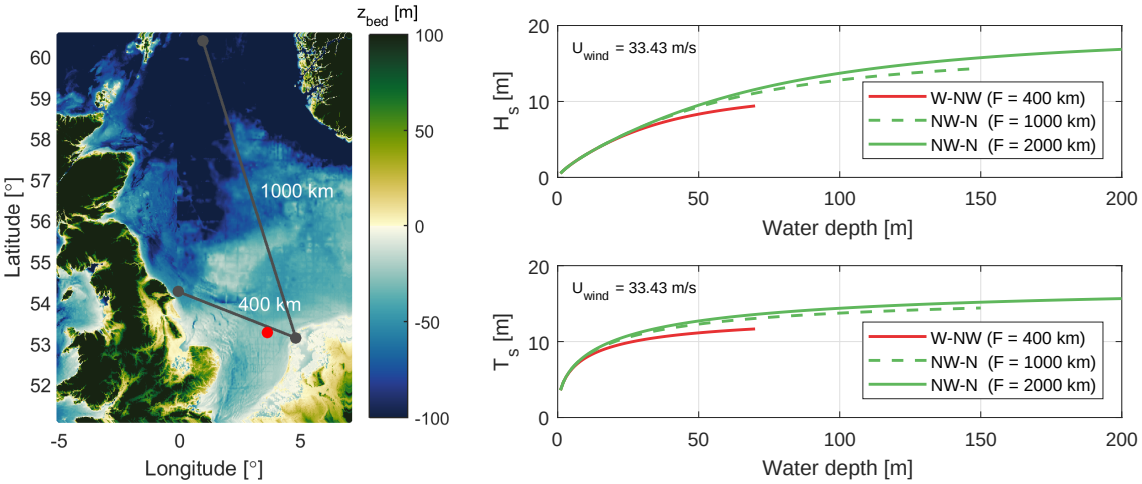

(a) Fetch length for WNW and NNW wave directions in the North Sea.

(b) Wave height and wave period over water depth calculated with the Bretschneider formulas (Bretschneinder, 1964). $U_{wind} = 33.43 m/s$ is the 1/3000 year wind speed based on the peak-over-threshold analysis of observed wind speeds at the A12 station (red dot in figure a) in appendix B.2.

Figure 3.5: Fetch analysis of waves from the WNW and NNW. Waves from the WNW have a smaller fetch than waves from the NNW. Waves from the NNW also develop in deeper water. This leads to a reduced maximum wave height and period for waves from the WNW. For W and WSW waves this is even more pronounced.

3.1.2. Topography and bathymetry over time

The historical migration of the gully is presented in figure 3.6. In every panel, the bathymetry of a specific year is given. The panels include arrows indicating the alongshore migration of the gully since the last measurement. The red arrows indicate migration due to a relocation. The black arrows indicate migration due to natural processes. For visualisation purposes, arrows have only been plotted for migrations larger than 50m.

From 1998 until 2013, in every period between relocations, the same trend can be distinguished. In the first year after a relocation there is a small amount of northward migration (1998-1999, 2005-2006, 2010-2011). In the next 1 or 2 years gully migration rates increase significantly (1999-2001, 2006-2007, 2011-2012). In the last years before a relocation gully migration decreases again annually (2001-2004, 2007-2009, 2012-2013) until it is positioned against the northern dune head. When it has reached this position it is relocated.

From 2014 until 2017 gully migration is directed southward. In the first year after the relocation the migration is very small (2014-2015). In the next year the migration is still very small and the migration of the mouth of the gully is directed northwards again (2015-2016). In the last year of the measurements the gully migration has increased and shifted southwards again.

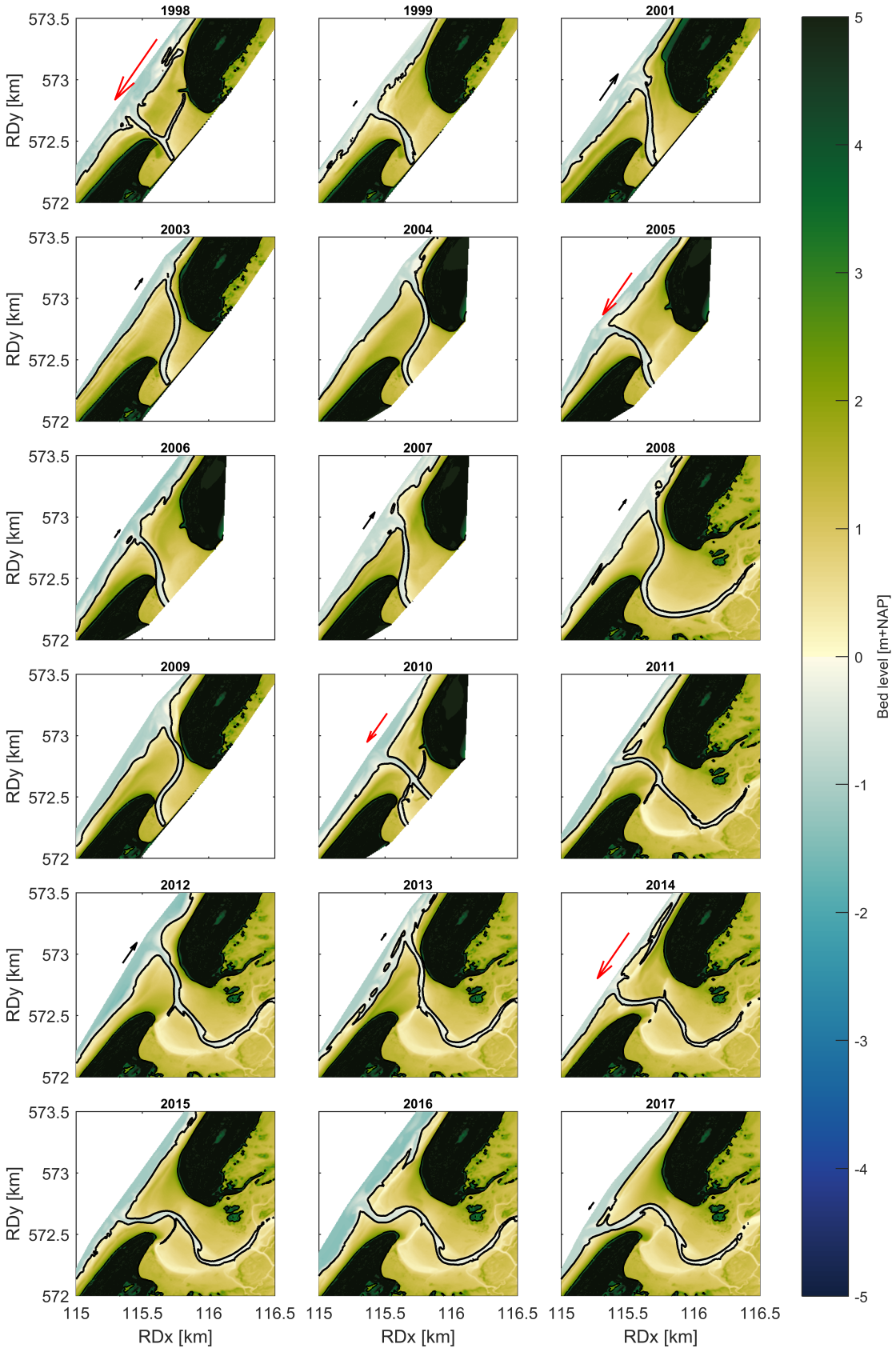

Figure 3.6: Annually measured gully position from 1998 until 2017. The arrows indicate the migration of the gully since the last measurement. Migration less than 50m has not been indicated with an arrow. The red arrows indicate migration due to relocations. Northward migration can be seen from 1998 until 2013. Then, after the relocation in 2013, a southward migration is seen from 2014 until 2017. Plots were made from Kusthoogte data.

3.1.3. Sediment distribution

As seen in figure 3.7, the spatial grain size distribution in De Slufter is not uniform. There is a fining trend present in landward direction, starting at the mouth. Sediment distribution on the beach flat and at the coastline is characterised by 'medium sand' (Wentworth, 1922). These are the orange and red dots. Further south the sediment is characterised by 'fine sand' (green and yellow dots) and at the most landward side the sediment is characterised by 'medium to coarse silt' (dark blue dots).

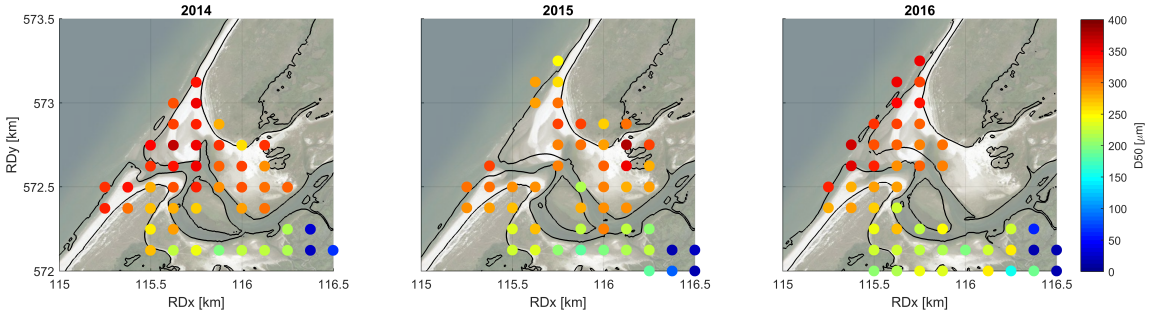

Figure 3.7: Spatial distribution of median grain size (D50) in 2014, 2015 and 2016. The contour lines represent the NAP+0.5m and NAP+3m contours to indicate the location of the gully and the dune heads. The largest grain sizes are found at the beach flat and the smallest are found on the landward side of the slufter valley.

Median grain sizes are coarse at the beach flat due to wave action and tidal currents there during inundated conditions. Assuming uniform sediment density in the area, these processes transport less of coarse (and thus heavier) grains than fine (and thus lighter) grains. Furthermore, during dry conditions, finer sediments are transported away from the beach flat by aeolian transport. Apart from decreasing intensity of wave action and tidal currents, the fining trend in landward direction is caused by the increased influence of aeolian transport and increasing terrain roughness (Holthuis, 2017). The increase in terrain roughness is caused by an increase in vegetational cover and topographical relief. Fine sediments are mainly transported as suspended sediment in the water column or by aeolian transport. They are therefore influenced less by the terrain roughness than coarse sediments which are mainly transported over the bed. Consequently, fine sediments are transported further landward than coarse sediments. The sediment on the dune heads is finer than on the beach flat due to aeolian transport.

Furthermore, there are differences between grain sizes over time at the beach flat. Sediment grain sizes in 2015 are smaller than in 2014 and 2016 at the seaward side, especially near the northern dune head (most northward yellow and orange dots in middle panel). All measurements are performed from the last week of march until mid-april (M. Prins, personal communication, December 2018). Therefore, it is cannot be caused by different measurement dates. An analysis into the unsteady, non-uniform distribution of sediment grain size is out of the scope of this study however. It is thus assumed that the mean of the grain sizes at the shoreline from 2014 to 2016 is representative for the actual grain size at the shoreline.

The mean D_{50} of all measurements at the beach from 2014 to 2016 is $316\mu m$. For the longshore transport calculations it is assumed that sediment grain size along the beach is uniform and equal to the mean D_{50}. This assumption will introduce errors in the calculations. However, these errors are considered acceptable because the goal of this study is to analyze trends and not exact quantifications. Furthermore, errors in the sediment grain size will mainly affect the bulk transport rates. It will not have a great effect on the net direction of longshore transport, which is the most important result of the analysis.

3.2. Longshore sediment transport

An analysis of (yearly averaged) wave-induced alongshore sediment transport (from here on called 'longshore transport') rates was performed with the goal of finding a correlation between net yearly longshore transport and gully migration. Longshore transport was calculated by using the following equation proposed by van Rijn (2013):

$$Q_{t,mass} = 0.00018 * K_{swell} * \rho_s * g^{0.5} * (tan(\beta))^{0.4} * (D_{50})^{-0.6} * (H_{s,br})^{3.1} * sin(2\theta_{br}) \tag{3.1}$$

In which:

$Q_{t,mass}$	longshore sediment transport volume	[m^3/year]
K_{swell}	swell factor	[-]
ρ_s	sediment density	[kg/m^3]
$tan(\beta)$	surf zone slope	[m/m]
D_{50}	sediment grain diameter	[m]
$H_{s,br}$	significant wave height of waves at the breaker line (location where 5% of waves are breaking)	[m]

where $K_{swell} = 1.05$ for the Dutch coast, based on van Rijn (2013). $\rho_s = 1650 kg/m^3$. Based on the slope in figure C.3 $tan(\beta = 0.008)$. Based on subsection 3.1.3 $D_{50} = 0.0003m$. Assuming a straight uniform coastline with parallel depth contours, the significant wave height at the breaker line is the ratio of the breaker depth h_{br} and the breaker coefficient γ:

$$H_{s,br} = \frac{h_{br}}{\gamma} = \frac{\left[\frac{H_{s,o}^2 c_o cos(\theta_o)}{\alpha \gamma^2 g^{0.5}}\right]^{0.4}}{\gamma} \tag{3.2}$$

In which:

$H_{s,br}$	significant wave height of waves at the breaker line	[m]
$H_{s,o}$	offshore significant wave height	[m]
c_o	offshore wave propagation speed	[m/s]
θ_o	offshore wave incidence	[°]
α	calibration coefficient	[-]
γ	breaking coefficient	[-]

where $\alpha = 1.8$ and $\gamma = 0.6$ which is representative for the Dutch coast (van Rijn, 2013). The wave incidence of wave at the breaker line is calculated with:

$$\theta_{br} = sin^{-1}\left(\frac{c_{br}}{c_o}\right) sin\theta_o \tag{3.3}$$

In which:

θ_{br}	wave incidence at the breaker line	[°]
c_{br}	wave propagation speed at the breaker line	[m/s]
c_o	offshore wave propagation speed	[m/s]
θ_o	wave incidence at the breaker line	[°]

Annual longshore transport rates have been calculated using the hydrodynamic data as input. The constants assumed for the calculation have been summarized in table 3.2.

Constant	Value
h_0	26
K_{swell}	1.05
D_{50}	0.0003
α	1.8
γ	0.6
$tan(\beta)$	0.02
g	9.81
ρ_s	1650

Table 3.2: Assumed constants in the van Rijn (2013) formula.

Table 3.3 shows the results of the calculation for every year since 1999. The results show that, except in 2010, the annual net sediment flux has constantly been directed northward since 1998.

	Sediment transport		
	Bulk south [10^3 m^3/year]	Bulk north [10^3 m^3/year]	Net [10^3 m^3/year]
1997	-182	200	18
1998	-252	669	418
1999	-108	635	527
2000	-214	358	144
2001	-307	373	66
2002	-156	305	150
2003	-279	360	82
2004	-186	587	401
2005	-395	427	32
2006	-192	303	111
2007	-356	630	274
2008	-197	515	317
2009	-188	292	103
2010	-338	253	-85
2011	-149	641	492
2012	-217	435	218
2013	-208	318	110
2014	-132	379	246
2015	-141	516	375
2016	-200	336	136
2017	-141	235	94

Table 3.3: Overview of annual bulk and net longshore transport rates calculated with the van Rijn (2013) formula. Southward transport is defined negative and northward transport is defined positive. Years indicate the period from January 1st until December 31st.

3.3. Gully migration

The analysis of historical gully migration and longshore transport is visualised in figure 3.8. The results show similar trends between longshore transport and gully migration for the first 15 years. However, in the last 4 years of measurements longshore transport and gully migration show opposing directions. It is thus expected that gully migration is governed by multiple driving processes. It is important to note that gully migration is defined along the blue transect in the figure instead of along the shoreline.

1998-2013: As described in subsection 3.1.2, the migration of the gully until 2013 differs in magnitude of annual migration and is generally directed northwards. As longshore transport was also directed northwards a link between longshore transport and gully migration direction thus seems plausible. Furthermore, similar trends between the magnitude of longshore transport and magnitude of gully migration can also be distinguished. This similarity in trends is not present every year though. For example: The gully had migrated 180m from 2006 to 2007. The longshore transport in that period was 110 000 m^3/year. The year after, 2007-2008, the gully migrated 115m. However, longshore transport in that period was 274 000 m^3/year. This means that longshore transport was more than twice as high while migration was only two thirds of the migration the year before.

2013-2017: After the relocation in 2013, the gully was located close to the southern dune. In the period from 2014 until 2017, gully migration shifted southward and showed only very limited migration. Longshore sediment transport remained directed northwards during that period. After 2013, no correlation between longshore transport and gully migration can thus be distinguished. The fact that longshore transport and migration direction do not always correlate means that gully migration cannot only be dominated by longshore transport. Other processes must therefore also play a role.

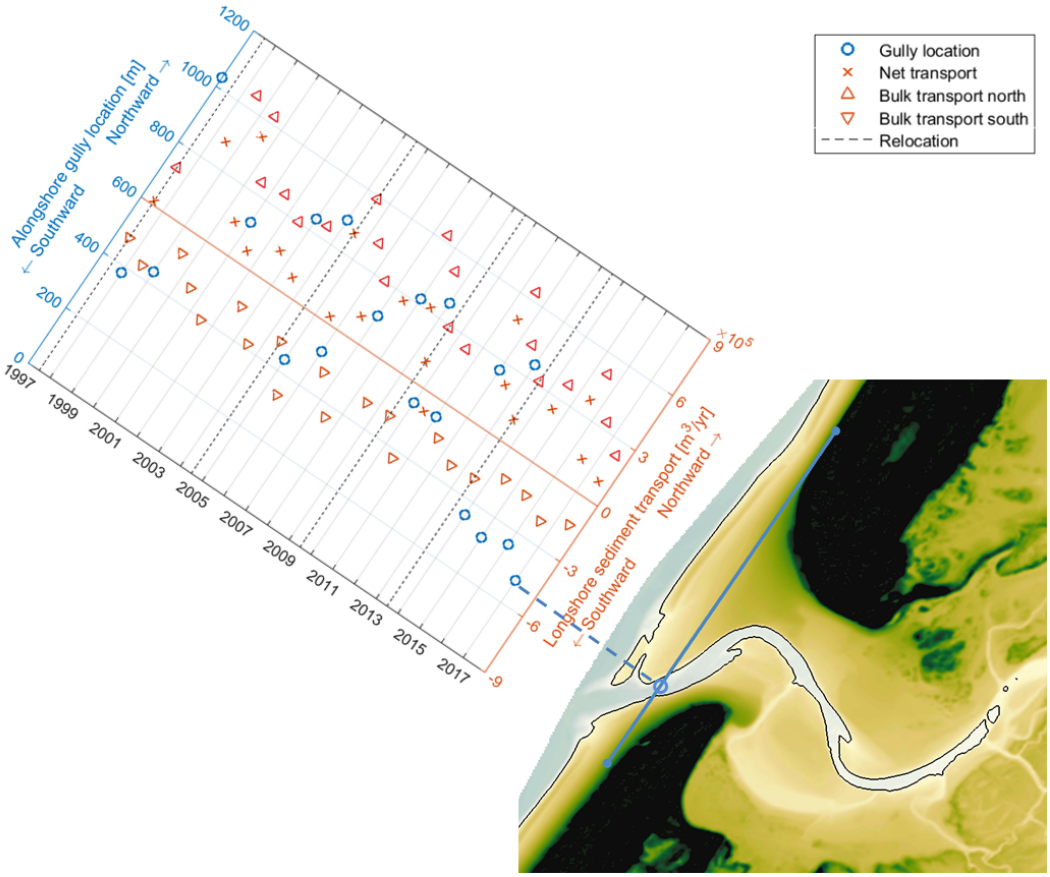

Figure 3.8: Alongshore gully position (blue circles, left axis, origin at the bottom) and longshore sediment transport according to van Rijn (2013) (red symbols, right axis, origin in the middle) over time. The years on the x-axis indicate the start of each year (i.e. January 1st). The map in the bottom right corner is the gully position as measured in 2017. The alongshore location of the gully is indicated as a blue circle on the blue transect. The blue left axis of the graph coincides with the length of the transect on the map.

Distance to dune head: The decrease of migration magnitude seen every (inter-relocation) period is correlated to the distance of the gully to the (northern) dune head. As the gully migrates towards the dune head, the bed level gradient increases in that direction which hinders further migration. This is evident from the period 2006-2009 in figure 3.6. From 2006 to 2008 there is a significant amount of migration and by 2008 the gully has reached the dune foot. Then, in between the 2008 and 2009 measurements no significant migration has occurred. The same is true for the periods 1999-2004 (large migration from 1999 until 2003, no migration from 2003 to 2004) and 2010-2013.

In the period after 2013 the same behaviour is recognized, only mirrored. After the relocation in 2013 the gully was already located near the dune foot. In the line of expectation, no significant migration was seen in the consecutive years. The migration that has occurred was in southward direction. Based on visual observations (e.g. the cover photo of this thesis) the migration since the last measurement has continued in southern direction.

Storm driven migration: To test the hypothesis that the gully migration might be storm driven, historical storm wave conditions and gully migration were compared, see figure 3.9. Storm wave conditions were assumed to be all measurements for which $H_s > 4\,m$. The general trend is similar to that of the total wave climate, with longshore transport mainly directed northwards. The magnitude is much lower however as is evident from the difference between the right y-axes.

In comparison to the total wave climate analysis, the correlation between longshore transport and gully migration seems to be slightly more pronounced from 1998 to 2004 and from 2010 to 2013. Large longshore transport magnitudes are generally followed by larger migrations. However, from 2005 to 2009 there is no correlation to be found. In that period, a southward directed longshore transport leads to a significant northward migration. From 2014 to 2017 northward longshore transports are followed by southward migration, as also seen for the total wave climate analysis.

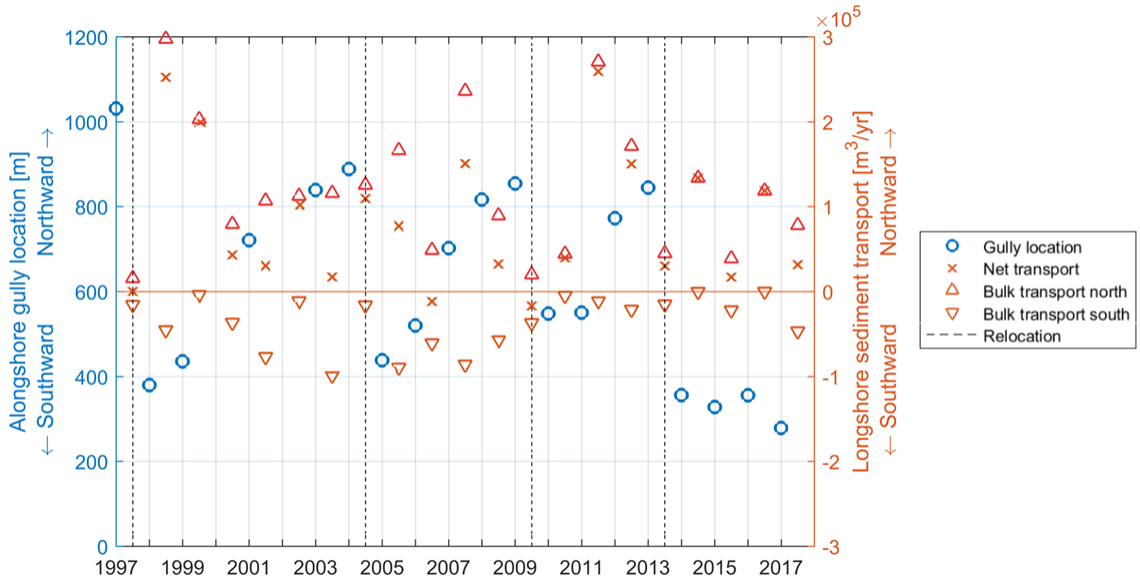

Figure 3.9: Alongshore gully position (blue circles, left axis, origin at the bottom) and longshore sediment transport during storm conditions ($H_s > 4\,m$) according to van Rijn (2013) (red symbols, right axis, origin in the middle) over time.

Secondary flow: Another possibility might be that the gully migration is influenced significantly by curvature-induced secondary flow in the bends during ebb flow, as was also suggested by Durieux (2003). This hypothesis is supported by the historical gully migration since 1998, as shown in figure 3.6. Due to secondary flow, the bends of the gully would lead to erosion of the outer bends and thus migration in that direction. This phenomena would likely be most pronounced when only the gully is filled with water, i.e. under calm conditions when tidal forcing is dominant. The effects of the tide will decrease as the tide travels further upstream into the gully. Therefore, the effect of secondary flow is likely highest at the first bend of the gully (viewed

from the mouth), suggesting that the shape of the gully near the shoreline is dominant for its migration. This behaviour is recognized in every measurement since 1998.

In figure 3.10 the correlation is visualised for 2010 to 2013 and 2014 to 2017. In addition to the red and black arrows, curved red lines are added to indicate the outer bends which would be eroded by secondary flow. In all years, the migration took place in the direction of these outer bends. This is also true for the years before 2010. The fact that the migration of the gully is mirrored when the outer bends are located on the southern side of the gully substantiates the hypothesis. Especially the initial shape of the gully after the relocation seems to govern whether or not migration is directed northwards or southwards.

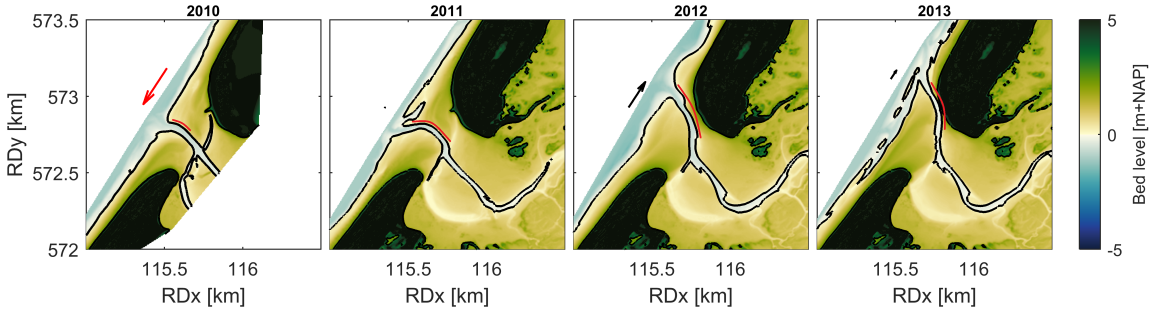

(a) 2010-2013

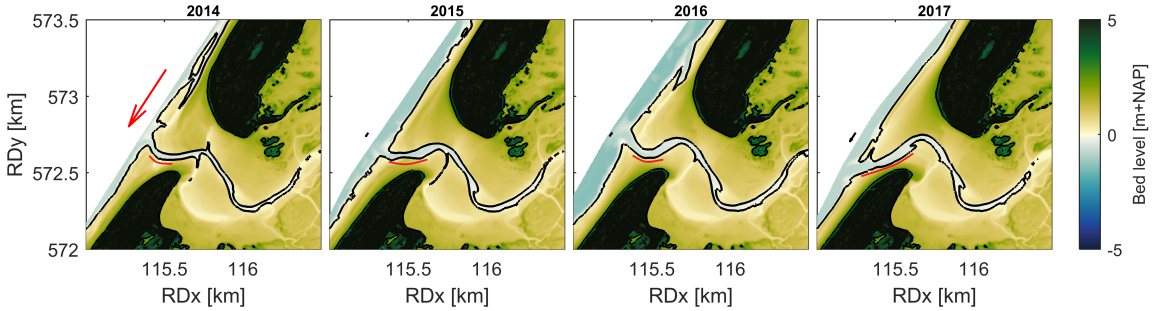

(b) 2014-2017

Figure 3.10: Gully position from 2010 to 2013 and from 2014 to 2017. The arrows indicate gully migration since the last measurement (red arrows for relocations, see figure 3.6). The outer bends to which the secondary flow hypothesis relates are indicated with red curved lines.)

If curvature-induced secondary flow is a governing process in the migration of the gully, then this should also be visible in the cross-gully profile. As explained in subsection 2.1.1, in an idealized situation curvature-induced secondary flow creates a profile in which the outer bend is steeper than the inner bend.

Figure 3.11 presents three cross-gully profiles of the measurements in 2005, 2010 and 2015. All profiles show a resemblance to the profile in subsection 2.1.1. The outer bend bank for each profile is steeper than the inner bend bank, resulting in a larger water depth in the outer bend than in the inner bend. The lower panel presents the gradients of the northern bank (red dots) and southern bank (blue dots) each year. The orange line indicates per year whether the southern or the northern bank was steeper. When the orange line is positive, the northern bank was steeper and vice versa. Until 2013, the northern bank was steeper. After 2013, the southern bank was steeper. This coincides exactly with the observed gully migration direction. This strongly suggests that curvature-induced secondary flow is of importance for gully migration.

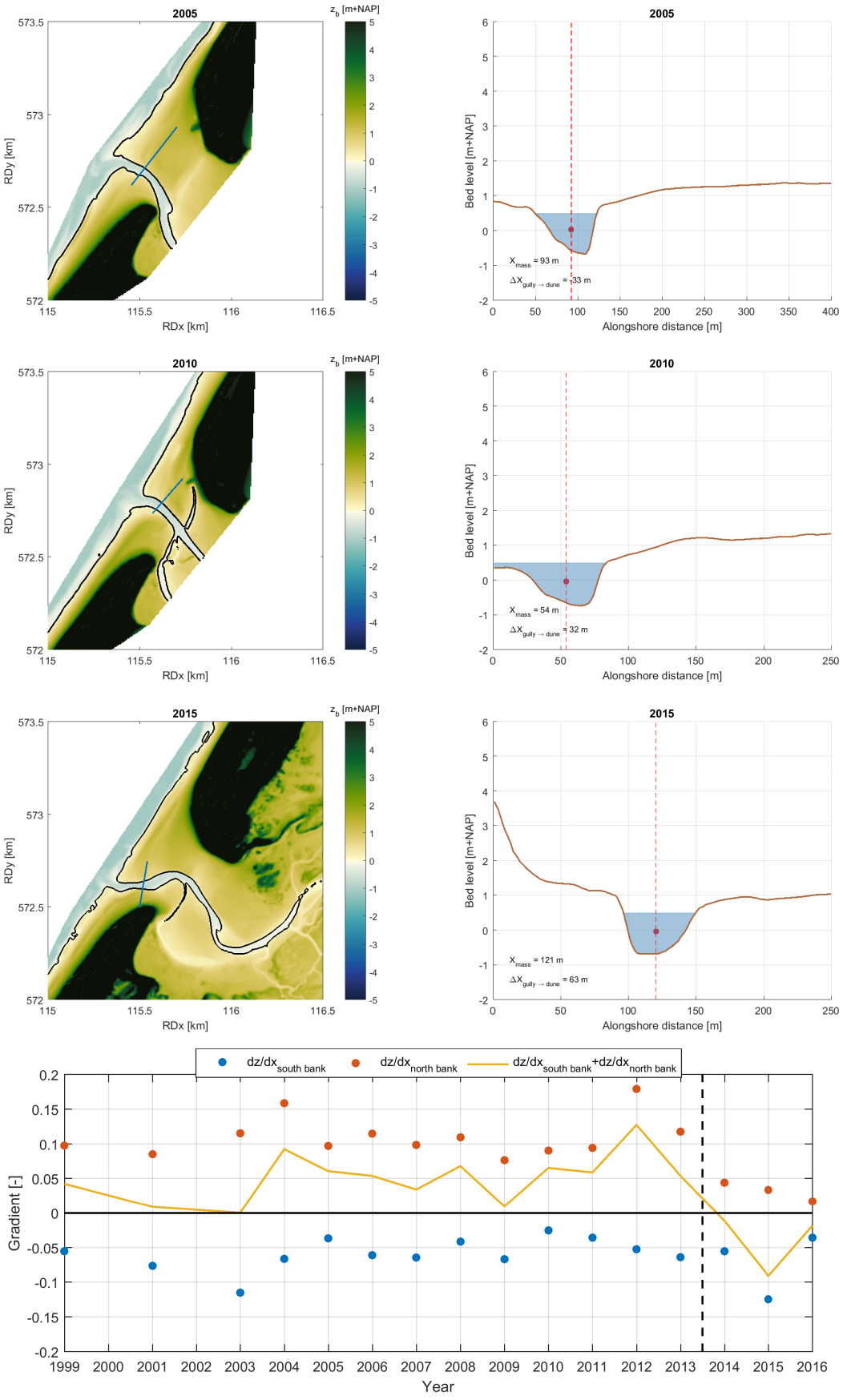

Figure 3.11: Analysis of inner and outer gully bank gradients. Until 2013 the northern bank (red dots in lower panel) was steeper than the southern bank (blue dots). The orange line, which indicates which bank gradient was larger per year, shows that this has shifted after 2013. This coincides with the observed gully migration direction. The top three panels present three representative slufter gully profiles 5 years apart.

The combined effect of the three expected important processes is analysed for 1998-2013 and 2013-2017 in figures 3.12 and 3.13, respectively. The inverse distance to the dune head is plotted to clearly visualise that the gully migration is inhibited more when the distance to the dune head becomes smaller. The inverse of the radius is given for a similar reason. A smaller radius of the bend would mean a stronger forcing by secondary flow.

1998-2013 Figure 3.12 suggests that gully migration is indeed governed by the 3 processes. The figure is discussed by dividing the total time period into three periods (between each relocation).

The first years of each period show an interesting behaviour. Longshore transport and curvature-induced secondary flow drive the migration north. This explains the northward migration. Also, the magnitude of migration in 2005 was larger than in 1998. In 2010, the gully did not migrate at all. The larger migration in 2005 could be explained by the larger influence of secondary flow compared to 1998. This would also explain the larger migration in 1999 compared to 2006. The absence of migration in 2010 is likely a result of the opposing forcing direction of the longshore transport and secondary flow. In 2011, the gully migrated more than 200m. This in turn coincides with the large increase in forcing due to secondary flow that year.

In the subsequent years (2000-2004, 2007-2009 and 2012-2013), the migration of the gully is inhibited significantly by the smaller distance to the dune head. In these years, longshore transport and forcing due to secondary flow seems to have less of an effect on the magnitude of migration. However, the direction is still governed by these processes.

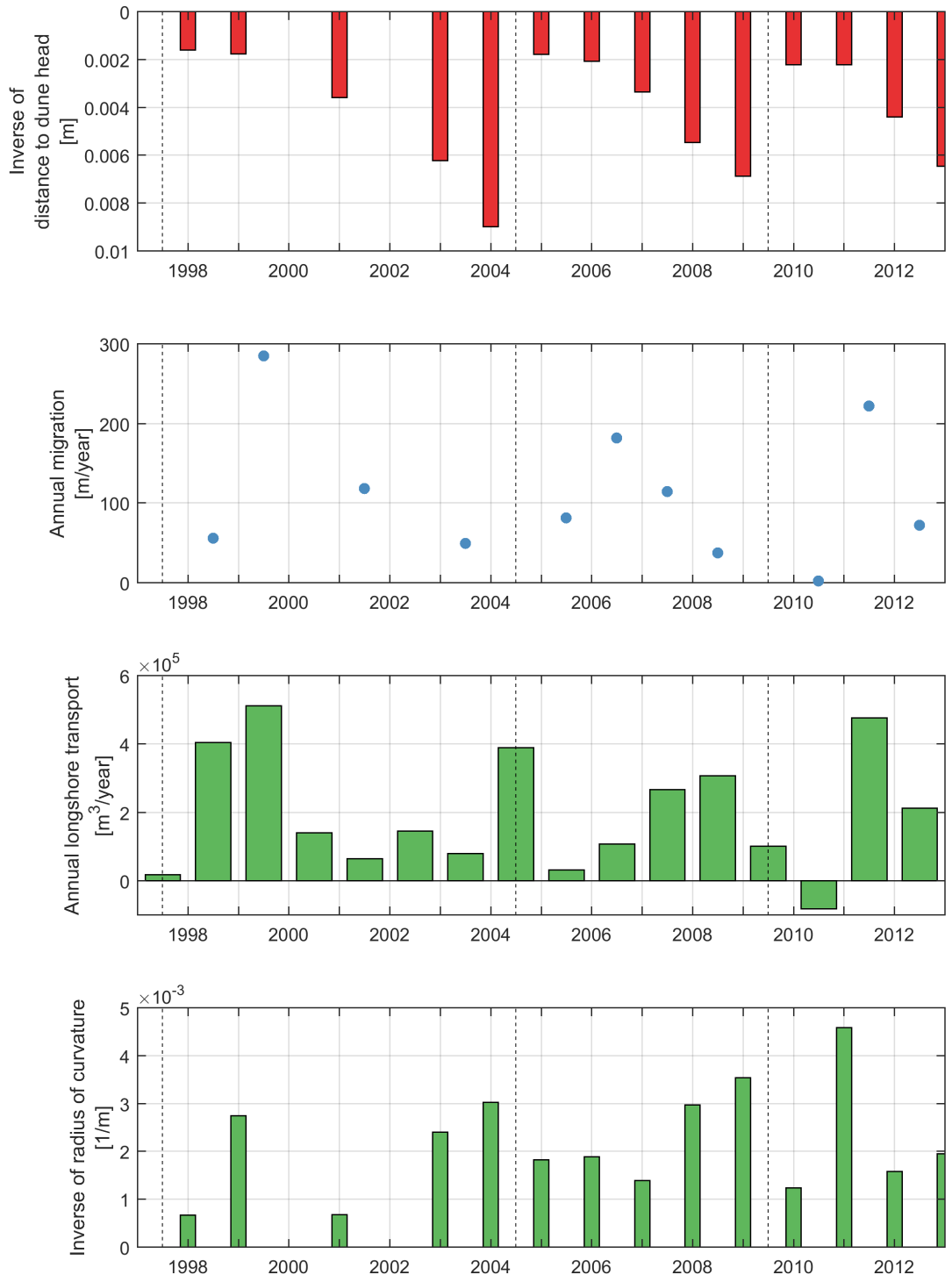

Figure 3.12: Analysis of gully migration and important driving and inhibiting mechanisms (1999-2013). The green and red bars indicate 'driving' and 'inhibiting' processes, respectively. In the top and bottom panels, bars are located on each year gridline. This is because these processes are measured at a certain moment at the beginning of the year and represent a 'starting position'. The bars in the third panel are located between years because they represent a process which was calculated for an entire year. The dots in the second panel represent gully migration that has taken place within a year and are therefore also located between years.

1998-2013 Figure 3.13 also shows interesting behaviour. First of all, gully migration after 2013 was generally smaller than before. The difference between the distance to the dune heads for all years is negligible. This thus not explains the differences per year. Therefore, the migration is likely explained by longshore transport and curvature-induced secondary flow. Northward migration took place in 2015, when the southward forcing by secondary flow was smallest and the northward forcing by longshore transport was largest. Vice versa in 2016, when southward migration was largest. This further suggests the equal importance of both longshore transport and secondary flow.

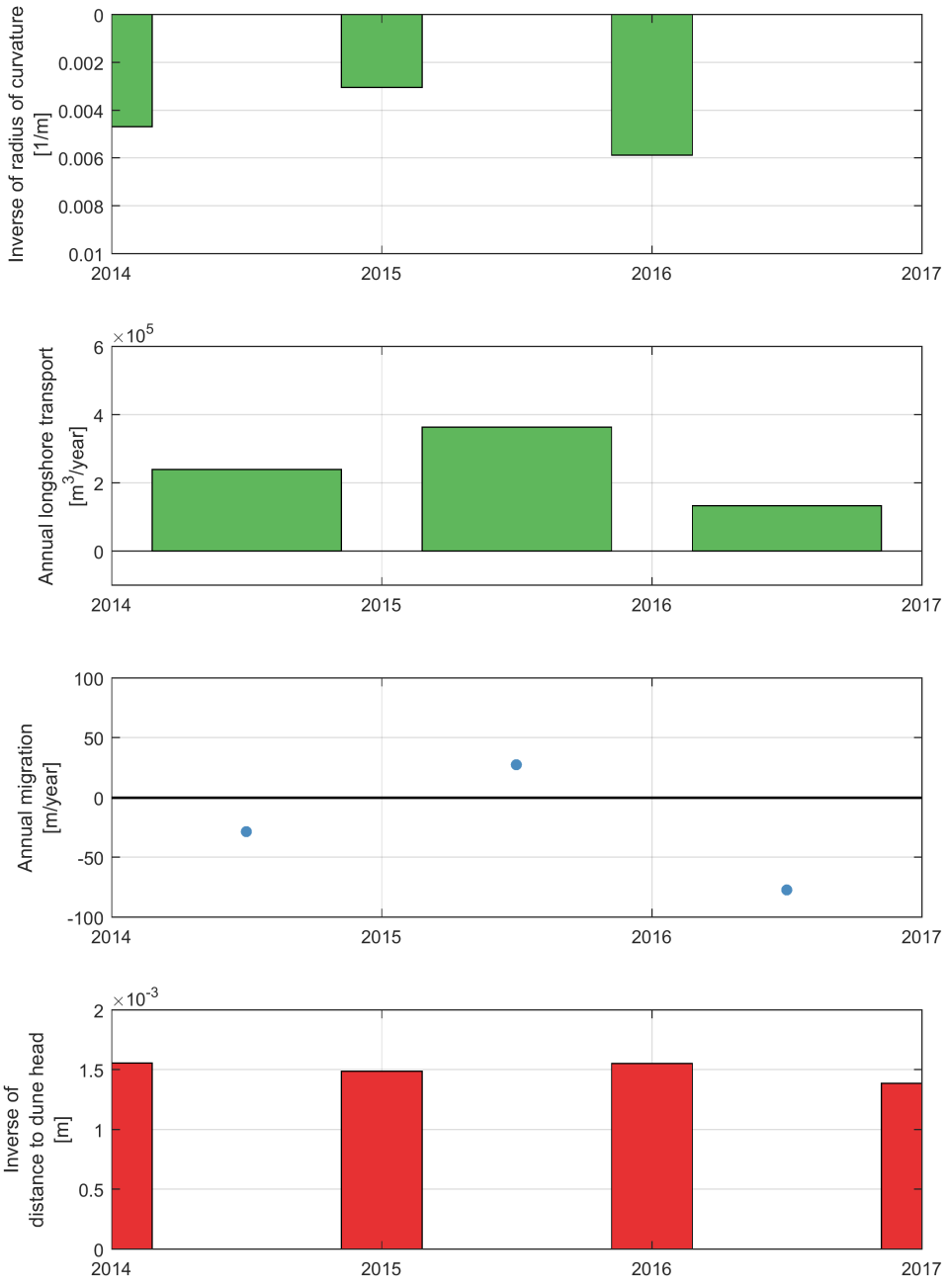

Figure 3.13: Analysis of gully migration and important driving and inhibiting mechanisms (2014-2017). The figure is similar to figure 3.12. However, as the migration for this period was southward, the positions of different panels have been interchanged for clarity.

Overwash during storms: As already discussed in the literature study it is expected that overwash over the beach flat into the gully also drives the migration of the gully. To analyse the effect of this on long term morphological development more frequent 2DH bed level measurements are necessary. These are not available. However, a measurement campaign by Utrecht University does provide a pre- and post-storm location of the gully for a small storm event (see figure 3.14). These locations show a slight outward migration of the bend, which could be attributed to overwash over the beach flat. The eastern blue line shows a slight outward migration of the bend. This is likely caused by the widening of the gully cross-section during ebb flow (which mainly takes place in the gully). Overwash is considered a short-term process however as the beach flat is inundated infrequently. Therefore, it is expected that overwash has a small effect on gully migration compared to the other processes. Still, overwash can alter the shape of the gully such that the gully curvature becomes more pronounced. This increases the effect of curvature-induced secondary flow on long-term gully migration.

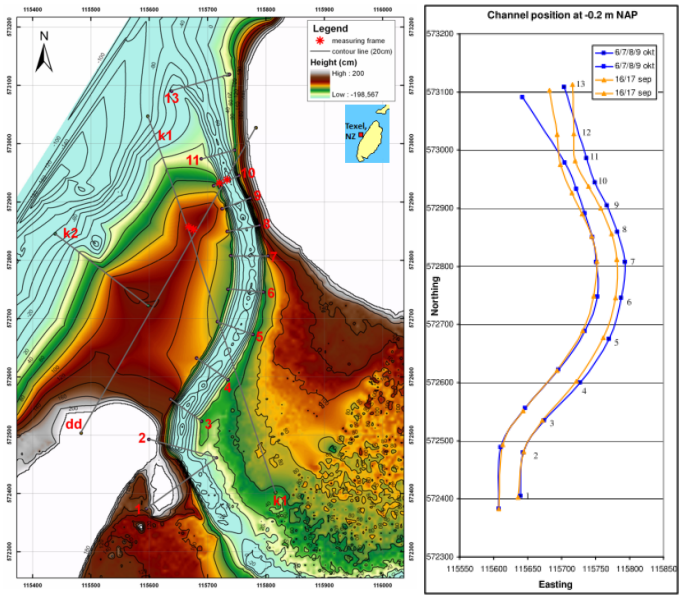

Figure 3.14: Overview of measured transects during the 2008 measurement campaign (Van Puijvelde, 2010).

3.4. Conclusion

This field data analysis has shown that the migration direction and magnitude of the gully cannot only be governed by net annual longshore transport. A correlation is found though between the northward directed net annual longshore tranport and the northward directed gully migration from 1998 to 2013. Since 2014 the migration mirrored and has generally been directed southwards. However, in this period longshore transport was still directed northwards. An analysis of storm conditions ($H_s > 4m$) also could not substantiate that longshore transport during storms is the governing process in gully migration direction or magnitude. It was thus further investigated which other processes were governing.

It was concluded that the erosion in the outer bends due to curvature-induced secondary flow is deemed a possible driving process for the migration of the gully. This means that the gully migration direction could be dependent on the initial shape and location of the gully after a relocation. This hypothesis is supported by a few indicators. First, the observed migration direction of the gully has coincided with the location of the outer bend of the most seaward section of the gully for all years. Second, an analysis of cross-gully profiles shows that for all measurements the gradient of the outer bend of the gully was steeper than the inner bend. This indicates a profile comparable to the idealized cross-gully profile due to curvature-induced secondary flow. Furthermore, overwash during storms or spring tide events is expected to increase the curvature of the gully. This further increases the effect of curvature-induced secondary flow. In this respect, overwash during storms has an effect on long-term migration. However, in itself it is only a short-term process and is not considered a driving mechanism.

It is expected that gully migration is thus governed by three processes:

- Net annual wave-induced longshore transport
- Curvature-induced secondary flow
- Distance to the dune head

The net annual wave-induced longshore transport and curvature-induced secondary flow are considered 'driving processes'. The distance to the dune head is considered an 'inhibiting process'. The hypothesis was tested by comparing observed annual migration to the calculated annual longshore transport, the inverse radius of the gully bend and the inverse distance to the dune head for two periods, 1999 until 2013 and 2013 until 2017. Based on this analysis, it is concluded that the observed gully migration is likely explained by the three processes with the sidenote that overwash over the beach flat during storms has a stimulating effect on curvature-induced secondary flow.

4

Model setup

In this chapter the setup of the XBeach model is elaborated on. In section 4.1 the grid and bathymetry are discussed. The model settings that deviate from the default XBeach (Kingsday version) settings are explained in section 4.2, as well as the spatially varying bed friction used in the model. The hydrodynamic boundary conditions of the model are presented in section 4.3.

4.1. Grid and bathymetry

The origin of the XBeach grid is located at RDx = 105.5 km and RDy = 573.5 km. The offshore grid boundary has an angle of 33 degrees relative to the North so that it complies to the coordinate system used by XBeach. The grid covers an area of approximately 9 kilometers in cross-shore direction (7.5 kilometers open sea, 1.5 kilometer land) and 7.5 kilometers in alongshore direction (figure 4.1). Cross-shore grid cell sizes vary from 40 meters at the offshore boundary to 3 meters around the mouth and the sand dike. Alongshore grid cell sizes vary from 33 meters at the lateral boundaries to 8 meters in the center. The model grid thus consists of 333 936 grid cells (773 cross-shore cells x 432 alongshore cells).

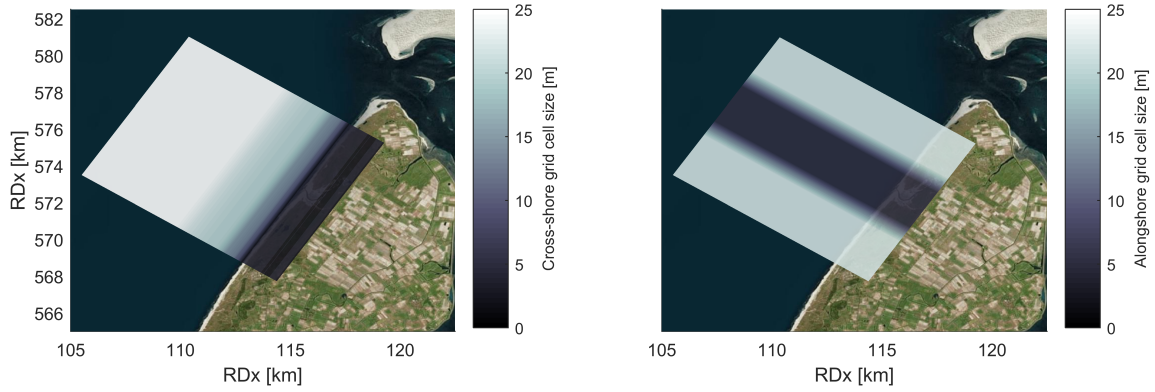

(a) Cross-shore grid cell size (2D)

(b) Alongshore grid cell size (2D)

Figure 4.1: Grid cell sizes of the XBeach model. Cross-shore and alongshore transects of grid cell sizes are shown in appendix C.

The model grid was chosen such that it contains the entire slufter valley including the sand dike and that it extends far enough offshore to allow a (manually created) mild slope due to the deepening of the offshore boundary. Deepening the offshore boundary was necessary to prevent waves from breaking upon entering the model. Alterations to the model bathymetry have been elaborated on in appendix C. Figure 4.2 shows the final model bathymetry that was used for the case study.

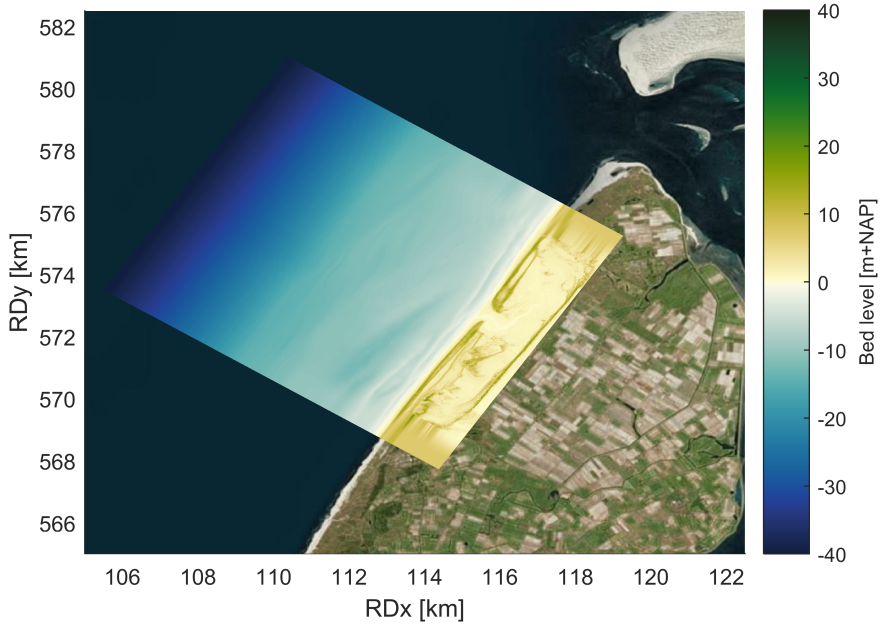

Figure 4.2: XBeach model bathymetry. 2015 data was used because it was the most complete and recent dataset.

4.2. Model settings

When possible, default settings associated with the XBeach Kingsday version were used in the model. Deviations from the default settings are explained in this section.

To preserve wave groupiness waves have been imposed with the *single_dir* option. With *single_dir* (Roelvink et al., 2017), the wave direction is solved at regular intervals using the stationary solver. The wave energy is then propagated along the mean wave direction. Cyclic boundary conditions were used in the model. With cyclic boundary conditions, waves that exit the model on a lateral boundary enter the model on the other lateral boundary. This allows for a more 'narrow' model (in alongshore direction) because no 'shadow zones' are formed. The interval between wave module calls is set to 60 seconds with the *waveint* parameter. Lastly, even though it is the default, it is important to state clearly that no morphological acceleration was used. The reason for this is that the interaction between tide and storm surge is important in De Slufter. This interaction cannot be modelled correctly with a morphological acceleration factor. In appendix F the sensitivity of the model to a higher morfac is shown. An overview of all relevant parameters is given in appendix C.3.

The Manning bed friction formulation was used in this model. Bed friction was defined spatially varying in the model and was specified according to Manning's bed friction formulation (figure 4.3). To account for the influence of vegetation in the slufter valley the model area was divided into a vegetated and a non-vegetated part. Based on C-CAP[1] (NOAA Office for Coastal Management, 2016), a Manning coefficient [n] of 0.05 was specified for the grid cells in vegetated areas. A Manning coefficient of 0.02, which is the default Manning value for sandy coasts in XBeach, was chosen in all non-vegetated grid cells. Due to smoothing, which was necessary for numerical stability, the Manning coefficients at the interfaces between the vegetated and non-vegetated areas are in between 0.02 and 0.05.

In addition to bed friction, an appropriate (spatially uniform) wave friction factor of $f_w = 0.06$ (Smyth and Hay, 2002) was added to the model. The wave friction factor only affects the wave action equation and thus only short wave height.

[1] Coastal Change Analysis Program

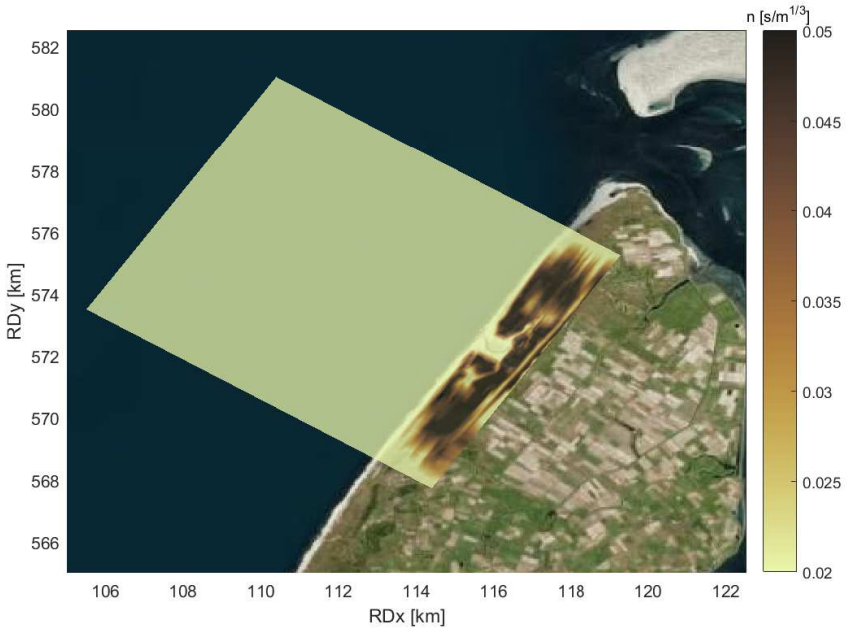

Figure 4.3: Spatial distribution of Manning coefficient 'n'.

4.3. Boundary conditions

The hydraulic boundary conditions are imposed on the offshore model boundary and are time dependent. They consist of a water level component and a wave component. For the model validation the offshore boundary conditions were created from historical data. For the case study the offshore boundary conditions are storm surge hydrographs as described by Steetzel (1993) with coinciding peak wave and water levels to represent extreme storm conditions. The landward boundary was imposed with a still water level (NAP+0 m).

Water levels

For simplicity, the normative water level boundary conditions at the offshore boundary consist of an M2-tide with associated amplitude (≈NAP+0.79 m) and the local NTR (section 3.1.1). The choice for the M2-tide component was a pragmatic one. Using the maximum tidal water level gave normative levels which, based on earlier official reports (ENW, 2007), were considered to overestimate realistic conditions. NTR values for different return periods were determined with a peak-over-threshold analysis on the measured water level data (appendix B.2.1). The normative water level with a certain return period (*Dutch: toetspeil*) is the sum of the (constant) M_2 tidal amplitude and the non-tidal residual water level with that return period.

$$\eta = amp(M_2) + z_{NTR} \tag{4.1}$$

Waves

For simplicity reasons it was decided to model waves from the Northwest (315°). As subsection 3.1.1 shows, waves from the West are fetch limited and cannot reach heights higher than 10m. Waves from the North-northwest or North are assumed to have less of an impact on the sand dike due to their high obliqueness. Also, the location of the mouth in relation to the sand dike leads to the assumption that wave from the North-northwest or North have a lower wave impact on the sand dike. Therefore waves from these wave directions were considered of less interest than waves from the Northwest.

The imposed maximum significant wave heights at the offshore boundary have been determined with a peak-over-threshold analysis on the measured wave height data of subsection 3.1.1. The peak-over-threshold analysis is shown in appendix B.2.2. It is not possible to perform a peak-over-threshold analysis on the wave period. Instead, a representative wave steepness was assumed based on Eierlandse Gat measurements. Combined with the already determined wave heights the accompanying wave periods were calculated. In appendix B.2.2 the calculation of the wave boundary conditions is explained in detail.

Final model boundary conditions

Table 4.1 presents the hydrodynamic boundary conditions to be used in the model. The 1/3000 year boundary condition was chosen to assess the exceedance of the signalling norm, discussed in section 2.3. This is the most conservative safety norm for De Slufter.

ID	Boundary condition	η [m+NAP]	H_{m0} [m]	T_p [s]	Dir
1	1/1 storm	2.3	5.9	9.5	NW
2	1/10 storm	2.9	7.6	11.2	NW
3	1/100 storm	3.5	9.1	12.8	NW
4	1/3000 storm	4.3	11.2	15.2	NW

Table 4.1: Hydraulic boundary conditions used in the modelling study.

The evolution of the boundary conditions over time is based on a storm surge hydrograph as described by Steetzel (1993). The hydrograph is composed of a surge component and a tide component. Figure 4.4 shows the boundary conditions over time for a storm with a return period of 3 000 years.

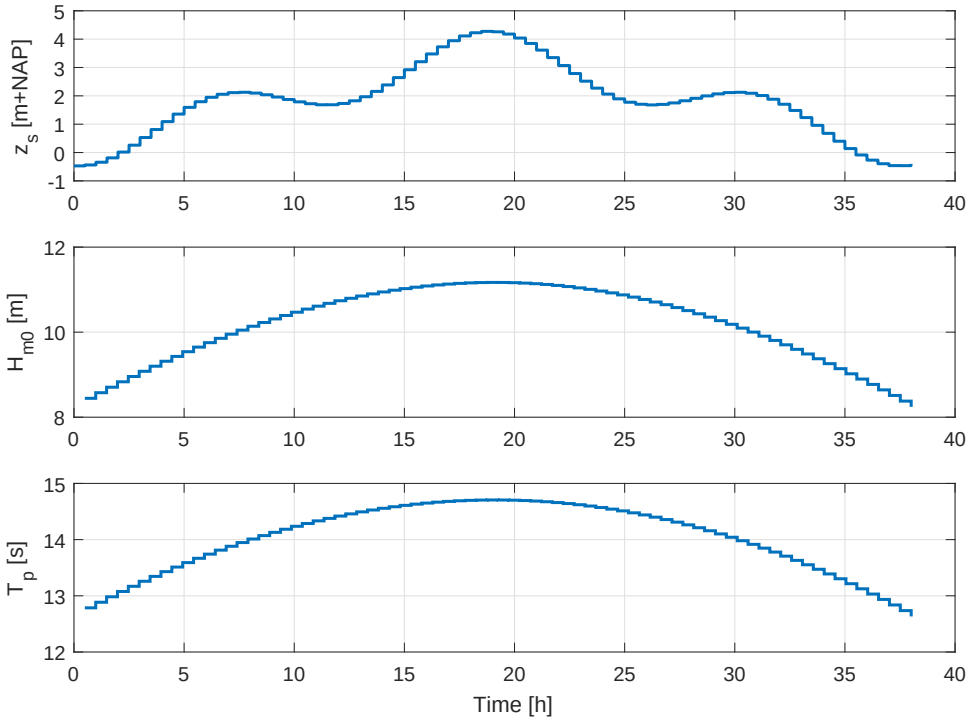

Figure 4.4: Model boundary conditions for a 1/3 000 year storm lasting 37 hours. The top panel represents the water level. The middle panel represents the significant wave height. The bottom panel represents the peak wave period. Wave direction is assumed constant over time.

5

Validation

The validation of the XBeach model is divided into two parts:

- **Hydrodynamic validation**. Bed level changes in XBeach are turned off. The hydrodynamic results of the XBeach model are quantitatively compared to field measurements.
- **Morphological validation**. Bed level changes are turned on. The resulting bed levels are qualitatively compared to field measurements. The resulting gully migration is compared quantitatively.

5.1. Hydrodynamic validation

For the hydrodynamic validation, the model is set up as described in chapter 4. Water level data inside De Slufter from the 2015-2016 Utrecht University measurement campaign (appendix D.1) was used to validate the hydrodynamic results of the XBeach model. The measurement locations P1-8 on which the hydrodynamic data was validated are shown in figure 5.1.

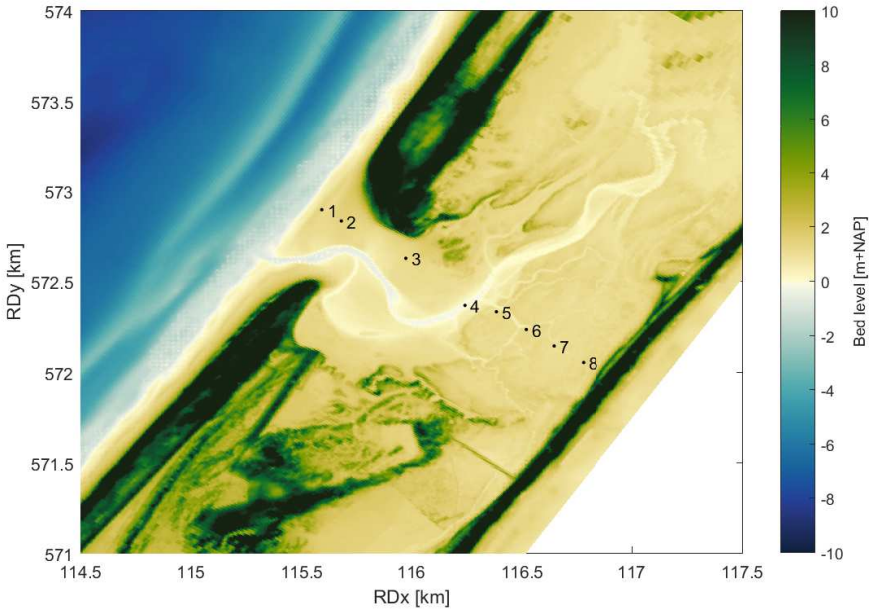

Figure 5.1: Locations of the measurement points on which the hydrodynamic results are validated. The bathymetry in the map is the bathymetry used in the validation.

5.1.1. Hydrodynamic conditions

The storm event with the highest maximum water level, which started 28-11-2015 12:00 and ended 01-12-2015 00:00 (lasting 60 hours), was modelled for the hydrodynamic validation. Figure 5.2 shows the hydrodynamic boundary conditions imposed on the offshore boundary.

The wave direction during the storm was predominantly WSW to WNW with a maximum wave height of 5.33 meters. The maximum offshore water level was NAP+1.97m. The peak wave height and peak water level almost coincide on 29-11 at 23:00. At that time the mean wave direction was in between West and West-northwest.

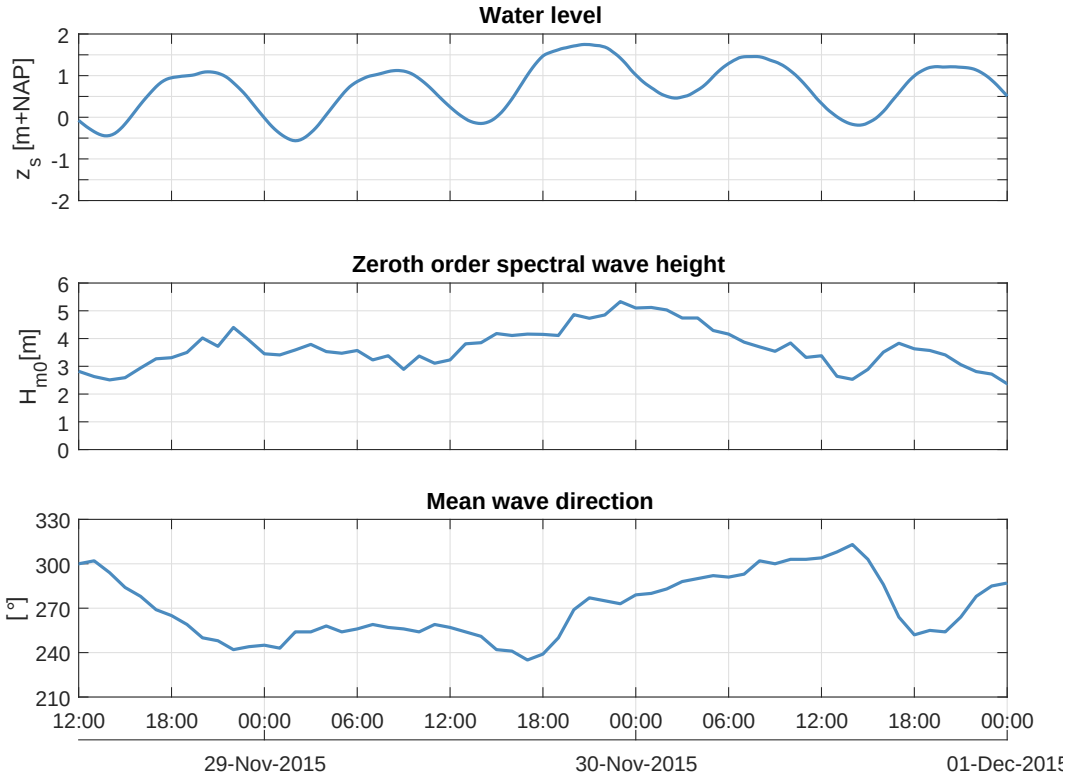

Figure 5.2: Offshore hydraulic boundary conditions for the hydrodynamic validation storm.

5.1.2. Results

Water levels

Figure 5.3 shows the comparison between measured and modelled water levels in De Slufter during the 2015 validation storm. The comparison is quantified with three statistical errors (Root-mean-squared-error (RMSE), scattered interpolant (SCI) and bias:

$$RMSE = \sqrt{mean(z_{computed} - z_{measured})^2} \tag{5.1}$$

$$SCI = \frac{RMSE}{(max(\sqrt{mean(z^2_{measured})}, abs(mean(z_{measured}))))} \tag{5.2}$$

$$Bias = mean(z_{computed} - z_{measured}) \tag{5.3}$$

The results shows a very good resemblance to the measurements, with root-mean-squared errors not exceeding $10cm$ and scattered interpolant values not exceeding ~5%. Only the results at the P1 modelling station differ significantly. However, this is due to errors in the measurements, as explained in appendix D.1.

The largest errors in the other locations are found around midnight, during ebb flow. The water level in the results drops slightly later than in the measurements. This is likely caused by the fact that the bathymetry used in the model is not identical to the actual bathymetry during the measurements. The gully depth in the model is likely underestimated slightly due to interpolation. Furthermore, as water levels during the validation are relatively low, water is mainly transported through the gully during ebb. For equal tidal prisms, the water level in the model will then be slightly higher in the model than in the measurements. An elaboration on the water level validation is given in appendix F, in which the sensitivity of the results to the bed friction for vegetated areas is also analysed.

Overall, the water levels are very well represented however.

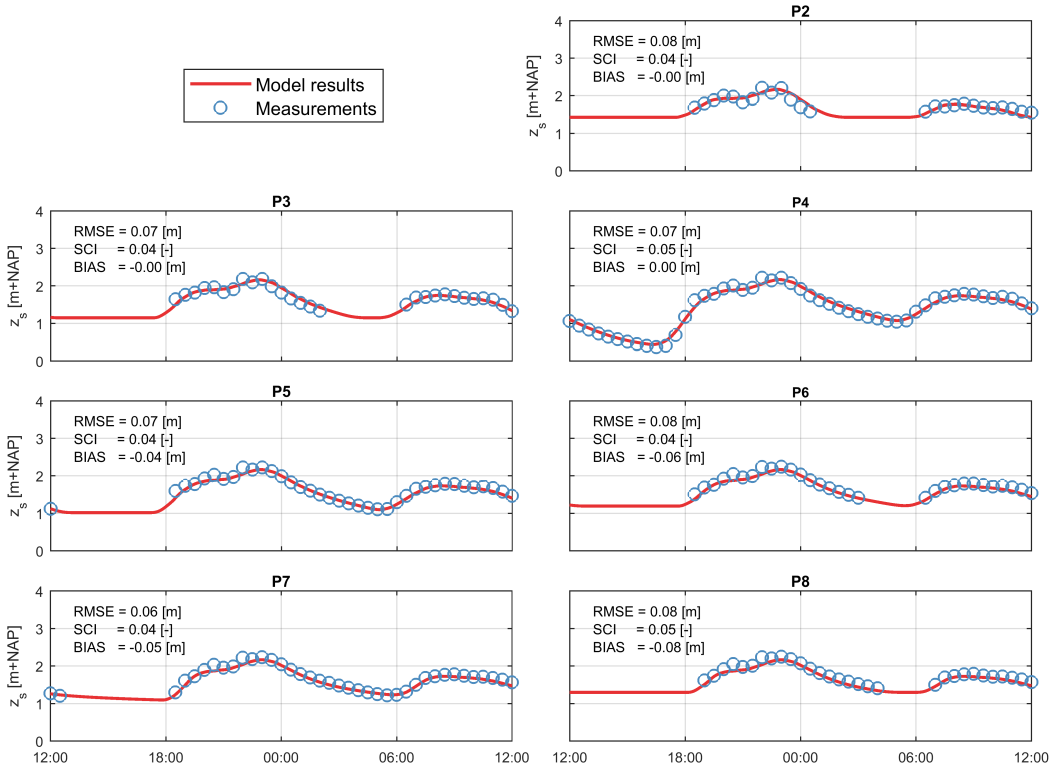

Figure 5.3: Comparison between measured water levels and XBeach results over time for $n_{non-vegetated} = 0.02$ and $n_{vegetated} = 0.05$. P1-8 refers to the measurement locations in figure 5.1, where P1 is located in the mouth and P8 is located near the sand dike. For visual purposes, only every second measurement has been plotted.

Tidal wave shape

Figure 5.4 shows the analysis of the tidal wave shape of both the observed and modelled water levels (top panel) and the modelled flow velocity (bottom panel) for measurement station P4 (figure 5.1), which is located in the static part of the gully (velocities were not measured during the campaign). The model results resemble the observations well, even though the rising water level period is overestimated. The model shows longer ebb periods with higher maximum ebb velocities ($\sim 0.76 m/s$) and shorter flood periods with lower maximum flood velocities ($\sim 0.69 m/s$). This behaviour in the gully has also been described in literature (Van Der Vegt and Hoekstra, 2012). The model thus qualitatively resembles the velocities inside the gully during a small storm event.

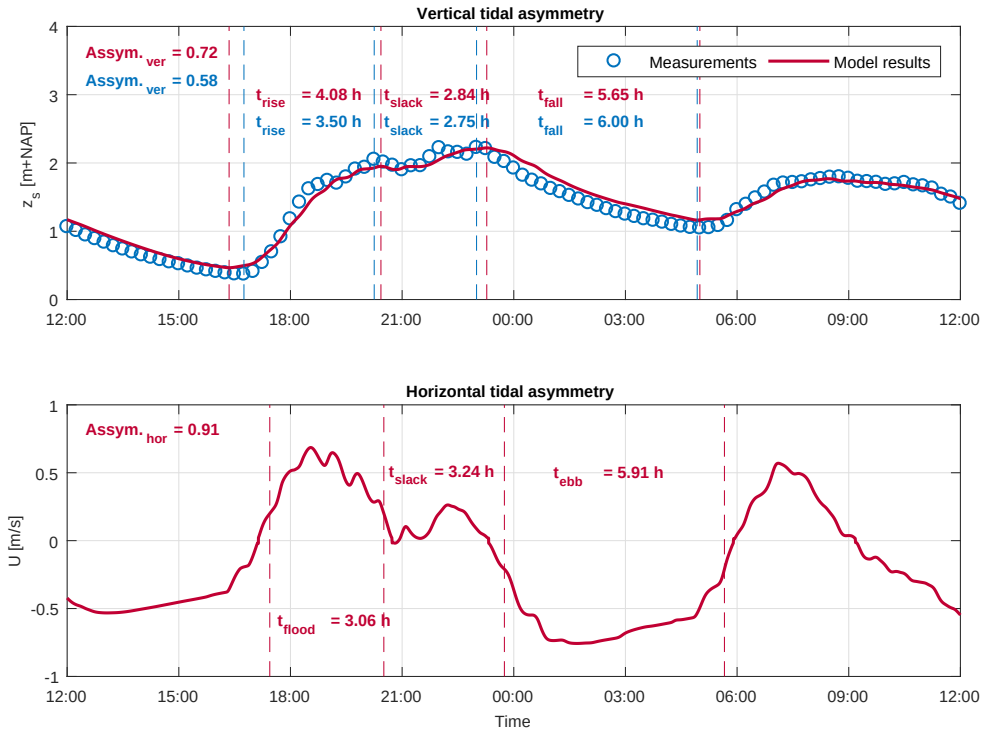

Figure 5.4: Analysis of vertical tidal asymmetry (measured and modelled water levels) and horizontal tidal asymmetry (only modelled velocities) for measurement location P4 (figure D.2). Vertical tidal asymmetry is defined as $\frac{t_{flood}}{t_{ebb}}$. Horizontal tidal asymmetry is defined as $\frac{max(u_{flood})}{max(|u_{ebb}|)}$.

Waves

To account for the effect of vegetation on the short wave height inside De Slufter, a wave friction coefficient '*fw*' of 0.06 was chosen. Figure 5.5 shows the significant short wave height over time inside De Slufter at measurement locations P2-8. The modelled short wave heights show a very good resemblance to the measurements. The difference at P4 can likely be attributed to wind wave growth (A.C. Engelstad, personal communication, May 14, 2018), as it is located in the gully. Wind wave growth is not included in the model.

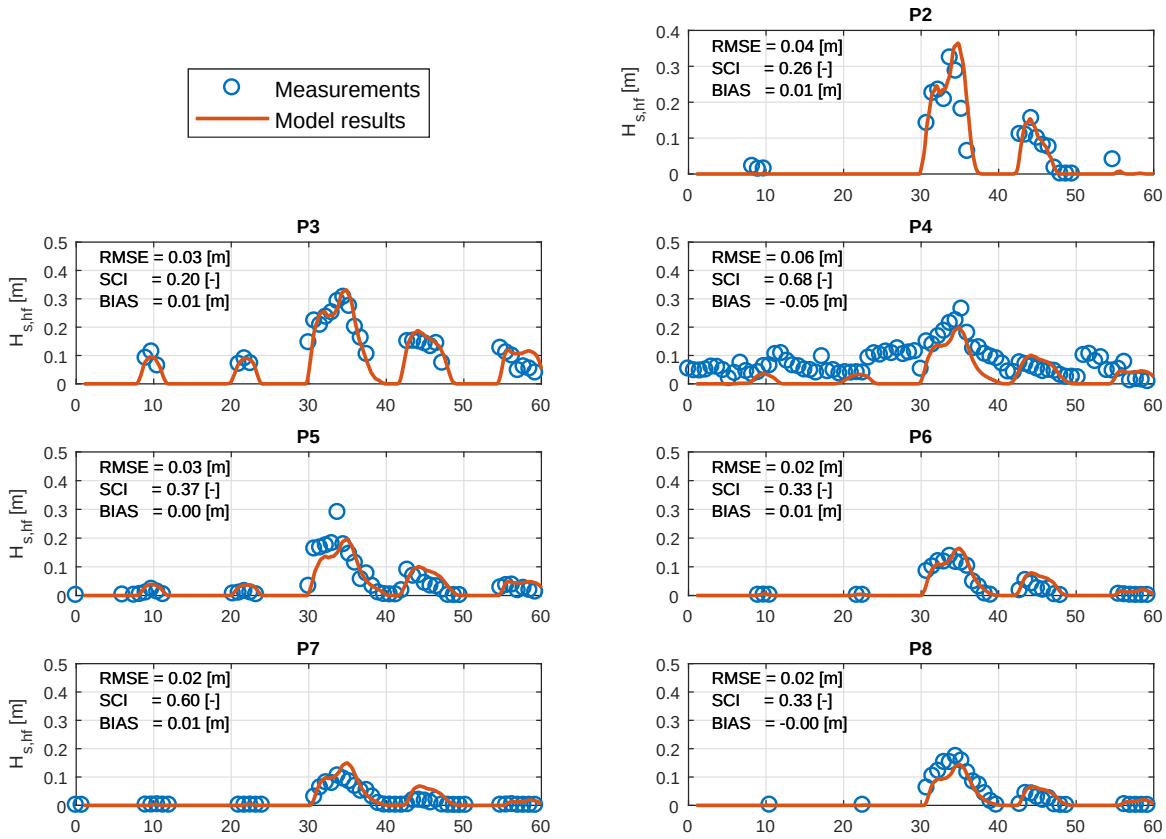

Figure 5.5: Comparison between high frequency (>0.05 Hz) significant wave height measurements and results over time for points P2-8. Please note that point P2-8 refers to the points in figure 5.1.

Figure 5.6 shows the significant long wave height over time inside De Slufter at measurement locations P2-8. The long wave height time series of the model results were determined by first dividing the water level results into segments of 1 hour. For each segment a variance density spectrum was computed. The peaks seen in the results are caused by this method of calculation. Next, the significant wave height for every hour was calculated. The lower and upper frequency limits were chosen to coincide with the limits of the long wave height data, with periods ranging between 20-200s (0.005-0.05Hz). The long wave height is underestimated at the entrance of the slufter mouth while it is slightly overestimated at the sand dike. Near the sand dike, where the long wave motions are most important, the RMSE values do not exceed 1 cm which is considered a good match.

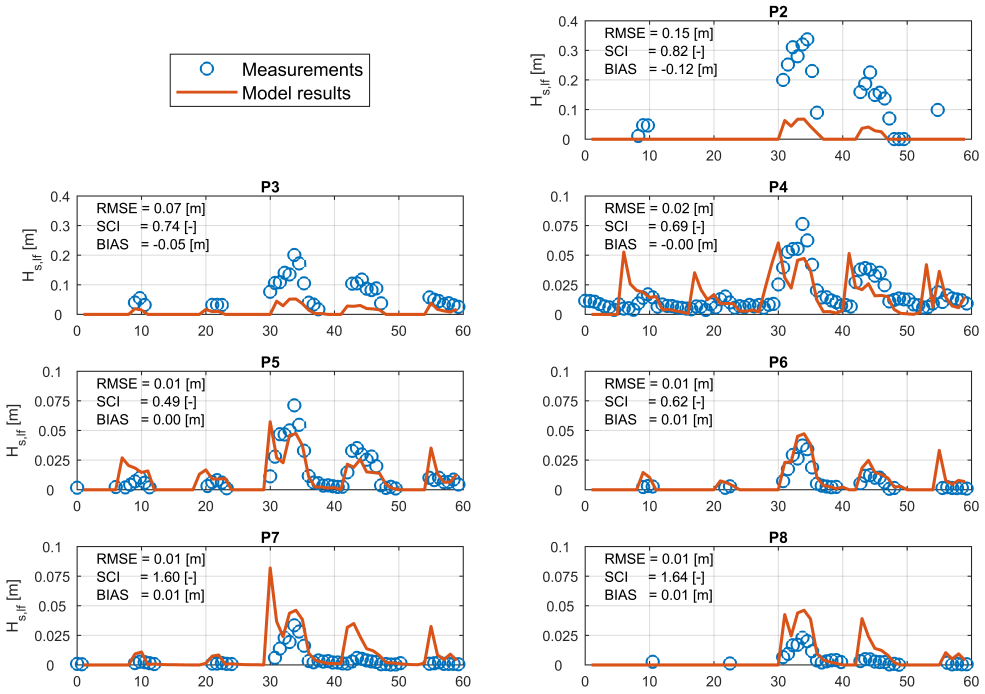

Figure 5.6: Comparison between low frequency (0.005-0.05 Hz) significant wave height measurements and results over time for points P2-8. Please note that point P2-8 refers to the points in figure 5.1.

5.2. Morphological validation

For the morphological validation the model was set up as described in chapter 4 with the exception of the bathymetry, which was created from 2008 datasets (appendix B).

The morphological development of De Slufter is validated on the gully transect measurements described in appendix D. As discussed in the field data analysis the migration of the gully is expected to be driven by longshore transport, curvature-induced secondary flow and storm-driven overwash. During storms, secondary flow will be negligible as the beach flat will be flooded due to the storm surge. This means that water is not constrained to the gully system anymore. Consequently, a water level gradient does not occur between the inner and outer gully bends. During storms, out of the three identified processes, only longshore transport and overwash will thus be of importance. For the morphological validation, the fact that XBeach cannot model 3D processes such as curvature-induced secondary flow is thus not considered to significantly influence the results.

5.2.1. Hydrodynamic conditions

The storm event that was identified by Van Puijvelde (2010) started 29-09-2008 18:00 and ended 02-10-2008 06:00, lasting 60 hours. During this storm, the wave direction was predominantly West with a maximum wave height of 4.39 meters (which is lower than the storm for the hydrodynamic validation). The maximum water level was NAP+1.53m. Figure 5.7 shows the hydrodynamic boundary conditions imposed on the offshore model boundary.

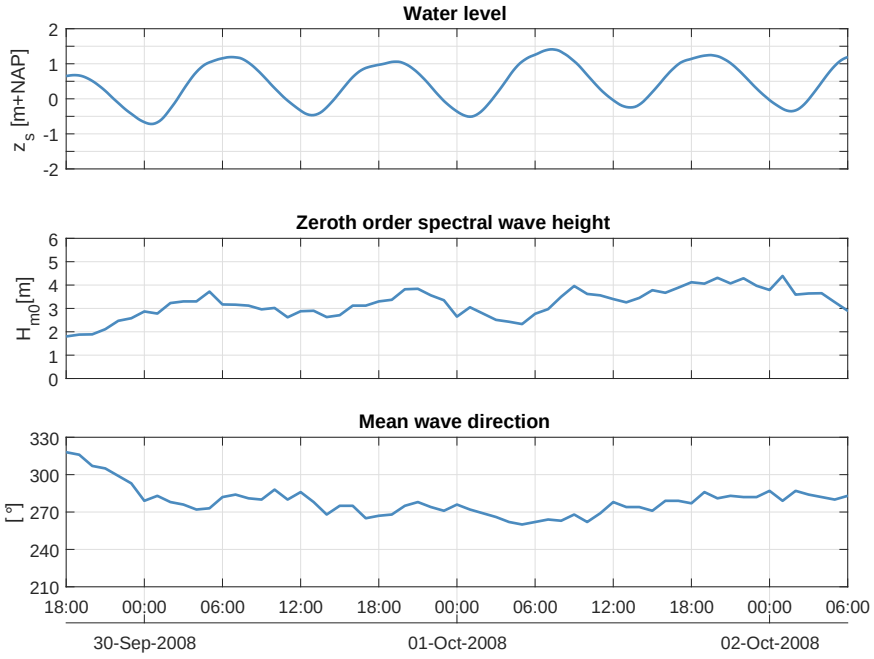

Figure 5.7: Offshore hydrodynamic boundary conditions for the morphological validation storm.

5.2.2. Results

Channel migration

Figure 5.8 shows transect 2, which is located near the southern dune foot. The pre-storm location of the gully is not exactly equal for the measurements and the model results. Even though, the results show a good resemblance to the measurements. The direction and order of magnitude of the migration is very similar. The model does underestimate the decrease in conveying cross-section (defined as the transect area below NAP+1 m). This is likely caused by the location of the gully in the model. In the measurements, the transect is located on the valley side of the beach flat. Sediment is eroded from the beach flat and deposited into the channel. In the model however, the gully transect is 'shielded' by the higher dune foot over which less overwash into the gully takes place. This leads to less deposition in the gully.

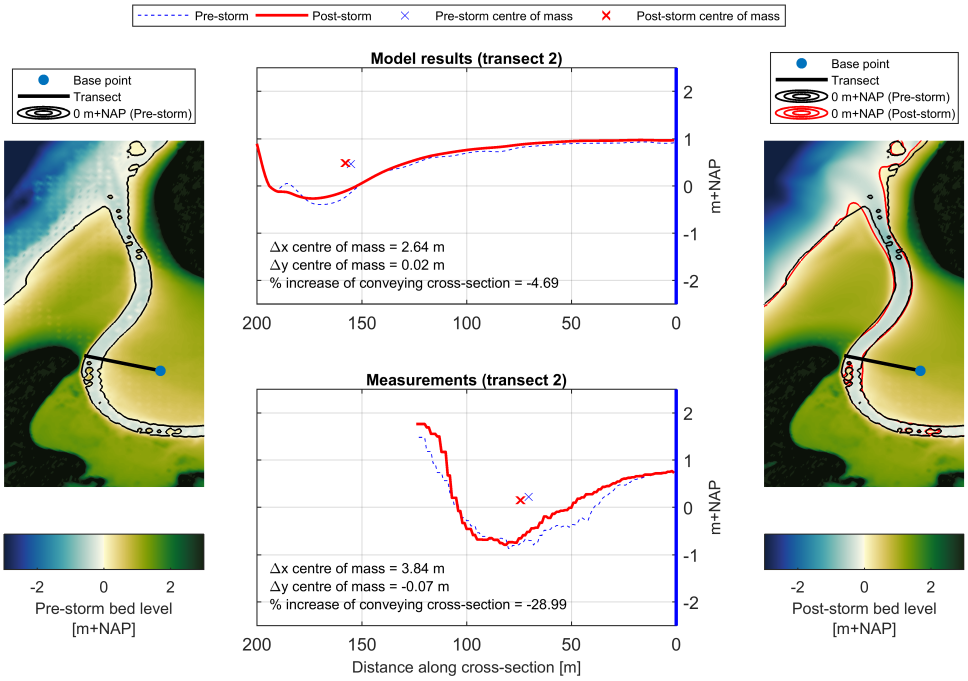

Figure 5.8: Migration of gully transect 2. The transect number refers to the transect numbers in figure D.1.

The migration of gully transect 4 is shown in figure 5.9. The model results show a very good resemblance to the measurements in this part of the gully. It shows erosion on the valley side and deposition on the seaward side of the gully which results in a migration towards the valley in the order of 5-10 meters.

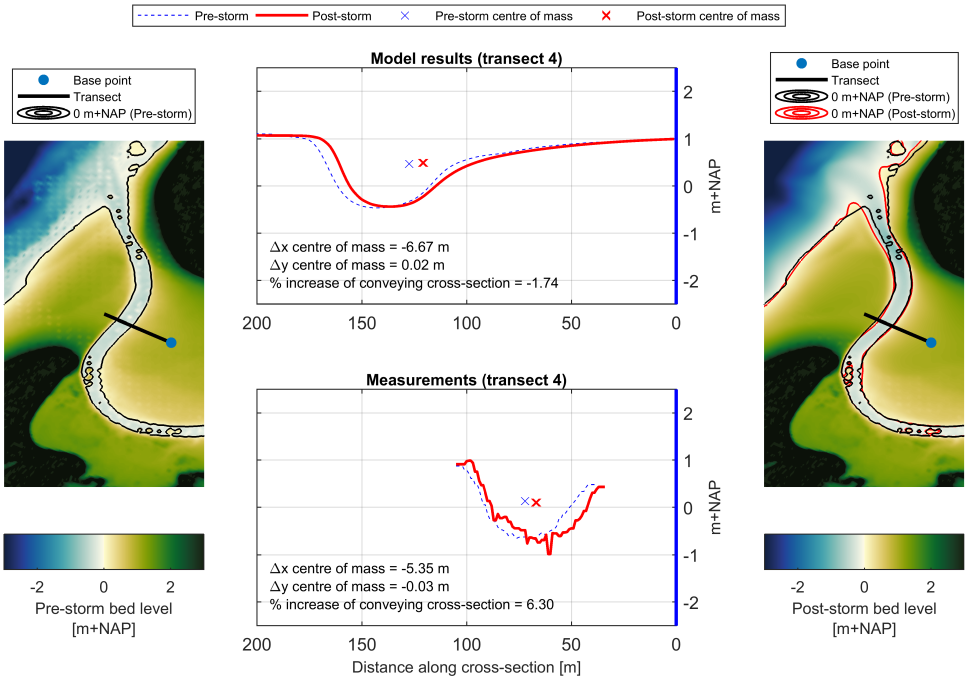

Figure 5.9: Migration of gully transect 4. The transect number refers to the transect numbers in figure D.1.

The migration of the more seaward gully transects 6 and 10 also show good results, with gully migration in the same direction and order of magnitude as the measurements. The model results show a significantly larger increase in conveying cross-section. A likely cause is the initial depth of the gully in the model

bathymetry. The gully is much shallower here than in the measurements. This leads to higher flow velocities in the gully during ebb and thus more erosion (which leads to more deepening).

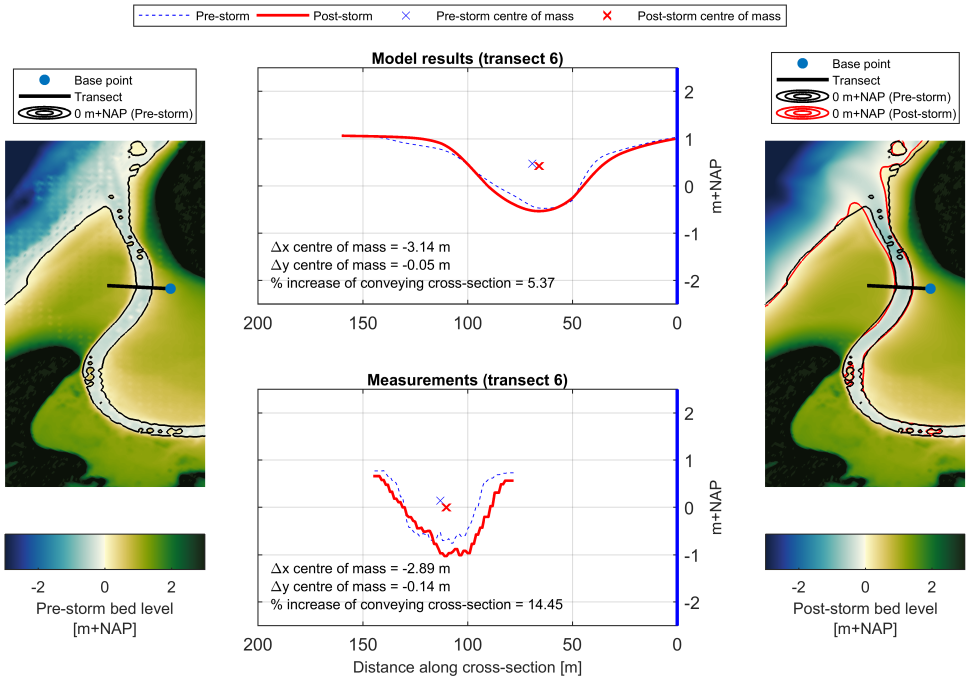

(a) Gully transect 6.

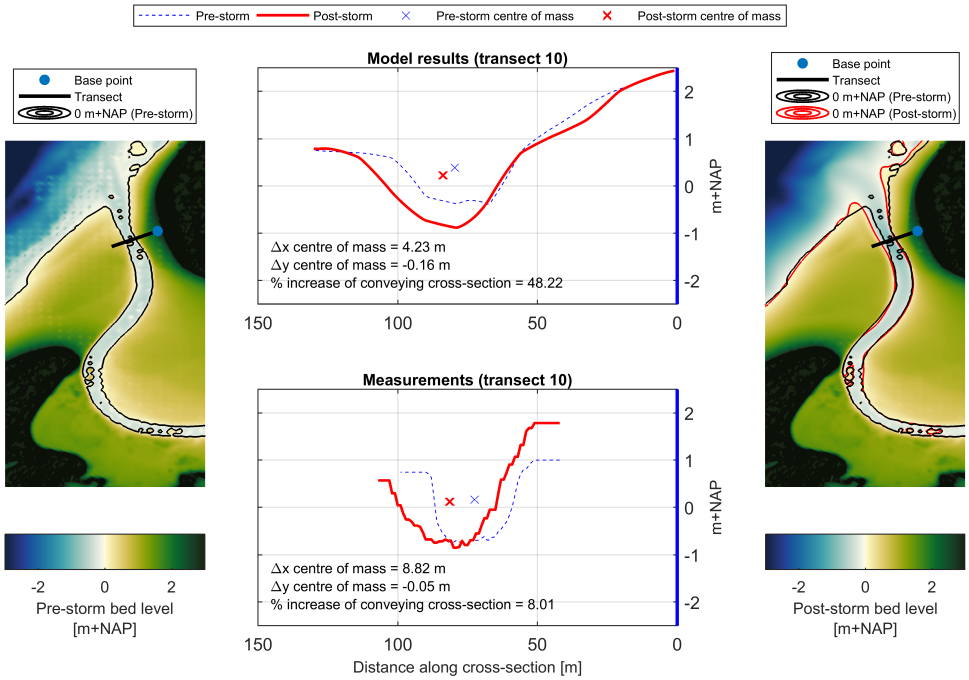

(b) Gully transect 10.

Figure 5.10: Transects near the gully mouth. The transect number refers to the transect numbers in figure D.1.

5.3. Conclusion

The hydrodynamics in the model generally match well with the field observations by Van Der Vegt and Hoekstra (2012). Root-mean-squared errors for short wave heights do not exceed 6cm and those of the water levels do not exceed 8cm (excluding the faulty measurements at P1). Also, resulting from the corresponding water levels, the tidal asymmetry in the model was in accordance with observations.

However, long waves are not exactly in accordance with observations. At the mouth, long wave height results are lower than the observations. When the waves propagate further into the valley the observed and modelled wave heights converge due to dissipation until, at the sand dike, observed wave heights are even slightly lower than the modelled wave heights (approximately 2cm). The fact that long waves there are larger in the model will therefore lead to conservative dune erosion volumes. For the purpose of this study, being the assessment of coastal safety, the capacity for accurately resolving hydrodynamic processes are thus considered sufficient.

As no short-term measurements of dune and sand dike erosion were available, the morphological validation was performed on field measurements of gully migration. As both the beach flat and the gully are inundated during the storm, the fact that XBeach does not resolve curvature-induced secondary flow is not considered a problem. The gully migration trends that were modelled are in agreement with the observations by Van Der Vegt and Hoekstra (2012) and show that the model can accurately model the validatable storm-driven morphological changes during storm events.

Therefore, combining the track record of XBeach Surfbeat in modelling dune erosion for dissipative sandy coastal systems with the fact that hydrodynamic and morphological observations are well in accordance with results in the model, the model is considered adequate for this study.

6 Results

In this chapter the results of the modelling study will be treated. First, in section 6.1, the model scenarios are presented as well as the failure assessment methods used in this study. In section 6.2 the results of the present scenarios will be discussed and assessed on failure. In section 6.3 the same is done for future scenarios.

6.1. Model scenarios and failure assessment

6.1.1. Model scenarios

The main goal of this study is to assess the present and future coastal safety of the Wadden island Texel. Both present (i.e. without SLR) and future (i.e. with SLR) coastal safety will therefore be evaluated for different morphological configurations. The scenarios can thus be divided into two general categories:

1. **Present scenarios**
2. **Future scenarios**

Hereafter, both categories will be elaborated on in terms of bathymetry configuration and assumed hydrodynamic boundary conditions. Excluding consecutive storm scenarios (which consist of rerunning the 1/1, 1/10, 1/100 and 1/3000 year storms three times), 15 scenarios have been run for this study: 9 present scenarios to represent possible situations in the short term ('Present') and 6 scenarios to represent possible situations in the year 2100 ('Future'). An overview of the present and future scenarios is given in tables 6.1 and 6.2, respectively.

Present scenarios

In all present scenarios, sea level rise is not included. It is however assumed that different bathymetry configurations can occur, i.e. a wider mouth or a second, more northerly located mouth. Visualisations of these configurations are presented in figure 6.1. For the wider mouth scenarios. the bed level of the newly formed beach flat is assumed similar to the beach flat height in the reference scenario. While it is highly unlikely that bathymetric changes of such a scale might occur within a short period of time it is interesting to model as it sheds light on the interdependence of the mouth, the valley and the sand dike.

For the present scenarios, storms of different return periods are modelled, i.e. with 1, 10, 100 and 3000 year return periods. Scenarios in which series of consecutive storms occur are also included. Consecutive storms have been assumed to be identical to the previous storm. The difference lies in the model bathymetry, which is equal to the resulting bathymetry of the previous storm. These consecutive storms have not been included in the table to keep it clear and orderly.

Scenario number 4 is from here on referred to as the 'reference scenario'.

Nr.	ID	Mouth config.	SLR [m]	BLR [m]	Storm	Wave Dir.
1	S0B1R1_1NW	Reference	0	0	1/1 year	NW
2	S0B1R10_1NW	Reference	0	0	1/10 year	NW
3	S0B1R100_1NW	Reference	0	0	1/100 year	NW
4	S0B1R3000_1NW	Reference	0	0	1/3000 year	NW
5	S0B2aR3000_1NW	800 m	0	0	1/3000 year	NW
6	S0B2bR3000_1NW	1000 m	0	0	1/3000 year	NW
7	S0B2cR3000_1NW	1250 m	0	0	1/3000 year	NW
8	S0B2dR3000_1NW	1500 m	0	0	1/3000 year	NW
9	S0B3R3000_1NW	Second mouth	0	0	1/3000 year	NW

Table 6.1: Overview of present model scenarios. The column 'mouth config.' refers to the configurations in figure 6.1 (numerical values indicate width). The 'reference' is equal to the location and width of the current mouth (400 m wide), see figure 6.1. The column SLR indicates the amount of sea level rise assumed in the scenario. The column BLR indicates the amount of bed level rise. Both SLR and BLR are 0 m for present scenarios. The entries in the column 'Storm' refer to the hydraulic boundary conditions in table 4.1. All storms were assumed northwesterly. Consecutive storm events were not included in the overview for clarity. These consist of rerunning scenarios 1,2,3 and 4 three times.

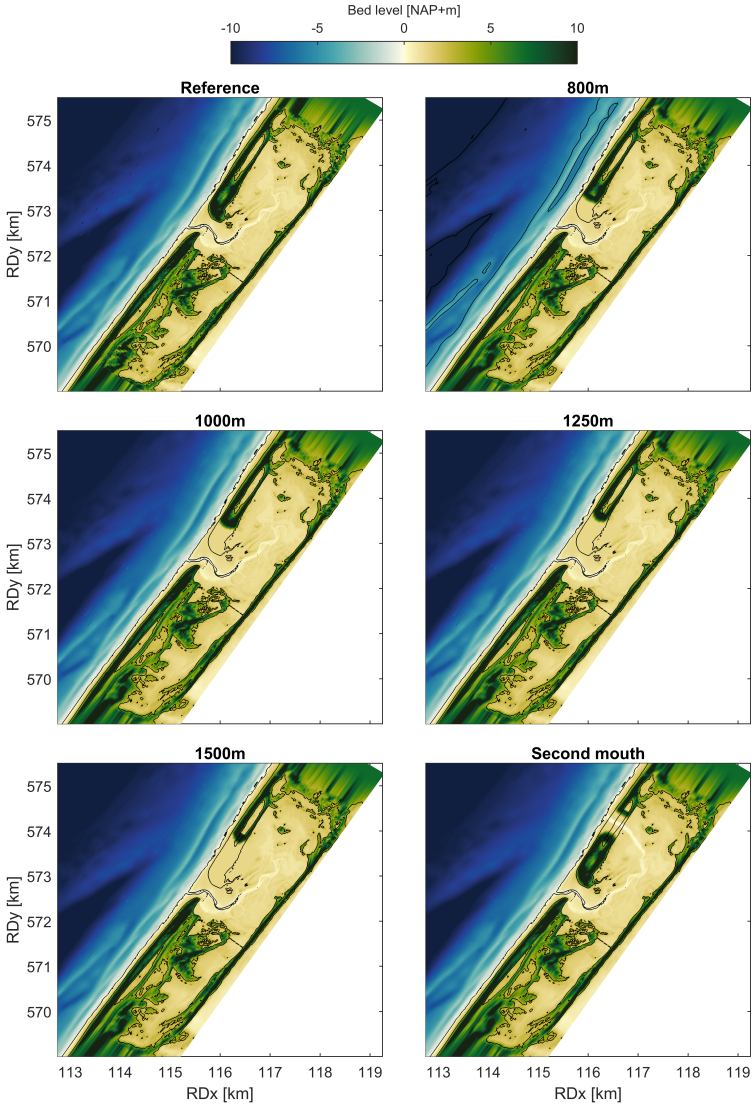

Figure 6.1: Overview of the 6 different bathymetry configurations of the 'present scenarios'. The black lines represent the NAP+0m and NAP+3m contour lines of the 'Reference' scenario (top left panel).

Future scenarios

In all future scenarios, SLR is included. For this study, 3 SLR scenarios are considered, based on subsection 2.1.3:

- **SLR1:** RCP8.5, Lower boundary - 0.75 meters
- **SLR2:** RCP8.5, Median - 1.95 meters
- **SLR3:** RCP8.5, Upper boundary - 3.17 meters

While the likelihood of especially the upper scenarios is very uncertain, these extreme scenarios were chosen because they give a wide range of possible scenarios which is expected to lead to more conclusive results. Furthermore, bed level rise (BLR) is assumed to either be equal to sea level rise (SLR) or to be 0 m. These two extremes were chosen because they represent the boundaries of expected morphological development, rather than a most likely morphology. From a coastal safety perspective this is preferable as basing conclusions on extremes will lead to the most conservative conclusion.

Figure 6.2 shows a cross-shore profile for every BLR scenario. The location of these profiles is given in the top left figure. For situations with BLR it was assumed that morphological activity had only taken place in areas that are regularly inundated. As the dunes are never inundated it was assumed that these had not risen. As BLR equals SLR, each SLR scenario with BLR can thus also be characterised as a present scenario in which only the dunes have been lowered.

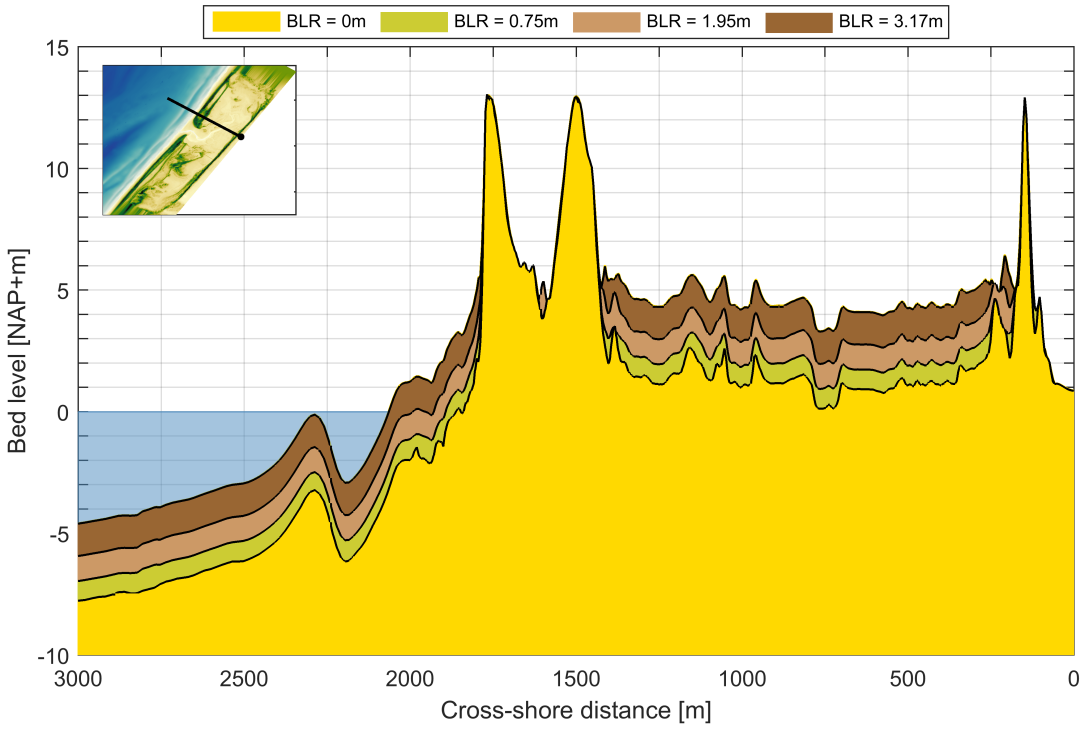

Figure 6.2: Alongshore transect showing the profiles for different BLR scenarios. The yellow profile

To limit the amount of runs, only storms with a return period of 3000 years and with 1 mean wave direction were modelled for future scenarios. For simplicity reasons northwesterly storms were modelled because they represent almost normally incident wave conditions. Also, northwestern waves are in the range of highest possible wave heights, as treated in subsection 3.1.1.

Nr.	ID	Mouth	SLR [m]	BLR [m]	Storm	Wave Dir.
10	S1B1R3000_1NW	Reference	0.75	0	1/3000 year	NW
11	S1B4aR3000_1NW	Reference	0.75	0.75	1/3000 year	NW
12	S2B1R3000_1NW	Reference	1.95	0	1/3000 year	NW
13	S2B4bR3000_1NW	Reference	1.95	1.95	1/3000 year	NW
14	S3B1R3000_1NW	Reference	3.17	0	1/3000 year	NW
15	S3B4cR3000_1NW	Reference	3.17	3.17	1/3000 year	NW

Table 6.2: Overview of future model scenarios. The column 'mouth config.' refers to the configurations in figure 6.1. The column SLR indicates the amount of sea level rise assumed in the scenario. The column BLR indicates the amount of bed level rise. BLR has been visualised in figure 6.2. The entries in the column 'Storm' refer to the hydraulic boundary conditions in table 4.1.

6.1.2. Failure assessment

In this modelling study, failure is assessed on 2 failure mechanisms: 'Grensprofiel' and 'Initiation of flooding'.

Grensprofiel: The 'Grensprofiel' failure mechanism defined in this report consists of two aspects. First, each post-storm cross-shore sand dike profile must contain a minimum transect volume of 20 m^3/m above SSL. For this purpose, the post-storm volume above SSL is calculated for 223 cross-shore transects along the sand dike, spaced 22.5m apart. If the volume above SSL is less than $20m^3/m$ for any transect, failure has occurred. This failure mechanism can only be assessed for a reasonably straight dune row. Therefore, only the sand dike is assessed (and not the lateral edges).

Second, the post-storm sand dike profile must contain a limit profile, equal to the limit profile discussed in subsection 2.3.1. If the limit profile does not fit into the post-storm sand dike profile, failure has occurred.

Initiation of flooding: The 'Initiation of flooding' failure mechanism used in this report is identical to the 'Puddles' failure mechanism defined by Von Gronau (2017) and has only been given a different name. In the definition by Von Gronau (2017), 'Puddles' failure occurs when at any point behind the 'Legger' (the 'Waterstaatswerk' boundary in this study) there is at least 20 cm of water depth.

Due to the manual topographic changes at the lateral edges of De Slufter, the model topography there deviates from the actual topography. To assess the 'Initiation of failure' mechanism, it is therefore first analysed what the weak (read: lowest) spots are in the ridge running around the valley. The ridge being the sand dike and the lateral edges combined. These are the locations through which inundation will occur first. Next, the maximum water level in the model (thus including long wave motion) is compared to the lowest point along the ridge. Figure 1.4 shows that if water flows over the ridge of De Slufter, it immediately flows into Texel and thus past the 'Waterstaatswerk' boundary. If the maximum water level is higher than the lowest point along the ridge, failure has thus occurred. The bed level of this lowest point is NAP+6.70 m, as will be discussed later. To assess the 'Initiation of flooding' mechanism at the sand dike a 1D analysis is performed on maximum water levels at the sand dike and height of the sand dike.

As the occurrence of 'Initiation of flooding' indicates water overflowing over the sand dike, this almost certainly means that there is a transect without a volume above SSL. Therefore, 'Grensprofiel' can be considered a more conservative assessment of failure than 'Initiation of flooding'.

Summary In summation, in this modelling study failure has occurred if:

- **1**: there is a location behind the 'waterstaatswerk' boundary with a water depth of more than 20cm.
  - for the lateral edges this occurs when the storm surge level is higher than the lowest point along the slufter ridge (NAP+6.70 m).
- **2A**: there is a cross-shore profile along the sand dike which cannot contain the corresponding limit profile.
- **2B**: there is a cross-shore profile along the sand dike which does not contain at least 20 m^3/m above SSL.

The round panels in figure 6.3 indicate examples of 'safe' and 'failed' situations for a generic sand dike cross-section. Panels with a green outline indicate 'safe' situations. Panels with a red outline indicate 'failed' situations. The numbers in the red panels refer to the list above.

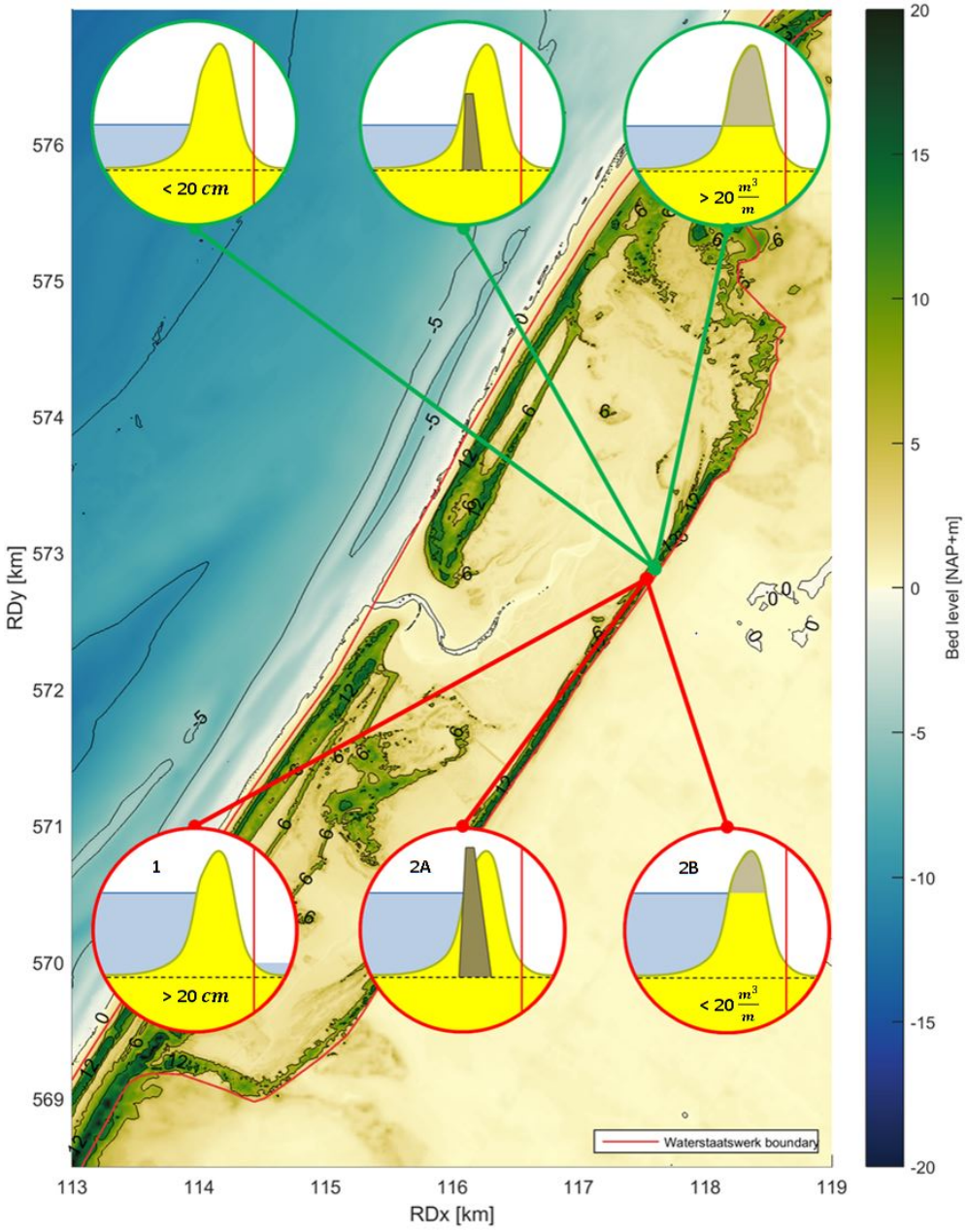

Figure 6.3: Overview of failure mechanisms used in this study. Green and red outlined panels indicate 'safe' and 'failed' situations, respectively. The values in the bottom of the left and right panels indicate water depth behind the 'waterstaatswerk' boundary and volume above SSL, respectively.

6.2. Present coastal safety

In this section, the hydrodynamic and morphological response of De Slufter to storms without SLR will be elaborated on. First, the response to a 1/3000 year storm is treated in detail in subsection 6.2.1. The hydrodynamic and morphological processes are treated first (i.e. the 2D variability of mean water levels and SSL, the wave attack on the sand dike and water depths in the valley, dune and sand dike erosion). Afterwards the occurrence of failure mechanisms (i.e. 'Grensprofiel' and 'Initiation of flooding' (Von Gronau, 2017)) during the storm will be treated as these are most important from a coastal safety perspective. After the detailed elaboration on the 1/3000 year storm, the response to storms due to different bathymetry configurations will be covered in subsections 6.2.2 and 6.2.3. At the start of each subsection the associated scenario(s) is/are presented.

6.2.1. 1/3000 year storm

This scenario (the 'reference scenario') represents the response of De Slufter in its present configuration and without SLR or BLR to a normative 1/3000 year storm.

Nr.	ID	Mouth	SLR [m]	BLR [m]	Storm	Wave Dir.
4	S0B1R3000_1NW	Reference	0	0	1/3000 year	NW

Table 6.3: Overview of scenarios that were analysed for this subsection.

Spatially varying water level

The maximum storm surge level is an important factor in the amount of dune and sand dike erosion during a storm. From figure 6.4 it becomes clear that mean water levels, which indicate SSL, are not uniformly distributed over the model domain, which is consistent with findings by Van Der Vegt and Hoekstra (2012).

In figure 6.4, phase 1 (upper left panel) indicates the first storm peak and marks the first moment in which the tide turns from flood to ebb. Phase 2 (upper right panel) indicates the flood period leading up to the peak of the storm. Phase 3 (lower left panel) marks the high peak of the storm and subsequently, the turning of the tide again. In this phase, water levels, wave heights and peak periods are highest, see figure 4.4. Phase 4 (lower right panel) marks the ebb flow after the peak of the storm.

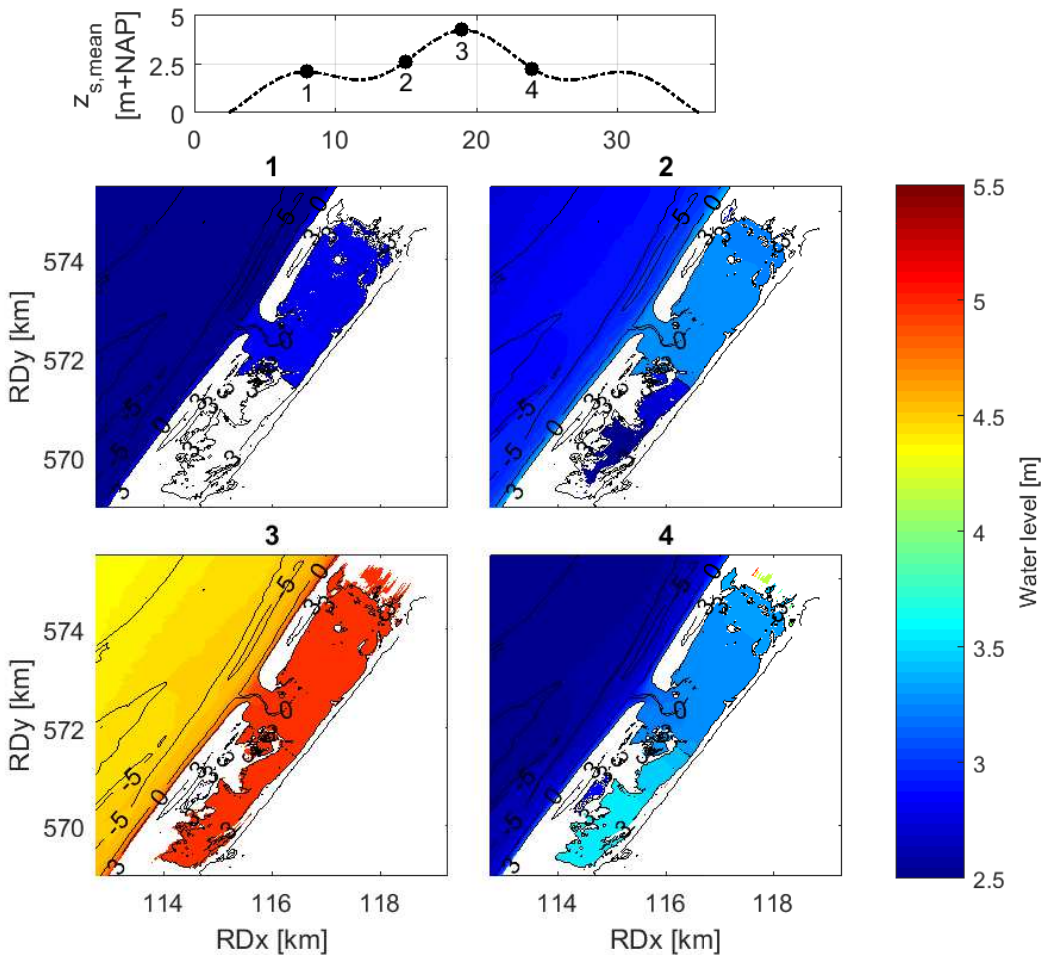

Figure 6.4: Mean water levels in the slufter during a 1/3000 year storm. For all phases it is clear that the water level is not uniformly distributed. At the peak of the storm the SSL at the offshore boundary is 4.3 m+NAP. Near the sand dike this has increased to 5 m+NAP.

During all four defined phases water levels show significant spatial variability. For all phases, a positive water level gradient ($\frac{d\eta}{dx} > 0$) is present in cross-shore direction from the offshore boundary to De Slufter due to wave setup. In the area in and just in front of the slufter mouth the (positive) water level gradient is largest (see transfer of orange to red in phase 3). As treated later in this section, this is the area in which most wave breaking occurs, leading to a negative gradient in short wave height ($\frac{\delta H_{s,HF}}{\delta x} < 0$), see figure 6.7. Consequently, a large negative radiation stress gradient ($\frac{\delta S_{xx}}{\delta x} < 0$) is present in onshore direction. This gradient leads to an onshore directed force which subsequently leads to a positive water level gradient.

$$F_x = -\frac{\delta S_{xx}}{\delta x} = \rho g h \frac{d\eta}{dx} \tag{6.1}$$

Further into the valley the (positive) water level gradient decreases significantly. This is due to the fact that there is less wave breaking (as only lower waves propagate further into the valley) and thus a smaller gradient in wave energy decrease (visible later on in figure 6.7). Subsequently, the radiation stress gradient becomes smaller and the water level gradient as well. The water level gradients can be seen more clearly in figure 6.5, which shows the Δh relative to the offshore water level for the 4 phases.

During phase 2 and 4, an additional gradient is visible between the southern and northern valley. During phase 2, a flooding phase, water levels in the southern valley are lower than in the northern valley. This is caused by the fact that the southern valley is still in the process of filling up. During phase 4, an ebb phase, the opposite is true as the southern valley is in the process of emptying. Furthermore, the water level head between the offshore boundary and the northern valley is significantly larger during phase 4 than during phase 2. This is the case because the large volume of water stored in the valley needs time to empty. Furthermore,

there is a lag between the offshore forcing and the response inside De Slufter due to the 8km cross-shore distance. In phase 3, at the peak of the storm, no water level gradient is present along the sand dike. This is due to the fact that both valleys have completely filled up and because of the low velocities inside the valley due to the slack tide.

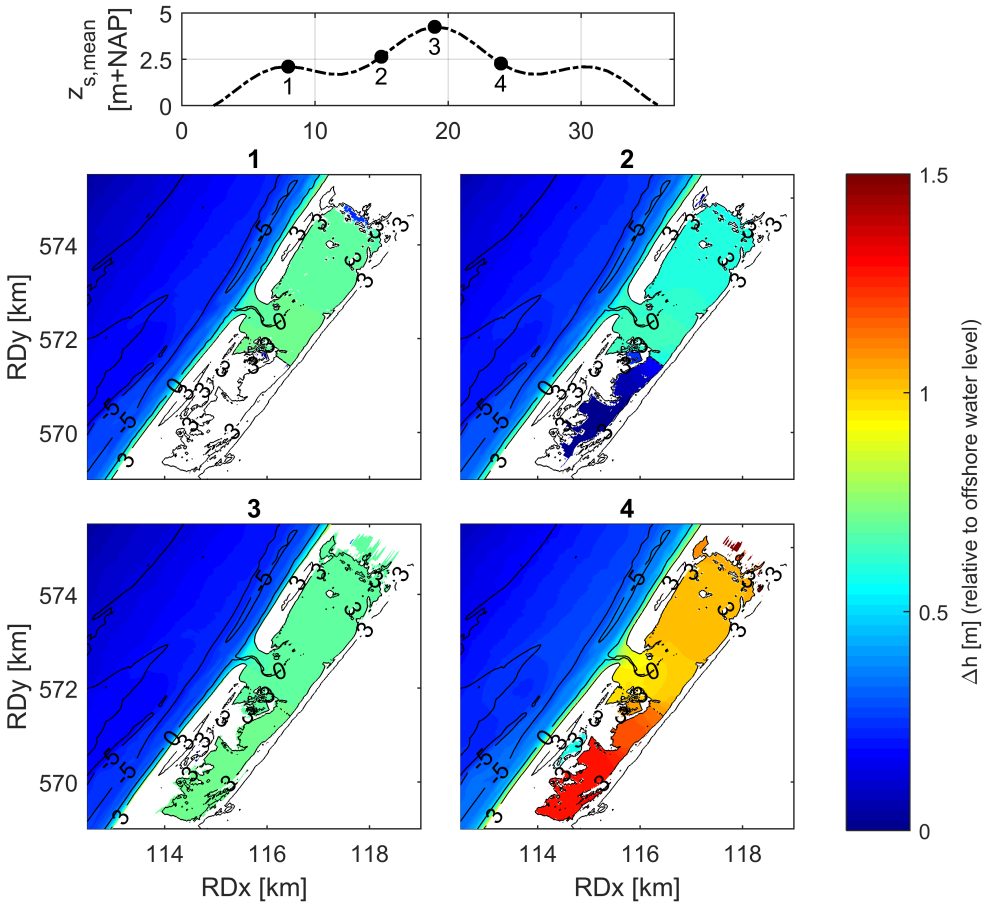

Figure 6.5: 2D maps of mean water level head relative to the mean water level at the offshore boundary. The 4 phases of these maps coincide with the phases in figure 6.6.

The presence of these water level gradients means that the maximum SSL (in phase 3, the peak of the storm) near the sand dike is much larger than the maximum SSL imposed on the offshore boundary (approximately 0.7m larger). It also means that SSL varies over the valley and thus along the sand dike when the southern valley is in the process of filling or emptying. During the peak of the storm however, when the southern and northern valleys have filled up, mean water levels in the entire slufter valley are uniform.

Wave attack

An important factor in the amount of dune erosion that occurs at the sand dike during a storm is the amount of wave energy that is capable of reaching the sand dike. In the model, a large part of the wave energy that propagates through the slufter mouth is dissipated while crossing the slufter valley. The driving forces behind this dissipation are depth-induced wave breaking and wave friction, of which the effects diminish with increasing water depths. As the water depths inside and outside De Slufter increase during a storm less wave energy is thus dissipated and more wave energy is capable of entering De Slufter and reaching the sand dike. This dependance is clearly visible from figure 6.6. During the peak of the storm (phase 3), water depths in the area from the mouth to the sand dike are approximately 3-4m. With these water depths, a significantly larger amount of wave energy enters De Slufter than during phase 2 in which water depths are 2-2.5m

The waves imposed on the offshore model boundary have been given a large directional spreading. This causes the 'fanning out' of short wave energy propagating into De Slufter. During phase 1, the water depths in De Slufter are still small. Wave energy cannot propagate far northwards as it is hindered by a small object,

indicated with a red arrow in figure 6.6-(b). The consequent narrow spreading of wave energy due to the blocking by the mound is a result of the fact that XBeach does not resolve diffraction. In reality, while wave energy would be lower behind the object, it would diffract around the object and propagate further. During phase 3, the object is inundated and waves propagate over it, resulting in a wider section of the sand dike under short wave attack. In reality the spreading of wave energy due to diffraction would also lead to lower wave heights at the sand dike directly in front of the mouth, due to the spreading of wave energy along the wave crest.

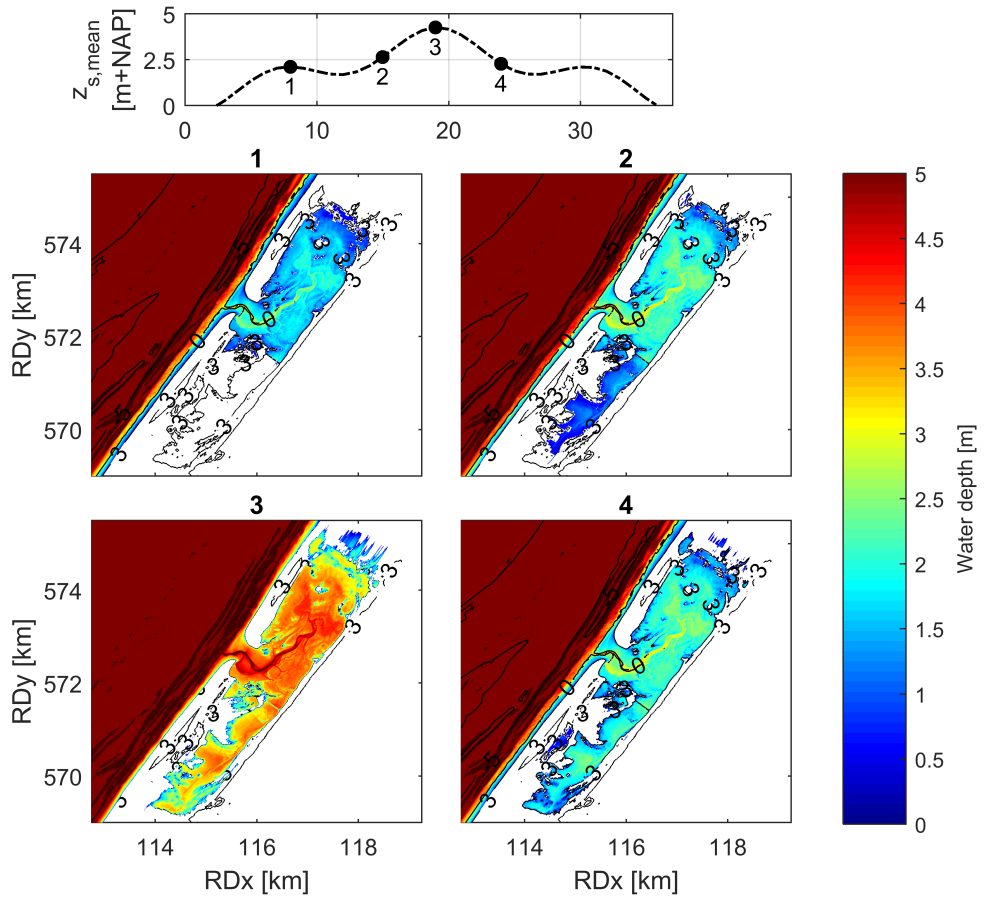

(a) Water depth

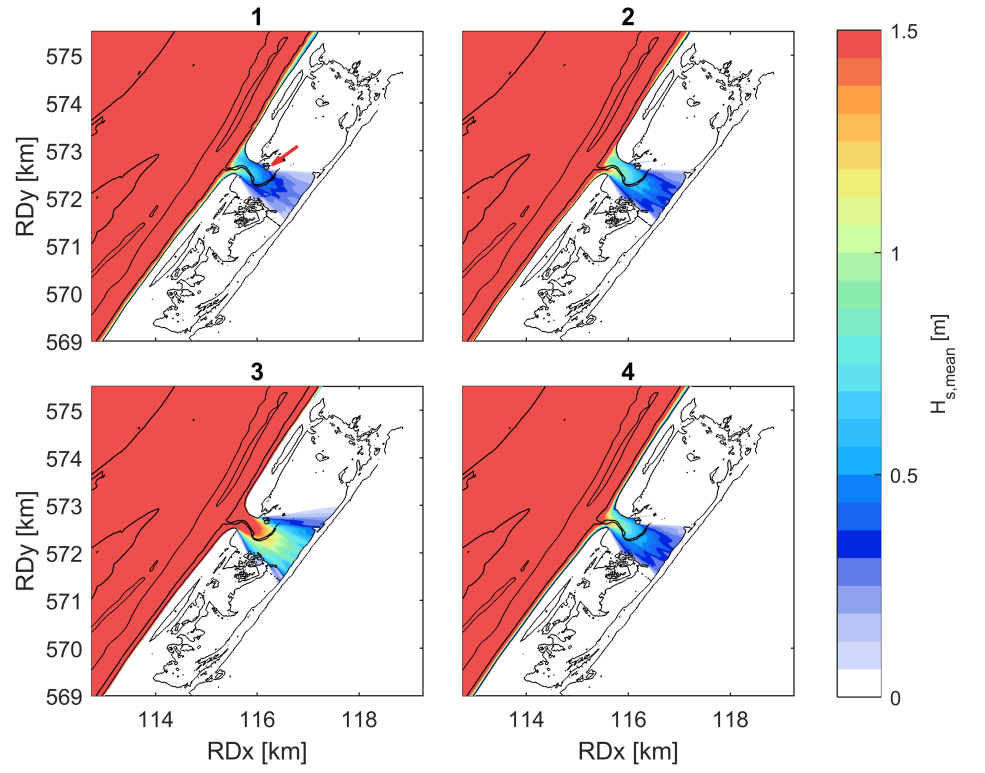

(b) Short wave height

Figure 6.6: Water depth and short wave height in the slufter valley during 4 different phases of a 1/3000 year storm. In phase 1, the southern area of De Slufter has not yet been inundated. The red arrow in figure b indicates a mound which blocks the propagation of wave energy. In phase 2, the southern area has been inundated by further rising water levels. In phase 3, water depths are at their highest. Phase 4 presents water depths during ebb flow at equal offshore water levels as phase 2. At phase 4 water depths in the southern part of the valley are higher than in phase 2 even though offshore storm surge levels are equal.

The mean significant short wave height just in front of the mouth ($x = 2km$ in figure 6.7) during the peak of the storm (phase 3) is approximately 3.40m. Near the sand dike directly in front of the mouth ($x = 0km$) this has decreased to 0.86m. At the peak of the storm the long wave height is 0.49m just in front of the mouth ($x = 2km$ in figure 6.8). At the sand dike this is 0.23m ($x = 0km$), a decrease of 53%.

These values (which have been summarized in table 6.4) show that the capacity of the slufter valley for diminishing wave attack on the sand dike is significant but that this capacity decreases when water depths increase. However, at the peak of the storm, 75% of short wave height and 50% of long wave height are still dissipated. This means that, even during the peak of a normative 1/3000 year storm, De Slufter acts as a formidable wave dissipator which reduces wave attack on the sand dike significantly. Furthermore, the table shows that relative short wave height dissipation is larger than relative long wave height dissipation but that short wave height is still larger than long wave height near the sand dike (≈3.7 times larger).

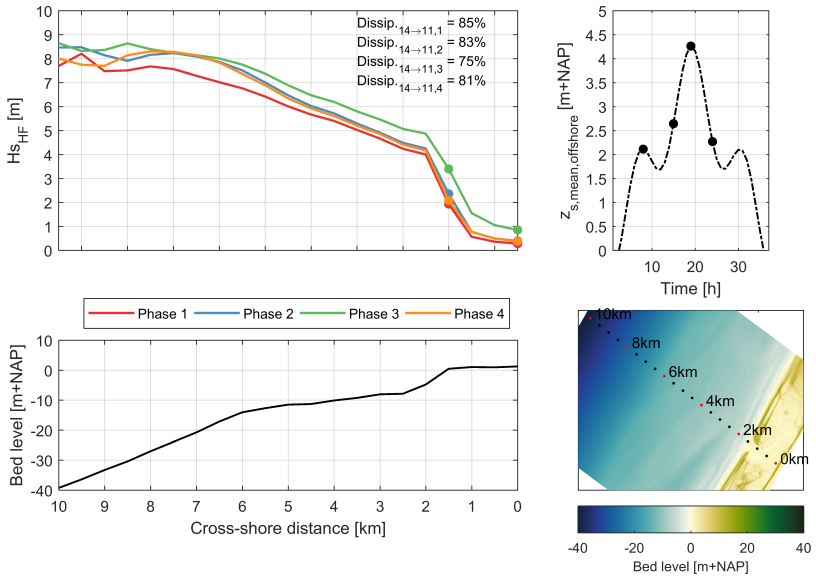

Figure 6.7: Short wave height transect in the slufter valley during 4 phases of a 1/3000 year storm.

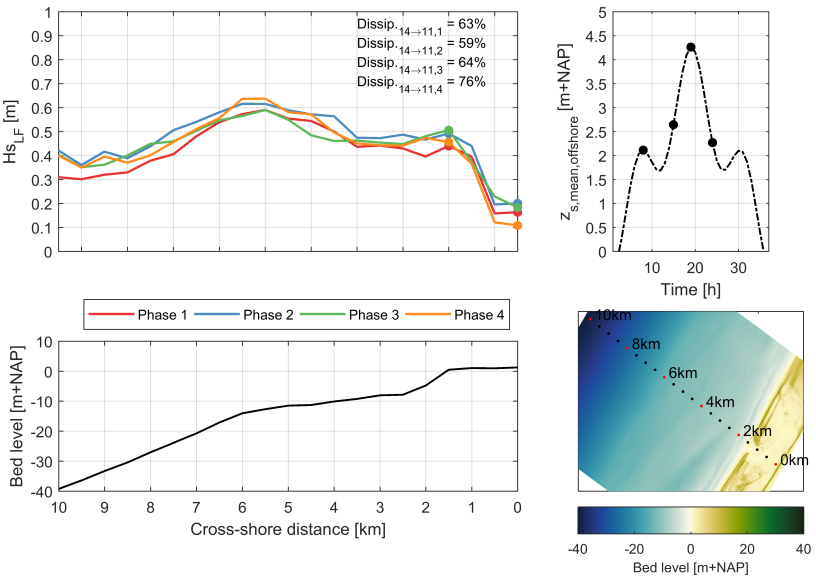

Figure 6.8: Long wave height transect in the slufter valley during 4 phases of a 1/3000 year storm.

HF	$H_{s,x=2km}$ [m]	$H_{s,x=0km}$ [m]	ΔH_s [m]	Dissipation [%]
Phase 1	1.96	0.29	-1.67	85.2
Phase 2	2.38	0.40	-1.98	83.2
Phase 3	3.40	0.86	-2.54	74.7
Phase 4	2.08	0.39	-1.69	81.3

LF	$H_{s,x=2km}$ [m]	$H_{s,x=0km}$ [m]	ΔH_s [m]	Dissipation [%]
Phase 1	0,39	0,11	-0,28	71,8
Phase 2	0,44	0,16	-0,28	63,6
Phase 3	0,49	0,22	-0,27	55,1
Phase 4	0,43	0,10	-0,33	76,7

Table 6.4: Overview of wave heights just in front of the mouth and near the sand dike with wave height decrease and dissipation included.

Dune and sand dike erosion

Figure 6.9 shows the erosion volumes above NAP+3 m after a 1/3000 year storm for the sand dike (yellow) and the front dune row (green). The NAP+3 m limit is used for all transects as an approximation of dune foot height. The maximum dune erosion is 118 m^3/m and is located at the northern dune head. The maximum sand dike erosion is 6.8 m^3/m and is located in front of the slufter mouth.

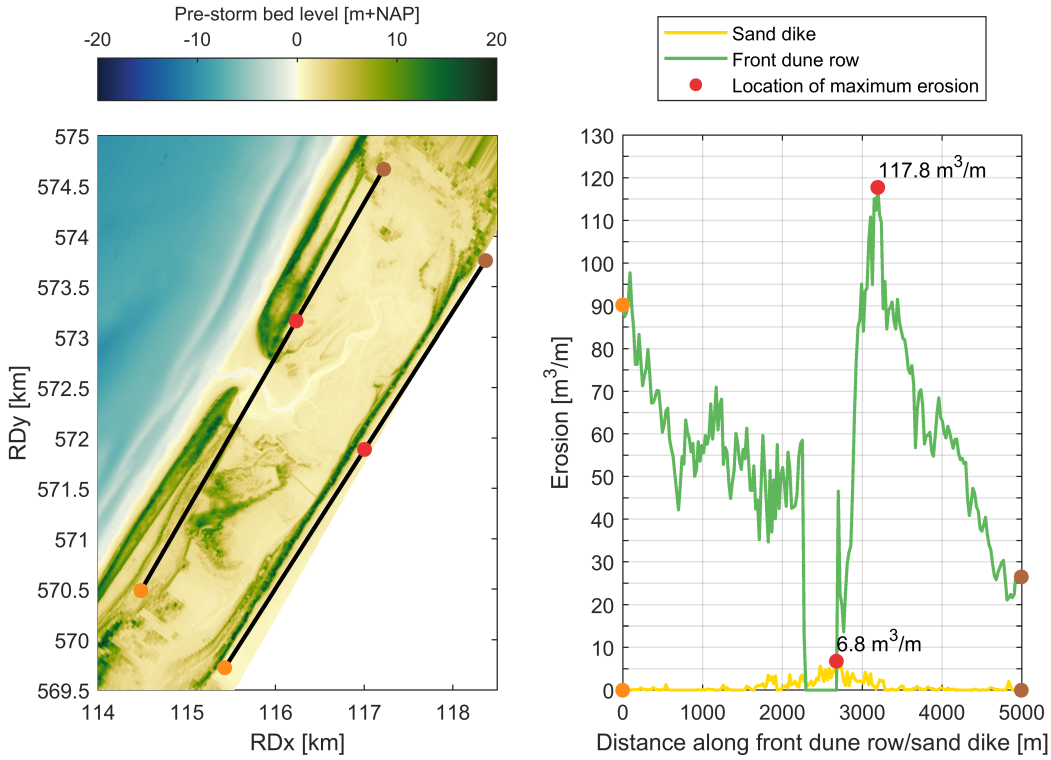

Figure 6.9: Erosion along the sanddike and the front dune row after a 1/3000 year storm. The peak erosion is caused by a smaller duneform in front of the sand dike.

Front dune row Two downward trends in alongshore direction are distinguished in dune erosion. The first is visible between the most southern point in the transect (x = 0m in figure 6.9) and the southern dune head (x = 2200m). The second trend is visible between the point of maximum erosion (x = 3240m) and the most northern point of the transect (x = 5000m).

These trends coincide with trends in beach widths along the front dune row, which variate significantly. Wider beaches will dissipate more wave energy before waves reach the dune profile and will thus lead to

less dune erosion. In this study, the beach width is assumed to be the area in front of the dune in which NAP+0m< z_b <NAP+3m. In figure 6.10 the beach width is plotted for two transects: The transect with the maximum erosion (middle panel) and a transect further north (lower panel) with much less erosion. A clear distinction in beach width can be distinguished. Namely, the transect with little erosion has a beach width of 136m and the transect of maximum erosion has a beach width of only 49m.

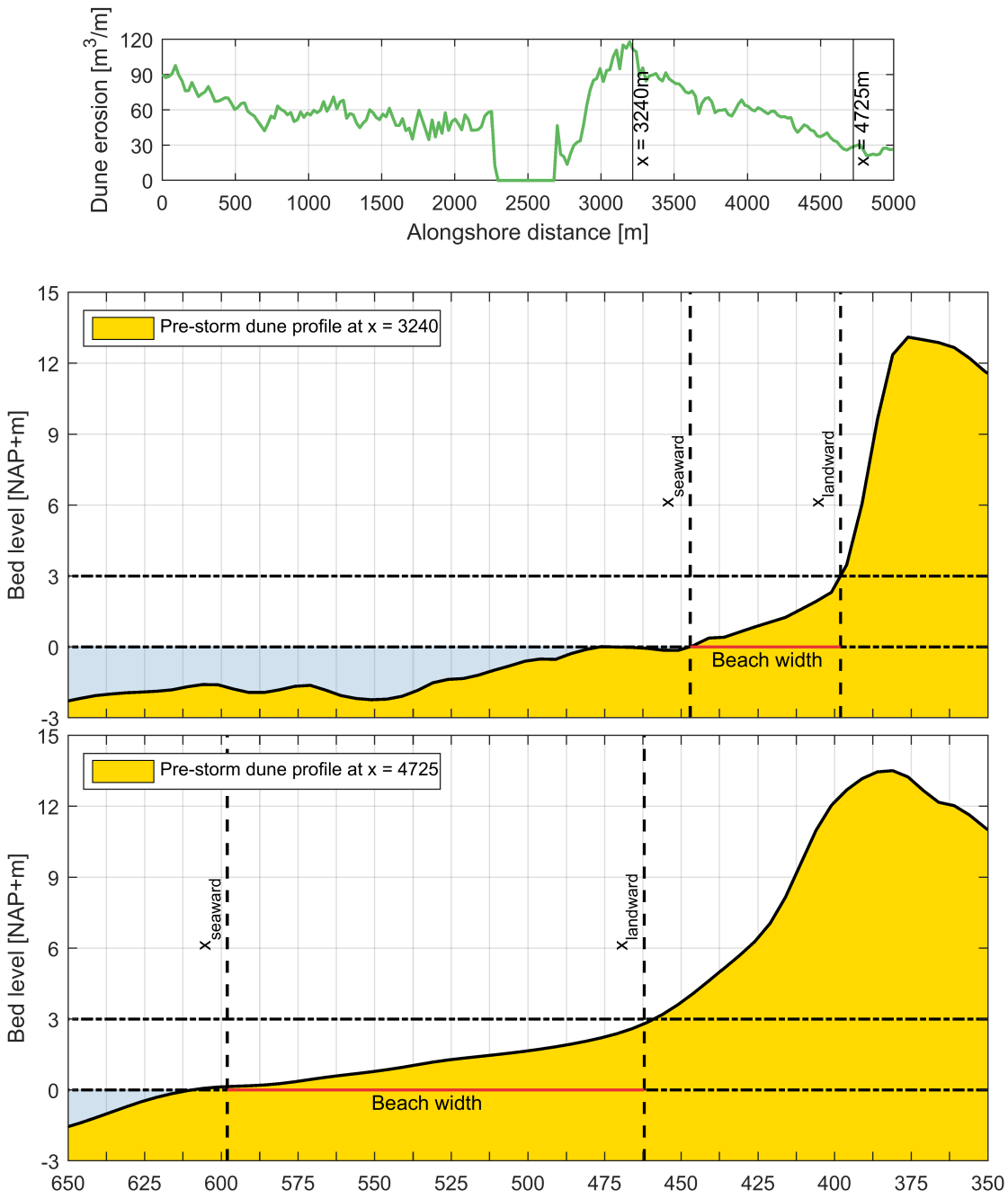

Figure 6.10: Beach width for maximum erosion transect and a transect more northward with much less erosion.

The correlation between beach width and dune erosion during storms is present along the entire front dune row, as is evident from figure 6.11. For transects in which the beach width is 110m or more the erosion volumes do not exceed 60 m^3/m during a 1/3000 year storm. For transects with beach widths of 70m or less the erosion volumes are at least 60 m^3/m. To mitigate erosion of the front dune row it is thus important to maintain a minimal beach width.

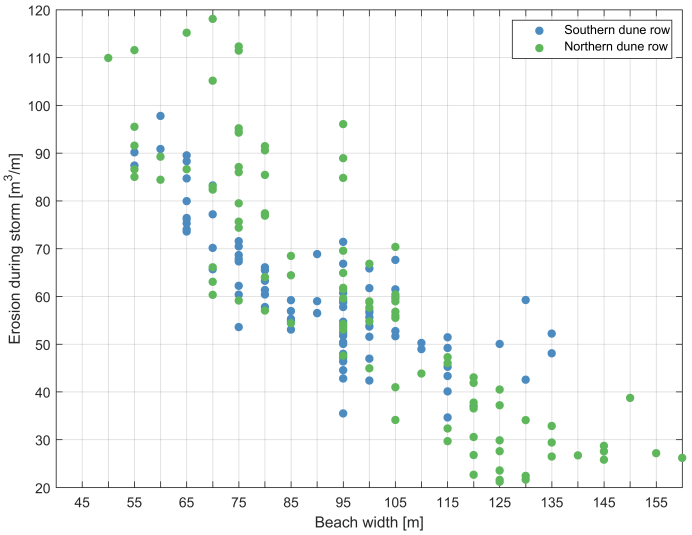

Figure 6.11: Scatter plot of dune erosion over beach width for the southern dune row (blue dots) and the northern dune row (green dots). A clear downward trend in dune erosion is present for increasing beach widths.

Furthermore, the maximum dune erosion at the northern dune head is explained by the flow velocity there at the peak of the storm, presented in figure 6.12. Large currents develop when the valley fills up through the mouth. These currents lead to high flow velocities around the northern dune head. Furthermore, these currents transport sediment that erodes from the dune in cross-shore direction away from the transect in alongshore direction towards the mouth.

Without longshore transport of sediment, the erosion of the duneface and subsequent accretion on the shoreface lead to a more gentle slope. This in turn leads to less dune erosion as a storm progresses. In this case however, as the accreted sediment is transported in alongshore direction, the sedimentation of the beach is counteracted (but not stopped). This means that the decrease in dune erosion during a storm is counteracted as well and explains why the maximum dune erosion is located at the northern dune head.

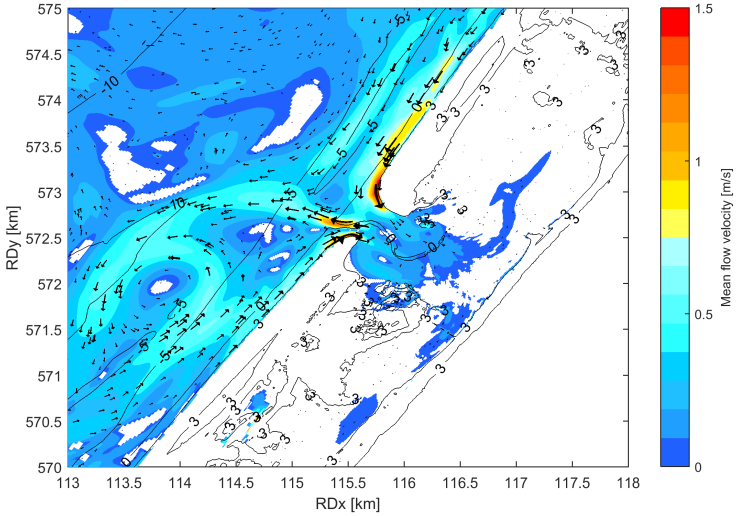

Figure 6.12: 2D map op mean flow velocity during the peak of a 1/3000 year storm. Strong currents can be seen along the northern dune head.

Sand dike Figure 6.6 shows that sand dike erosion is largest in the area in front of the mouth. This is a result of the fact that this area is under most wave attack when the valley is inundated, as is discussed later on. As more wave energy hits the duneface in this area, more dune erosion occurs.

Another interesting aspect is that the sand dike erosion volumes are small compared to the front dune face (the erosion of the sand dike itself does not exceed approximately 7 m^3/m). The maximum sand dike erosion is thus only 6% of the maximum dune erosion. This is a consequence of the large amount of wave dissipation that occurs in the slufter valley, as explained earlier in this section. These erosion volumes have no significant influence on the cross-shore shape of the sand dike, as is evident from figure 6.13, which shows the transect at which this maximum erosion has taken place. The large difference in erosion volumes between the front dune face and the sand dike indicates the importance of dissipation in the slufter valley for the coastal safety of the sand dike.

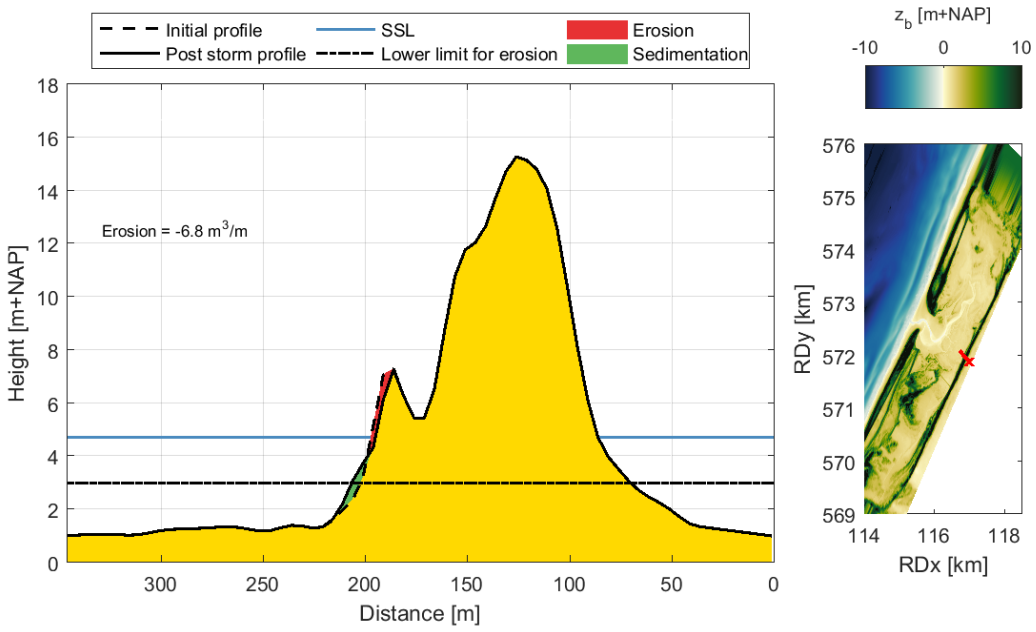

Figure 6.13: Cross-shore transect of the sand dike at the location in which the most sand dike erosion has taken place after a 1/3000 year storm. The red line and cross in the map indicate the 2D transect location.

Failure mechanisms

Grensprofiel - The maximum storm surge level near the sand dike is NAP+5 m which is significantly higher than the offshore storm surge level (NAP+4.3 m). A dune section is considered 'failed' when the volume above maximum SSL in a transect is lower than 20 m^3/m. Figure 6.14 shows that the post-storm volume above maximum SSL in any transect along the sanddike does not fall below 173 m^3/m.

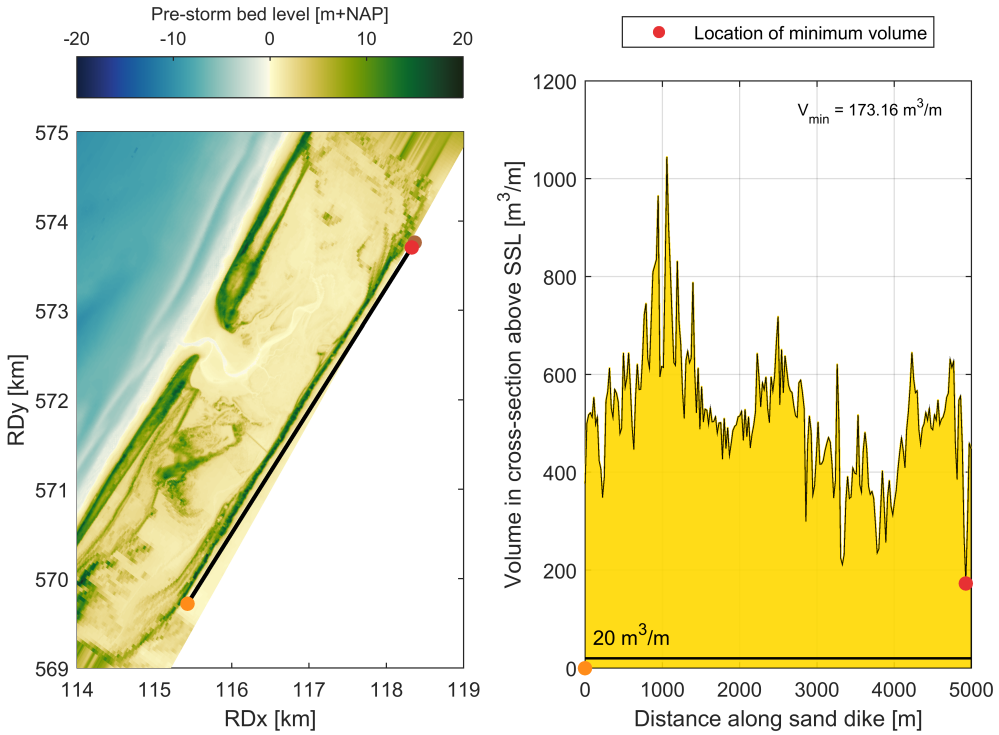

Figure 6.14: Volume in transect above SSL (5 m+NAP at the sand dike) for a 1/3000 year storm.

Figure 6.15 shows that for both the transect of maximum erosion and the transect with the minimum volume above SSL, the cross-shore profile still envelops the limit profile. For the maximum erosion transect, the limit profile can easily be fit into the post-storm sand dike profile. In the transect with minimum volume, the limit profile also fits into the post-storm profile. However, the vertical margins for this profile are small. For the maximum sand dike profile this is approximately 1 m. However, wave attack at that location is small because it is shielded by a narrower dune (between $x = 270$ m to $x = 200$ m) and no overtopping is expected to occur. Therefore, based on the minimum transect volume and the limit profile, all transects can be labeled 'safe'.

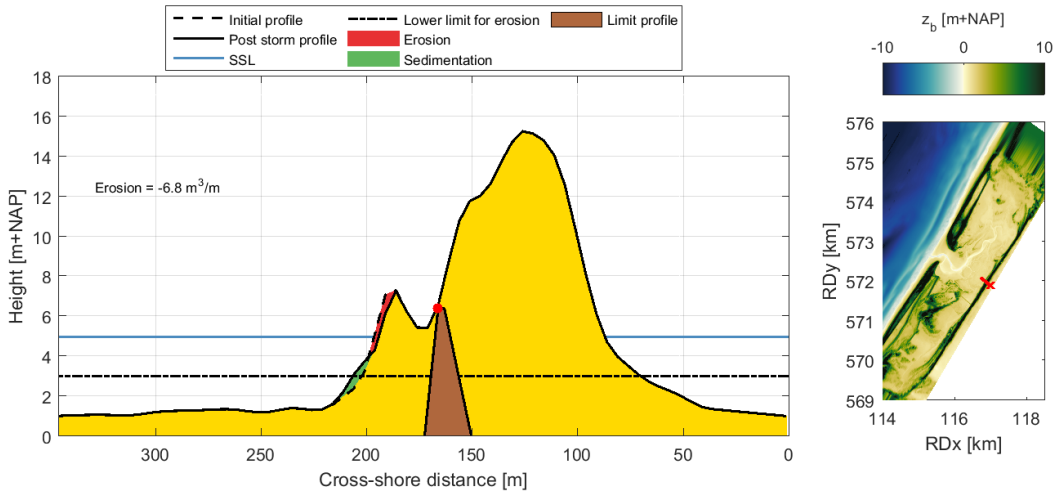

(a) Maximum erosion transect

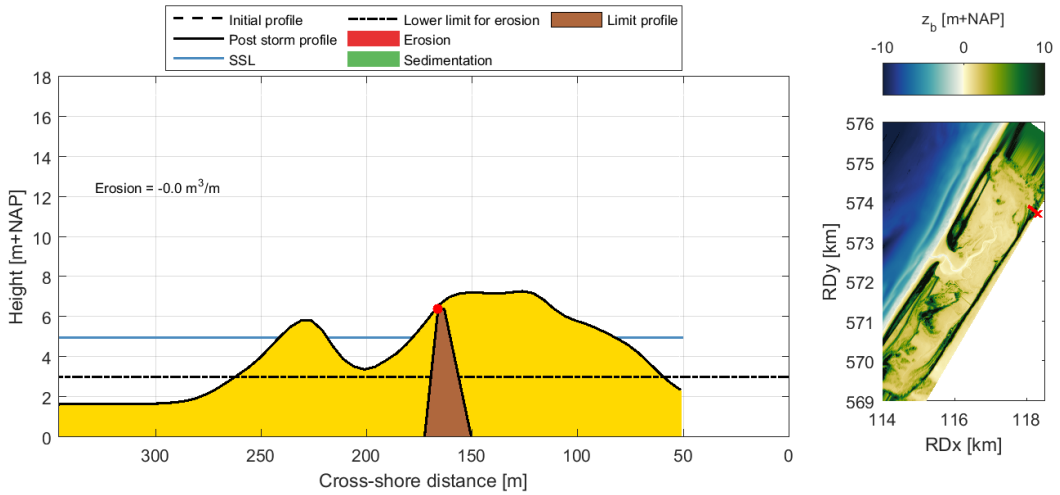

(b) Minimum volume transect

Figure 6.15: 'Grensprofiel' assessment concerning the limit profile.

Initiation of flooding - While there is dune erosion at the sand dike, there is no morphological activity on the ridge of the sand dike. In other words, the height of the primary coastal defence is not lowered by a 1/3000 year storm. This is concluded from figure 6.16, which shows the maximum sand dike height in relation to the maximum water level at the sand dike during the peak of the storm (for the same alongshore transect as figure 6.14).Pre- and post storm sand dike height are equal, which is why only the pre-storm sand dike height is plotted. Infragravity wave overtopping is included by plotting the maximum water level over an hour. Just as short wave attack, long wave attack is focussed around the area directly in front of the mouth. From figure 6.16 it is evident that wave overtopping of the sand dike will not occur during a 1/3000 year storm in present conditions. The minimum vertical distance between maximum water level and sand dike height is more than 2m.

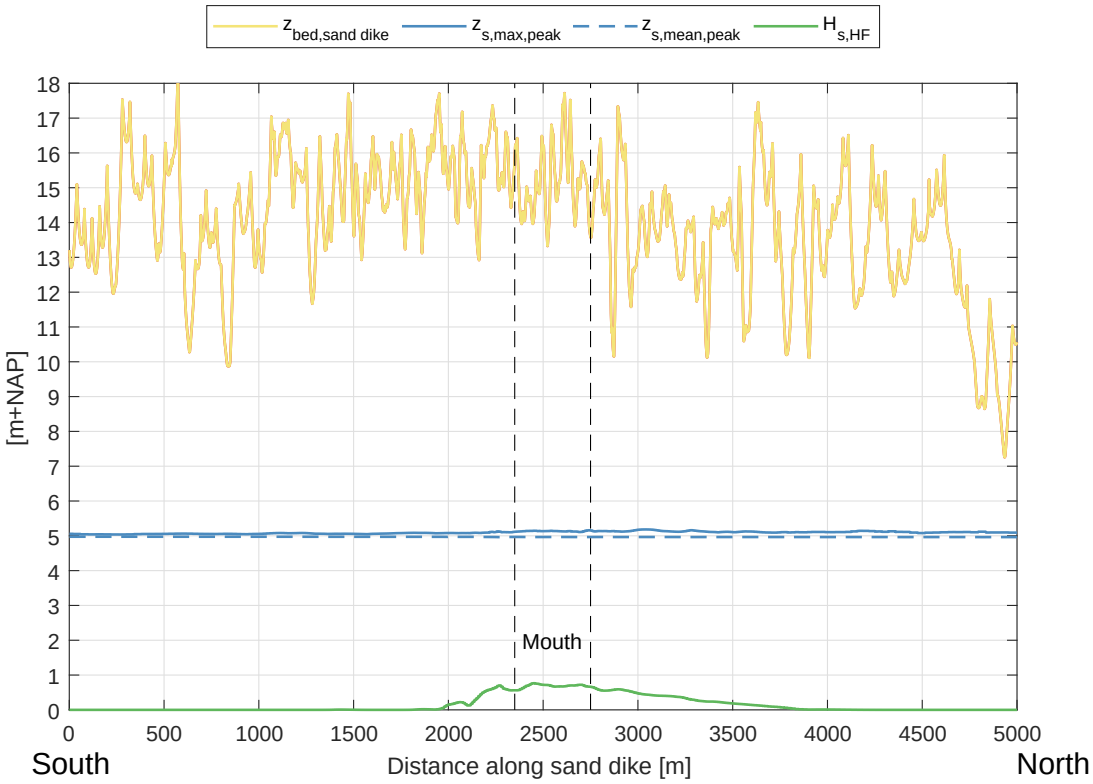

Figure 6.16: Height of the sand dike ridge compared to the maximum water level at the peak of the storm. No lowering of the ridge has taken place during the storm. The figure shows the maximum water level plus the short wave height near the sand dike during the storm peak.

For the assessment of the 'Initiation of flooding' criterium, the southwestern and northeastern edges of De Slufter are dominant. These edges are lower than the sand dike and are therefore more prone to overflowing due to the high SSL inside the slufter valley. To assess the potential overtopping and inundation of water, the minimum observed dune height in 2015 in these areas is compared to the maximum water level during the peak of the storm. The dune height in 2015 was chosen as it is as much in accordance with the model bathymetry as possible. Furthermore, no significant morphological changes in these areas are expected as they are rarely inundated.

A 2D map of maximum water levels in the valley during a 1/3000 year storm is presented in figure 6.17. Contrary to the mean water levels, maximum water levels during the storm are not uniformly distributed over the valley. This is caused by long wave energy propagating through the mouth into the valley. In the northeast of the northern valley the presence of the spatial variability of maximum water levels is caused by long waves reflecting from the steep sand dike. In the southern valley, the absence of maximum water level variability is caused by the dike that separates the northern and southern valley and which prevents long wave energy from propagating further. This difference in maximum water level means that the northern edge must be higher to be considered safe than the southern edge.

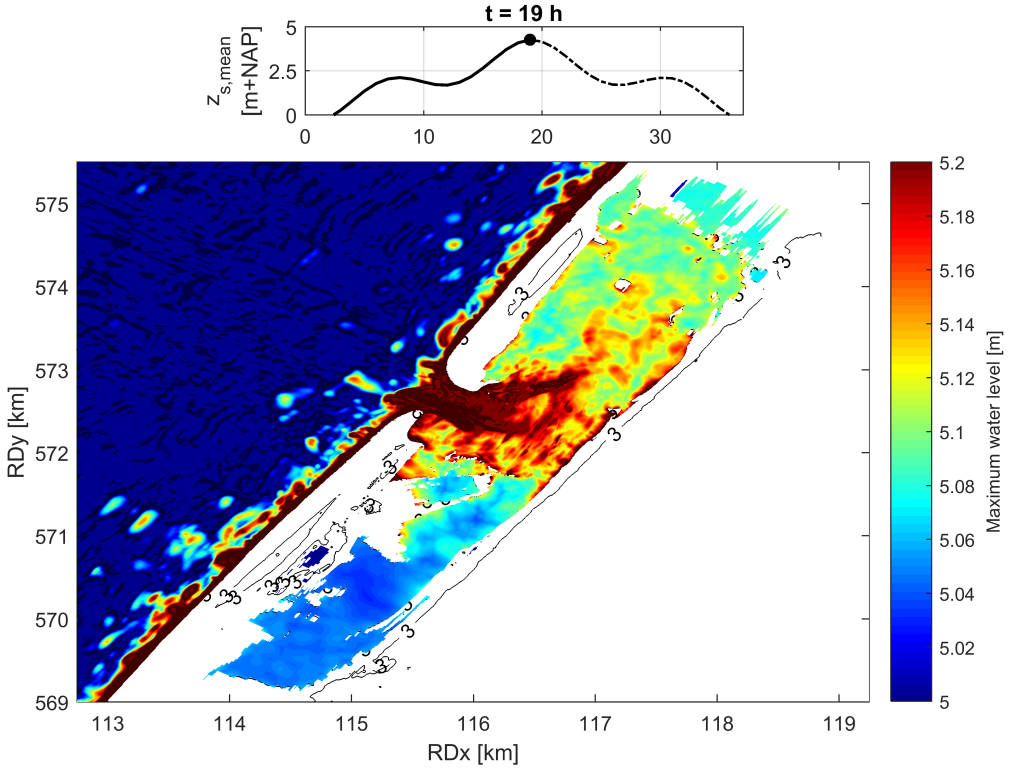

Figure 6.17: 2D plot of maximum water levels in De Slufter during the peak of a 1/3000 year storm. There is a striking difference between the northern valley and the southern valley in terms of maximum water level. This is mainly caused by long wave energy propagating through the slufter mouth.

Based on topographic data from 2015, the maximum possible bathymetry contour was determined for which a contiguous line was still present. Figure 6.18 shows the bathymetry contour 10 cm higher to properly visualise the weak spots in the ridge around De Slufter. From the figure it is deduced that overwash and even inundation over the ridge will occur when maximum water levels reach NAP+6.70 m or higher. The locations of these weak spots have been marked with red circles. As maximum water levels at the lateral edges do not exceed NAP+5.20 m for a 1/3000 year storm, no failure will occur.

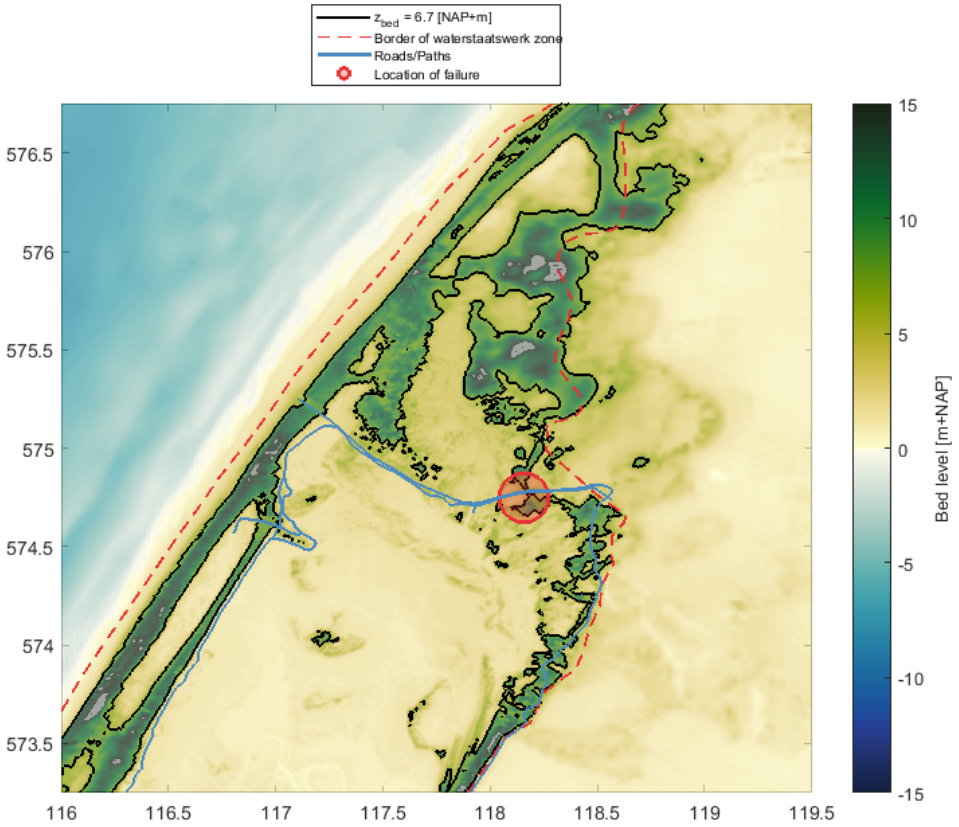

(a) Northern edge

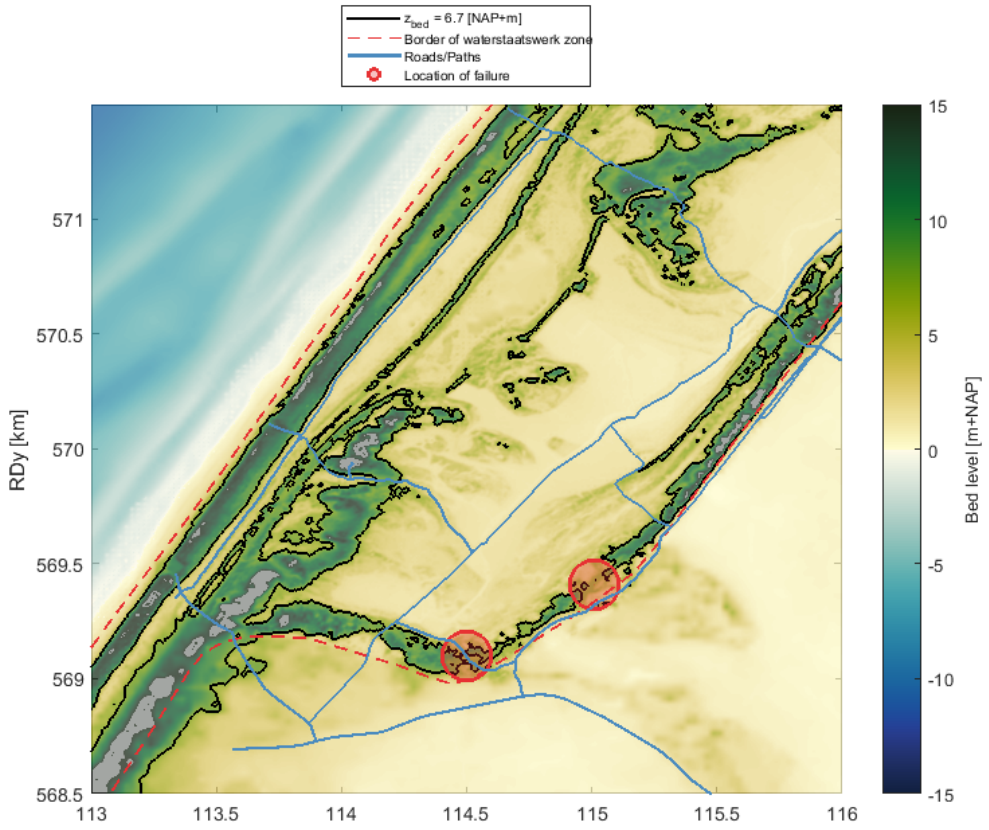

(b) Southern edge

Figure 6.18: 2D maps of the topography of the southwestern and northeastern edges of De Slufter. The bathymetry contours indicate the maximum contiguous sand dike ridge along the edges, based on the 2015 data. The red circles indicate the lowest locations along the ridge where overflow will occur when water levels rise high enough.

Conclusions

With present sea level conditions and its present bed configuration, water entering De Slufter through the mouth is contained to the slufter valley for a 1/3000 year storm. Based on the assessment of two failure mechanisms, 'Grensprofiel' and 'Initiation of flooding', De Slufter is thus capable of protecting Texel from flooding against a normative storm.

Only a relatively small amount of erosion takes place at the sand dike and at all locations alongshore the sand dike retains its maximum height. Also, the transect volume at any location along the sand dike does not fall below 173 m^3/m and all post-storm cross-shore sand dike profiles are large enough to fit in a 'limit profile'. Therefore, 'Grensprofiel' failure does not occur either. Wave overtopping over the sand dike does not take place.

To assess the occurrence of 'Initiation of flooding', the maximum water level at the sand dike during the peak of the storm was analysed. In the north, in which the sand dike height is lowest, the sand dike height is well above the maximum water level (more than 2m). No overtopping will thus occur. Furthermore, assuming negligible short wave action in the northeast and the southwest, the 'Initiation of flooding' criterion has been further assessed by comparing bathymetry contours with maximum water levels during the storm. A contiguous outer ring of bed levels higher than the maximum water level is present. Therefore, it is concluded that inundation will not take place. As there is also no long wave overtopping over the sand dike, 'Initiation of flooding' failure does not occur.

6.2.2. Wider mouths

Nr.	ID	Mouth	SLR [m]	BLR [m]	Storm	Wave Dir.
4	S0B1R3000_1NW	Reference	0	0	1/3000 year	NW
5	S0B2aR3000_1NW	800 m	0	0	1/3000 year	NW
6	S0B2bR3000_1NW	1000 m	0	0	1/3000 year	NW
7	S0B2cR3000_1NW	1250 m	0	0	1/3000 year	NW
8	S0B2dR3000_1NW	1500 m	0	0	1/3000 year	NW

Table 6.5: Overview of scenarios that were analysed for this subsection.

Spatially varying water level

The mean water levels in De Slufter during the peak of a 1/3000 year storm do not differ significantly for different widths of the slufter mouth. The only variations are found around the mouth itself, as areas that were covered by dune in the reference scenario have been flooded. However, these variations have no effect further landwards in the valley, as the water level near the sand dike does not change.

The valley does flood faster however, i.e. for a width of 1500 m the southern valley starts flooding at t = 6h instead of t = 9h (like in the reference scenario). The cause of this faster flooding is the increase in conveying cross-section due to the wider mouth. As the water levels in and around the mouth stay the same for the different scenarios a larger discharge of water can flow into the valley and fill it up quicker. This has no effect on the water levels during the peak of the storm however, as in all scenarios the valley has completely filled up before the peak of the storm is reached.

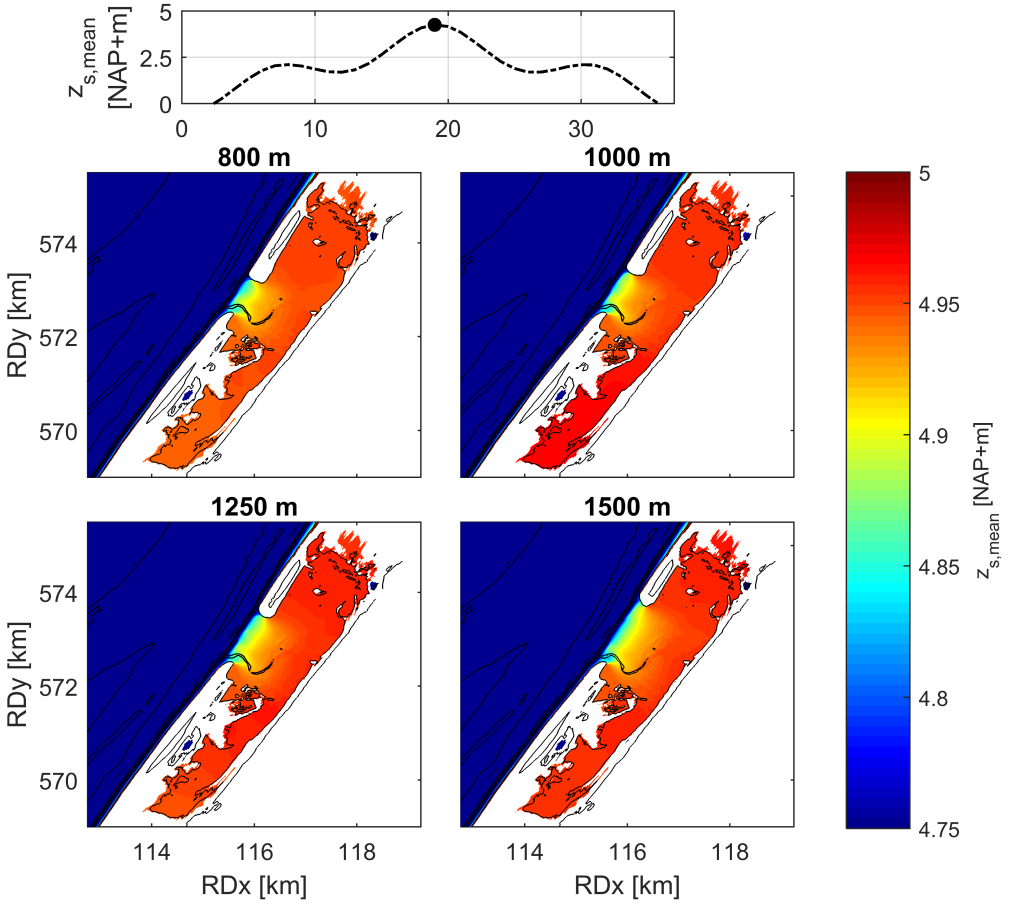

Figure 6.19: Water levels at the peak of a 1/3000 year storm for different widths of the slufter mouth. There is virtually no difference between the scenarios apart from the areas around the newly formed beach flat.

Wave attack

As the slufter mouth becomes wider, wave energy is allowed to spread out and reach a wider area of the sand dike. However, compared to the reference scenario, the maximum short wave height along the sand dike does not significantly increase in case of a wider mouth, see figure 6.20. For both the reference scenario and the 1500m wide mouth scenario, the maximum short wave height along the sand dike is approximately 1m.

These results do not agree with the earlier study by Van Rooijen and Van Thiel de Vries (2014) in which a significant increase in short wave attack on the sand dike was identified for a wider mouth. This difference is mainly a result of a difference in bathymetry configuration, in which Van Rooijen and Van Thiel de Vries (2014) assumed the bed level of the newly formed beach flat to be lower (≈NAP+0 m) than the present beach flat. In this study however, the newly formed beach flat height is assumed to be equal to the present beach flat height, which is approximately NAP+1.25 m. Consequently, wave dissipation due to depth induced breaking as well as wave and bottom friction remain approximately the same for the wider mouths in the present study.

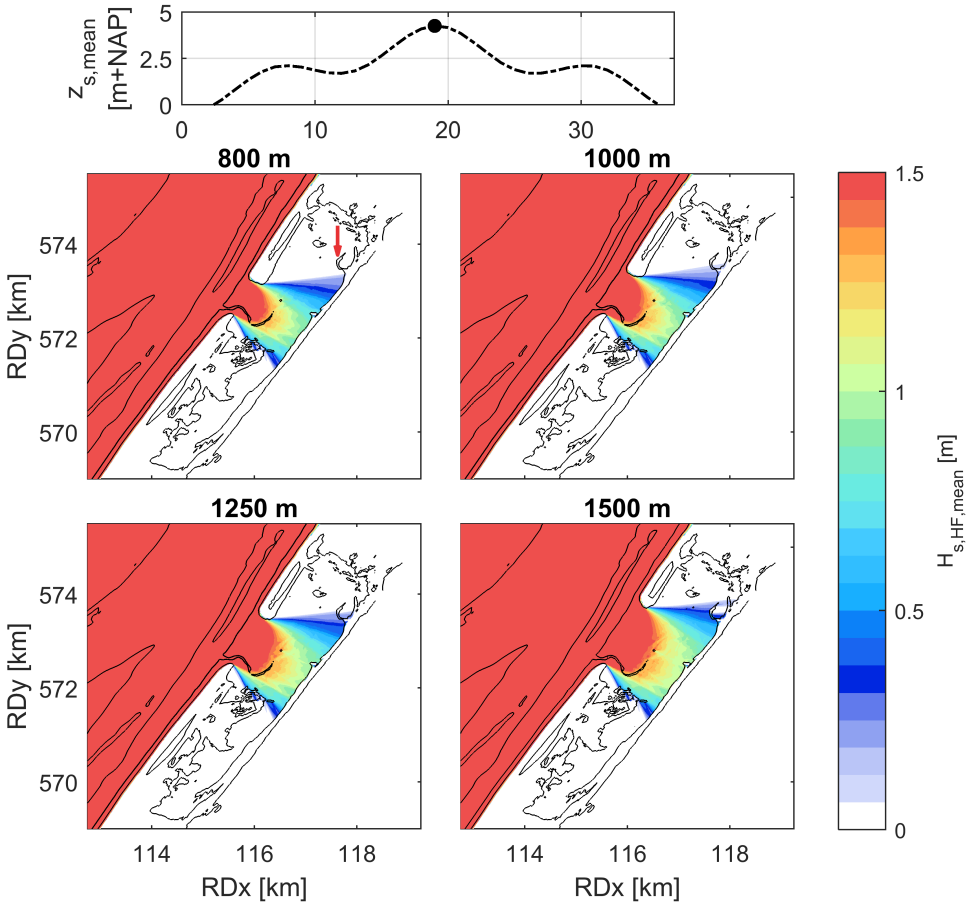

Figure 6.20: Short wave height during the peak of a 1/3000 year storm for different assumed widths of the slufter mouth.

Figure 6.21 shows that, while the maximum short wave height along the sand dike does not significantly change for different widths, the alongshore distribution does. In area A (area of the sand in front of the mouth in the reference scenario) short wave heights are approximately equal for all scenarios. In area B a correlation between width and short wave height is already starting to become visible and in areas C-E a clear correlation can be distinguished.

The short wave height distribution of the 1500 m scenario shows a sudden drop at approximately $x = 4600 - 4700$ m. This drop is caused by a mound blocking the propagation of wave energy, as seen in figure 6.20 (upper left panel, indicated with the red arrow). The peak at $x = 4800$ m is thus only the resumption of the undisturbed wave alongshore wave height.

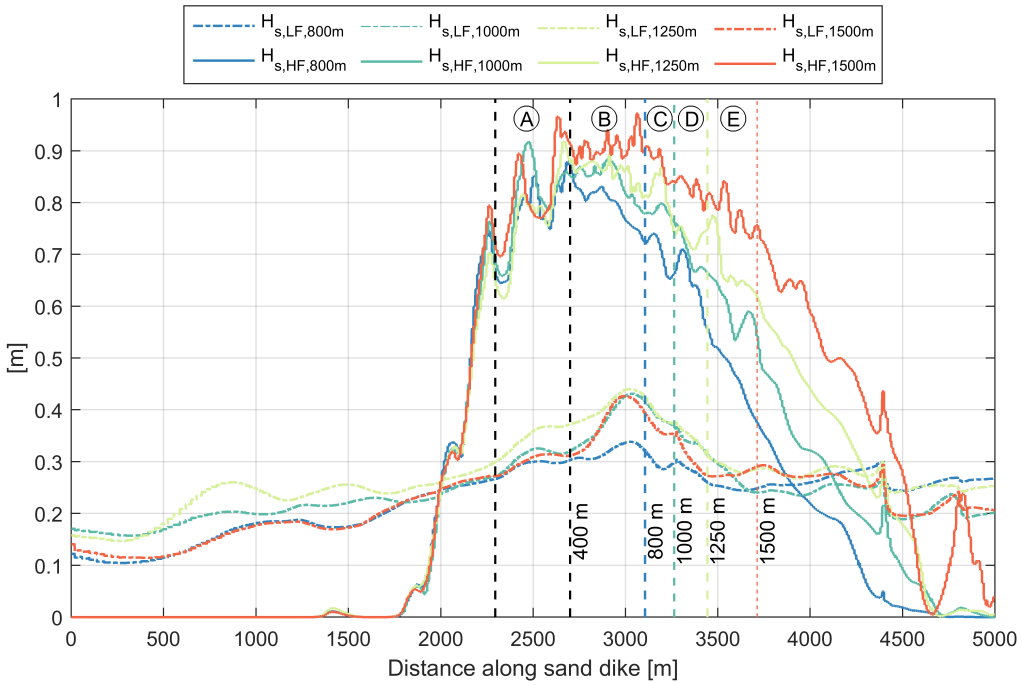

Figure 6.21: Short (solid lines) and long (dash-dot lines) wave height at the sand dike during the peak of a 1/3000 year storm for different widths of the slufter mouth. The long wave height was calculated with $H_{s,LF} = \sqrt{2} * \sqrt{8 * |z_{s,var}|}$.

There seems to be no significant correlation between long wave height and width of the mouth. As water levels are near equal for wider mouth scenarios this could be caused by the randomness of the forcing. However, a clear explanation cannot be given.

Sand dike erosion

As stated earlier, mean water levels and maximum wave heights in De Slufter do not vary significantly for different widths of the mouth. However, a wider mouth does lead to a larger area of the sand dike being attacked (figure 6.20) and, consequently, higher short wave heights in the northeastern part of De Slufter.

Dune erosion along the sand dike for the different widths is plotted in figure 6.22. The striped vertical lines indicate which parts of the sand dike are directly in front of the mouth for different widths. The alongshore erosion shows behaviour similar to the alongshore short wave height: similar erosion volumes in area A, a weak correlation between mouth width and erosion volume in area B and a strong correlation in area C-E and beyond.

The figure shows that erosion volumes in area B are twice as high for the wider mouth scenarios as for the reference scenario. The erosion volumes are still relatively small however. The peak erosion volume is caused by the shape of the profile there. A small duneform is present in front of the sand dike which is almost fully inundated during the peak of the storm. Larger erosion volumes, which are a result of overwash processes, are thus included in the calculation due to the NAP+3m limit. Figure 6.23 shows the pre- and post storm profiles of this transect. Due to the duneform, the sand dike itself remains relatively unaffected. The transect of maximum erosion has been presented in figure 6.23. The shape of the sand dike profile is also the reason that the overall erosion increases from $x = 2700m$ to $x = 3400m$. The individual spikes in erosion north of $x = 3400m$ are also caused by the smaller duneforms in front the sand dike.

Figures 6.21 and 6.22 show that the alongshore distribution of sand dike erosion is strongly correlated to the alongshore distribution of short wave height at the sand dike. There is no clear correlation between mouth width and long wave height (see figure 6.21) and mean water levels along the sand dike are practically equal for different widths (see figure 6.25). This means that the short wave height increase as a result of the wider area of wave attack is the main reason for the difference in dune erosion between the scenarios.

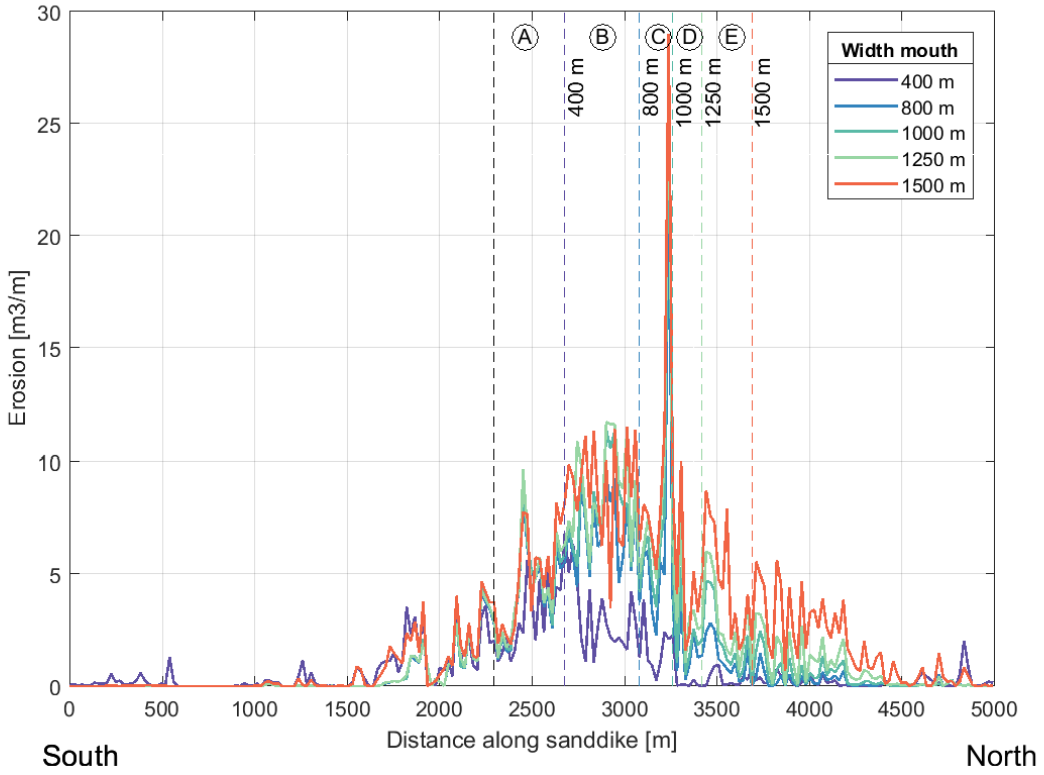

Figure 6.22: Erosion along the sanddike for a 1/3000 year storm for different widths of the slufter mouth. The vertical striped lines indicate the locations of the southern (most leftward) and northern boundary of the mouth for the different scenarios. The isolated peaks are caused by the dune shape in that location, as already explained in figure 6.9.

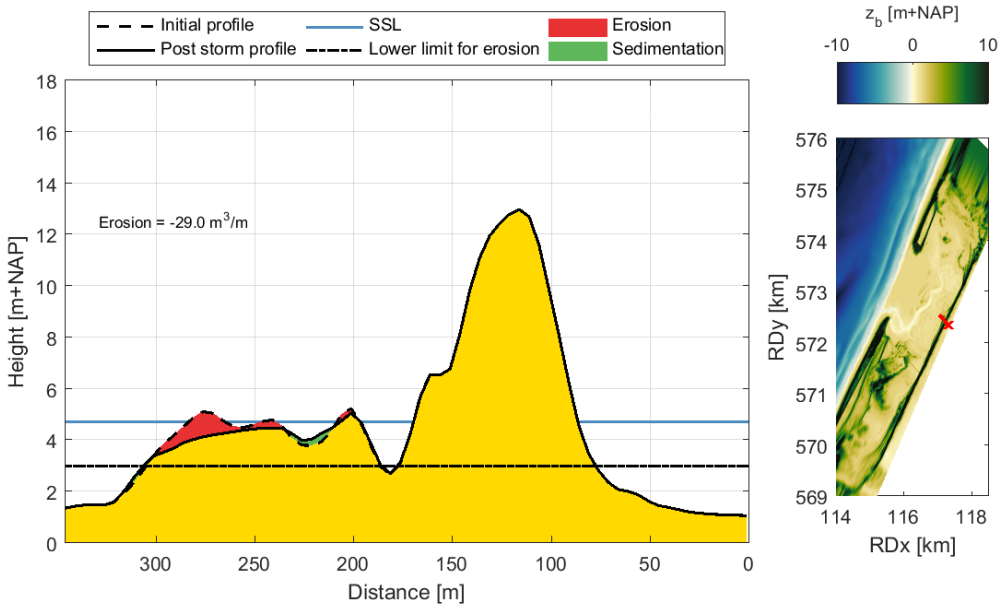

Figure 6.23: Sand dike transect showing the location of maximum erosion for the wider mouth scenarios at x = 3200m.

Failure mechanisms

The failure assessment for the wider mouths is performed in the same manner as for the reference scenario. The results are summarized in this subsection.

Grensprofiel - Table 6.6 shows that (over all scenarios) the lowest minimum transect volume above SSL, which occurs for the 1500m wide mouth scenario, is $118 m^3/m$. Therefore, based on the 'Grensprofiel' criterium, failure does not occur for any of the wider mouth scenarios. A clear downward trend is visible in the minimum volume between the scenarios. As the mean water levels are practically equal, the difference in minimum transect volume between the different scenarios is caused by an increase in sand dike erosion and not by an increase in SSL. This is in agreement with the results in figure 6.22. The location of minimum volume is equal to the reference scenario.

Width [m]	**max. SSL** [m+NAP]	$z_{s,max,north}$ [m+NAP]	$z_{s,max,south}$ [m+NAP]	**Min. volume** [m^3/m]
400	4.95	5.15	5.06	173
800	4.95	5.17	5.05	151
1000	4.95	5.15	5.10	131
1250	4.95	5.13	5.07	124
1500	4.95	5.15	5.07	118

Table 6.6: Minimum transect volume for different widths of the slufter mouth. All minimum volumes were located in the same place as in figure 6.14.

In figure 6.24 two cross-shore sand dike profiles have been visualised with the associated limit profile. The figure shows that the profile at which maximum erosion occurs and the profile with the minimum transect volume both do not fail. Furthermore, no 'Grensprofiel' failure occurs in any of the transects along the sand dike.

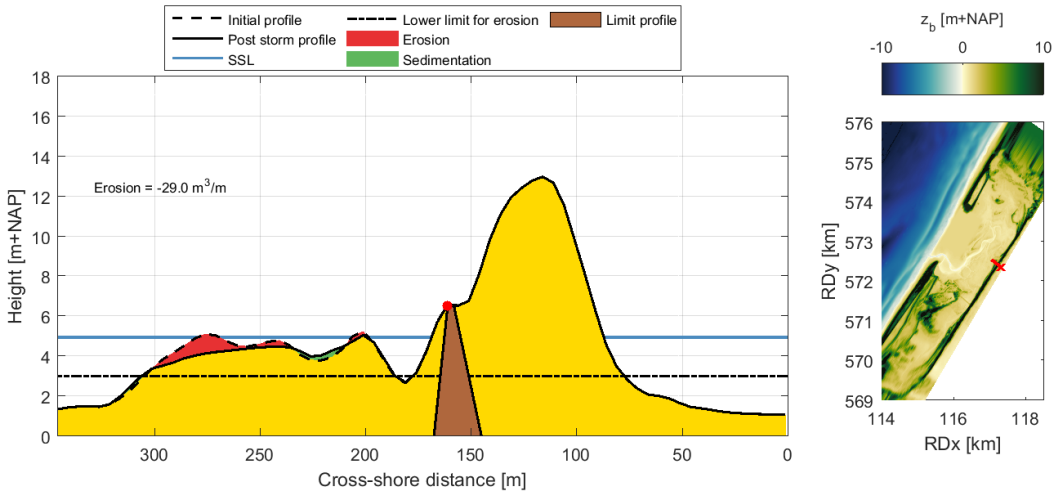

(a) Maximum erosion transect

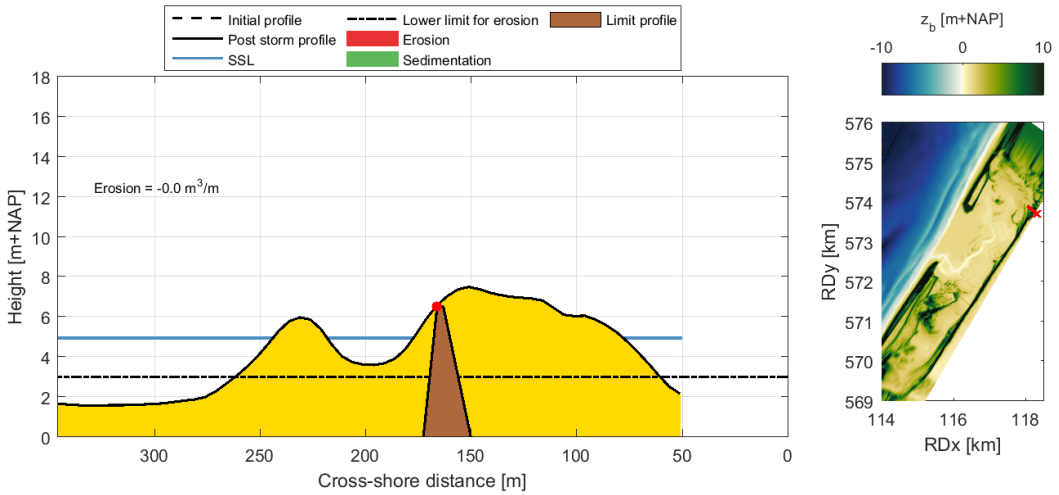

(b) Minimum volume transect

Figure 6.24: 'Grensprofiel assessment concerning the limit profile for the 1500m wide mouth scenario.

Initiation of flooding - Figure 6.25 shows that, even when the front dune row has almost disappeared, maximum water levels along the sand dike stay well below the sand dike height. No overtopping is therefore expected to occur. Just as in the reference scenario the highest deviation of the maximum water level from the mean water level is located in front of the mouth where the sand dike height is at least NAP+10 m (at approximately $x = 2700m - 3300m$).

The more southern and northern part of the sand dike in figure 6.25 show that the maximum water level does not trend with the wider mouths.

While the difference is small, there is still a slight difference in maximum water levels at the southwestern and northeastern edges of the valley compared to those of the reference scenario. These maximum water levels are presented in table 6.6. Based on the topography in figure 6.18 no overtopping or inundation will take place and 'Initiation of flooding' failure will not occur.

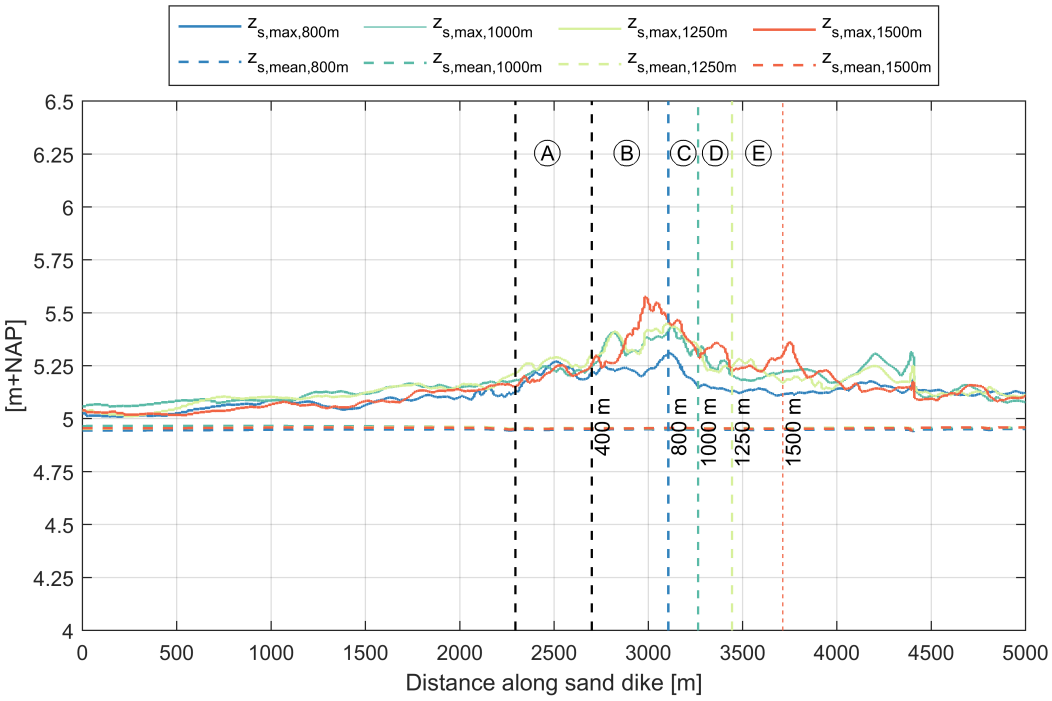

(a) Mean and maximum water level

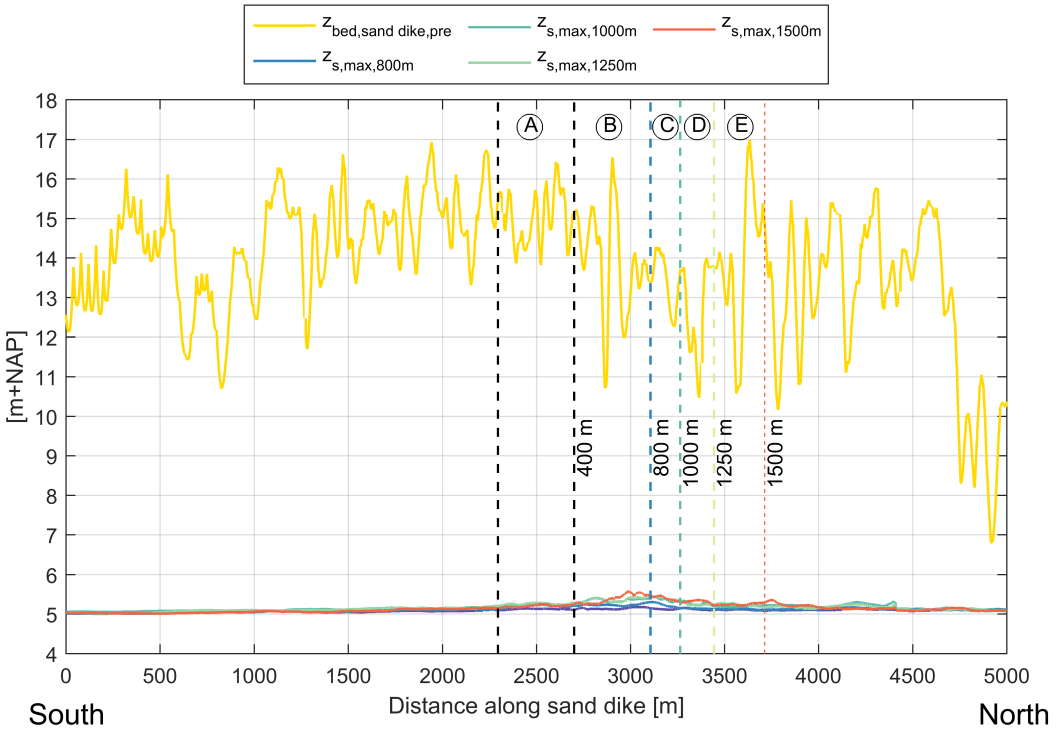

(b) Sand dike height and maximum water level.

Figure 6.25: Height of the sand dike ridge compared to maximum water level and mean water level compared to maximum water level during the peak of a 1/3000 year storm. The different colors represent scenarios with different widths of the slufter mouth. No lowering of the ridge has taken place during the storm and the post-storm height has thus not been plotted.

6.2.3. Second mouth

Nr.	ID	Mouth config.	SLR [m]	BLR [m]	Storm	Wave Dir.
4	S0B1R3000_1NW	Reference	0	0	1/3000 year	NW
8	S0B2dR3000_1NW	1500 m	0	0	1/3000 year	NW
9	S0B3R3000_1NW	2 mouths	0	0	1/3000 year	NW

Table 6.7: Overview of scenarios that were analysed for this subsection. See figure 6.1 for the bathymetry configurations.

Spatially varying water level

The 2D water level distribution for two mouths during the storm peak is the same as for the reference scenario or for the wider mouth scenarios. Due to the second mouth the valley does fill up quicker though, as also seen for the wider mouths. As in the wider mouth scenarios this is caused by a higher discharge into the valley as a result of an increase in conveying cross-section.

Wave attack

Apart from differences in the area around the newly formed mouth, the water depth in the valley at the peak of the storm is very similar to that of the reference scenario and the wider mouth scenarios. Wave dissipation in the valley is thus also similar. Therefore, as expected, short wave height development for both mouths is similar to that of the reference scenario.

Short waves from the second mouth are now also attacking the northern edge of De Slufter, which is generally lower than the sand dike. However, the largest short wave height in this area is only approximately 0.3m.

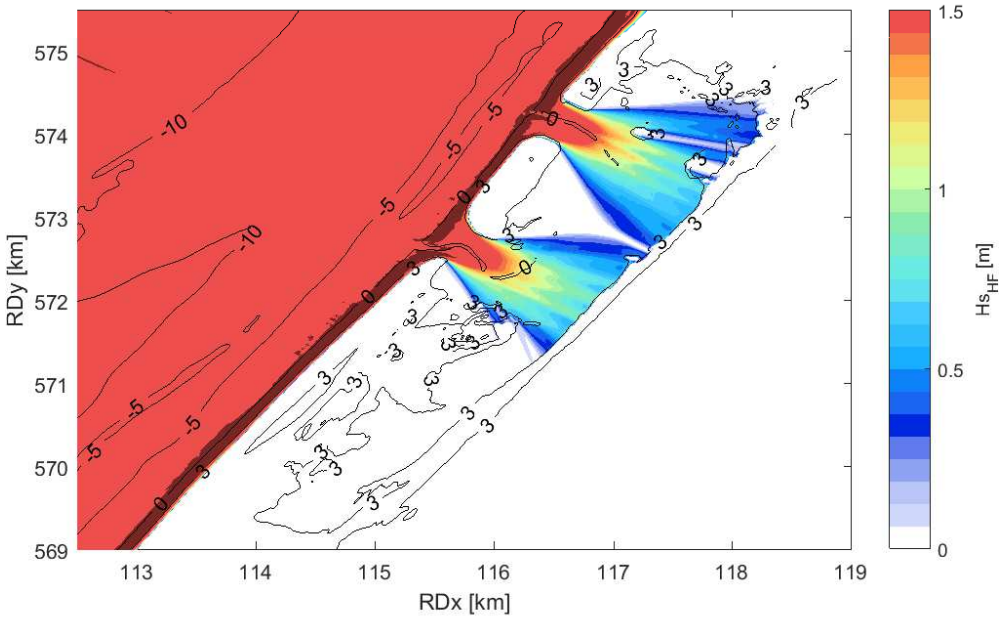

Figure 6.26: Short wave height during the peak of a 1/3000 year storm for a second mouth

The alongshore wave height distribution shown in figure 6.27 compares the reference, 1500m wide mouth and second mouth scenario. In area A (the area in front of the mouth for the reference scenario) the wave heights do not differ significantly for the reference and the second mouth scenario, as expected. Maximum wave heights range from 0.75 m for the reference scenario to 0.85 m for the second mouth scenario. However, the difference between the two is attributed to the variability that is present due to the randomness of the offshore forcing. This is substantiated by the fact that in area A the wave heights in the second mouth scenario are not constantly larger than those in the reference scenario. Wave heights in the 1500m wide mouth scenario are slightly larger, as already treated in section 6.2.3.

In area B, the wave heights for the 1500m wide mouth scenario are significantly higher than the rest. Furthermore, in all three scenarios a downward trend in short wave height is visible, caused by the spreading of wave energy (see figure 6.26).

In area C, the area in front of the second mouth, the short wave height for the second mouth scenario is higher than for the wider mouth, as expected. While the 2D distribution of short wave height was very similar for both mouths, figure 6.27 shows that the wave heights in front of the northern mouth are actually lower than in front of the southern mouth. This is caused by the fact that the bed level in this area is slightly higher than further south, which thus leads to a smaller water depth and more wave dissipation. The dips seen for both scenarios between $x = 4500m$ and $x = 5000m$ are again caused by the mounds there which block the propagation of wave energy, as also explained in subsection 6.2.2.

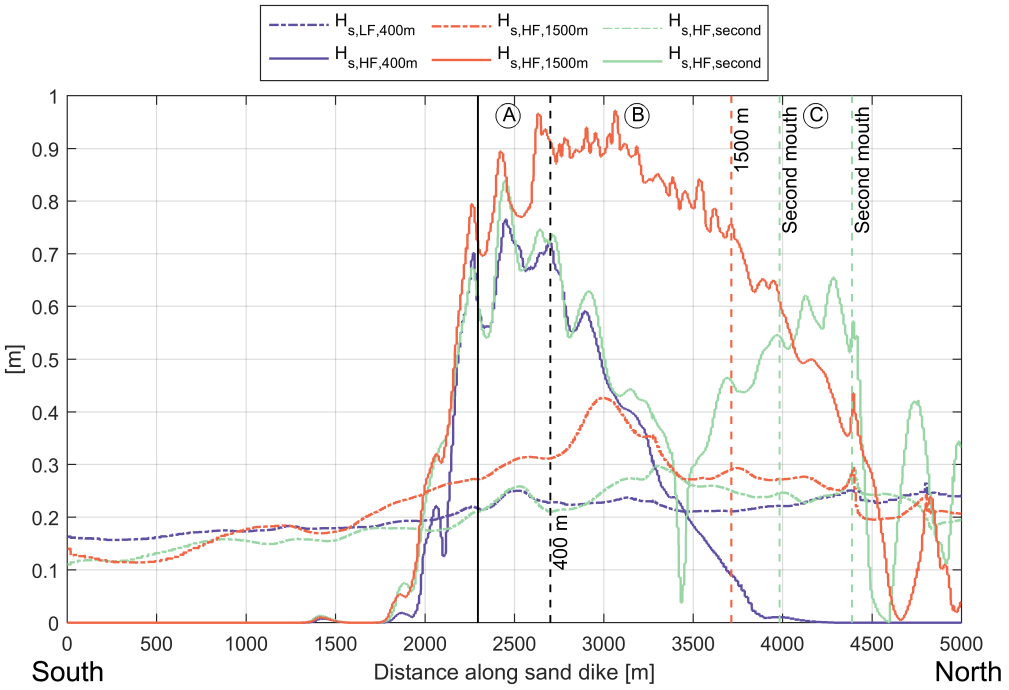

Figure 6.27: Short (solid lines) and long (dash-dot lines) wave height at the sand dike during the peak of a 1/3000 year storm for different configurations of the slufter mouth (reference, 1500m wide mouth, second mouth). The long wave height was calculated with $H_{s,LF} = sqrt(2) * sqrt(8 * abs(z_{s,var}))$.

In terms of long waves, the same difference is noticed for the second mouth scenario: higher long wave height in front of the wider mouth scenario but no trends in the north and south.

Dune erosion

Figure 6.28 shows that sand dike erosion in a scenario with 2 mouths (green line) is smaller than in a scenario with one 1500m wide mouth (red line). However, similar to figure 6.22, in areas where the sand dike is under equal wave attack for all scenarios the erosion is similar. The area of the sand dike that is in front of the northern mouth is not in front of the 1500m wide mouth (see the green and red lines in figure 6.28). As expected, the erosion there is slightly larger for the second mouth scenario.

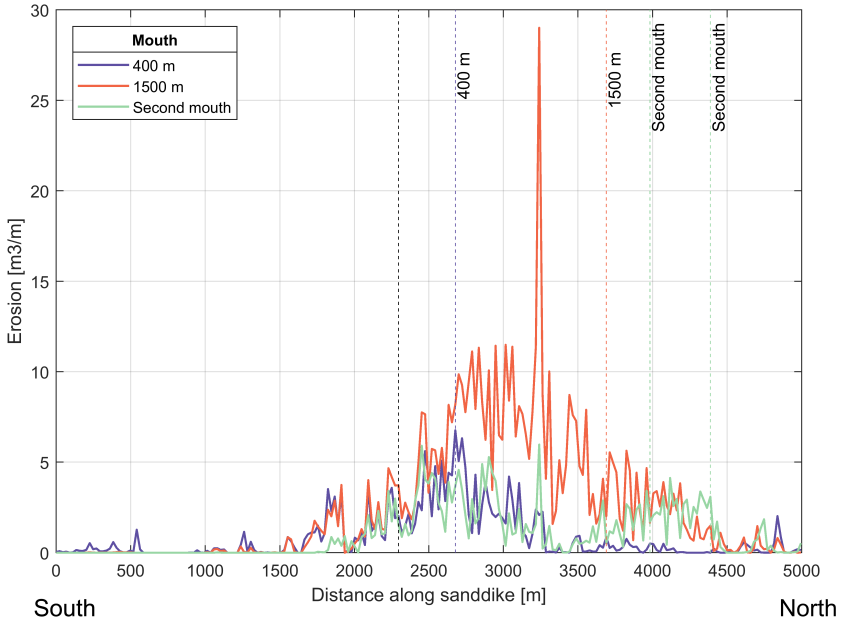

Figure 6.28: Erosion along the sand dike for a 1/3000 year storm for a second mouth. The vertical striped lines indicate the locations of the southern and northern boundaries of the mouth(s). The black striped line indicates the southern boundary of both the 400 m and 1500 m wide mouth. The isolated erosion peaks are caused by the cross-shore shape of the dune there, as explained in subsection 6.2.1.

Failure mechanisms

Grensprofiel - The minimum transect volume along the sand dike is at least 184 m^3/m as is clear from figure 6.29. This is a higher volume than for the reference scenario which is remarkable as there is more wave attack there for the second mouth. The increase is expected to be caused by smoothing of the model bathymetry which was necessary for numerical stability after the manual creation of the second mouth.

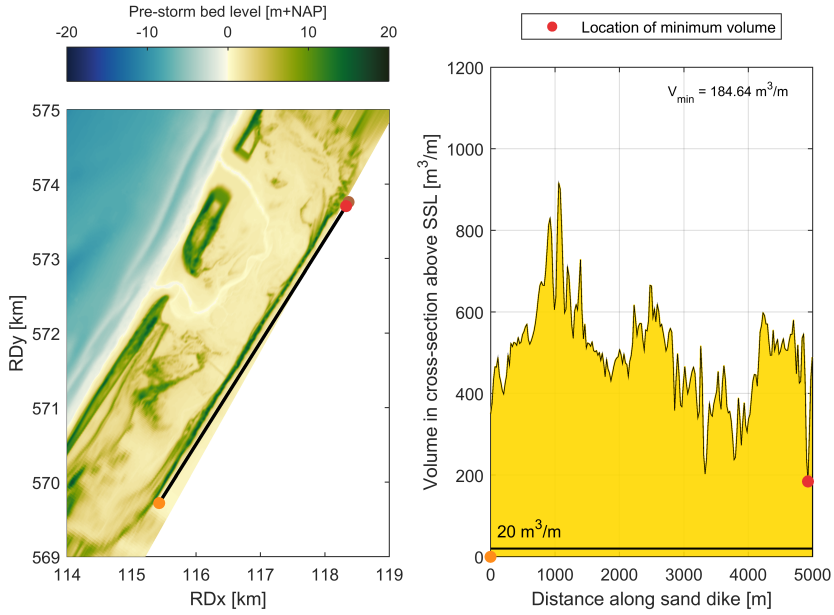

Figure 6.29: Volume in transect above SSL for a 1/3000 year storm with a second mouth.

Initiation of flooding - Figure 6.30 shows that for the second mouth scenario no overtopping will occur over the sand dike as the maximum water levels stay well below the sand dike level. In the area directly in front of the second mouth the maximum water level at the sand dike is equal or greater than for the 1500m wide mouth.

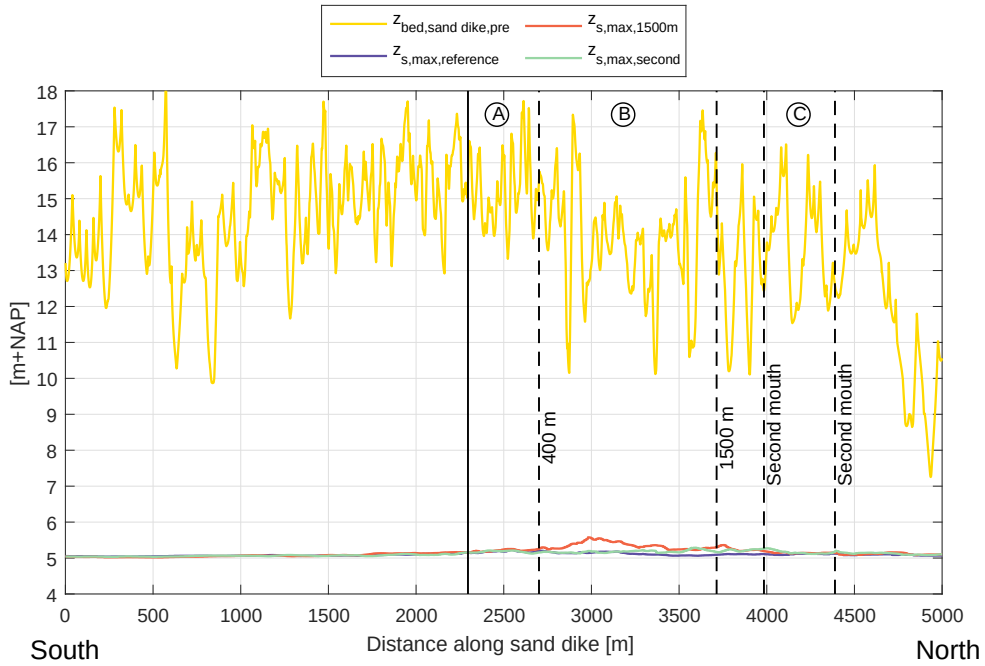

Figure 6.30: Height of the sand dike ridge and maximum water levels for scenarios with different mouth configurations. No lowering of the ridge has taken place during the storm.

6.2.4. Consecutive storm events

After assessing the coastal safety for a normative storm event of 1/3000 years it is also important to assess the cumulative effect of a series of storms. As evident from figure 6.31 most of the erosion along the sand dike occurs during the first storm. In the consecutive storms additional erosion takes place in front of the mouth. No significant additional erosion takes place further north or south however. This behaviour is in agreement with section 2.1.2. Each storm event shapes the dune and sand dike profiles closer to the equilibrium profile. This decreases the relative effect of processes such as dune avalanching and wave impact on the dune face due to wave uprush in later storms.

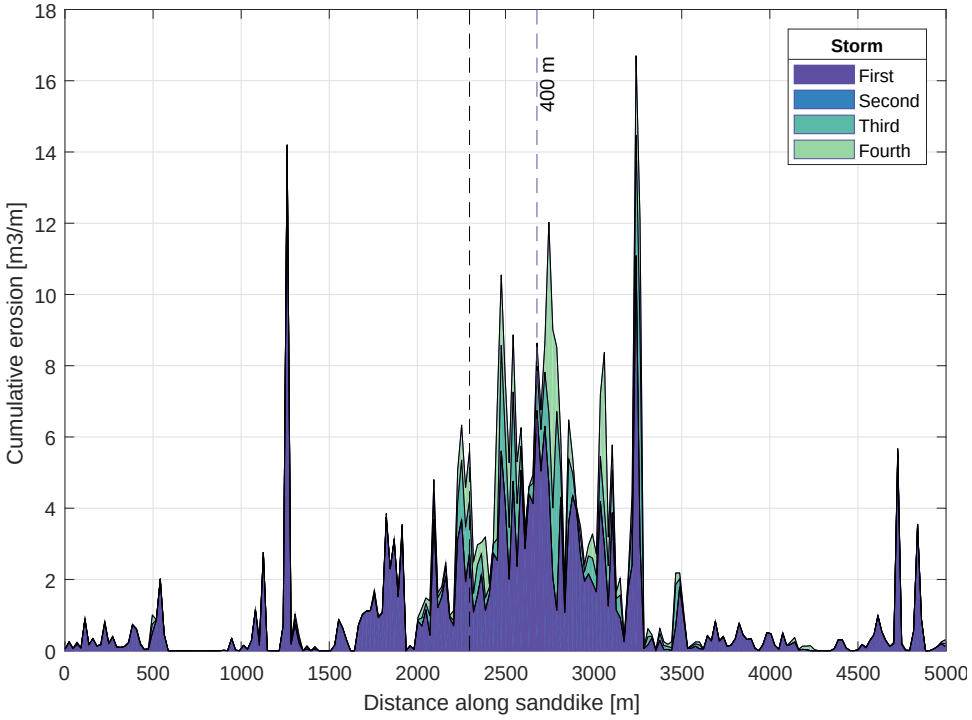

Figure 6.31: Cumulative erosion along sand dike for 1,2,3 and 4 1/3000 year storms.

The significant decrease of erosion seen in figure 6.31 is quantified in figure 6.32. For a 1/3000 year storm the erosion during the second storm is only 35% of the erosion during the first storm. By the fourth storm it is only 25%.

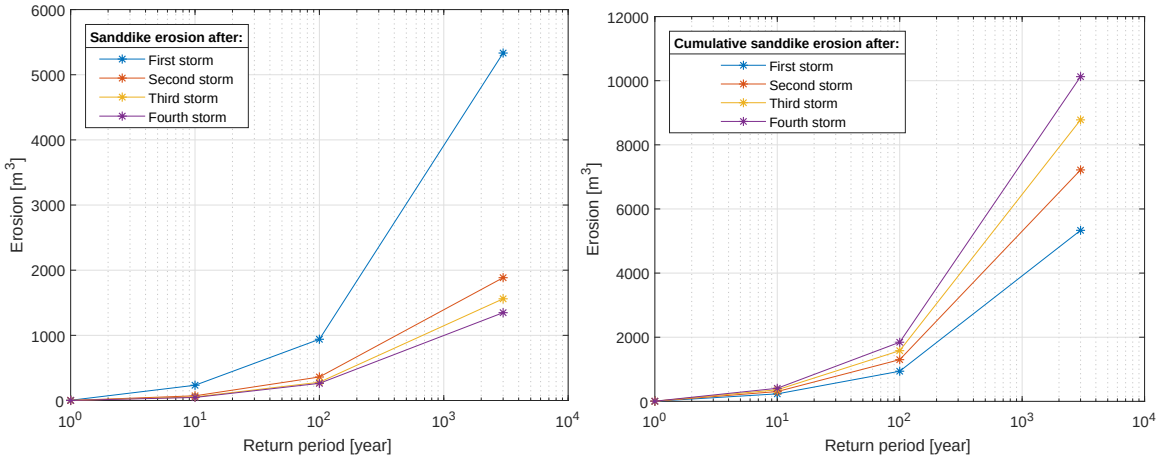

(a) Stepwise (b) Cumulative

Figure 6.32: Total sanddike erosion for series of storms with return periods of 1, 10, 100 and 3000 years. The left panel shows sand dike erosion per individual storm event. The right panel shows the cumulative sand dike erosion after each consecutive storm event.

6.3. Future coastal safety

In this section, future coastal safety is assessed by modelling possible scenarios for the year 2100. No probability of a scenario is assumed. Instead, a broad range of scenarios is analysed to draw conclusions on the limits of possibilities. In subsection 6.3.1 the effect of SLR is assessed for scenarios without BLR. In subsection 6.3.2 the effect of SLR is assessed for scenarios with BLR.

6.3.1. 1/3000 year storm, without bed level rise

Nr.	ID	Mouth	SLR [m]	BLR [m]	Storm	Wave Dir.
4	S0B1R3000_1NW	Reference	0	0	1/3000 year	NW
10	S1B1R3000_1NW	Reference	0.75	0	1/3000 year	NW
17	S2B1R3000_1NW	Reference	1.95	0	1/3000 year	NW
24	S3B1R3000_1NW	Reference	3.17	0	1/3000 year	NW

Table 6.8: Overview of scenarios that were analysed for this subsection.

Water levels

Figure 6.33 shows that the water level head between the valley and the offshore boundary is still present in the SLR scenarios. The magnitude of the water level head does decrease however as is evident from figure 6.34. Due to increasing water depths, there is less wave energy dissipation in De Slufter, leading to a smaller negative radiation stress gradient and subsequently a smaller positive water level gradient. This behaviour is not recognized in the SLR = 3.17 m scenario. This is because, at the peak of the storm, large quantities of water are flowing out through the southwestern and northeastern edges of De Slufter, lowering the water level in the valley. This is evident from the water level gradient which is visible in the southwest of De Slufter for SLR = 3.17 in figure 6.33. The overflow of water that causes the gradient can be seen east of the sand dike (dark blue patch). Overflow of water has also occurred in the SLR = 1.95 scenario in the southwest.

Figure 6.33 shows that the southwestern and northeastern edges of De Slufter are weak spots in the coastal defence. Water that flows over these edges will flow directly into Texel (see figure 1.4).

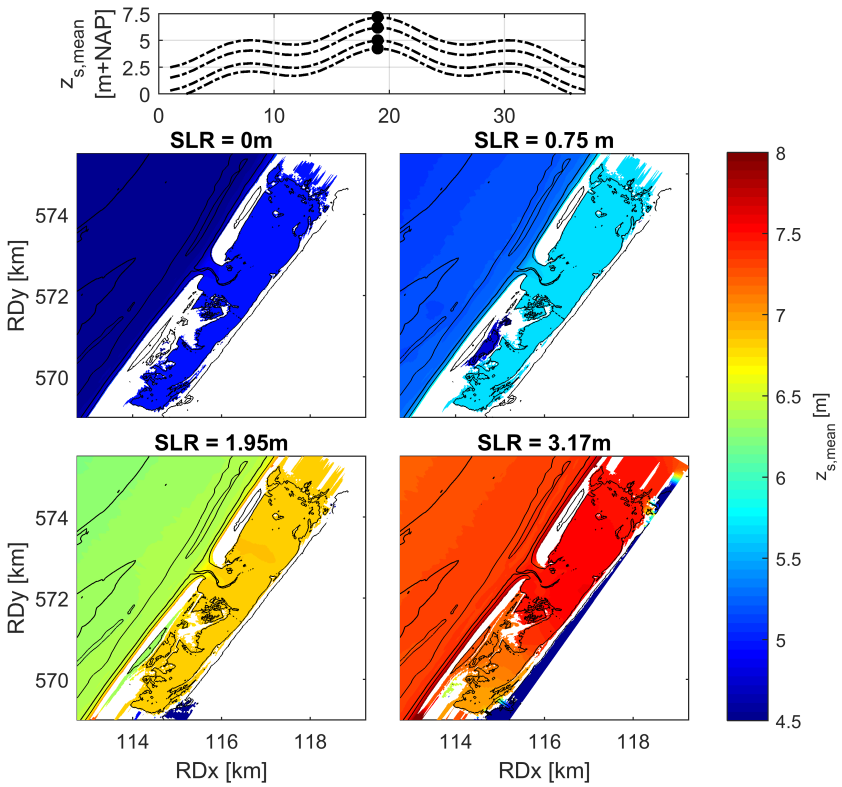

Figure 6.33: Mean water levels in De Slufter for different SLR scenarios.

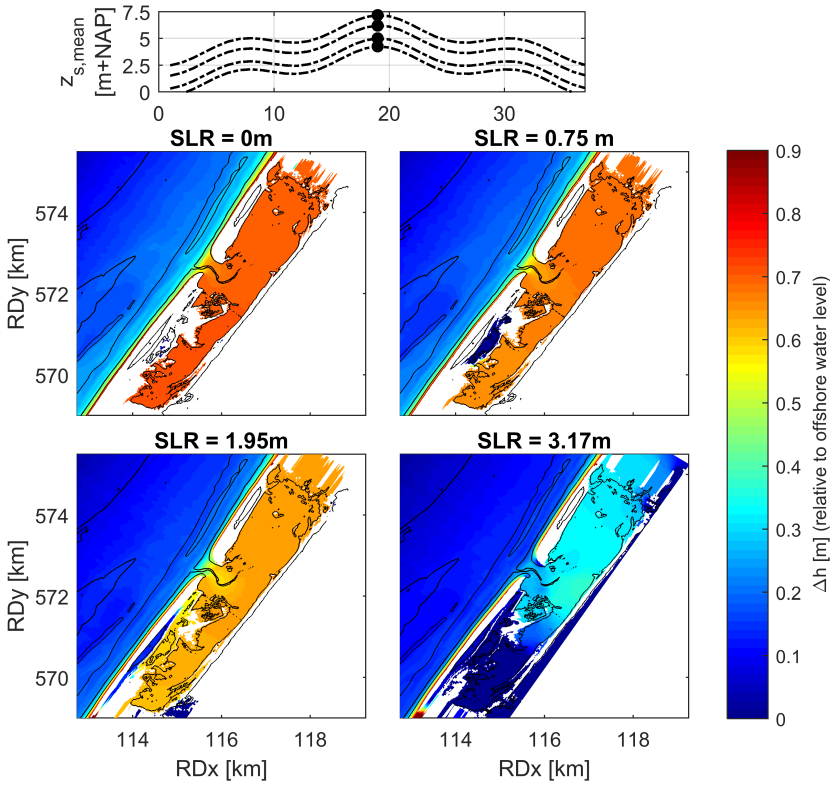

Figure 6.34: 2D maps of mean water level head relative to the mean water level at the offshore boundary.

Wave attack

From the offshore boundary to approximately $x = 3500m$, there is no correlation between SLR magnitude and short wave height, see figure 6.35. Waves do not break yet in that area. After $x = 3500m$ however, waves start breaking and the short wave height becomes depth limited. Apart from wave breaking, which is the dominant factor, the effects of wave and bottom friction also increase for shallower water, leading to an even stronger correlation.

The strong depth dependence of short wave height means that the influence of the offshore wave height on the wave height in De Slufter is not that significant. The water level is of great significance however. A higher water level, and a subsequent greater water depth, leads to an immediate increase in short wave height, as evident from $x = 3500m$ to $x = 8500m$ in the top left panel of figure 6.35.

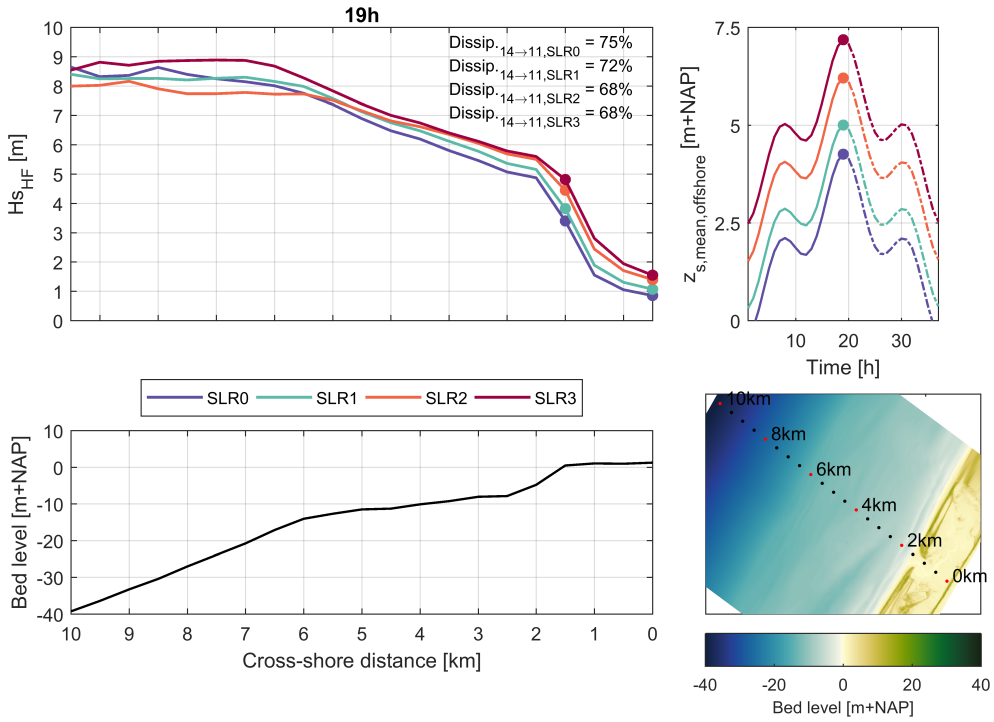

Figure 6.35: 1D transects of mean short wave height development during the peak of a 1/3000 year storm for different SLR scenarios. The top left graph starts at the offshore boundary (left) and ends at the sand dike (right).

Due to SLR the short wave height in the valley thus increases and more wave energy is allowed to enter De Slufter, as shown in figure 6.36. For the lowest SLR scenario the significant short wave height near the sand dike rises with 20cm to 107cm. For the most extreme SLR scenario it rises with 69cm to 155cm.

The spreading of short wave energy is practically the same in the SLR = 3.17 m scenario as it is in the reference scenario (apart from the increased spreading southward, due to wave energy capable of propagating over the inundated sand dike there). As seen in figure 6.37 however, the maximum wave height does increase. This is the most important consequence of SLR on short wave action and also the major difference between the effects of wider mouths and the effects of SLR. Wider mouths lead to a larger spreading of wave attack and SLR leads to higher maximum wave heights at the sand dike.

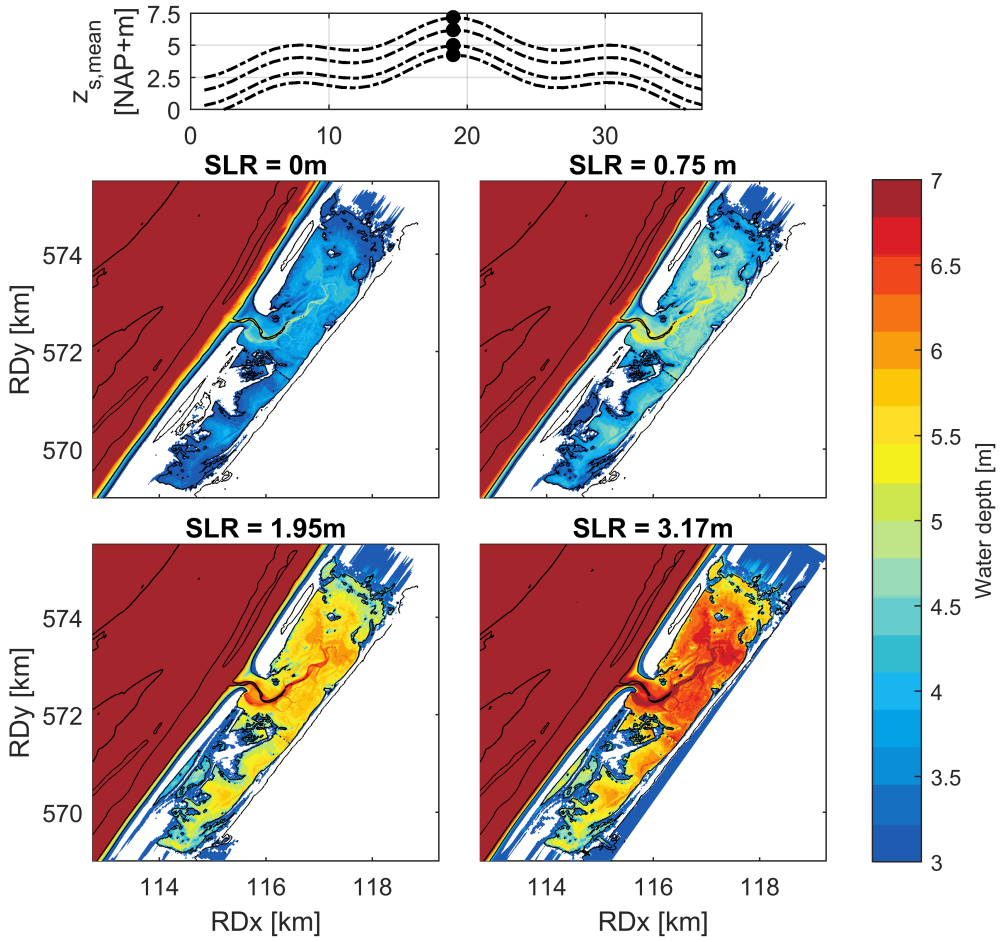

(a) Water depth

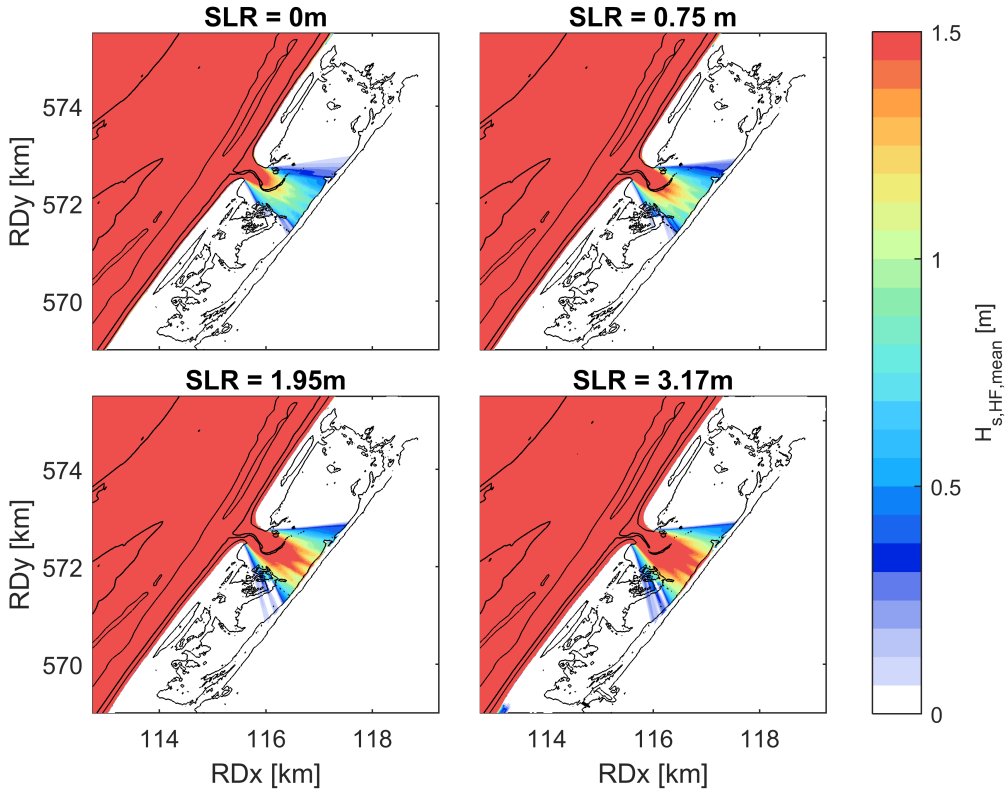

(b) Short wave height

Figure 6.36: Water depth and short wave height during the peak of a 1/3000 year storm for different SLR scenarios without BLR.

Contrary to short wave height, long wave height remains relatively constant in front of the mouth at the sand dike for different SLR scenarios (≈15-25cm), see figure 6.37. Further to the north and south long wave heights decrease as sea level rises. This inverse correlation between water level and long wave height is caused by increasing water depths in De Slufter, leading to less shoaling.

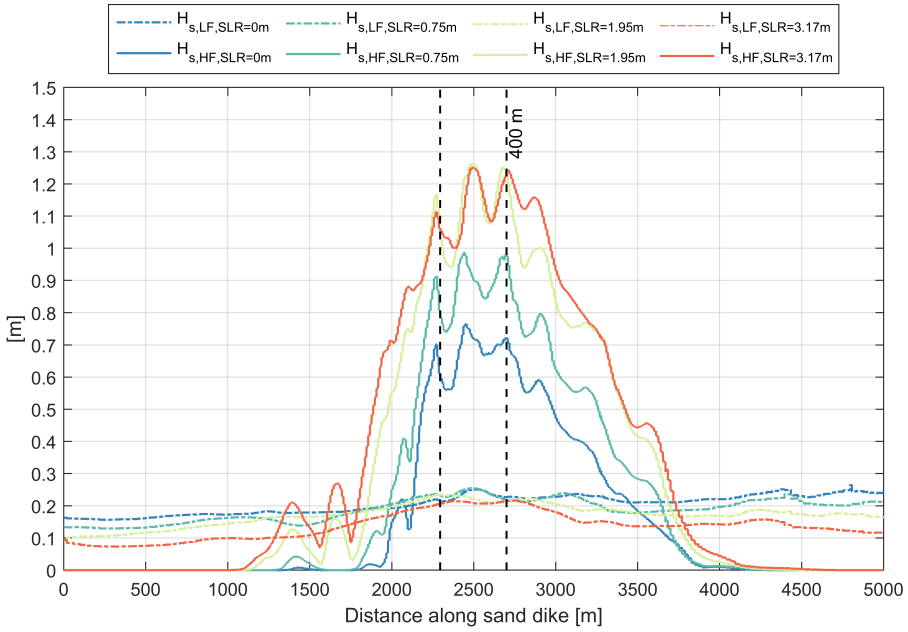

Figure 6.37: Short (solid lines) and long (dash-dot lines) wave height at the sand dike during the peak of a 1/3000 year storm for different SLR scenarios. The long wave height was calculated with $H_{s,LF} = sqrt(2) * sqrt(8 * abs(z_{s,var}))$.

Dune and sand dike erosion

Figure 6.38 indicates the significant influence of the water level, or storm surge level, on dune erosion. For SLR = 3.17 m, the maximum erosion is located at the same location as in the reference scenario but is 4 times larger, with more than 400 m^3/m erosion. This leads to the almost complete erosion of the front dune row. For SLR = 0.75 m erosion already leads to a large horizontal displacement of the dune foot. Transects of this location for both SLR scenarios are shown in figure 6.39

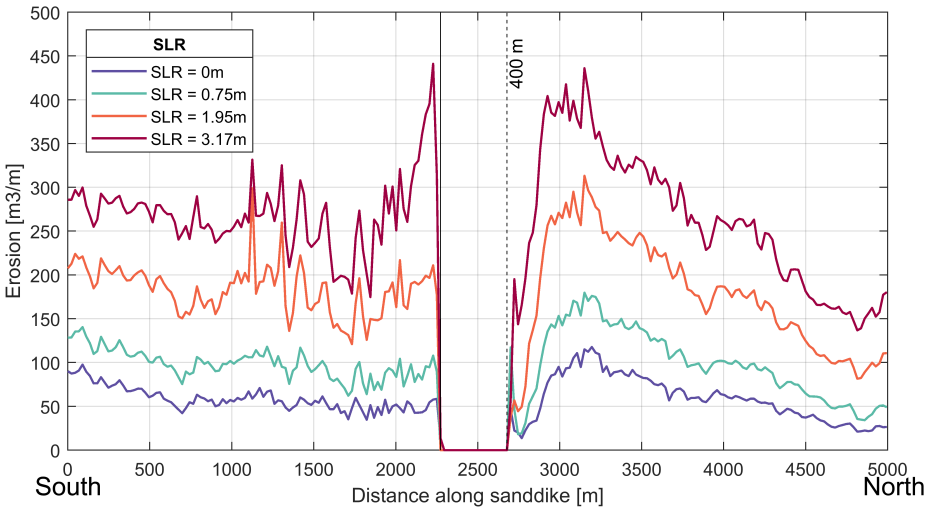

Figure 6.38: Overview of alongshore dune erosion for all SLR scenarios.

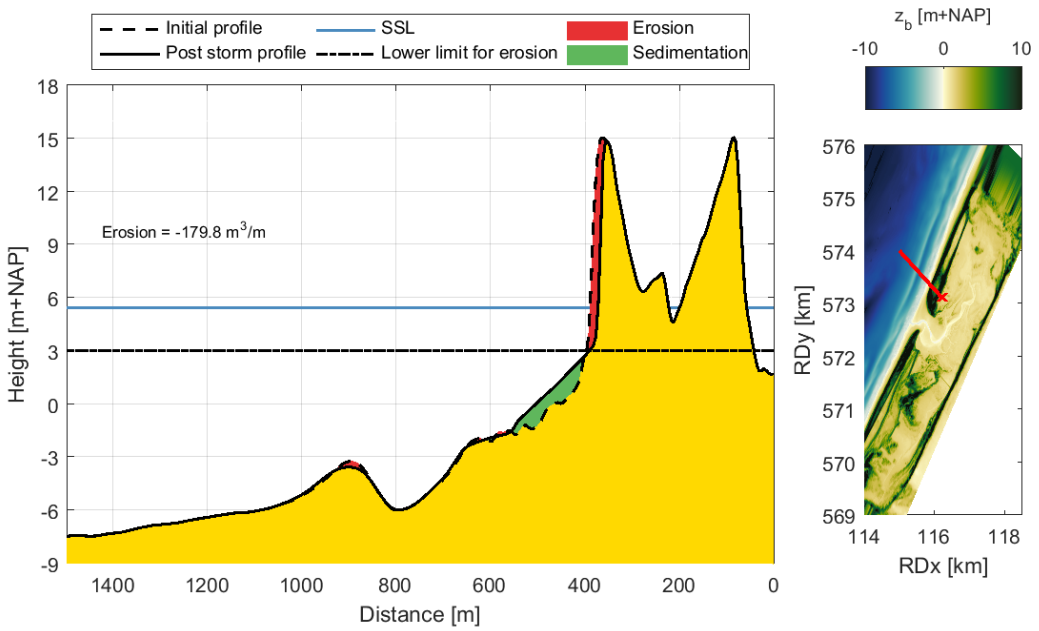

(a) SLR = 0.75 m

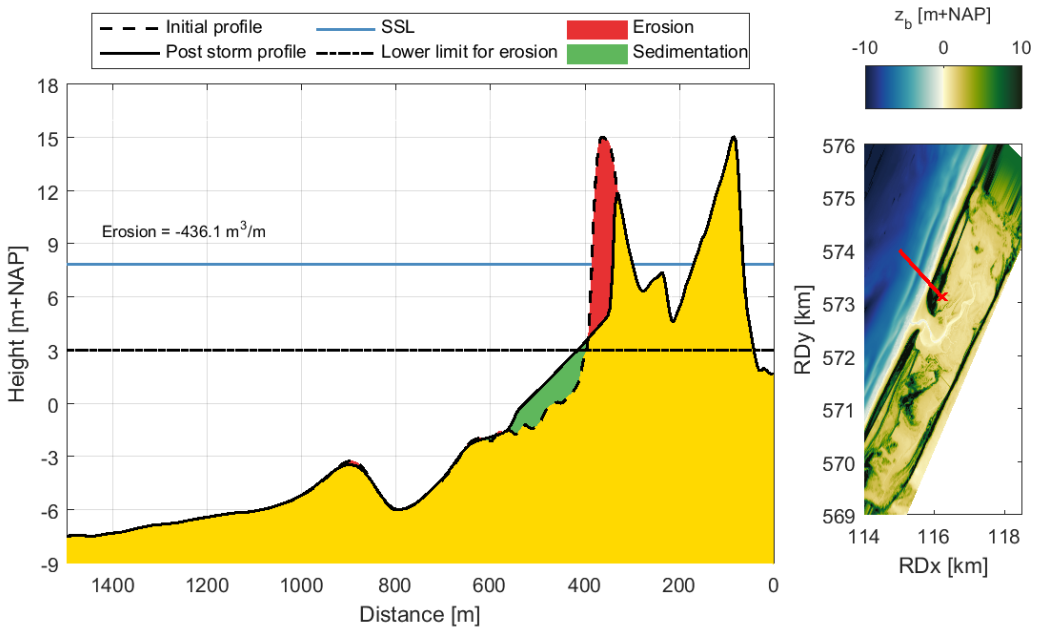

(b) SLR = 3.17 m

Figure 6.39: Transect of maximum dune erosion for SLR without BLR.

Erosion also increases along the sand dike as SLR increases, see figure 6.40. The ratios between sand dike erosion for different SLR scenarios is similar to that of the front dune row. Up until SLR = 1.95 m the main increase in sand dike erosion is found in the area in front of the mouth, where erosion was already largest. In this area the sand dike is relatively high. The high erosion peak at $x = 4700 - 5000m$ is caused by overwash and later inundation over the sand dike there, leading to a large amount of erosion.

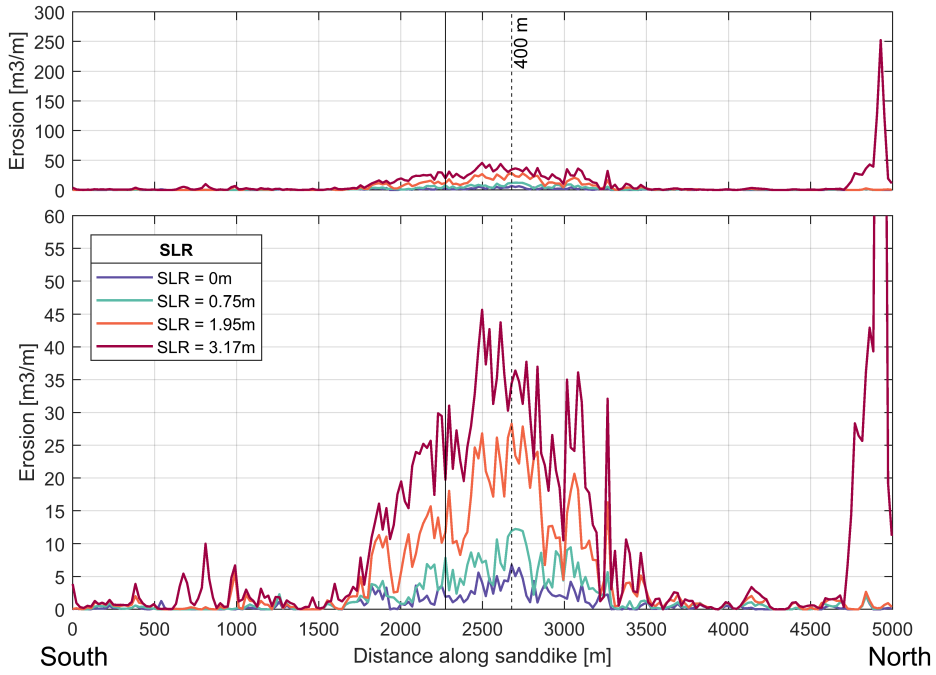

Figure 6.40: Erosion along the sand dike after a 1/3000 year storm for different SLR scenarios without BLR. The top and bottom graph only differ in y-scale. Apart from the erosion in the North, the isolated erosion peaks are caused by the cross-shore shape of the dune there, as explained in subsection 6.2.1. As bed levels have not risen, the limit above which dune erosion is calculated has not changed either (NAP+3m).

At the location of maximum sand dike erosion in front of the mouth for SLR = 3.17 m, a large part of the sand dike has been eroded, almost $45 m^3/m$. In the case of SLR = 0.75 m this is significantly less. The impact of sea level rise on the post-storm profile thus severely increases for more extreme scenarios.

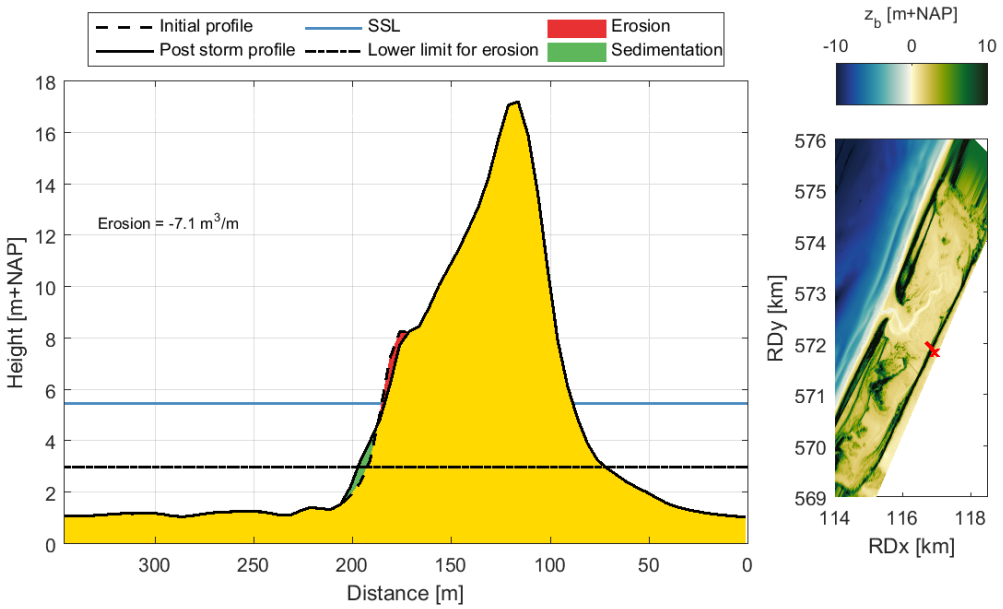

(a) SLR = 0.75 m

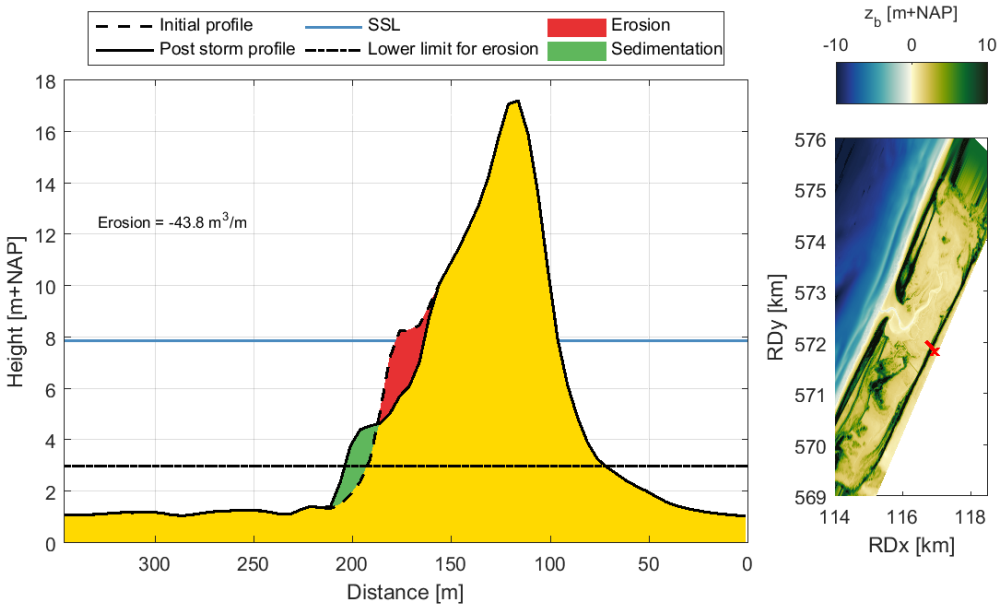

(b) SLR = 3.17 m

Figure 6.41: Transect of maximum sand dike erosion for SLR without BLR.

More importantly however, for SLR = 3.17 m extreme erosion takes place in the northeastern part of the sand dike in between $x = 4500 - 5000m$. This extreme erosion is caused by overwash and later inundation over the sand dike. The pre- and post-storm transects at this location are presented in figure 6.42 and show that the post-storm maximum sand dike height has decreased from NAP+7.2 m to NAP+5.1 m. This means that overflowing water will pour into Texel. The location of this overwash can be distinguished in figure 6.33 as the small green patch in the northeastern corner of the lower right map.

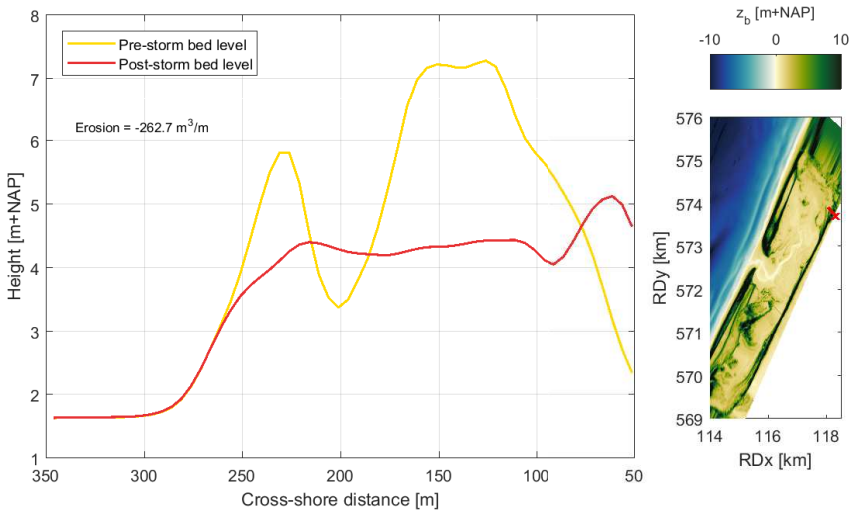

Figure 6.42: Sand dike transect at the location of maximum erosion (x = 4930m) during a 1/3000 year storm for SLR = 3.17 m.

Failure mechanisms

Grensprofiel - As is clear from table 6.9, the minimum volume for the SLR = 0.75 m scenario is still well above the 'Grensprofiel' limit with 92 m^3/m. For the SLR = 1.95 m scenario however, the minimum transect volume has fallen below the 20 m^3/m limit to 15 m^3/m. In the SLR = 3.17 m scenario the SSL is higher than the post-storm minimum sand dike height and the minimum transect volume is thus 0 m^3/m. Based on the 'Grensprofiel' criterium, failure therefore occurs at a point somewhere in between SLR = 0.75 m and SLR = 1.95 m. As in the reference scenario, the location of this minimum volume is in the north of the sand dike only. The rest of the sand dike adheres to safety standards.

This 'Grensprofiel tipping point', is approximated by analysing post-storm bed levels for the SLR = 1.95 m scenario. This is done by iteratively setting storm surge level such that the minimum volume above SSL is 20 m^3/m. This tipping point occurs when SLR = 1.84 m. In this analysis it is assumed that the water level head between the offshore boundary and the storm surge level in the valley remains constant for sea level rise between 0.75 m and 1.95 m, which is a valid assumption as will be discussed later on in this section.

SLR [m]	**max. SSL** [NAP+m]	$z_{s,max,north}$ [NAP+m]	$z_{s,max,south}$ [NAP+m]	**Min. volume** [m^3/m]
SLR = 0m	4.96	5.15	5.06	173
SLR = 0.75 m	5.69	5.85	5.75	92
SLR = 1.84m	*6.73*	-	-	*20*
SLR = 1.95 m	6.84	7.05	6.90	15
SLR = 3.17 m	7.56	7.60	7.30	0

Table 6.9: Minimum transect volume for different SLR scenarios. All minimum volumes were located in the same place as in the reference scenario. 'Grensprofiel' failure occurs for SLR = 1.95 m and SLR = 3.17 m. The values for SLR = 1.84m are not model results but an approximation based on the model results for SLR = 1.95 m. Therefore, they are presented in italics.

Figure 6.43 presents the profile at which maximum sand dike erosion occurs (in front of the mouth) and at which the post-storm transect volume is lowest (in the north of the sand dike). For the transect of maximum erosion, there is still more than enough area to fit in the limit profile. However, for the minimum volume transect, 'Grensprofiel' failure occurs. This type of failure occurs in multiple transects in the north of the sand dike. For SLR = 3.17 m, more transects fail than for SLR = 1.95 m, which is visualised in figure 6.44.

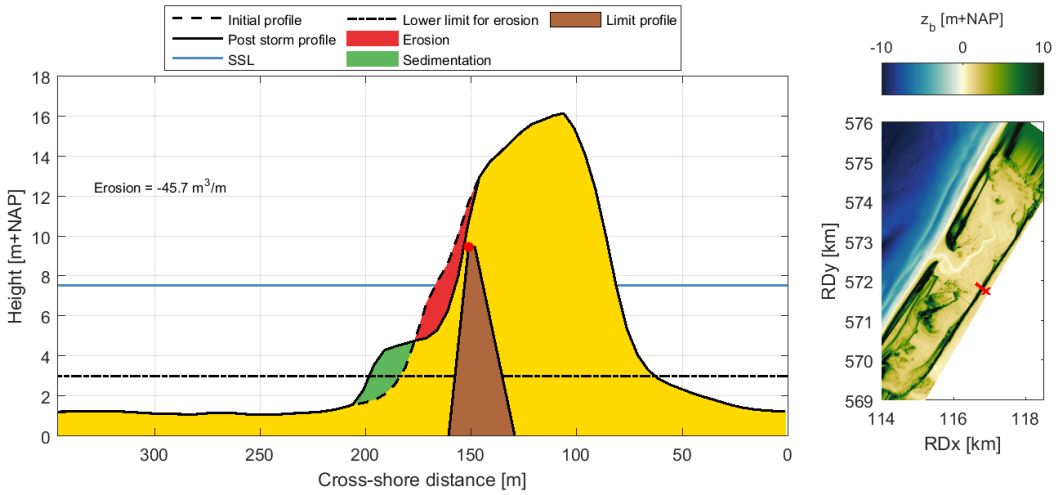

(a) Maximum erosion transect excluding the northern weak spot of the sand dike

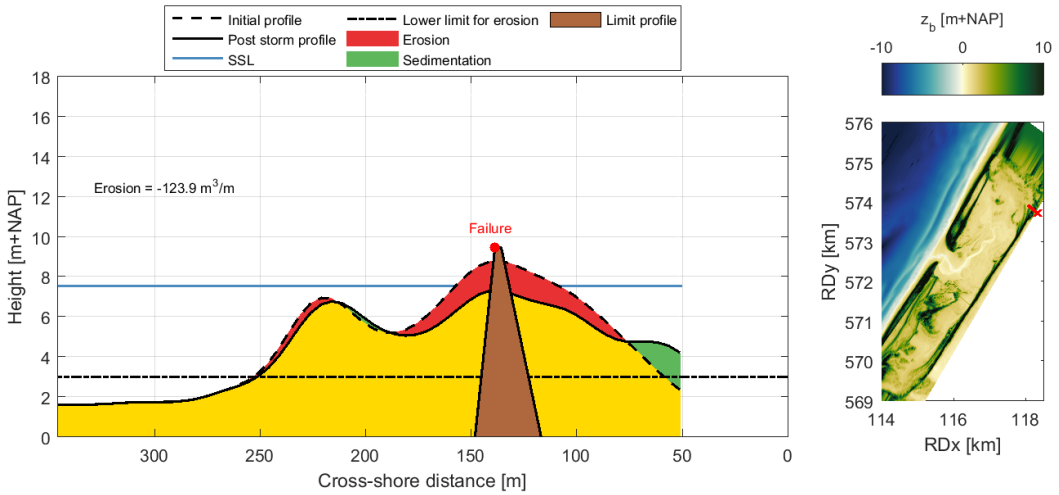

(b) Minimum volume transect

Figure 6.43: 'Grensprofiel' assessment concerning the limit profile for SLR = 3.17 m.

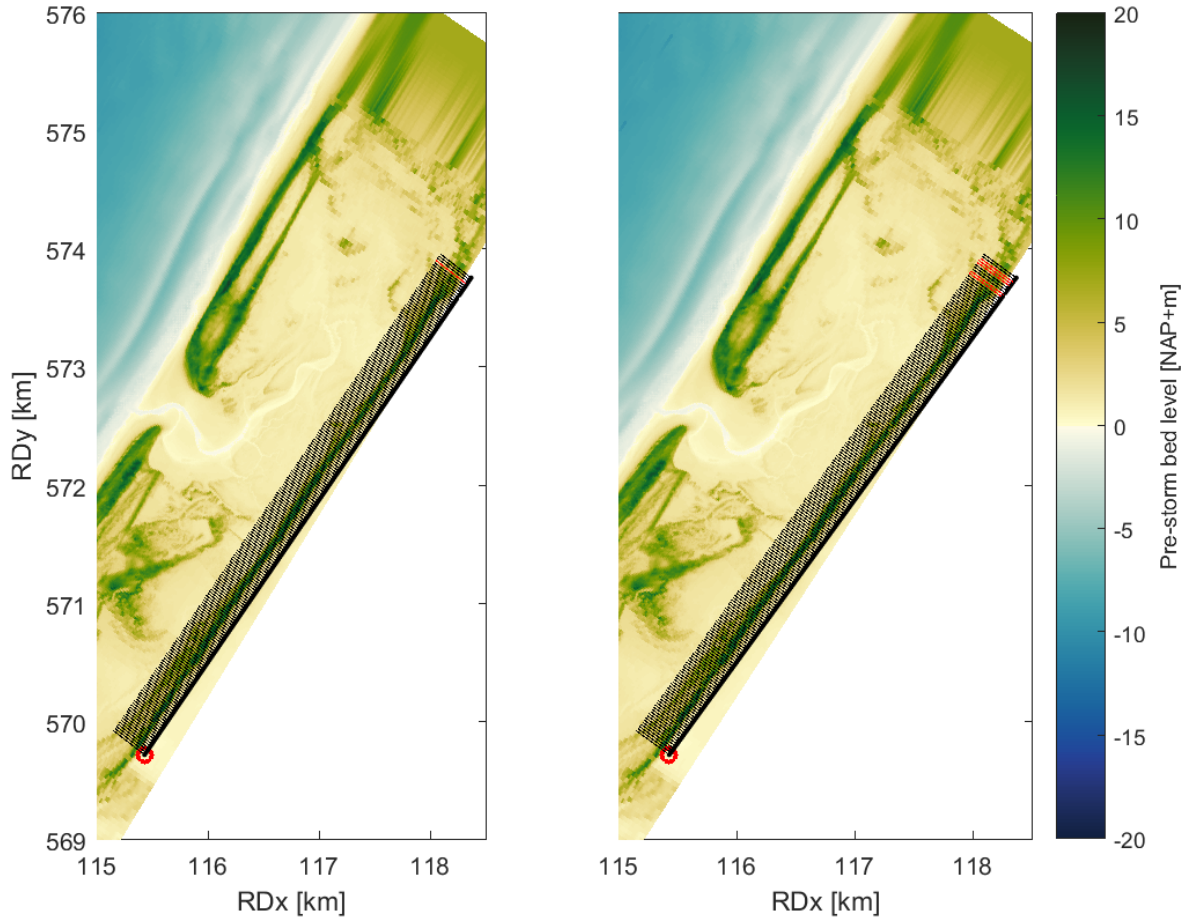

(a) SLR = 1.95 m

(b) SLR = 3.17 m

Figure 6.44: 2D map of transects that have failed according to the 'Grensprofiel' criterium. A black line indicates a 'safe' transect. A red line indicates a 'failed' transect.

Initiation of flooding - Figure 6.45 shows the previously discussed overwash from another perspective. The sand dike height is plotted against the maximum water levels at the peak of the storm (t = 19 h) for different SLR scenarios.

The overwash occurs when the maximum water level exceeds the sand dike height, which is NAP+7.2 m at the location in question. At t=17 h, the maximum water level at the overwash location (x = 4800m) is slightly higher than the bed level of the sand dike, which results in erosion of the sand dike. At t=18 h, the maximum water level has risen further and erosion has increased. At t=19 h - the peak of the storm - the bed level has lowered significantly to less than NAP+7 m. This allows inundation and leads to more erosion. At this point, the land behind the sand dike has flooded and is covered with 2.5 m water at some points. At t=24 h the sand dike height is only NAP+4.3 m. In appendix E.2 the development of this overwash in time is given for t=17 h to t=22 h.

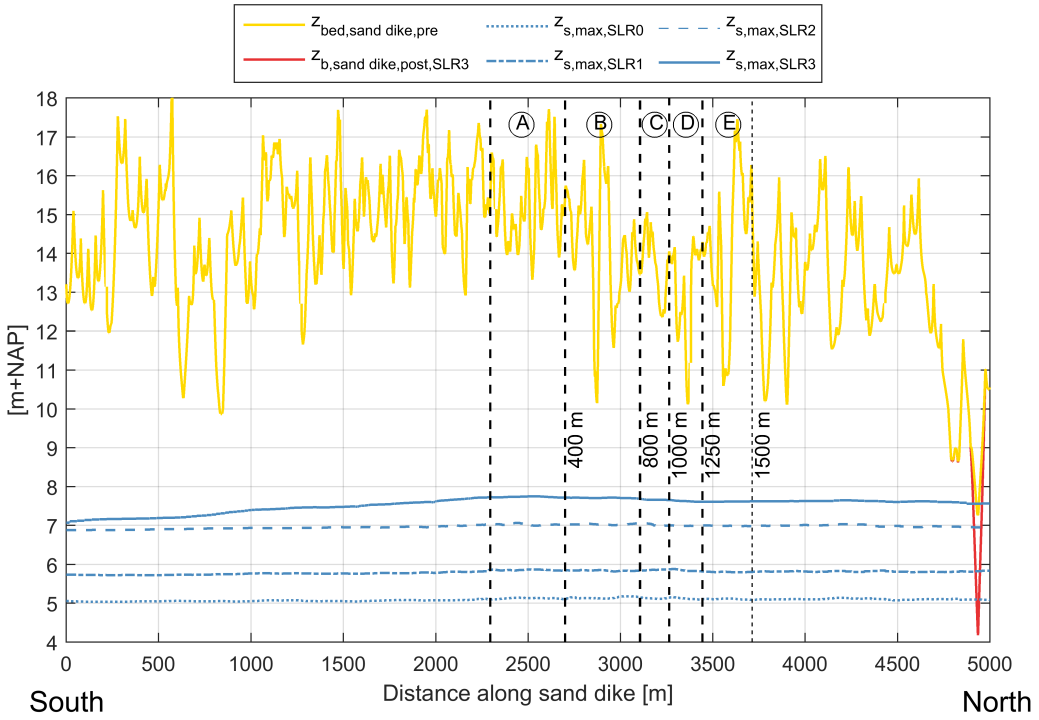

Figure 6.45: Alongshore sand dike height with maximum water levels during the peak of a storm for different SLR scenarios. The figure includes water levels corresponding to 4 different SLR scenarios. The red line in the north indicates the post-storm bed level of the sand dike in that location. Overflow of water has taken place and has eroded the sand dike there. The development of this overwash in time is given for t=17h to t=22h is presented in appendix E.2.

'Initiation of flooding' will occur over both the southwestern and the northeastern lateral edges of the sand dike for SLR = 1.95 m and SLR = 3.17 m. This occurs even before the overwash of the sand dike in figure 6.45. The water level head between the offhore boundary and the valley is near constant for all SLR scenarios, see figure 6.46. Therefore, based on the bed level of the 'weak spots' in the lateral edges (see figure 6.18) the 'Initiation of flooding tipping point' occurs at NAP+1.70 m.

$$SLR_{max,allowable} = 6.70m - 4.30m - 0.70m = 1.70m \tag{6.2}$$

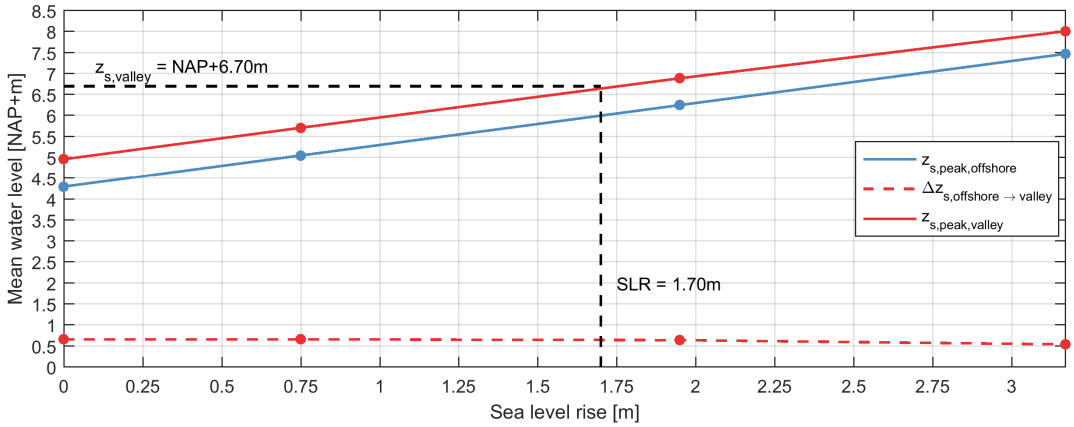

Figure 6.46: 'Tipping point' analysis. The striped red line indicates the water level head between the offshore boundary and the storm surge inside De Slufter. The continuous blue and red line represent the offshore water level and the storm surge level inside De Slufter, respectively. NAP+6.70 m is the lowest crest level height of the ridge around De Slufter, as discussed earlier. Therefore, 'Initiation of flooding' failure is expected to occur at the lateral edges when SLR = 1.70 m.

Conclusions

Apart from one specific location in the north, the sand dike adheres to safety standards. This specific location is weaker than the rest of the sand dike because it is lower (less than NAP+8m instead of at least NAP+10 m). Failure occurs there for the SLR = 3.17 m scenario due to overwash. According to the 'Grensprofiel' mechanism failure even occurs for SLR = 1.95 m. Assuming a constant water level head between the offshore boundary and the valley, the 'tipping point' of De Slufter, based on the 'Grensprofiel' criterium, is at SLR = 1.84 m.

However, inundation of water occurs over the southwestern and northeastern edges of the sand dike for these water levels. These edges are much lower than the sand dike and thus cannot protect against the (extreme scenarios of) increasing sea level rise. Based on 'Initiation of flooding' the tipping point is at SLR = 1.70 m. 'Initiation of flooding' at the lateral edges is thus the dominant failure mechanism. The areas where the lowest bed levels are located could be reinforced by raising bed levels there. However, raising these areas in the southwestern and northeastern edges would require much effort and capital. Furthermore, one cannot simply intervene manually in the dune areas as it is a Natura2000 area. Due to the less readily available solution, these edges are therefore considered to be the weak spots of De Slufter in the future.

6.3.2. 1/3000 year storm, with bed level rise

As bed levels below NAP+3.5 m have risen equally to sea levels these scenarios all have virtually the same hydrodynamic response as the reference scenario. The scenarios could also be described as 'the reference scenario in which the dunes have been lowered with different magnitudes'. Therefore, please refer to subsection 6.2.1 for the hydrodynamic response. In this subsection only deviations of the reference scenario are treated.

Nr.	ID	Mouth	SLR [m]	BLR [m]	Storm	Wave Dir.
4	S0B1R3000_1NW	Reference	0	0	1/3000 year	NW
16	S1B4aR3000_1NW	Reference	0.75	0.75	1/3000 year	NW
23	S2B4bR3000_1NW	Reference	1.95	1.95	1/3000 year	NW
30	S3B4cR3000_1NW	Reference	3.17	3.17	1/3000 year	NW

Table 6.10: Overview of scenarios that were analysed for this subsection.

Sand dike erosion

When comparing figures 6.40 and 6.47 two major differences stand out. First of all, sand dike erosion in the scenarios with BLR is generally lower than in the situations without BLR. This has two main causes: as bed levels have risen equally to water levels, wave heights do not increase significantly and thus neither does sand dike erosion. Also, as bed levels have risen, the dune foot has risen as well. This means that the limit above which erosion can be considered sand dike erosion has to be heightened. Otherwise, changes in sand dike erosion could be caused by bed level changes in the valley. Consequently, as the sand dike has become relatively lower there is less volume above the limit to erode, leading to smaller erosion volumes.

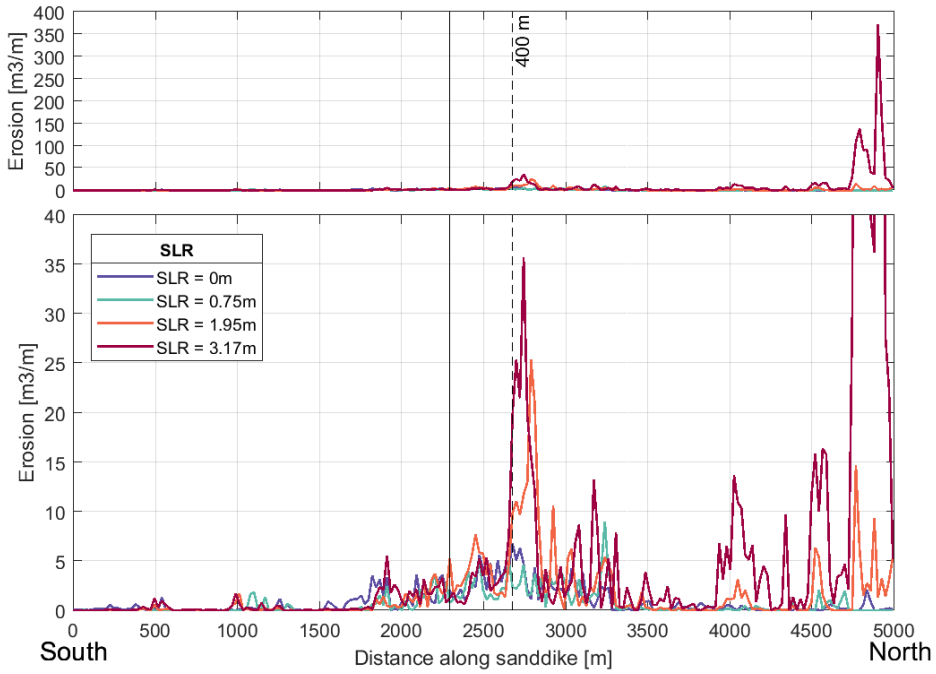

Figure 6.47: Erosion along the sanddike after a 1/3000 year storm for different SLR scenarios with BLR. The top and bottom graph only differ in y-scale. As bed levels have risen, the dune foot has risen as well. Therefore, the limit above which dune erosion is calculated has increased equal to SLR (e.g. the limit for SLR = 3.17 is now 3 + 3.17 = NAP+6.17m).

Second, sand dike erosion is relatively similar for the different scenarios. At some locations there are large differences however. These are caused by the cross-shore shape of the sand dike there, combined with the higher SSL for higher SLR scenarios. Due to smaller duneforms in front of the sand dike, the sand dike is shielded from wave attack in the lower SLR scenarios. When the SSL becomes higher than the peaks of these

duneforms, the sand dike itself is attacked and erosion increases significantly. This can be clearly identified in figure 6.48, which shows a sand dike transect with such a duneform for 2 SLR (with BLR) scenarios.

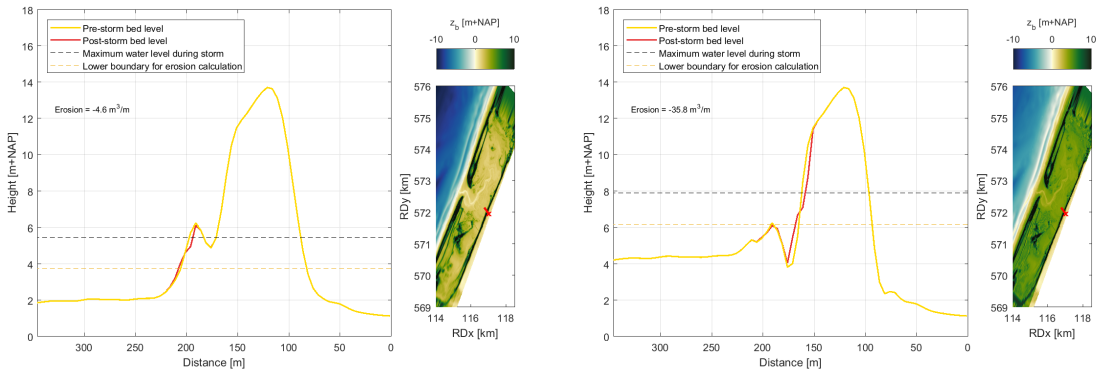

(a) SLR = 0.75 m

(b) SLR = 3.17 m

Figure 6.48: Sand dike erosion transects for SLR showing the influence of small dune forms on sand dike erosion.

Failure mechanisms

Grensprofiel - The differences in transect volume above storm surge level between scenarios with and without BLR are small. For scenarios with BLR storm surge levels are higher but only in the order of centimeters. Only for SLR = 3.17 m the difference is significant but this is due to the fact that there is no overflow over the southwestern edge. This, in turn, is due to the manually heightened bed level there which was necessary for numerical stability (as explained in appendix C.2). It is assumed that, just as the lower SLR scenarios, the SSL will be higher but only in the order of centimeters. As table 6.11 shows, the minimum transect volumes in the profile are too low for the two highest SLR scenarios. Just as in the scenarios without BLR, 'Grensprofiel' failure thus occurs somewhere in between SLR = 0.75 m and SLR = 1.95 m. Based on the constant water level head again, failure will likely occur for SLR = 1.83 m.

SLR [m]	**max. SSL** [m+NAP]	$z_{s,max,north}$ [m+NAP]	$z_{s,max,south}$ [m+NAP]	**Min. volume** [m^3/m]
SLR = 0m	4.96	5.15	5.06	173
SLR = 0.75 m	5.71	5.85	5.75	90
SLR = 1.83 m	*6.78*			*20*
SLR = 1.95 m	6.89	6.96	6.91	11
SLR = 3.17 m	8.01	7.85	8.12	0

Table 6.11: Minimum transect volume for different SLR scenarios. All minimum volumes were located in the same place as in the reference scenario.

Initiation of flooding - Just as in the SLR = 3.17 m scenario without BLR, overwash occurs in the northeast of the sand dike. Due to necessary smoothing, the sand dike height is slightly lowered (approx. 50cm) in some locations, including the northeast. This is the reason that some extra erosion is present in that area for the scenario with BLR.

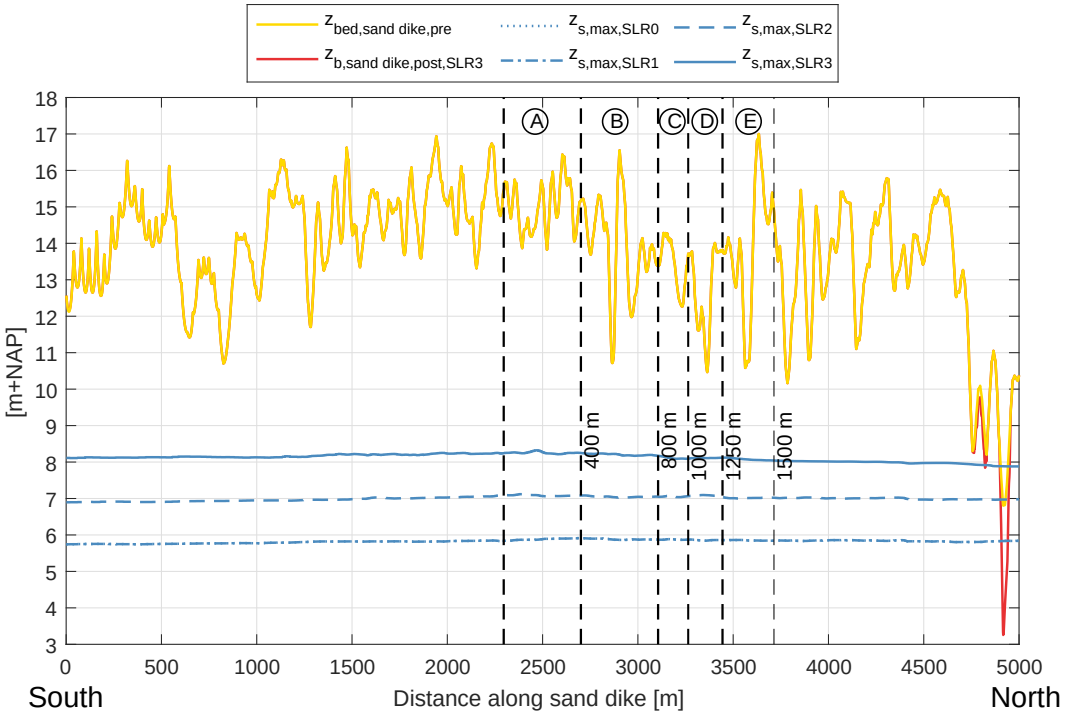

Figure 6.49: Alongshore sand dike height with maximum water levels during the peak of a 1/3000 year storm (t=19h). The figure includes water levels corresponding to 3 different SLR scenarios. The red line in the north indicates the post-storm bed level of the sand dike for SLR = 3.17 m. Overwash and later inundation has taken place and has eroded the sand dike there.

Based on the 1DH analysis of 'Initiation of flooding' no overwash occurs for SLR = 1.95 m. However, erosion due to overwash does take place in the lower parts of the transect. As only the maximum bed level per transect is used in the calculation of the height along the sand dike, the lower parts are hidden behind higher parts of the sand dike. This is visualized in figure 6.50, which shows the bed level in the northeast of De Slufter before and after the overwash event (in the red circle). The bed level is lowered here from NAP+6.8 m to NAP+4 m, proving that overwash and inundation do indeed occur.

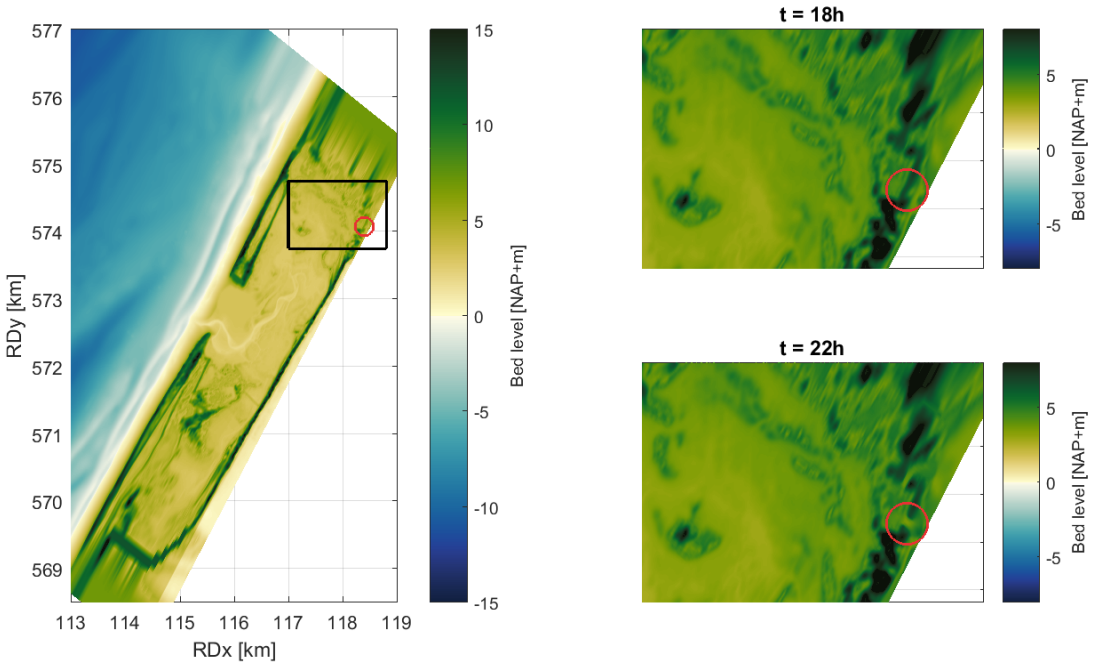

Figure 6.50: 2D bed level of the northeastern corner of De Slufter before and after the overwash event when SLR = 1.95 m. The red circle indicates the location of the overwash.

The hydrodynamic processes inside De Slufter for SLR scenarios with BLR are very similar to those in the reference scenario. Wave attack on the sand dike is thus much lower than in SLR scenarios without BLR. The fact that the sand dike is relatively lower and the wave attack is smaller means that sand dike erosion is also smaller than for the scenarios without BLR. However, overwash does occur in the same locations. Furthermore, overwash for scenarios with BLR also occurs for SLR = 1.95 m. In the same locations as for the scenarios without BLR, inundation of water takes place over the lateral edges. The 'Initiation of flooding' failure thus occurs. For SLR = 1.95 m and SLR = 3.17 m 'Grensprofiel' failure also occurs. The 'Initiation of flooding tipping point' is equal to that of the scenarios without BLR: NAP+1.70 m.

6.3.3. Failure maps

Figures 6.51, 6.52 and 6.53 present the locations at which failure occurs for different SLR scenarios (SLR = 1.70m, SLR = 1.95 m and SLR = 3.17 m, respectively). The first type of failure, which happens at SLR = 1.70m, is 'Initiation of flooding' failure. This failure occurs at the northeastern and southwestern lateral edges of the sand dike. In the northeast, the weak spot is the road leading to 'Strandpaal 28'. This road has locally lowered the dune ridge. In the southwest, the weak spots are a footpath running from the main road along the sand dike into De Slufter and a naturally lower area in the southwestern lateral edge, see figure 6.51.

For SLR = 1.95 m, both 'Initiation of flooding' and 'Grensprofiel' failure occur at multiple locations along the slufter ridge. Again, the locations are centered around the northeastern and southwestern areas of De Slufter where the ridge is characterised by a more heterogeneuously shaped dune area, contrary to the man-made sand dike.

For SLR = 3.17 m, the locations at which failure occurs are equal to those for SLR = 1.95 m. This means that again, apart from 1 weak spot in the north, no failure occurs at the sand dike itself. It is therefore concluded that the sand dike is very robust in combination with the highly dissipative slufter valley.

Table 6.12 presents an overview of all present and future scenarios and the occurrence of failure.

Scenario	**SSL** [m+NAP]	$z_{s,max,north}$ [m+NAP]	$z_{s,max,south}$ [m+NAP]	**Min. volume** [m^3/m]	**'Grensprofiel'**	**'Initiation of flooding'**
400m wide mouth	4.95	5.15	5.06	173	No	No
800m wide mouth	4.95	5.17	5.05	151	No	No
1000m wide mouth	4.95	5.15	5.10	131	No	No
1250m wide mouth	4.95	5.13	5.07	124	No	No
1500 m wide mouth	4.95	5.15	5.07	118	No	No
Second mouth	4.95	5.14	5.06	184	No	No
SLR = 0 m	4.95	5.15	5.06	173	No	No
SLR = 0.75 m	5.69	5.85	5.75	92	No	No
SLR = 1.95 m	6.84	7.05	6.90	15	Yes	Yes
SLR = 3.17 m	7.56	7.60	7.30	0	Yes	Yes
SLR = 0.75 m incl. BLR	5.71	5.85	5.75	90	No	No
SLR = 1.95 m incl. BLR	6.89	6.96	6.91	11	Yes	Yes
SLR = 3.17 m incl. BLR	8.01	7.85	8.12	0	Yes	Yes

Table 6.12: Overview of scenarios and the occurrence of failure. The columns 'Grensprofiel' and 'Initiation of flooding' indicate whether that type of failure has occurred (Yes) or not (No).

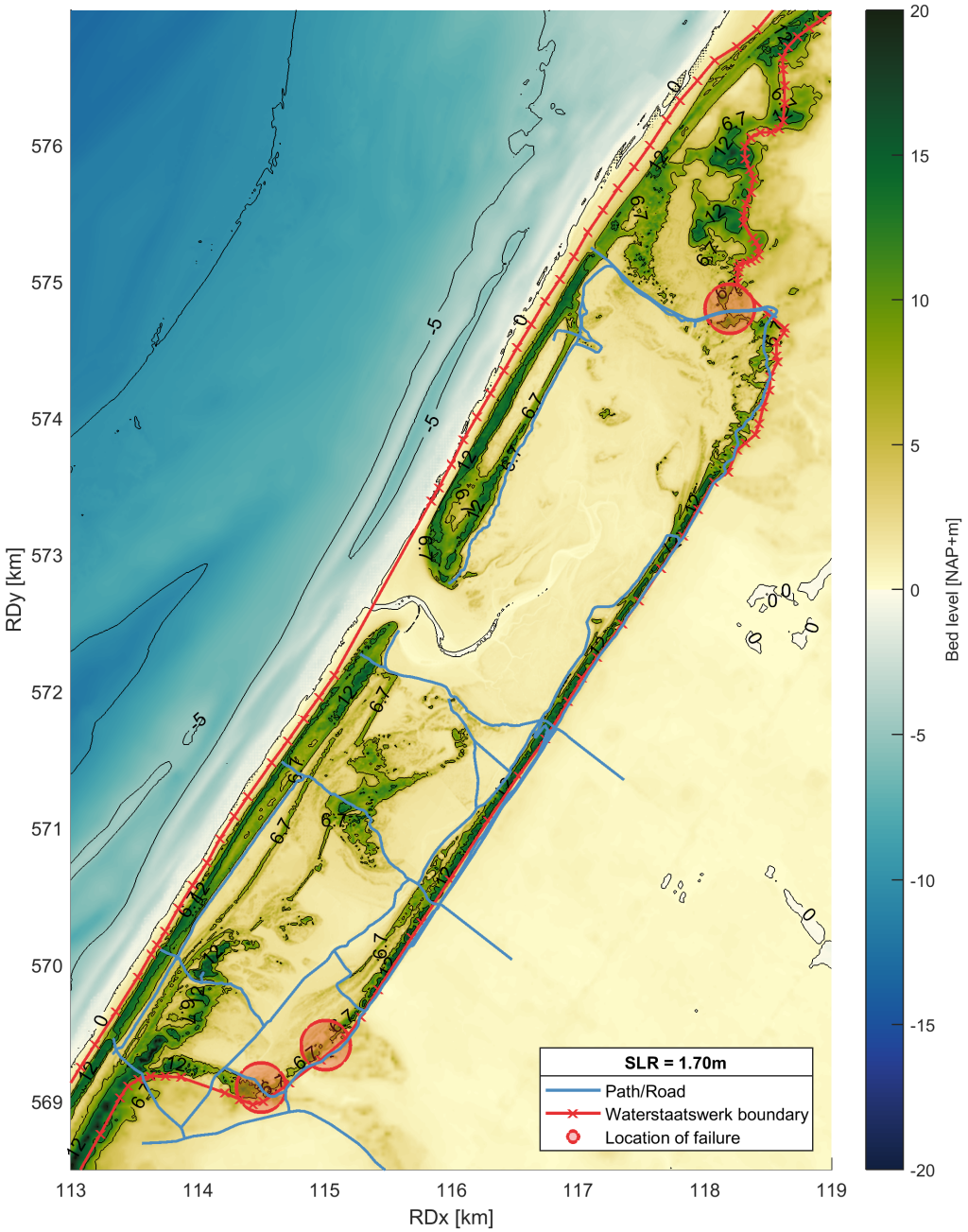

Figure 6.51: 2D map of De Slufter indicating locations of failure for a 1/3000 year storm and 1.70m sea level rise.

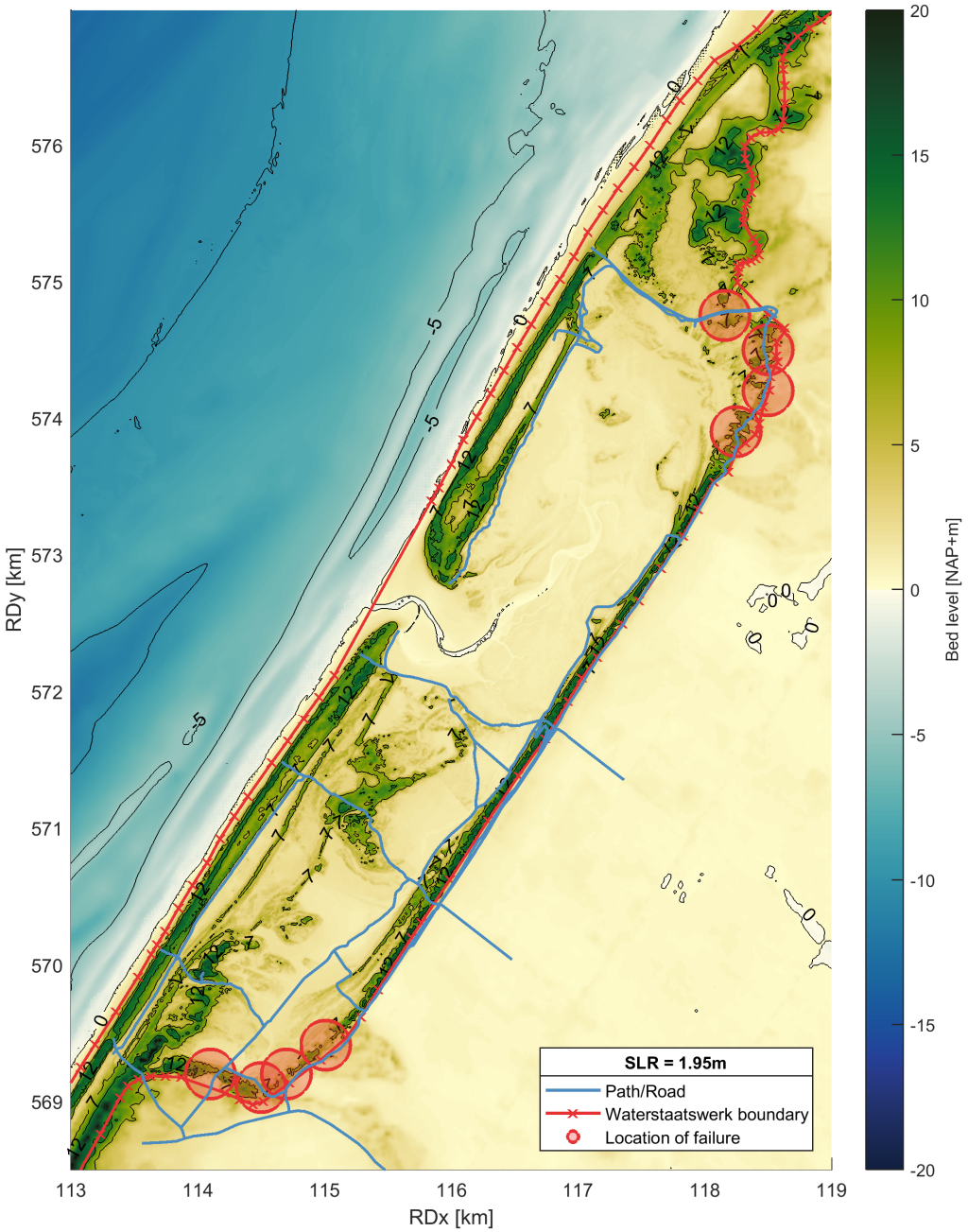

Figure 6.52: 2D map of De Slufter indicating locations of failure for a 1/3000 year storm and 1.95 m sea level rise.

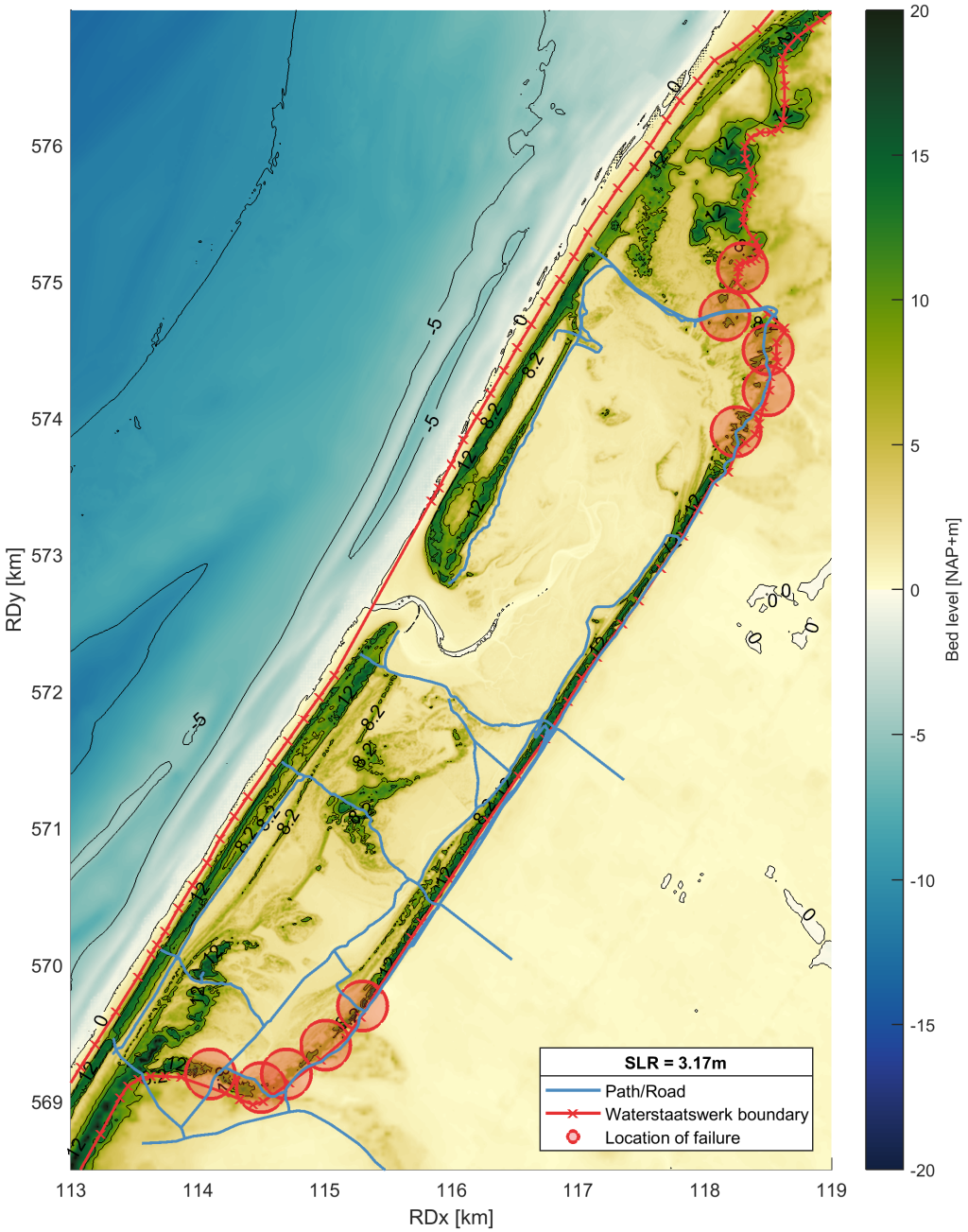

Figure 6.53: 2D map of De Slufter indicating locations of failure for a 1/3000 year storm and 3.17 m sea level rise.

7

Discussion

In this chapter the method in which this research was conducted as well as certain made assumptions are critically reflected upon. The contents of this chapter provide an understanding of the strengths and limitations of the (results of the) research before any conclusions are made in chapter 8.

7.1. Gully migration

High frequency (three-hourly) wave observations made it possible to test two hypotheses. First, the hypothesis that gully migration is dominated by wave-driven longshore transport during all conditions. Second, the hypothesis that longshore transport during storm conditions dominates gully migration. Furthermore, the availability of annual gully location measurements and high frequent hydrodynamic data made it possible to analyse the long-term behaviour of the gully. However, there were some limitations to the used data which will likely be overcome in future studies.

Recent developments In this thesis, gully migration was analysed from 1997 to 2017. In this period, annual bathymetry and topography measurements were available. Longshore transport during that period was calculated from high frequent wave and water level measurements available in the area. However, due to the infrequent measurements of the topography in the mouth, the forcing data cannot be utilized to its full potential. The direct response of the gully to variations in forcing could thus not yet be analysed. Recent developments in the quality and availability of satellite imagery will likely overcome this issue however.

Furthermore, the gully has migrated southward in recent years. At the time of writing, the gully has migrated so far that it is presently eroding the southern dune head. The interaction between the dunes and the gully has not been analysed in detail as it was out of the scope of this study. However, this interesting behaviour will be of importance if the HHNK decides to cease relocations of the slufter gully.

Also, recent photographs suggest that the 'extremely' southern location of the gully has led to a very narrow beach flat. A storm event could well create a new opening for the gully towards the sea. If this were to happen, it would suggest that the gully is relocated by natural processes. However, at the time of writing no storm events of significance have occurred yet in 2018. This must therefore be investigated in a future study.

Uncertainty in exact dates of measurements The exact dates of the Kusthoogte measurements were unclear. This introduces inconsistencies in the comparison between annual gully migration and driving processes. E.g. while the annual longshore transport was always calculated from January 1st to December 31st, the gully migration was calculated from measurements performed at different times of the year. The same is the case for the calculations of the bend radius and the distance to the dune heads, as these were based on the measured position of the gully. In reality, gully migration magnitudes could thus have been smaller or larger. However, the aim of this study was to identify the driving processes behind gully migration. While an exact knowledge of measurements would improve the accuracy of this analysis, the present measurements were sufficiently frequent to describe clear long-term trends in gully behaviour.

7.2. Model limitations and strengths

In this study, new and valuable knowledge has been developed concerning De Slufter using the 2DH process-based modelling program XBeach Surfbeat. This study has further emphasised the importance of using XBeach (or similar models) over DUROS+ for the analysis of complex systems such as De Slufter. First of all, the DUROS+ model requires a profile from at least NAP-5 m to NAP+5 m, which means that the sand dike erosion could not have been modelled. Second, it was found that the slufter valley is a powerful wave dissipator and that the sand dike is therefore very well able to withstand wave attack in the present and future wave climate. From this it was found that the sand dike is not dominant for the coastal safety of De Slufter. Instead, the lateral edges are. DUROS+ does not resolve the hydrodynamics within the profile, does not resolve time-dependent morphology (only pre- and post-storm profiles) and cannot resolve complex 2DH processes. Therefore, such conclusions could not have been drawn with DUROS+.

Furthermore, valuable insight was gained in the effects of sea level rise on the hydro- and morphological response of De Slufter to extreme storm events. De Slufter was concluded to comply to safety standards for sea level rise up to 1.70 m. At that magnitude, water levels inside De Slufter will be so high that inundation takes place over the lateral edges of the valley. These conclusions are substantiated by the fact that the hydrodynamic validation showed that the hydrodynamics inside the model correspond well to observations. No morphological validation on dune and sand dike erosion was possible however. It can therefore not be definitively concluded that observed erosion rates are exactly in accordance with reality. Therefore, one should not focus on this study in a quantitative but in a qualitative sense.

7.2.1. Hydrodynamic forcing and model settings

For the model, assumptions and simplifications were made that influence the results of this study. The sensitivity of these parameters is discussed in appendix F. The most important parameters are discussed below.

Storm shape and duration First of all, in line with Steetzel (1993), the duration of storms in this study was assumed such that 2.5 tidal waves were modelled. This means that the tidal forcing is sufficiently included in the model. Second, the shape of the storms in this study was assumed such that the peak water level is the sum of a tidal water level and the maximum non-tidal residual water level. The storm and tide are thus assumed to be in phase. However, in reality this is not necessarily the case. As shown in this study, the maximum water level inside De Slufter is one of the dominant parameters for the coastal safety of De Slufter. The fact that in reality the surge and high water do not always coincide means that the maximum simulated total water level could be higher than observed.

The conclusions made in this study are thus based on conservative water levels. Therefore, a more realistic storm shape and duration will thus presumably lead to a less extreme situation and consequently a safer Slufter.

Bed friction The spatially varying bed friction used in this study is a gross simplification of the real life effects of vegetation on wave dissipation. Only two parameters were assumed: a vegetated and a non-vegetated Manning coefficient. In reality, different types of vegetation are present in De Slufter which all have different associated bed friction values. The model validation shows that the effect of bed friction on the water levels in De Slufter is insignificant though.

Generalization of wave parameters To create wave forcing for the model, one wave condition (i.e. significant wave height, peak wave period and mean wave direction) per return period was determined from an analysis of historical measurements. To generalize the entirety of the wave climate into 4 wave conditions it was assumed that all storms were north-westerly. This has led to near normally incident waves. This does not necessarily lead to the most conservative erosion volumes. Westerly 1/3000 year storms could lead to more sand dike erosion. However, as discussed in this thesis, westerly 1/3000 year storms are not realistic due to a limitation in the fetch.

The wave periods for the storm conditions were determined with a wave steepness value. It was assumed that all waves have the same wave steepness. However, there is quite a significant variability in wave steepness in reality with lower waves generally having a lower steepness than high waves. The mean of wave steepness

values of NW-N waves above 5.9 m was assumed to be a representative value for general wave steepness in the area. This means that wave periods will either be shorter or longer than resolved in the model. Therefore, one should not focus too much on the absolute values but rather on the relative effects presented in this study (i.e. qualitative not quantitative).

Spreading parameter 's' Due to a mistake in the setup of the wave boundary conditions, an unrealistic directional spreading parameter was chosen, leading to a large directional spreading of wave energy. Unfortunately, this mistake was discovered in a very late stage of the research which meant that there was too little time to redo all the model runs. However, as is elaborated on in appendix E, the effect on the results inside De Slufter are small due to the dissipation in the valley. This high amount of dissipation (due to wave breaking and wave friction) means that wave heights inside De Slufter are governed by depth and not so much by offshore wave height.

The large spreading did have a significant effect on dune erosion of the front dune row, with more erosion for the more realistic (narrower) direction spreading than in this thesis. However, the modelled patterns in failure did not change. The trends in dune erosion remained similar, with minimum and maximum erosion in equal locations.

7.2.2. Hydro- and morphodynamic processes in the model domain

The XBeach Surfbeat model used in this study has certain limitations and strengths regarding the ability to model hydrodynamic and morphological processes.

Absence of short wave runup As individual short waves are not resolved in XBeach Surfbeat, the effect of short wave runup is not included in the failure assessments. However, short wave attack on the sand dike is relatively low. Therefore, the effect of individual short waves on sand dike overtopping is considered negligible. Near the lateral edges of De Slufter, short wave energy is low and is thus also expected not to have a significant effect. Only in the second mouth case, short wave attack is significant on the lateral edge. However, the wave heights near the ridge are still low ($< 0.5m$).

Lack of short-term dune erosion observations The lack of short-term data concerning dune erosion in or near De Slufter made it impractical to validate dune erosion in the model. This was unfortunate as it is an important process for this study. However, it was shown that validatable morphological processes, i.e. the migration of the gully during a small storm event, were well in accordance with observations.

Furthermore, the hydrodynamics in the model near the sand dike were shown to be in agreement with observed hydrodynamics. Though individual short wave runup was not included, short wave height throughout the model corresponded well to observations. The short wave impact on the sand dike was thus well represented in the model. Where model results did not match observations, e.g. for long wave heights, the results were generally such that they led to more conservative conclusions.

7.2.3. Differences with earlier studies

As already discussed, an earlier study has been performed by Van Rooijen and Van Thiel de Vries (2014), who studied the effects of different bathymetry configurations on present coastal safety.

There are considerable differences between the previous study and this study in terms of dune and sand dike erosion. A likely reason for this is the different choice of critical bed level slope under wet conditions. Van Rooijen and Van Thiel de Vries (2014) scaled down the associated parameter such that the maximum bed level slope for inundated grid cells was less steep. Furthermore, the maximum erosion speed was scaled up. The reason for the changes in these parameters is unclear.

In this thesis it was chosen to use default parameters as much as possible. Each XBeach release is elaborately tested using a large number of standard validations (skillbeds). Also, the default parameter for the critical bed level slope under dry and wet conditions is in line with the physical internal angle of friction of sand. Therefore, the results of this study are considered more realistic than those of the previous study. Both changes in parameters lead to less dune and sand dike erosion in the present study compared to the study by

Van Rooijen and Van Thiel de Vries (2014).

These two parameters thus explain the decrease of both dune and sand dike erosion compared to the previous study. However, another explanation likely lies in the assumption of beach flat height in the wider mouth scenarios. In the previous study it was assumed that the front dune row had been 'dug out'. Therefore, the area that was previously dune was assumed to be NAP+0 m. In this thesis it was assumed that the bed level in this area was equal to the present beach flat, which is considerablly higher than NAP+0 m. This will affect the wave height in the valley and, consequently, sand dike erosion. Compared to the previous study wave heights and sand dike erosion will thus be lower. The assumption for the beach flat in this study is considered more realistic as it was based on physical observations of the present beach flat.

7.3. Effects of sea level rise

The XBeach Surfbeat model allowed an analysis of the effects of sea level rise on coastal safety. Multiple combination of sea level rise and bed level rise provided insight into the future response of De Slufter to storm events assuming different developments of De Slufter over time.

Bed level rise assumption For simplicity reasons, it was assumed for the future scenarios that bed level rise was either equal to sea level rise or that no bed level rise had occurred at all. In reality the magnitude of bed level rise will likely lie somewhere in between. Observations of hydro- and morphodynamic processes will thus also lie in between the model results of this study (e.g. wave heights, water levels, sand dike erosion). However, it was found that failure occurred for the same conditions (i.e. SLR magnitude, return period of storm) in scenarios with and without bed level rise. Therefore, the results approach the expected behaviour of De Slufter under future extreme conditions well.

Slufters and coastal safety This study has shown that De Slufter in its present configuration complies to the associated safety standards, even when the mouth has widened significantly. The large amount of dissipation of wave energy propagating through the valley has been shown to contribute significantly to this capability. Furthermore, high SLR scenarios were shown to lead to extreme erosion volumes at the front dune, leading to significant weakening. However, while sand dike erosion increased with approximately the same proportion as the front dune row erosion, the sand dike erosion volumes remained small. This means that slufters in general could be an effective type of coastal zone area for the protection against the effects of SLR on coastal safety. A reservation to this hypothesis is that this study focussed on storm-driven morphology. In the case of sea level rise, slufter morphology will be increasingly governed by calm conditions due to the constant inundation of the valley. This means that the observed bed level rise will presumably be more complex than assumed in this report (i.e. spatially non-uniform, growth not constant over time).

8

Conclusions and recommendations

8.1. Conclusions

The objective of this research was to assess the impacts of a different coastal management strategy with respect to the slufter gully and of sea level rise on the present and future coastal safety of Texel. To meet this objective the following research question was posed:

"What will be the effect of ceasing human interventions into the slufter gully on the present and future coastal safety of the Wadden island Texel?"

For the purpose of answering this question three subquestions were defined. In this section the conclusions are divided into one subsection per subquestion. In every section the relevant conclusions leading to the answer of a research question are discussed before the research question itself is answered.

8.1.1. Gully migration

The dynamic behaviour of the slufter gully is considered to be a dominant factor determining the width of the slufter mouth. Therefore, it was investigated which processes govern the direction and magnitude of the migration of the gully.

Gully migration is not only dominated by annual net alongshore sediment transport: The yearly averaged net sediment flux was calculated with the van Rijn (2013) longshore transport equation. The results were compared to the historical migration of the gully for a period of 18 years (1998-2017). For the first 14 years net sediment flux direction and gully migration direction were both directed north and thus correlated well. Similar trends in longshore transport magnitude and gully migration magnitude can also be distinguished, albeit less clearly defined.

However, for the last 4 years a southward gully migration is observed while net sediment flux was directed north. Therefore, wave induced longshore transport cannot be the only dominant process in gully migration.

Gully migration is not driven by wave-induced longshore transport during storms: The same analysis as for the total wave climate was performed for storm conditions ($H_s > 4m$). The results were again compared to historical gully migration. Annual longshore transport due to storms and historical gully migration showed less correlation than for the total wave climate. Long-term gully migration is therefore concluded not to be governed by longshore transport during storm events.

Gully migration is possibly governed by curvature-induced secondary flow due to tidal forcing: Based on the first measurement of the gully position after each relocation, it is expected that curvature-induced secondary flow is a governing process in gully migration. The gully is not straight but is curved (seen from above) and it differs per year how much curvature there is in the gully in the mouth and where this curvature is directed. Until 2013, the outer bend of the most seaward curve was mainly located on the north side of the gully. However, after the relocation in 2013, this outer bend was located on the south side of the gully. In nearly all annual measurements since 1998, the gully has migrated in the direction of this outer bend.

Curvature-induced secondary flow could possibly explain this behaviour. This process would only be present when water is contained to the gully. When this is the case, only the tidal forcing induces currents inside the gully. Hence 'curvature-induced secondary flow due to tidal currents'.

Answer to research subquestion 1

"Which processes govern the direction and magnitude of migration of the slufter gully?"
Gully migration is not, as was expected, only dominated by wave-induced longshore transport. This was concluded as longshore transport and gully migration have been opposingly directed since 2013. Based on annual topography and bathymetry measurements it is expected that the gully migration is further governed by curvature-induced secondary flow due to tidal forcing, overwash from the beach flat into the gully during storms and by the distance to the dune heads (which inhibits migration).

8.1.2. Present coastal safety

To assess the present coastal safety of Texel the hydro- and morphodynamic response of De Slufter was modelled for different possible near-future scenarios (i.e. the present configuration of De Slufter, a wider mouth and a second, more northerly located mouth). In these scenarios, sea level rise was not included.

In all present scenarios, waves impacting the sand dike are relatively low: The wave dissipation in the valley significantly lowers wave heights as waves propagate towards the sand dike. 11.2m high wave heights imposed on the offshore boundary reduce to less than 1m high wave heights at the sand dike. While a wider mouth increases the area of the sand dike that is under wave attack, it does not significantly increase the maximum wave height on the sand dike. This means that, in the area of the sand dike that is in front of the mouth in the present situation, sand dike erosion does not significantly increase. As the mouth grows wider towards the north, the wave height near the sand dike does increase in the areas of the sand dike newly in front of the mouth. This leads to a shift of the maximum wave height northwards. Consequently, maximum sand dike erosion also shifts northwards. For a situation with a second mouth located in the north, wave heights in front of the second mouth show the same two-dimensional development as those in front of the present mouth.

Failure does not occur for a 1/3000 year storm for any configuration of the mouth: De Slufter was exposed to a (normative) 1/3000 year storm. Based on failure mechanisms defined by Von Gronau (2017) and ENW (2007) and on an analysis of maximum water levels and minimum dune height, 'Grensprofiel' and 'Initiation of flooding' failure do not occur. It is therefore concluded that De Slufter in its present configuration meets the legal safety standards for a normative 1/3000 year storm.

For situations equal to the reference scenario but with wider mouths (800m, 1000m, 1250m, 1500m), safety standards inside De Slufter are still met. Apart from a wider area of wave attack there is no significant difference in hydrodynamic response (e.g. maximum storm surge level) compared to the reference scenario. As the mouth grows wider, the sand dike erosion increases in areas that are then under wave attack (and were not in narrower mouth scenarios). However, in areas that were already under wave attack, the increase in sand dike erosion is not significant. In all wider mouth scenarios, dune erosion remains below $15 m^3/m$, apart from one transect in which a small duneform in front of the sand dike causes a large spike in erosion volume. Furthermore, there is no significant rise in maximum water level in the southwestern and northeastern corners of De Slufter. Inundation of Texel through these areas will thus not occur.

For a situation with a second mouth in the north of De Slufter (e.g. due to a dune breach) safety standards are still met. Maximum water levels in the northeastern part of De Slufter do not increase significantly and the wave attack on the sand dike is generally lower than for the 1500m wide mouth scenario.

Failure does not occur for a series of consecutive storms: De Slufter was exposed to 4 consecutive 1/3000 year storms. The effect of each consecutive storm on sand dike erosion decreases exponentially. This was expected, as each storm forces the cross-shore sand dike profile closer to the equilibrium profile. The total erosion along the sand dike also decreases exponentially for each consecutive storm. After the 4 storm events,

no failure mechanism occurs. The Slufter can thus adequately protect Texel from flooding, even for a series of 4 normative 1/3000 year storms.

The slufter valley is essential for the coastal safety of De Slufter: It is evident from the short wave energy distribution during storm events that the wave dissipation due to depth-induced breaking and wave friction is essential for the coastal safety of Texel as it severely mitigates sand dike erosion. The shallow water depths in the valley during storm events are governing for these processes. It is thus essential that the bed levels inside the valley do not lower. This would cause wave heights at the sand dike to increase and would lead to an increase in sand dike erosion.

Answer to research subquestion 2

"How will the proposed new coastal management strategy affect the present coastal safety of Texel?" Based on a range of possible scenarios in the near future, the new coastal management strategy will not jeopardize the coastal safety of Texel. Even for a situation in which the slufter mouth has grown 1500m wide or in which 4 consecutive 1/3000 year storms occur back to back De Slufter meets safety standards. This is a result of the highly dissipative slufter valley, which reduces the wave energy significantly as it propagates through the valley towards the sand dike. The valley thus shelters the sand dike from large energetic conditions. Therefore, even though no conclusion can be drawn on the expected width and location of the slufter mouth, De Slufter will comply to safety standards assuming negligible bed level change inside the valley in the near future.

8.1.3. Future coastal safety

The southwestern and northeastern edges of the slufter valley are governing for the coastal safety assessment of De Slufter, not the sand dike: Before the 'Grensprofiel' failure occurs at the sand dike, inundation ('Initiation of flooding') already takes place over the lateral edges of De Slufter. The highest possible contiguous ridge around the valley is located on NAP+6.70m. This means that the sand dike is not the weakest link in the coastal defence but the lateral edges are as they are much lower in height. However, in this study it was assumed that dunes would remain the same height until 2100, which is not realistic. Still, the inundation over the edges clearly indicates that in the coastal defence of Texel, these edges are of much more significance than the sand dike, which is very resilient against any extreme scenario apart from a single weak spot in the north.

If sea levels at the Dutch coast rise 1.70 m or more, De Slufter does not comply to the legal safety standards: For SLR = 0.75 m De Slufter still meets the legally defined safety standards. No lowering of the sand dike is observed and no inundation takes place. However, when SLR = 1.95 m the minimum volume in the sand dike falls below the 'Grensprofiel' failure limit and inundation takes place over the southwestern and northeastern edges of De Slufter. This means that somewhere in between SLR = 0.75 m and SLR = 1.95 m failure starts occurring due to inundation ('Initiation of flooding') and 'Grensprofiel' failure. Based on the topography in the southwestern and northeastern edges of De Slufter and the constant water level head between the offshore boundary and the valley for different sea level rise scenarios, 'Initiation of flooding' failure occurs for SLR = 1.70 m. This is thus the 'tipping point' of De Slufter.

Answer to research subquestion 3

"How will the proposed new coastal management strategy affect the future coastal safety of Texel?" The model results suggest that De Slufter complies to legal safety standards if sea levels at the Dutch coast do not rise more than 0.75 m. If sea levels rise 1.95 m or more coastal safety is not guaranteed because inundation occurs over the lateral edges of De Slufter and because overwash occurs over the northern part of the sand dike. This means that somewhere in between SLR = 0.75 m and SLR = 1.95 m

there is a 'tipping point', beyond which De Slufter cannot comply to legal safety standards. Based on the current topography of De Slufter and the near constant difference between offshore mean water level and storm surge level in the valley for different SLR scenarios this failure will occur for SLR = 1.70 m.

8.2. Recommendations

Recommendations are made based on the discussion and conclusions in this study:

Investigate the contribution of curvature-induced secondary flow to gully migration: The migration of the gully is not only dominated by yearly averaged net alongshore sediment transport or by storms. It is thus important to study which other processes are of importance. Based on the historical gully migration data, it is expected that curvature-induced secondary flow due to tidal forcing is a governing process for the direction of gully migration, especially in the most seaward section of the gully. This theory is substantiated by the fact that after every relocation the gully has travelled in the direction of the most seaward outer bend.

However, curvature-induced secondary flow is a 3D process that cannot be modelled by the 2DH program XBeach Surfbeat. It is therefore recommended to study gully migration with a 3D modelling program (e.g. Delft3D). Using identical wave and flow conditions for different initial locations and shapes of the gully will then shed light on whether or not secondary flow plays a significant role in gully migration.

Cease the relocations of the slufter mouth but monitor the migration: As shown in this report, De Slufter complies to the safety standards under present conditions. As each relocation is a costly endeavor it is recommended to stop the relocations of the gully. Not only to save money but also to acquire valuable data and insight into the long-term dynamics of the gully. First of all, it is of great interest to see whether or not the gully will erode the dune heads or if the dune heads will stop further migration of the gully. If the first, a wider slufter mouth in the future is a likely scenario. If the second, the opposite is true. Second, it is of great interest whether or not the gully will naturally relocate itself by cut-offs. If this is the case it is also unlikely that the mouth will widen significantly in the near future.

Increase the frequency of bathymetry/bed level measurements in the slufter mouth: The developments in satellite imagery technology and availability can be used for frequently determining gully positions. The Google Earth Engine can now provide more frequent, higher quality and more readily availabile satellite imagery which can be used to investigate gully migration with a much higher temporal resolution.

However, accurate bed levels are also a necessity for a thorough analysis. Therefore, to properly study the migration of the gully it is advised to have more frequent measurements of the 2D bathymetry of the area in and around the mouth (similar to the current Kusthoogte measurements). With monthly measurements the link between hydrodynamic forcing and gully migration can be more accurately analysed than is currently the case. Even increasing the frequency from once to twice a year would be helpful as a distinction could then be made between storm season and non-storm season. The increase in measurement frequency would have to persist for at least a full year but preferably for multiple years. As more frequent 2D bathymetry measurements are an expensive option, a more economic option would be to perform bed level measurements along transects, similar to those described in appendix D. However, this could be difficult during the breeding season, when section of the gully could be off limits.

Study how to naturally raise the lateral edges of De Slufter and the northern part of the sand dike: As concluded in this study, the lateral edges are the weakest link of De Slufter in terms of coastal safety. To mitigate the probability of 'Initiation of flooding' failure in the future, it is recommended to investigate how to naturally raise the bed levels of the 'weak spots' at the lateral edges of De Slufter and the northern part of the sand dike. As one of the reasons for issuing this study was to increase the natural character of De Slufter it is not recommended to manually raise the dunes. Also, manual intervention into the dune area is not easy as De Slufter is a Natura2000 site. It is thus recommended to study and find nature-based solutions in which natural processes can be utilized to raise the lateral edges of De Slufter. The same must be done for the northern part of the sand dike.

As SLR is a long-term process, raising the bed level is not a short-term necessity. However, as natural processes are long-term it is recommended to study the possibilities on a short term. Furthermore, if natural processes cannot suffice, it is recommended to manually raise bed levels. This is certainly not preferable though. A minimum bed level of NAP+9 m is recommended. This will make De Slufter resilient against sea level rise of as much as 3.17 m.

Perform a long-term morphodynamic modelling study into De Slufter: In this study, possible future scenarios were modelled. No further conclusion was drawn on the probability of occurrence of each scenario. In the present configuration, the morphology of the slufter valley and sand dike is dominated by storm and springtide events. However, when sea levels rise, De Slufter will at some point become constantly inundated. If that happens, De Slufter will also be morphologically active during calm conditions. Therefore, it is recommended to study the long-term response of De Slufter to sea level rise under calm conditions.

It is recommended to perform a long-term study with a process-based numerical model incorporating a morphological acceleration factor. As discussed, using a *morfac* was not an option in this study because it would not properly portray the interaction between the tide and storm surge. However, when modelling calm conditions, this is no longer an issue.

Furthermore, due to the future dependance of morphology on both calm and storm conditions, it is recommended to incorporate a coupled Delft3D and XBeach Surfbeat model approach (Van Ormondt et al., 2017). This coupled model approach was out of the scope of this study. However, now that a fully functioning XBeach Surfbeat model is ready for further use, this could be within the scope of a future MSc Thesis. Such a model would be well validatable as the long-term modelling could be compared to the presently available annual measurements.

Bibliography

Baart, F., Leander, R., de Ronde, J., De Vries, H., Vuik, V., and Nicolai, R. (2014). Zeespiegelmonitor 2014. Technical report, Deltares.

Bolle, A., Mercelis, P., Roelvink, J., Haerens, P., and Trouw, K. (2010). Application and Validation of Xbeach for Three Different Field Sites. *Coastal Engineering Proceedings*, 1(32):40.

Bosboom, J. and Stive, M. J. F. (2012). *Coastal Dynamics I: Lectures Notes CIE4305*. VSSD, Delft, 0.5 edition.

Bretschneinder, C. (1964). Generation of Waves by Wind State of the Art. *International Summer Course Lunteren*, page 160.

CERC (1984). Shore protection manual. *US Army Corps of Engineers, Coastal Engineering Research Center, Vicksburg, MS*, 2.

DeConto, R. M. and Pollard, D. (2016). Contribution of Antarctica to past and future sea-level rise. *Nature*, 531(7596):591–597.

Delft University of Technology (2018). SWAN Cycle III user manual.

Deltares (2012). Orca GUI User Manual: Guidelines.

Deltares (2016). Assemblageprotocol WBI2017: Nadere uitwerking van het beoogde assemblageprotocol voor het wettelijke beoordelingsinstrumentarium. Technical report, Deltares, Delft, The Netherlands.

Deltares (2017). XBeach Documentation, Release pre-1.22.4344. Technical report, Deltares, Delft, The Netherlands.

Den Bieman, J., Stuparu, D., Hoonhout, B., Diermanse, F., Boers, M., and Van Geer, P. (2014a). Fully Probabilistic Dune Safety Assessment Using an Advanced Probabilistic Method. *Coastal Engineering Proceedings*, 1(34):9.

Den Bieman, J. P., Stuparu, D. E., Hoonhout, B. M., Diermanse, F. L., Boers, M., and Van Geer, P. F. (2014b). Fully Probabilistic Dune Safety Assessment Using an Advanced Probabilistic Method. *Coastal Engineering Proceedings*, 1(34):9.

Den Heijer, C. (2013). *The role of bathymetry, wave obliquity and coastal curvature in dune erosion prediction*. PhD thesis, TU Delft.

Den Heijer, C., Baart, F., and van Koningsveld, M. (2011). Assessment of dune failure along the Dutch coast using a fully probabilistic approach. *Geomorphology*, 143-144:95–103.

Dissanayake, D., Ranasinghe, R., and Roelvink, J. (2012). The morphological response of large tidal inlet/basin systems to relative sea level rise. *Climatic Change*, 113(2):253–276.

Durieux, M. (2003). *De Stabiliteit van de Slufter op Texel*. PhD thesis, Delft University of Technology.

Ecomare (2018). Dutch Wadden Sea Region: The Slufter.

ENW (2007). Technisch Rapport Duinafslag: Beoordeling van de veiligheid van duinen als waterkering ten behoeve van Voorschrift Toetsing op Veiligheid 2006. Technical report.

ENW (2016). Grondslagen voor hoogwater- bescherming. Technical report, Expertisenetwerk waterveiligheid, Breda, The Netherlands.

European Commission (2017). Environment: Natura2000, http://ec.europa.eu/environment/.

Fisher, J., Overton, M., and Chisholm, T. (1986). Field measurements of dune erosion. *Coastal Engineering*, (1986):1107–1115.

Haasnoot, M., Bouwer, L., Diermanse, F., Kwadijk, J., van der Spek, A., Oude Essink, G., Delsman, J., Weiler, O., Mens, M., ter Maat, J., Huismans, Y., Sloff, K., and Mosselman, E. (2018). *Mogelijke gevolgen van versnelde zeespiegelstijging voor het Deltaprogramma. Een verkenning*.

Holthuijsen, L. H. (2010). *Waves in oceanic and coastal waters*. Cambridge University Press, New York, USA.

Holthuis, M. (2017). *Establishing the link between vegetation and sedimentology in the Slufter, Texel*. Msc thesis, Vrije Universiteit Amsterdam.

Hoonhout, B. and Den Heijer, C. (2011). Reliability of dune erosion assessment along curved coastlines. *Coastal Engineering Proceedings*, 32(37):15.

Intergovernmental Panel on Climate Change (IPCC) (2014). Climate change 2014, Synthesis report: Summary for Policymakers. Technical report, IPCC.

KNMI, van den Hurk, B., Siegmund, P., Klein Tank, A., Attema, J., Bakker, A., Beersma, J., Bessembinder, J., Boers, R., Brandsma, T., Brink, H. V. D., Drijfhout, S., Eskes, H., Haarsma, R., Hazeleger, W., Jilderda, R., Katsman, C., Lenderink, G., Loriaux, J., Meijgaard, E. V., Noije, T. V., Oldenborgh, G. J. V., Selten, F., Siebesma, P., Sterl, A., Vries, H. D., van Weele, M., De Winter, R., and van Zadelhoff, G. (2014). KNMI'14: Climate Change scenarios for the 21st Century – A Netherlands perspective. Technical Report May, KNMI.

Le Bars, D., Drijfhout, S., and De Vries, H. (2017). A high-end sea level rise probabilistic projection including rapid Antarctic ice sheet mass loss. *Environmental Research Letters*, 12(4).

Ministerie van Verkeer en Waterstaat (2007). Hydraulische Randvoorwaarden primaire waterkeringen voor de derde toetsronde 2006-2011. Technical Report HR 2006.

Nidzieko, N., Hench, J., and Monismith, S. (2009). Lateral Circulation in Well-Mixed and Stratified Estuarine Flows with Curvature. *Journal of Physical Oceanography*, 39(4):831–851.

NOAA Office for Coastal Management (2016). Coastal Change Analysis Program Regional Land Cover and Change. Technical Report 5, NOAA Office for Coastal Management.

Oude Essink, G., van Baaren, E., and de Louw, P. (2010). Effects of climate change on coastal groundwater systems: A modeling study in the Netherlands. *Water Resources Research*, 46(10):1–16.

Pawlowicz, R., Beardsley, B., and Lentz, S. (2002). Classical tidal harmonic analysis including error estimates in MATLAB using TDE. *Computers and Geosciences*, 28(8):929–937.

Pedroli, G. and Hoekstra, A. (1992). Sluftervorming en natuurontwikkeling. Technical report, Waterloopkundig laboratorium | WL, Delft, The Netherlands.

Roelvink, J., McCall, R., Mehvar, S., Nederhoff, K., and Dastgheib, A. (2017). Improving predictions of swash dynamics in XBeach: The role of groupiness and incident-band runup. *Coastal Engineering*.

Roelvink, J., Reniers, A., Van Dongeren, A., Van Thiel de Vries, J., McCall, R., and Lescinski, J. (2009). Modelling storm impacts on beaches, dunes and barrier islands. *Coastal Engineering*, 56(11-12):1133–1152.

Sallenger, A. H. (2000). Storm impact scale for barrier islands. *Journal of Coastal Research*, 16(3):890–895.

Slootjes, N. and Wagenaar, D. (2016). Factsheets normering primaire waterkeringen.

Smyth, C. and Hay, A. E. (2002). Wave Friction Factors in Nearshore Sands. *Journal of Physical Oceanography*, 32(12):3490–3498.

Soulsby, R. (1997). *Dynamics of Marine Sands: A Manual for Practical Applications*. Thomas Telford Publications, London.

Steetzel, H. J. (1993). *Cross-Shore Transport During Storm Surges*. PhD thesis, Delft University of Technology.

Technische Adviescommissie voor de Waterkeringen (2002). Leidraad Zandige Kust. Technical report, Technische Adviescommissie voor de Waterkeringen, Delft, The Netherlands.

van der Most, H. (2011). Samenvatting van analyse van slachtofferrisico's en maatschappelijke kosten- batenanalyse Waterveiligheid 21e eeuw. Technical report, Deltares.

Van Der Vegt, M. and Hoekstra, P. (2012). Morphodynamics of a storm-dominated, shallow tidal inlet: The Slufter, the Netherlands. *Geologie en Mijnbouw/Netherlands Journal of Geosciences*, 91(3):325–339.

Van Der Wegen, M. (2013). Numerical modeling of the impact of sea level rise on tidal basin morphodynamics. *Journal of Geophysical Research: Earth Surface*, 118(2):447–460.

Van Dongeren, A., Bolle, A., Vousdoukas, M., Plomaritis, T., Eftimovas, P., Williams, J., Armaroli, C., Idier, D., Van Geer, P., Van Thiel de Vries, J., Haerens, P., Taborda, R., Benavente, J., Trifonova, E., Ciavola, P., Balouin, Y., and Roelvink, J. (2009). MICORE: dune erosion and overwash model validation with data from nine European field sites. *Proceedings of Coastal Dynamics 2009: Impacts of Human Activities on Dynamic Coastal Processes*, Dano:1–15.

Van Geer, P., den Bieman, J., Hoonhout, B., and Boers, M. (2015). XBeach 1D–Probabilistic model: ADIS, Settings, Model uncertainty and Graphical User Interface. *Tec. Rep*, pages 1209002–1209436.

Van Gent, M., Van Thiel de Vries, J., Coeveld, E., De Vroeg, J., and Van de Graaff, J. (2008). Large-scale dune erosion tests to study the influence of wave periods. *Coastal Engineering*, 55(12):1041–1051.

Van Ormondt, M., Nelson, T. R., Hapke, C. J., and Roelvink, J. (2017). Morphodynamic Modelling of the Wilderness Breach, Fire Island, New York. Part I: Model Set-up and Validation. Technical report.

Van Puijvelde, S. (2010). *Morphodynamics of De Slufter, morphodynamical processes in a small tidal inlet in the Netherlands*. Master thesis, Utrecht University.

van Rijn, L. (1984). Sediment Transport, Part III: Bed Forms and Alluvial Roughness. *Journal of Hydraulic Engineering*, 110(12):1733–1754.

van Rijn, L. (2007). Unified View of Sediment Transport by Currents and Waves . I : Initiation of Motion , Bed Roughness , and Bed-Load Transport. *Journal of Hydraulic Engineering*, 133(6):649–667.

van Rijn, L. (2009). Prediction of dune erosion due to storms. *Coastal Engineering*, 56(4):441–457.

van Rijn, L. (2013). A simple general expression for longshore transport of sand, gravel and shingle. *Coastal Engineering*, 90:23–29.

Van Rooijen, A. and Van Thiel de Vries, J. (2014). Stormgedreven morfodynamiek van De Slufter, Texel. Modelstudie naar het effect van het loslaten van de monding op de kustveiligheid en morfodynamiek.

Van Thiel de Vries, J. (2009). *Dune erosion during storm surges*. PhD thesis, Delft University of Technology.

Van Thiel de Vries, J., Van Gent, M., Walstra, D., and Reniers, A. (2008). Analysis of dune erosion processes in large-scale flume experiments. *Coastal Engineering*, 55(12):1028–1040.

Vennell, R. and Old, C. (2007). High-resolution observations of the intensity of secondary circulation along a curved tidal channel. *Journal of Geophysical Research: Oceans*, 112(11):1–13.

Von Gronau, C. (2017). *Using a process-based model for dune safety assessment, a case study of Delfland with a 2DH XBeach model*. Master thesis, Delft University of Technology.

Wentworth, C. K. (1922). A Scale of Grade and Class Terms for Clastic Sediments. *The Journal of Geology*, 30(5):377–392.

WL | Delft Hydraulics (2006). Dune erosion - Product 1: Deterministic dune erosion prediction methods. Technical report, WL | Delft Hydraulics.

Zijdenbos, G. (2015). Golfparameters in Aquo. Technical report, Rijkswaterstaat.

A

Literature study

A.1. Dune safety assessment

The limit profile in figure 2.7 consists of a 'front slope' of 1:1, a 3 meter wide top and a 'rear slope' of 1:2. The minimum height of the limit profile is determined by formula

$$h_0 = RP + 0.12 T_p * \sqrt{H_{0s}} \tag{A.1}$$

with

- RP = storm surge level
- T_p = Peak wave period
- H_{0s} = Expected value of significant wave height

B

Field data

B.1. Bathymetry

The bathymetry for the model was created from 3 different datasets which vary in spatial coverage, frequency of measurement and resolution:

Source	**Resolution [m]**	**Frequency of measurement** $[yr^{-1}]$
Actueel Hoogtebestand Nederland	25	0.2
KustLiDAR	5	1
Vaklodingen	20	0.25-1

Table B.1: Datasets used for the model bathymetry

The bathymetry for the model has been created by naturally interpolating all three datasets on a predefined grid (the 'interpolation grid'), see figure B.1. Natural interpolation assigns a value to a grid cell by taking into account all nearby datapoints and averaging these values. This method was used because it means that a dataset with a higher resolution (and thus more datapoints around a grid cell) will have a larger influence on the final value of a grid cell point, which is desirable.

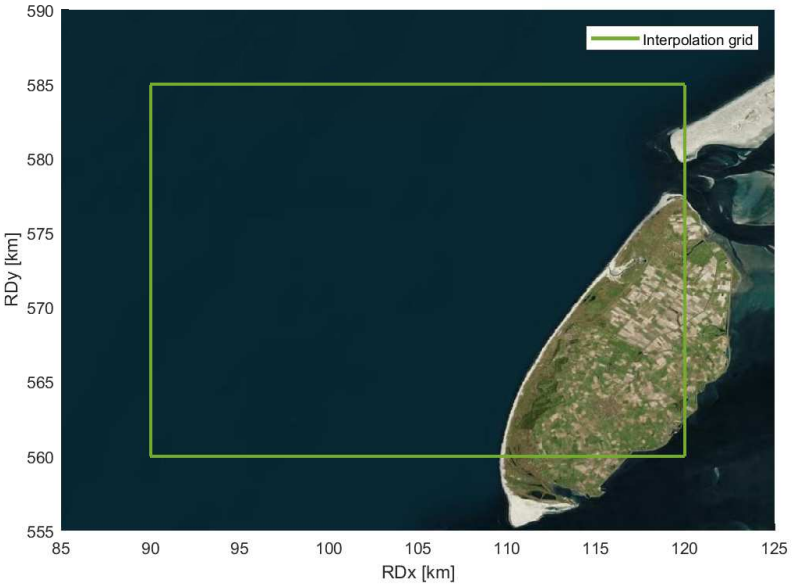

Figure B.1: Outline of the 'interpolation grid' which was used to combine all datasets on.

Figure B.2 shows the spatial coverage of the three different datasets (a-c) and the resulting (interpolated) bathymetry (d). From the 'Vaklodingen' data, all datapoints with values above 0 m+NAP were excluded. This choice was made because, considering the availability of the higher resolution KustLidar data and the AHN data, the surveying method of the 'Vaklodingen' data (which is measured from water) was considered less satisfactory for determing points on land. The 2015 final bathymetry consists of KustLiDAR data from 2015, AHN data from 2009 and Vaklodingen data from 2015.

The fact that older AHN was used is not considered an issue for two reasons. First, due to the natural interpolation method the higher resolution and more recent Kusthoogte dataset will have a much larger influence on grid cell values. Second, the area in which only AHN data is present are mainly areas in which no large morphological changes are expected.

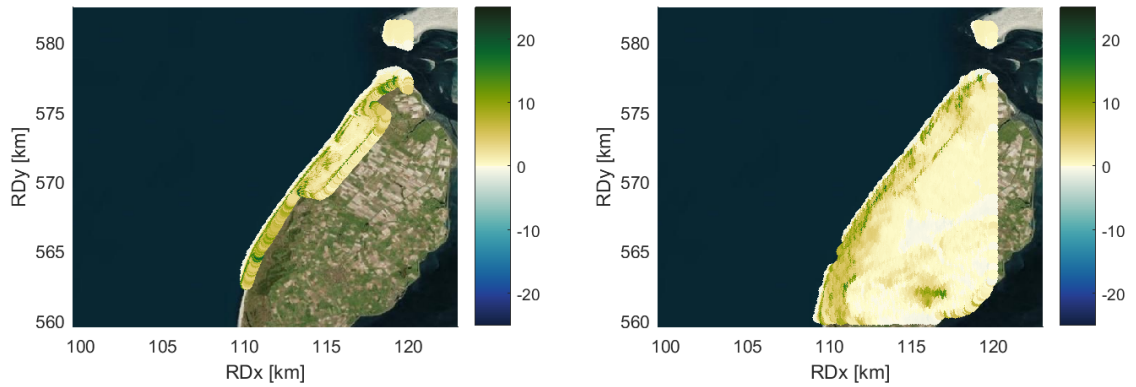

(a) Spatial coverage of KustLiDAR data (2015)

(b) Spatial coverage of AHN data (2009)

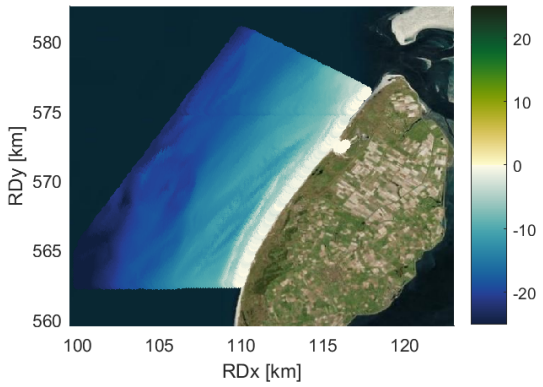

(c) Spatial coverage of Vaklodingen data (2015)

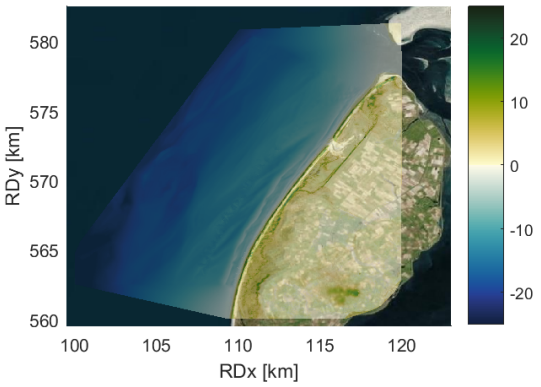

(d) Final bathymetry (2015)

Figure B.2: Final bathymetry and datasets used for the 2015 bathymetry.

Figure B.3 shows that the 2008 final bathymetry, which was used for the morphological validation, consists of KustLiDAR data from 2008, AHN data from 2009 and Vaklodingen data from 2009. The final 2008 bathymetry thus contains a lot of 2009 data. Nevertheless, the high resolution of the 2008 KustLiDAR data in the valley and the mouth makes it clearly distinct from the 2009 bathymetry.

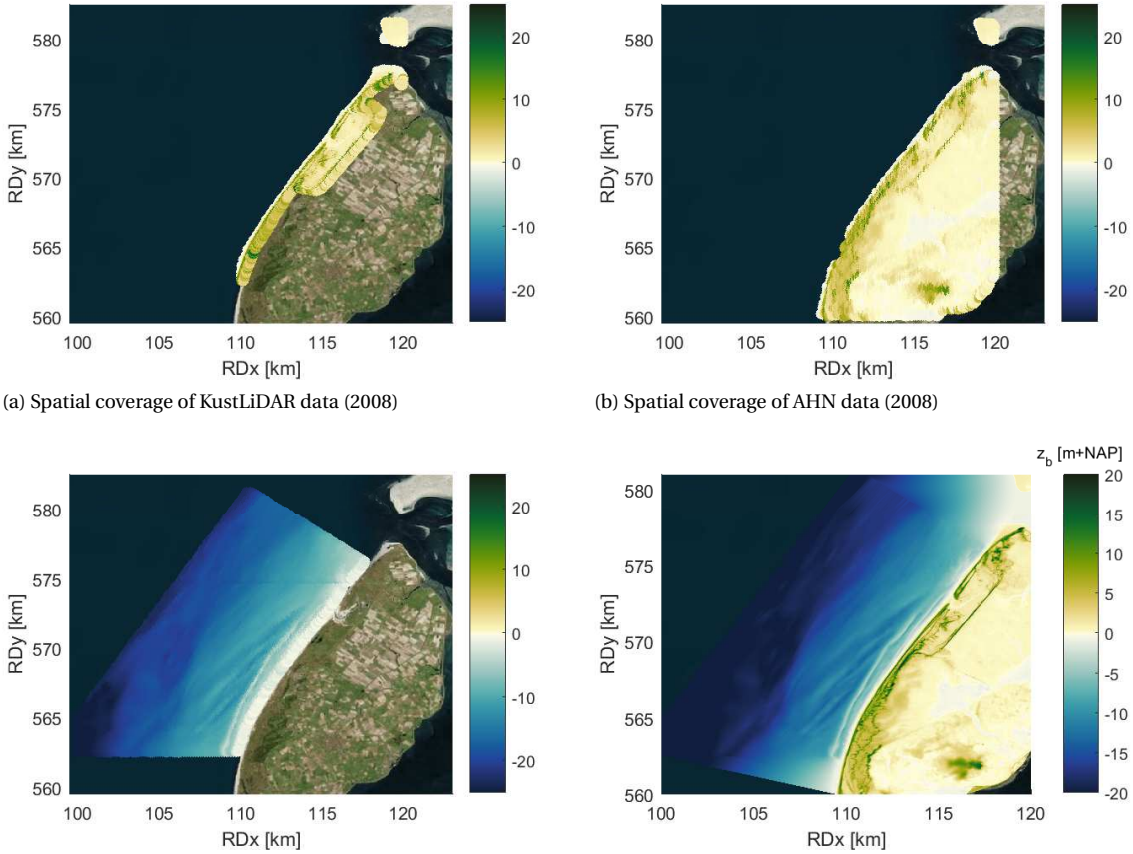

(a) Spatial coverage of KustLiDAR data (2008)

(b) Spatial coverage of AHN data (2008)

(c) Spatial coverage of Vaklodingen data (2009)

(d) Final bathymetry (2008)

Figure B.3: Final bathymetry and datasets used for the 2008 bathymetry.

B.1.1. Tidal constituents

For the creation of the tidal water level the tidal components of the water level time series at the Texel Noordzee buouy were analysed with T_TIDE (Pawlowicz et al., 2002). A list of all tidal constituents and their tidal period, amplitude and phase are presented in table B.2. Using these values as input, a representative tidal water level was created with T_PREDIC, spanning the entire period of the water level observations. The tidal water level was used for the creation of the model boundary conditions.

Tidal constituent	**Tidal period** [h]	**Amplitude** [m]	**Phase**	**Tidal constituent**	**Tidal period** [h]	**Amplitude** [m]	**Phase**
'M2 '	12,4	0,787	163,4	'MKS2'	12,4	0,008	302,2
'S2 '	12,0	0,225	225,5	'MK3 '	8,2	0,007	117,8
'N2 '	12,7	0,126	143,7	'MSK6'	4,0	0,007	275,7
'M4 '	6,2	0,103	180,8	'M3 '	8,3	0,006	284,2
'SA '	8766,2	0,097	293,6	'RHO1'	26,7	0,005	128,0
'M6 '	4,1	0,090	261,9	'MF '	327,9	0,005	169,9
'O1 '	25,8	0,089	176,7	'SO3 '	8,2	0,005	344,4
'2MS6'	4,1	0,083	315,2	'TAU1'	25,7	0,005	392,9
'MU2 '	12,9	0,077	245,8	'2Q1 '	28,0	0,004	732,6
'K1 '	23,9	0,071	348,7	'H2 '	12,4	0,004	275,1
'MS4 '	6,1	0,058	244,2	'SN4 '	6,2	0,003	268,4
'K2 '	12,0	0,056	237,3	'3MK7'	3,5	0,003	136,5
'L2 '	12,2	0,051	171,8	'PI1 '	24,1	0,003	301,7
'2MN6'	4,2	0,049	233,2	'MSM '	763,5	0,003	320,6
'NU2 '	12,6	0,041	122,5	'SO1 '	22,4	0,003	157,1
'MN4 '	6,3	0,035	155,0	'PSI1'	23,9	0,003	279,0
'P1 '	24,1	0,031	338,3	'SIG1'	27,8	0,002	344,6
'LDA2'	12,2	0,030	165,4	'OO1 '	22,3	0,002	169,4
'Q1 '	26,9	0,028	117,0	'J1 '	23,1	0,002	755,2
'SSA '	4382,9	0,023	175,7	'NO1'	24,8	0,002	223,2
'H1 '	12,4	0,022	222,9	'PHI1'	23,8	0,002	323,6
'M8 '	3,1	0,021	313,5	'GAM2'	12,5	0,002	150,9
'2MK6'	4,1	0,019	329,5	'SK'	8,0	0,002	186,3
'MSN2'	11,8	0,018	416,4	'BET1'	25,0	0,002	194,5
'MM '	661,3	0,016	182,5	'S4'	6,0	0,002	356,9
'EPS2'	13,1	0,015	227,8	'ALP1'	29,1	0,002	163,1
'2SM6'	4,0	0,014	113,7	'SK4'	6,0	0,001	128,0
'MK4 '	6,1	0,014	260,9	'ETA2'	11,8	0,001	249,6
'MO3 '	8,4	0,014	272,1	'CHI1'	24,7	0,001	252,5
'2N2 '	12,9	0,013	124,1	'OQ2'	13,2	0,001	771,6
'S1 '	24,0	0,012	133,6	'R2'	12,0	0,001	348,7
'T2 '	12,0	0,012	194,0	'UPS1'	21,6	0,000	341,8
'MSF '	354,4	0,011	280,0	'THE1'	23,2	0,000	615,9
'2MK5'	4,9	0,010	235,2	'2SK5'	4,8	0,000	150,0

Table B.2: List of all tidal constituents and their period, amplitude and phase. The list is ordered based on amplitude.

B.2. Hydrodynamic conditions

The hydrodynamic conditions near De Slufter were derived from two wave buoys offshore from Texel, see table B.3.

Buouy	RDx [m]	RDy [m]	Data	Measurement period [yr]	Timestep [min]
Eierlandse Gat	106 602	588 068	Wave	39	180
Texel Noordzee	111 215	570 624	Water level	29	10

Table B.3: Wave buouy data information showing location, data type, measurement period and timestep of measurement data.

Figure B.4: Wave and water level buoy locations.

B.2.1. Water levels

As discussed in section 3.1.1, the non-tidal residual water level was calculated by subtracting the manually created tidal water level from the total water level,presented in figure 3.3. With ORCA (Deltares, 2012), a peak-over-threshold analysis was performed on the non-tidal residual water level, presented in figure B.5.

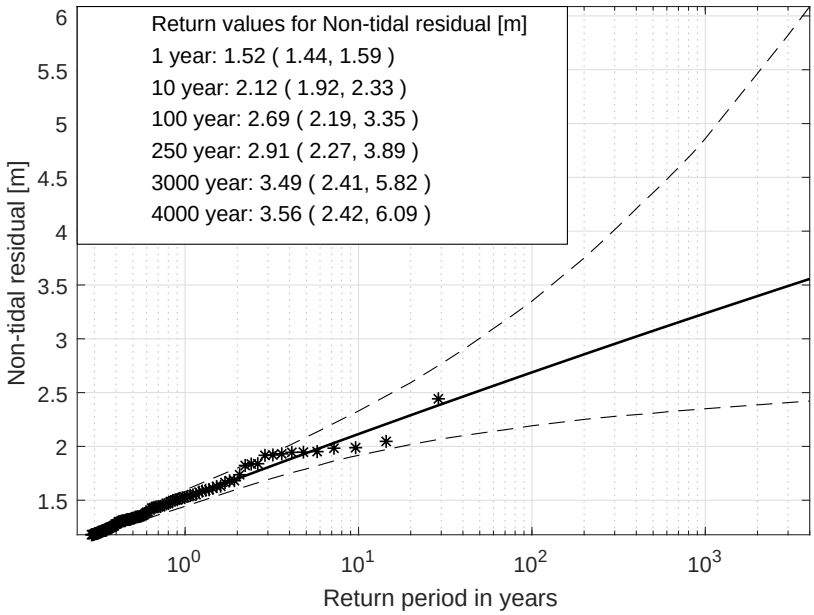

Figure B.5: Non-tidal residual in the North Sea near Texel as a function of return period. The solid line is the best fit based on the Pareto Distribution (GPD). The staggered lines are the borders of the 95% confidence interval.

The normative water level boundary conditions resulting from this analysis have been presented in table B.4.

Boundary condition	$z_{tidal,max}$ **[m+NAP]**	z_{NTR} **[m+NAP]**	η **[m+NAP]**
1/1 storm	0.79	1.52	**2.3**
1/10 storm	0.79	2.12	**2.9**
1/100 storm	0.79	2.69	**3.5**
1/3000 storm	0.79	3.49	**4.3**

Table B.4: Normative water levels for different return periods.

B.2.2. Waves

Wave height

With ORCA, a peak-over-threshold analysis was also performed on the significant wave heights measured by the 'Eierlandse Gat' buouy, leading to the top left values in figure B.6. The values for return periods of 1000 and 10 000 years were added to indicate the relatively small increase in wave height for return periods higher than 3000 years in relation to lower return periods.

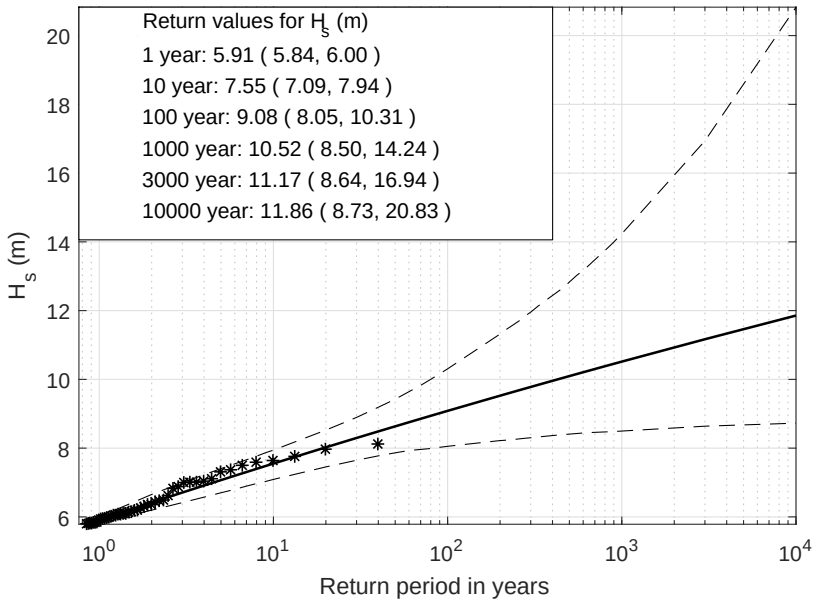

Figure B.6: Significant wave height in the Eierlandse Gat as a function of return period. The solid line is the best fit based on the Pareto Distribution (GPD). The staggered lines are the borders of the 95% confidence interval.

Wave period

The wave periods corresponding to the calculated extreme wave heights cannot be calculated through a peak-over-threshold analysis. Instead, they were calculated by using wave steepness (s) and height (H_{m0}) (figure B.7) in combination with the dispersion relation for arbitrary depths:

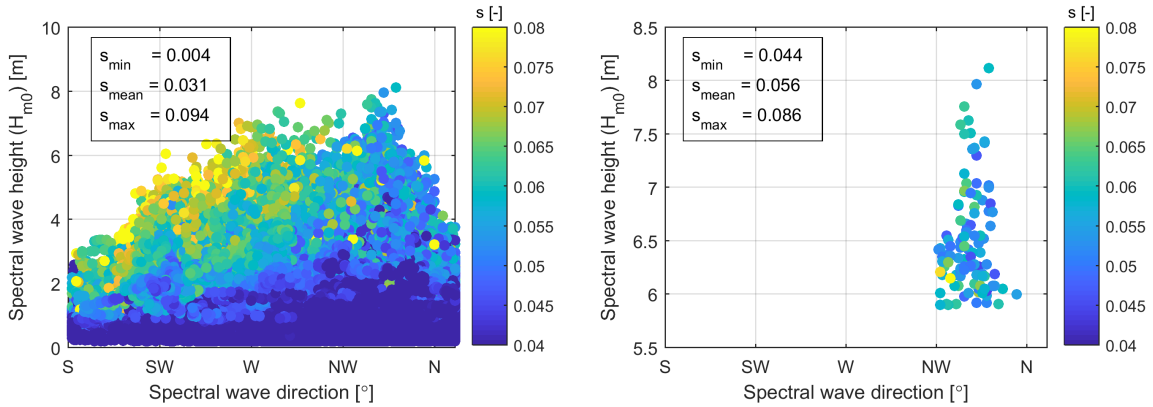

(a) All waves

(b) Waves from NW-N higher than 5.9 meters

Figure B.7: Wave steepness and direction calculated from measurements including minimum, mean and maximum wave steepness values.

$$T_{m02} = \sqrt{\frac{2\pi L}{g tanh(\frac{2\pi d}{L})}} = \sqrt{\frac{2\pi H_{m0}/s}{g tanh(\frac{2\pi d}{H_{m0}/s})}} \tag{B.1}$$

A representative wave steepness had to be assumed to derive one representative wave period per return period. To assume a representative wave steepness the following assumptions were made:

1. the nautical direction of all waves higher than 5.9 meters (1/1 per year storm wave height) is in the NW-N range (315-360°):
$$dir_{H>5.9} = 315 - 360° \tag{B.2}$$
2. all waves higher than 5.9 meters have the same steepness:
$$s_{H>5.9_1} = s_{H>5.9_2} = s_{H>5.9_i} \tag{B.3}$$
3. the steepness of all waves higher than 5.9 meters is equal to the mean steepness of all historically measured waves from the NW-N that were higher than 5.9 meters:
$$s_{H>5.9} = mean(s_{H>5.9}) \tag{B.4}$$

Assumption 1 is based on the geographical location of the United Kingdom and Scandinavia. Because of the limited fetch, waves from the S-NW and N-NE are limited in height (see figure B.8). It is therefore assumed that waves with return periods longer than 100 years can only arrive from the NW-N. Assumption 2 and 3 are necessary simplifications to encapsulate individual waves in representative boundary conditions. The choice for the mean steepness is supported by the distribution of wave steepness values (figure B.10), which shows that the majority of wave steepness values is centered around the mean. The wave steepness that follows from these assumptions is 0.056 [-].

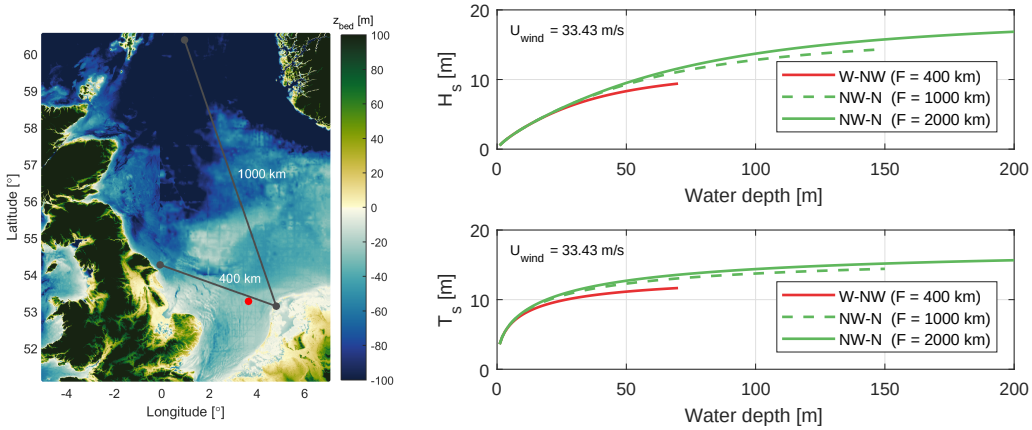

(a) Fetch length for WNW and NNW wave directions in the North Sea.

(b) Wave height and wave period over water depth calculated with the Brettschneider formulas (Bretschneinder, 1964).

Figure B.8: Fetch analysis of waves from the WNW and NNW. Waves from the WNW have a smaller fetch than waves from the NNW. Waves from the NNW also develop in deeper water. This leads to reduced maximum wave heigth and period for waves from the WNW compared to the NNW. $U = 33.43 m/s$ is based on the peak-over-threshold analysis of wind speeds in figure B.9 (for a 1/3000 year storm).

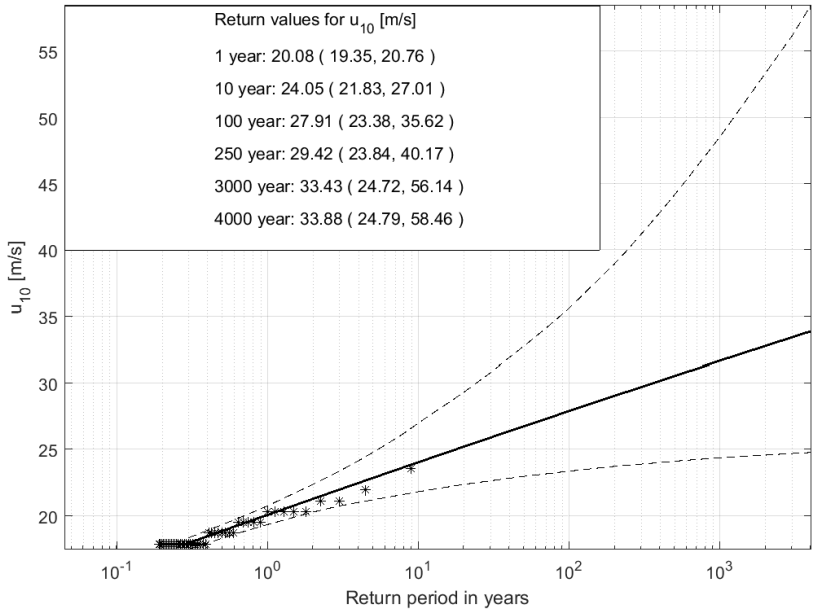

Figure B.9: PoT analysis on wind speeds at the A12 monitoring station located in the North Sea.

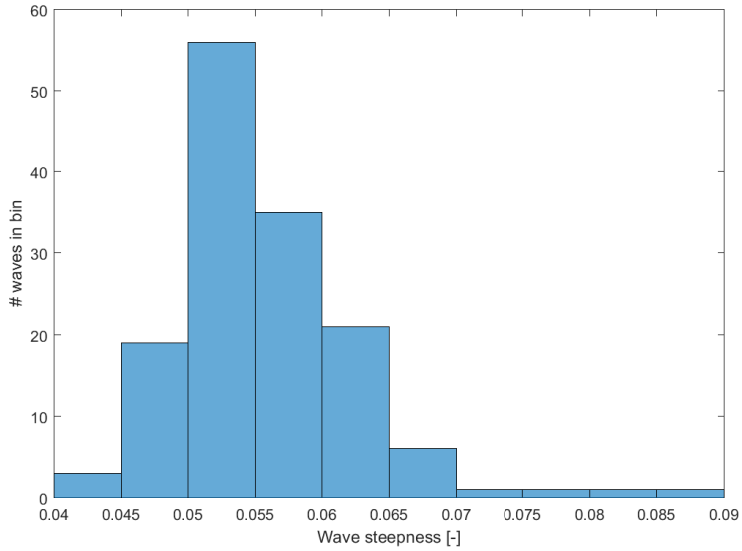

Figure B.10: Wave steepness distribution for waves from the NW-N range.

Please note that the steepness values from figure B.7 were calculated from (measured) T_{m02} values. Using these steepness values for the calculation of wave periods will therefore result in T_{m02} values. The peak period (T_p) is subsequently calculated with $T_p \approx 1.1 * T_{m02}$ (Holthuijsen, 2010).

ID	**Boundary condition**	H_{m0} **[m]**	T_p **[s]**	Dir
1	1/1 storm	5.9	9.5	NW
2	1/10 storm	7.6	11.2	NW
3	1/100 storm	9.1	12.8	NW
4	1/3000 storm	11.2	15.2	NW

Table B.5: Overview of representative wave conditions per return period.

C

Model setup

C.1. Grid

The model grid resolution was defined such that the highest resolution is found in the area near the slufter mouth and the lowest resolution is found near the lateral boundaries and the offshore boundary of the model. The cross-shore and alongshore distribution of grid cell sizes is presented in figure C.1.

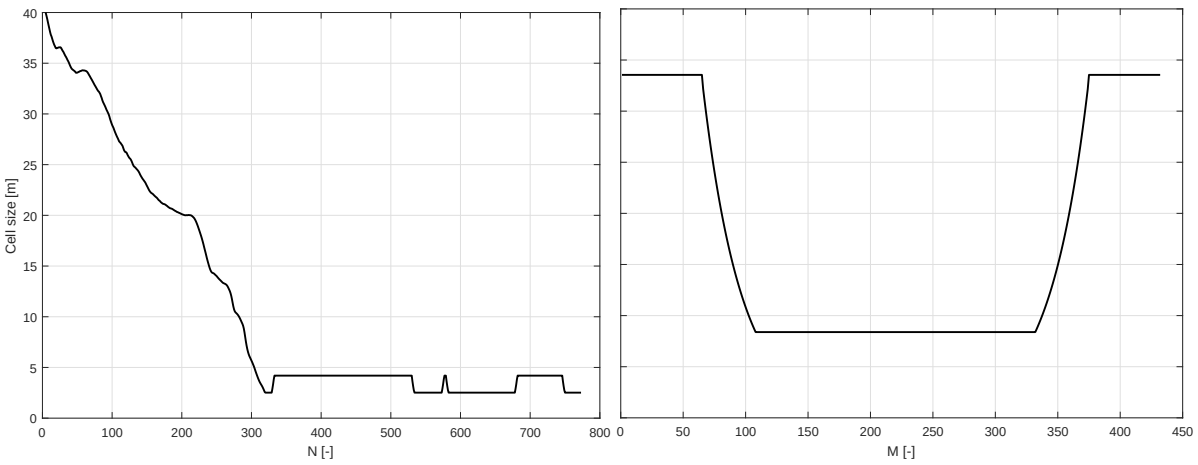

(a) Cross-shore grid cell size (starting at the offshore boundary)

(b) Alongshore grid cell size (starting at the southern lateral boundary)

Figure C.1: Grid cell sizes for the XBeach model

C.2. Bathymetry changes

For stability purposes, adjustments were made to the bathymetry data in the XBeach model. First, the offshore end of the model was deepened to prevent higher waves from immediately breaking upon entering the model. Based on figure C.2 and on the wave characteristics for a 1/10 000 year storm (see section B.2.2) the 3 offshore boundary cells were manually set to a depth of 40 meters. From the offshore boundary the depth was linearly interpolated over (alongshore) grid cells 4 to 100 (figure C.3-(a)).

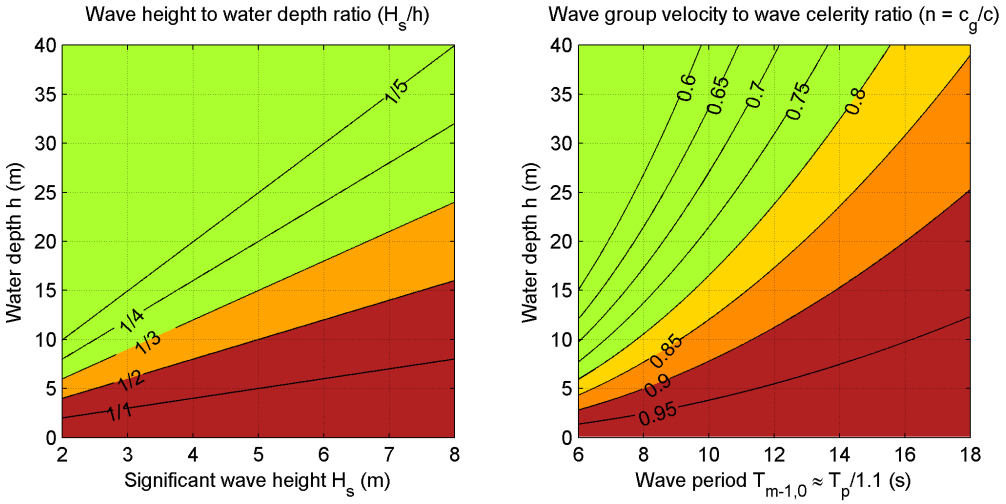

Figure C.2: Ratios used for the determination of the offshore boundary depth.

Second, both lateral boundaries were averaged to make them equal (figure C.3-(b)). This was done after a difference in depth between both lateral boundaries in combination with cyclic boundary conditions resulted in errors. Lastly, the bed level was manually elevated at both landward sides of the lateral boundaries to prevent water from flowing in through small gaps in the initial bathymetry. This was decided upon after the model showed water entering the model with extreme flow velocities in these locations, which resulted in numerical instability. The bed level there was changed such that the grid cells with bed level values lower than 7 meters were set to 7 meters (figure C.3-(c)). This prevented any water from entering the model through the landward lateral boundaries.

When running the scenarios with SLR, errors necessitated extra bathymetry changes. A wall was created in the southwestern corner of the slufter valley to prevent water from flowing out and causing numerical instability. This was in addition to the manually created walls at the lateral boundaries.

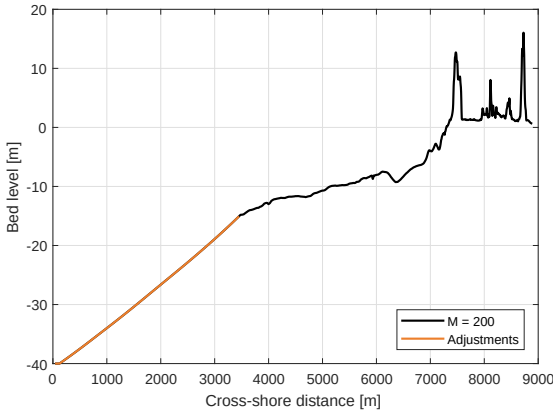

(a) Cross-shore transect. The cross-shore distance is measured from the offshore boundary.

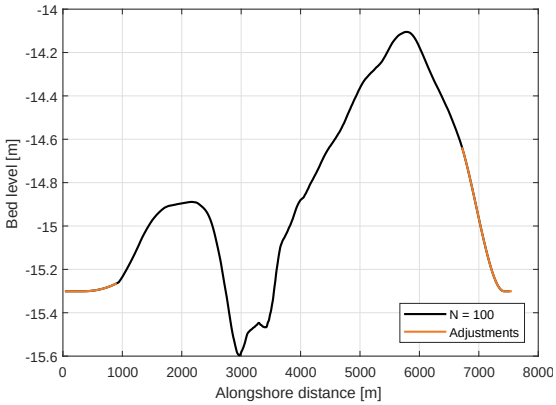

(b) Alongshore transect offshore. The alongshore distance is measured from the southern lateral boundary.

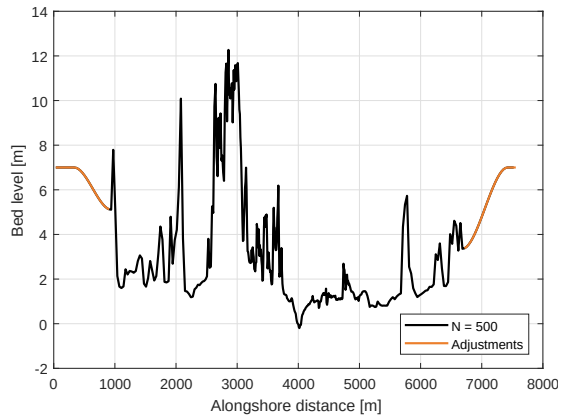

(c) Alongshore transect of the slufter valley. The alongshore distance is measured from the southern lateral boundary.

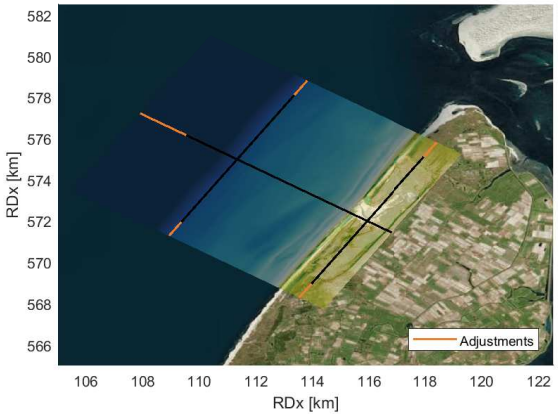

(d) Overview

Figure C.3: Adjustments made to the initial bathymetry before it was used in the model.

C.3. Model paramater settings

For the purpose of reproducability, the *params* file settings that were used for the validation and for the reference scenario are presented here. Table C.1 presents the hydrodynamic validation parameters. Table C.2 presents the reference scenario parameters.

Bed composition parameters	
D50	0.000339
D90	0.000390
Flow parameters	
bedfriction	manning
bedfricfile	*varying from 0.02 to 0.05*
General	
dtheta_s	10
single_dir	1
fw	0.06
Grid parameters	
depfile	bed_2015_20.dep
posdwn	-1
nx	773
ny	432
alfa	0
vardx	1
xfile	x_2015_20.grd
yfile	y_2015_20.grd
xori	0
yori	0
thetamin	0
thetamax	360
dtheta	360
thetanaut	1
MPI parameters	
mpiboundary	x
Model time	
tstop	215400
Morphology parameters	
morphology	0
morfac	1
Tide boundary conditions	
zs0file	tide_3000yr_storm_smalldt.txt
tideloc	2
Wave boundary condition parameters	
instat	jons_table
cyclic	1
Wave numerics parameters	
wavint	60
Wave-spectrum boundary condition parameters	
bcfile	jonswap_3000yr_storm_smalldt.txt
Output variables	
outputformat	netcdf
tintp	1
tintm	3600
tintg	3600
tstart	0

Table C.1: Parameter settings for the 2015 hydrodynamic validation.

Bed composition parameters	
D50	0.000339
D90	0.000390
Flow parameters	
bedfriction	manning
bedfricfile	*varying from 0.02 to 0.05*
General	
dtheta_s	10
single_dir	1
fw	0.06
CFL	0.5
Grid parameters	
depfile	bed_2015_23.dep
posdwn	-1
nx	773
ny	432
alfa	0
vardx	1
xfile	x_2015_23.grd
yfile	y_2015_23.grd
xori	0
yori	0
thetamin	0
thetamax	360
dtheta	360
thetanaut	1
MPI parameters	
mpiboundary	x
Model time	
tstop	133200
Morphology parameters	
morphology	1
morfac	1
Tide boundary conditions	
zs0file	tide_hydro_validation_2015.txt
tideloc	2
Wave boundary condition parameters	
instat	jons_table
cyclic	1
Wave numerics parameters	
wavint	60
Wave-spectrum boundary condition parameters	
bcfile	jonswap_hydro_validation_2015.txt
Output variables	
outputformat	netcdf
tintp	1
tintm	1800
tintg	3600
tstart	0

Table C.2: Parameter settings for the reference scenario.

D

Validation

In this appendix additional information is given on the validation data and method. In section D.1, the measurement data with which the model was validated is treated.

D.1. Measurement campaigns

Utrecht University (12/09/2008 - 15/10/2008)

In 2008, a 1-month measurement campaign by Utrecht University was executed in De Slufter. The measurements included: 13 gully transects, a dune-to-dune transect, a cross-basin transect and a shore transect (Van Puijvelde, 2010). In the course of the measurement campaign one storm event occurred during which a slight gully migration was identified (right figure). Apart from bed level measurements, hydrodynamic measurements (i.e. water level, velocity, wave height, wave period and wave direction) were also documented.

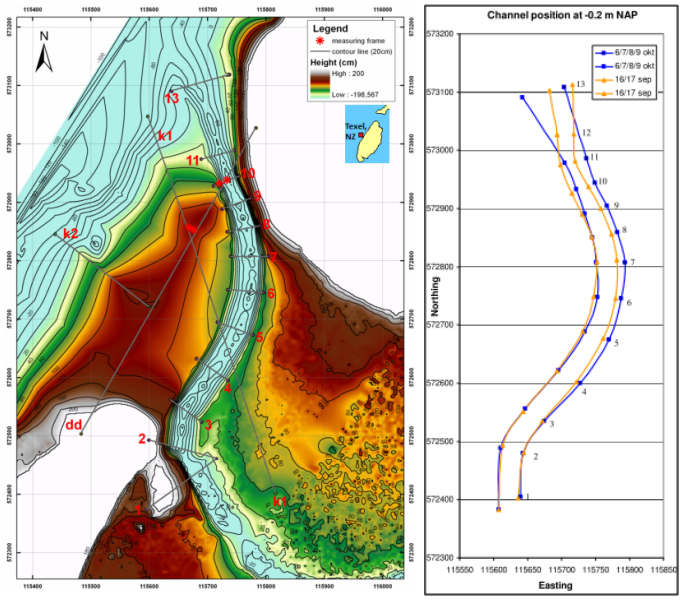

Figure D.1: Overview of measured transects during the 2008 measurement campaign (Van Puijvelde, 2010).

Utrecht University (17/11/2015-07/03/2016)

In november 2015, a research team from Utrecht University deployed 20 pressure sensors in De Slufter at strategic locations. 8 instruments were placed along a transect that extended from the slufter mouth to the sand dike, see figure D.2. During the campaign, three deeper events were identified that generated a substantial amount of hydrodynamic data. The high frequency wave height, low frequency wave height, mean wave period and peak frequency have also been derived from the pressure measurements.

Figure D.2 shows that very little measurements have been performed at location P2. The instrument at P2 was located too high. Therefore it has only measured 2 consecutive water level time series. The instrument at P1 not been calibrated accurately (A.C. Engelstad, personal communication, April 26, 2018) which has rendered the measurements unusablein this study.

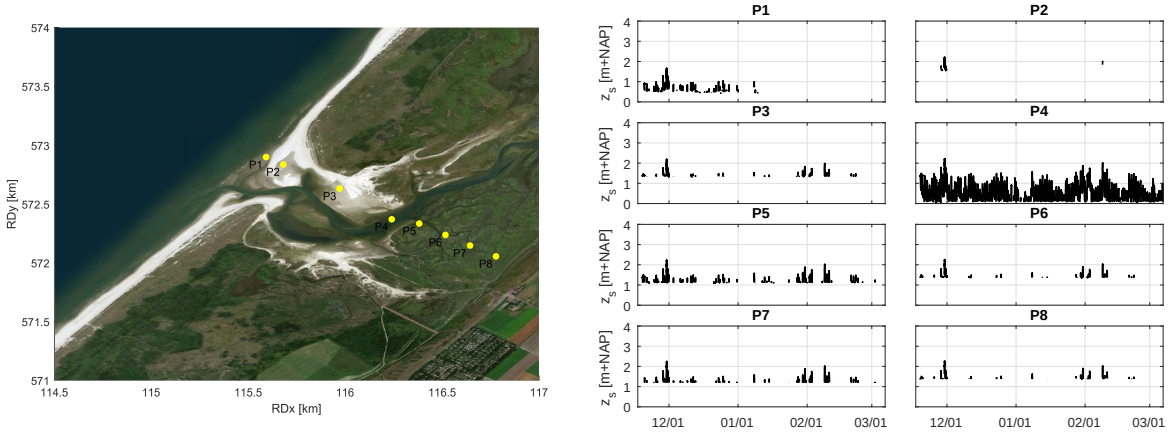

(a) Instrument locations

(b) Water level measurements

Figure D.2: 2015 measurement campaign data and measurement locations. The measurements at P1 have not been calibrated accurately and therefore have a strong bias (A.C. Engelstad, personal communication, April 26, 2018). The instrument at P2 has not generated much data because it was located too high.

E

Overwash development over time

In this appendix the development of the overwash in the northern part of the sand dike over time is presented. This overwash has taken place for a scenario with SLR = 3.17m. The red area in figure E.1 indicates the extent of the sand dike.

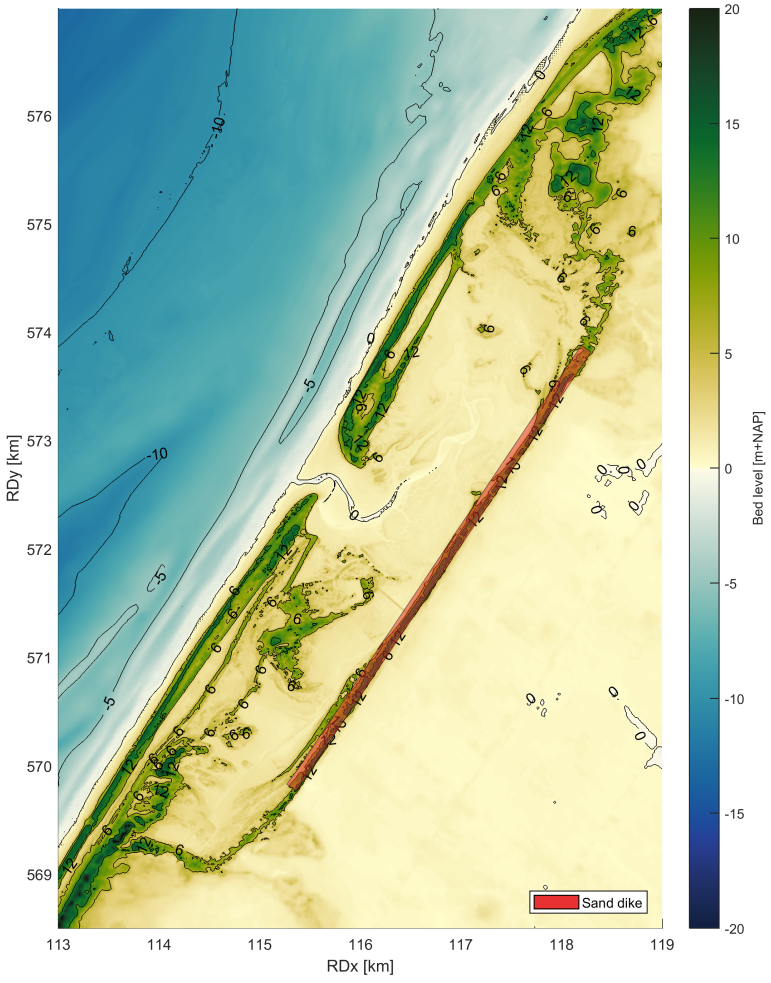

Figure E.1: 2D map of De Slufter indicating the sand dike.

Figure E.2 shows the development of sand dike height and water level over time for the overwash scenario in the SLR = 3.17m scenario. The red line indicates the development of the overwash at the northern part of

the sand dike. The outflow of water through the southern edge has already started at t=17h, as can be seen from the water level gradient from x=0m to x=2200m.

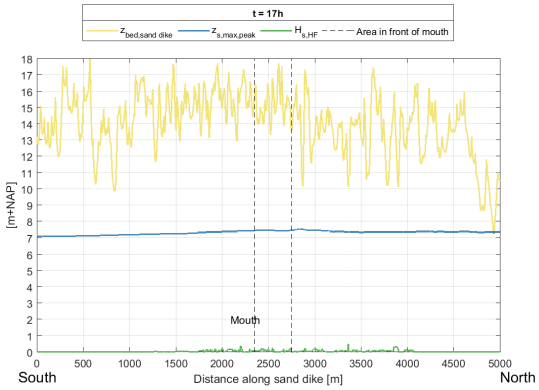

(a) t = 17h

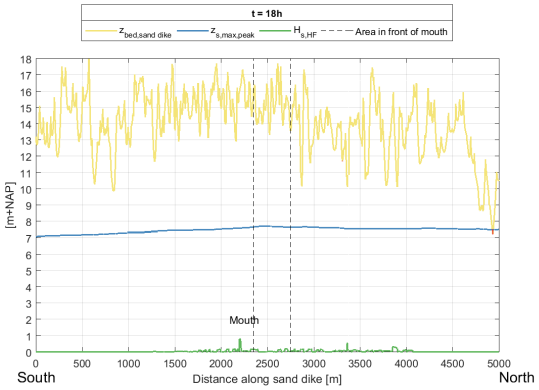

(b) t = 18h

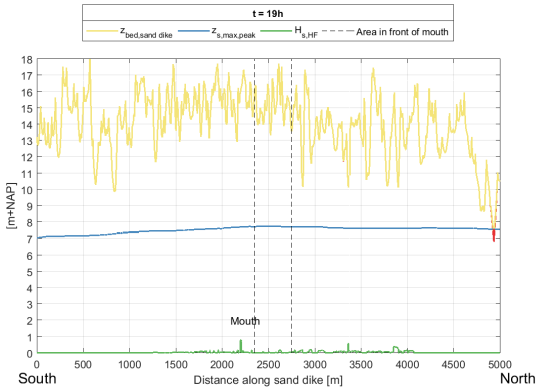

(c) t = 19h

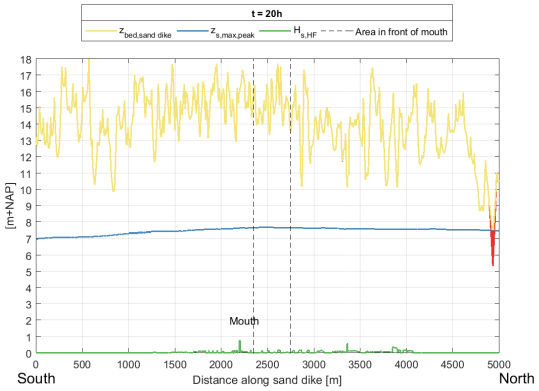

(d) t = 20h

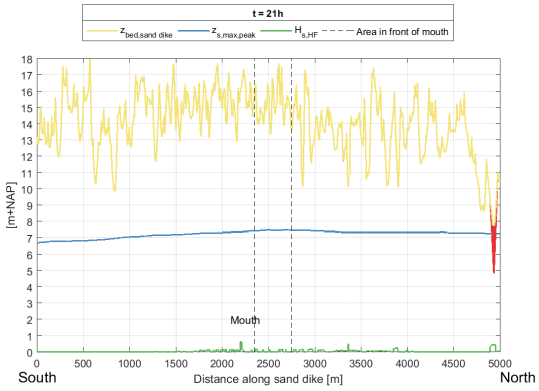

(e) t = 21h

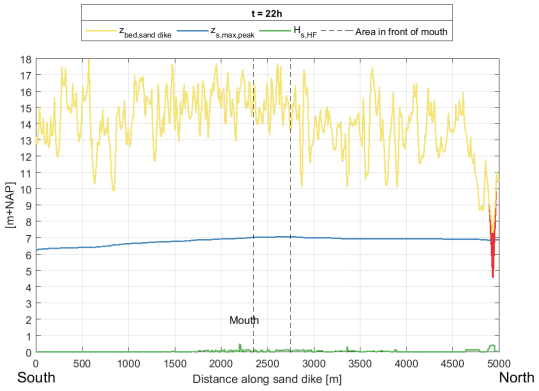

(f) t = 22h

Figure E.2: 1D alongshore transect of the sand dike showing the development of the overwash in the north over time. The yellow line represents the pre-storm sand dike height. The red line represents the post-storm sand dike height and the blue and green line indicate the maximum water level and short wave height, respectively

F

Sensitivity analysis

F.1. Bed friction

Figure F.1 shows the average errors (RMSE, scatter index and bias) of instrument locations P2-8 (see figure D.2). A clear downward trend can be distinguished in the results.

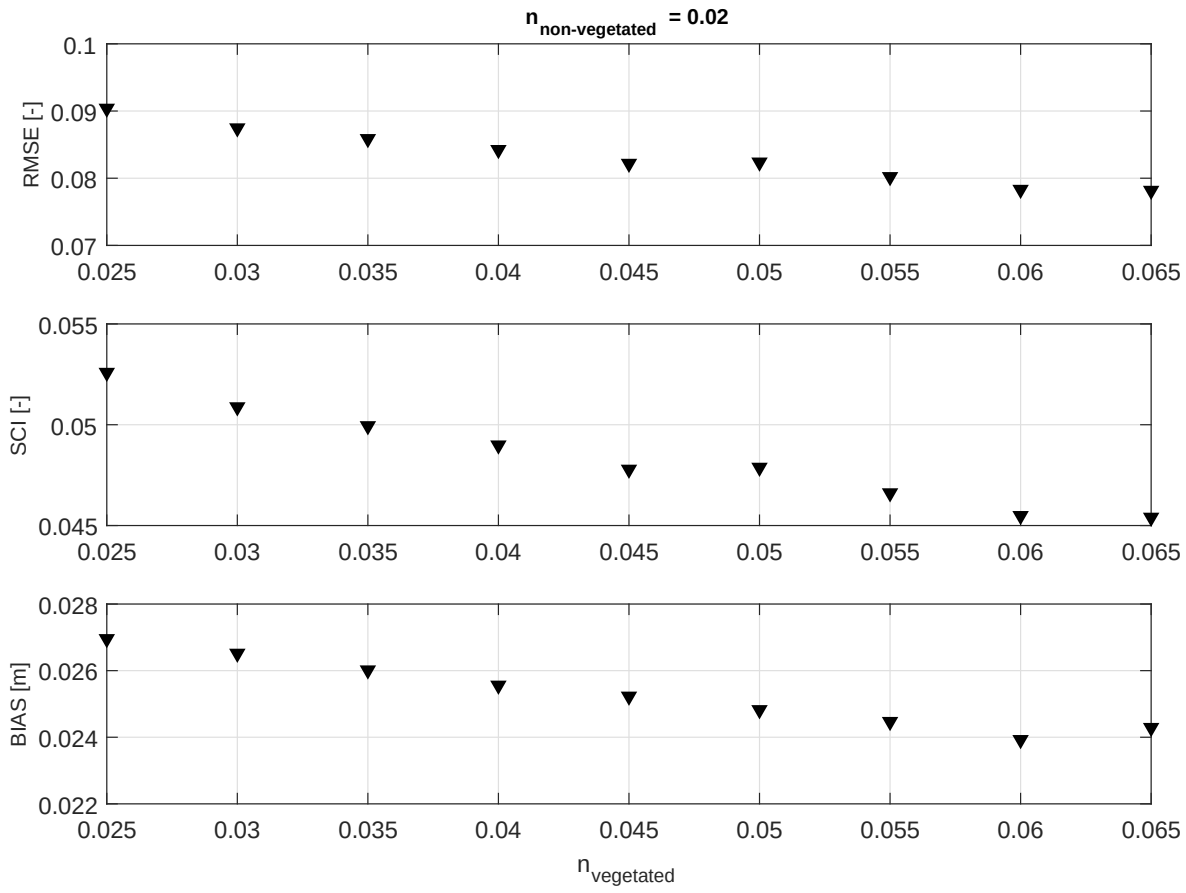

Figure F.1: Root-mean-squared error, scatter index and bias (averaged over locations P2-8) over Manning coefficient n. The x-axis represents the Manning coefficient for the vegetated area. The Manning coefficient for non-vegetated areas is a constant with value 0.02.

The fact that errors are smaller for an $n_{vegetated}$ of 0.065 than for 0.05 is contrary to the assumed value of 0.05. However, the assumption still stands for two reasons. First, differences between errors for different $n_{vegetated}$ are in a very narrow range (7.8% to 9%) and the influence of a different bedfriction is therefore very limited. Second, the validation has been performed with a small storm with (relatively) low water levels. In

chapter 5 it was shown that for low water levels, the ebb flow mainly takes place through the gully system. For equal tidal prisms the water level in a deep gully would be lower than in a shallow gully. It is likely that the gully depth is underestimated somewhat due to the interpolation between datapoints, which will always underestimate the maximum depth (if the datapoint is not located exactly on the maximum depth point). Also, the pre-storm gully location in the model is not exactly the same as the pre-storm gully location of the actual storm, which leads to an inaccuracy in the exact bed level at a measurement location.

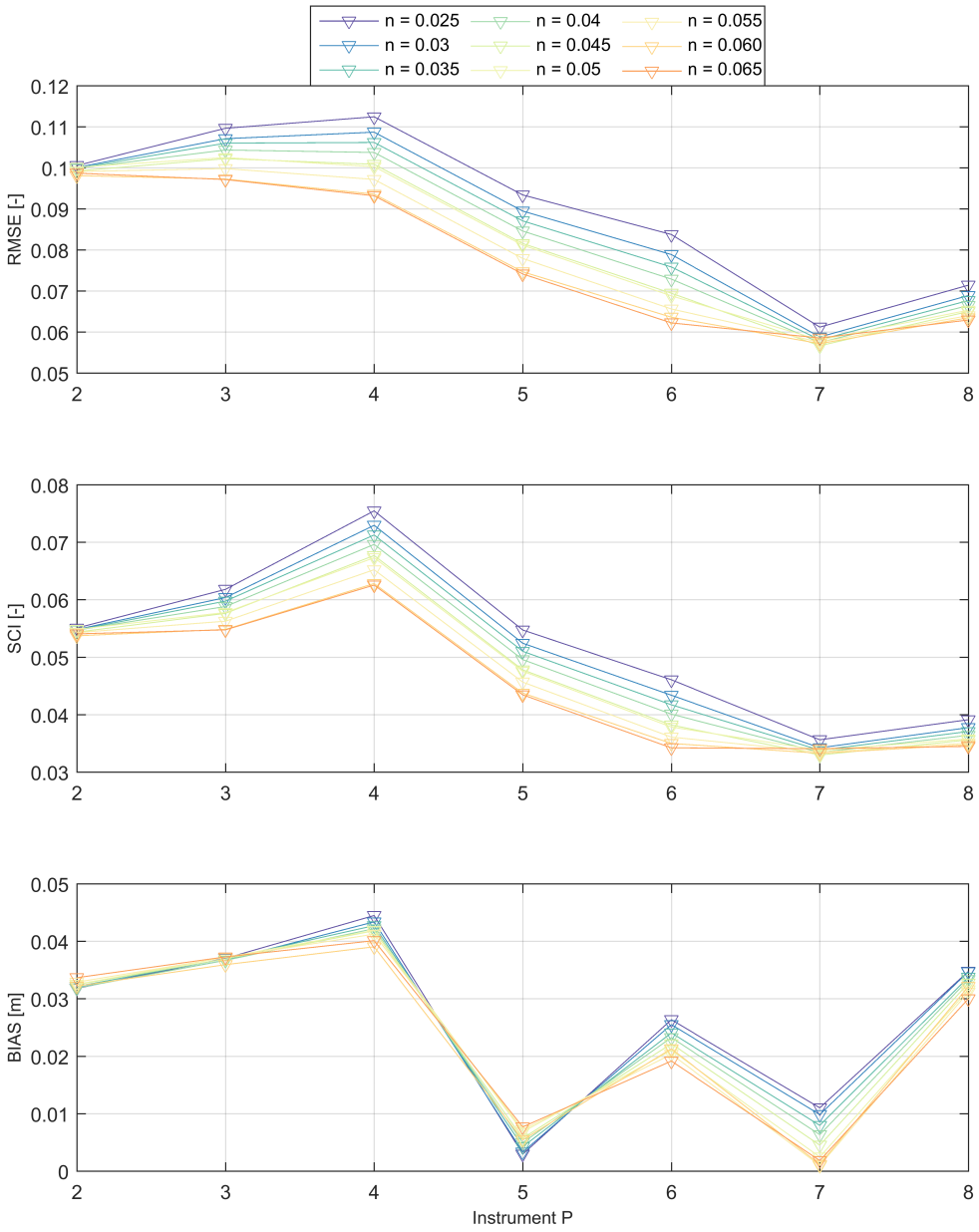

Figure F.2: Root-mean-squared error, scatter index and bias over measurement locations P2-8 for a range of $n_{vegetated}$.

Figure 5.3 shows that the largest errors occur when the water level drops later in the results than in the measurements. When the bed friction in De Slufter is higher, the water level will drop earlier. This reduces the error but only because it compensates for other errors. For higher water levels this effect will be reduced. Therefore, the bedfriction factor of 0.05 is acceptable.

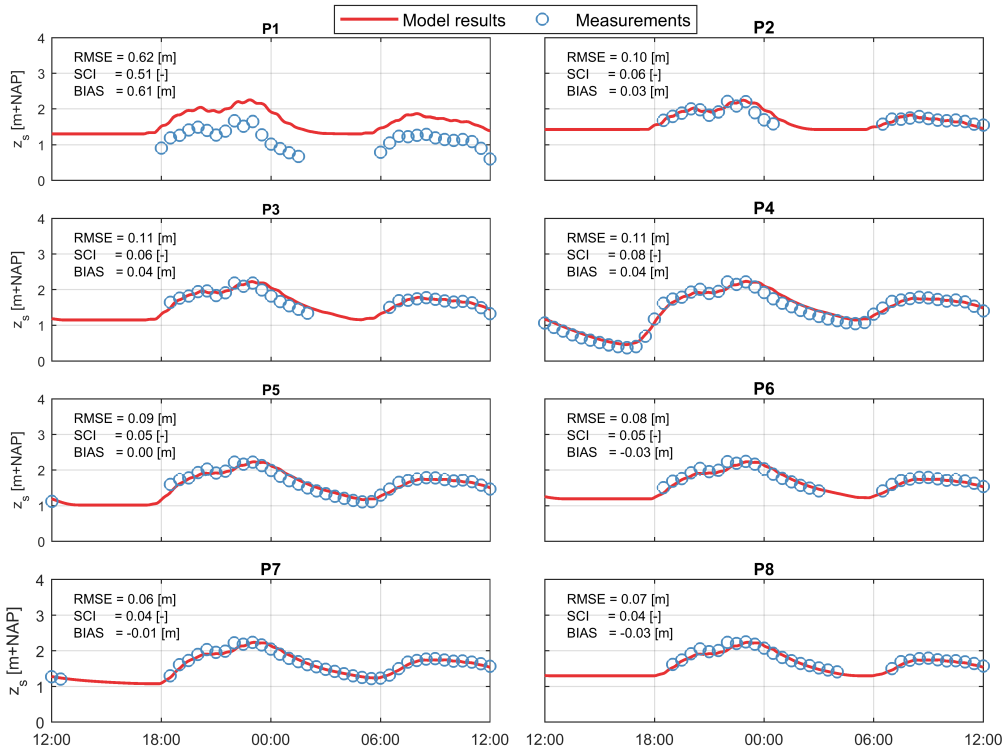

Figure F.3: Water level time series for instrument locations P1-8. $n_{vegetated} = 0.025$. The observations at P1 were incorrectly measured. P1 must thus be ignored.

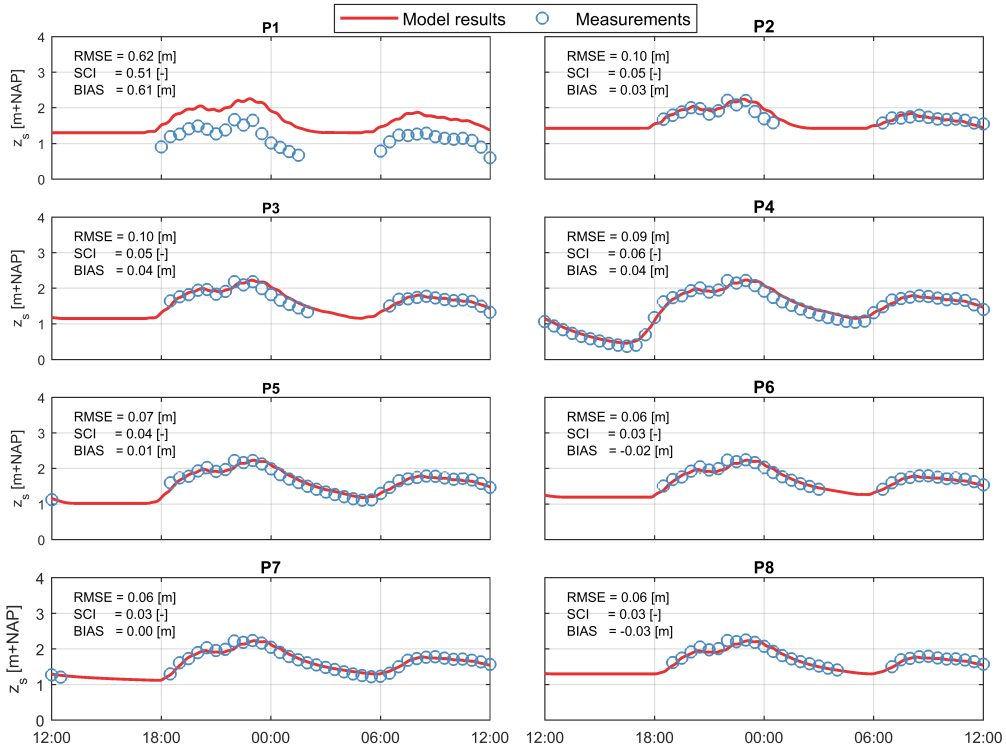

Figure F.4: Water level time series for instrument locations P1-8. $n_{vegetated} = 0.065$. The observations at P1 were incorrectly measured. P1 must thus be ignored.

F.2. Morphological acceleration factor

The default morphological acceleration factor (*morfac*) in XBeach is 1. Using a higher *morfac* for De Slufter (to reduce run times) is not allowed. Due to a higher morfac, the interaction between the tidal forcing and storm forcing is not well represented in the model anymore. This leads to an increase in overwash over the beach flat and more migration of the gully. This is evident from figures F.5 to F.8, which present 4 transects for both a *morfac* of 1 and 2.

Due to the higher *morfac*, the gully morphology due to tidal processes is mainly exaggerated in the south and middle part of the gully (section 1-3 and 4-6, respectively). The larger gully migration, compared to the reference scenario, in the middle section is caused by an increased sediment import over the beach flat into the gully during flooding.

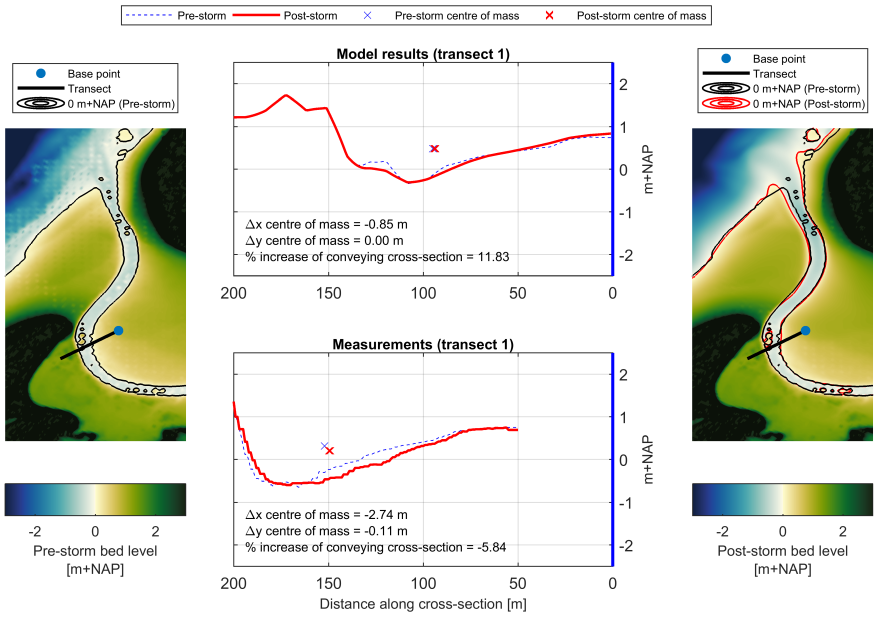

(a) *morfac = 1*

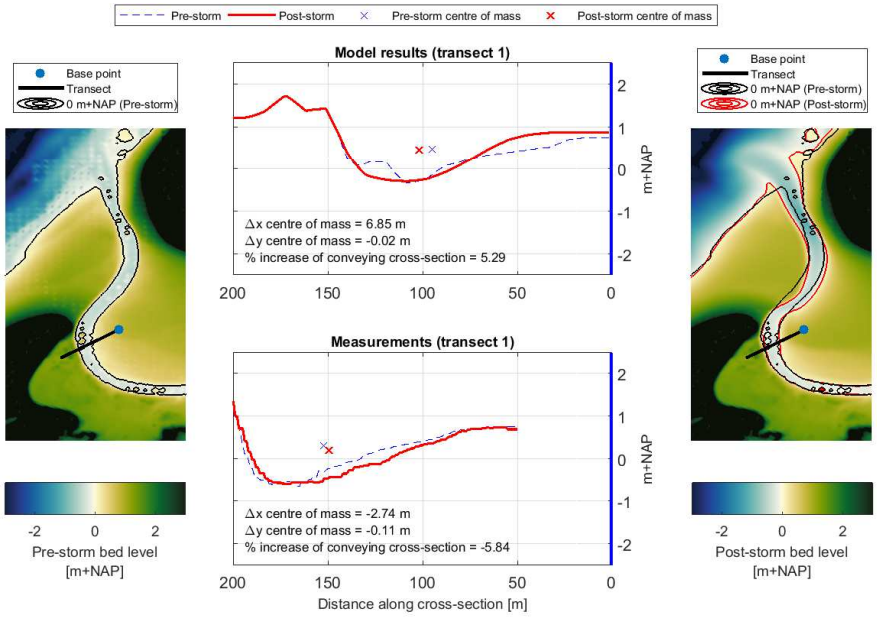

(b) *morfac = 2*

Figure F.5: Gully migration transect 1

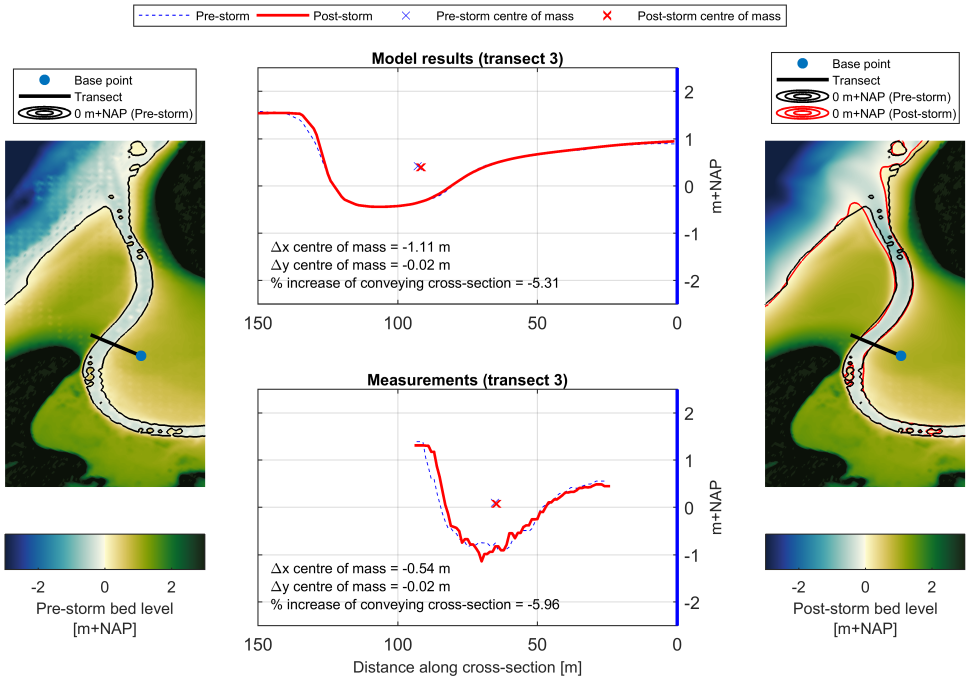

(a) *morfac = 1*

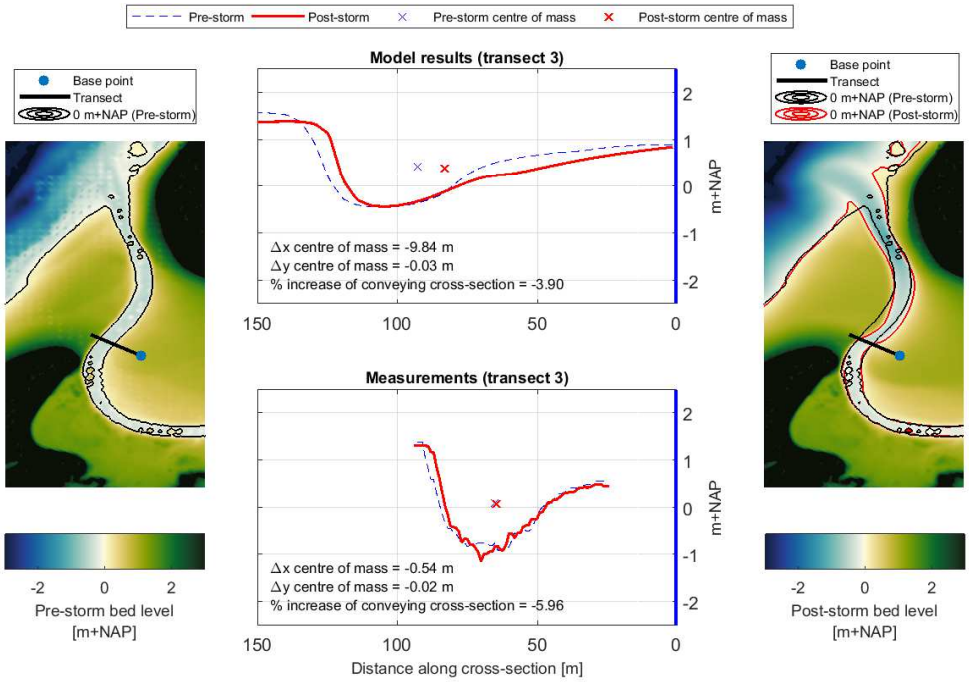

(b) *morfac = 2*

Figure F.6: Gully migration transect 3

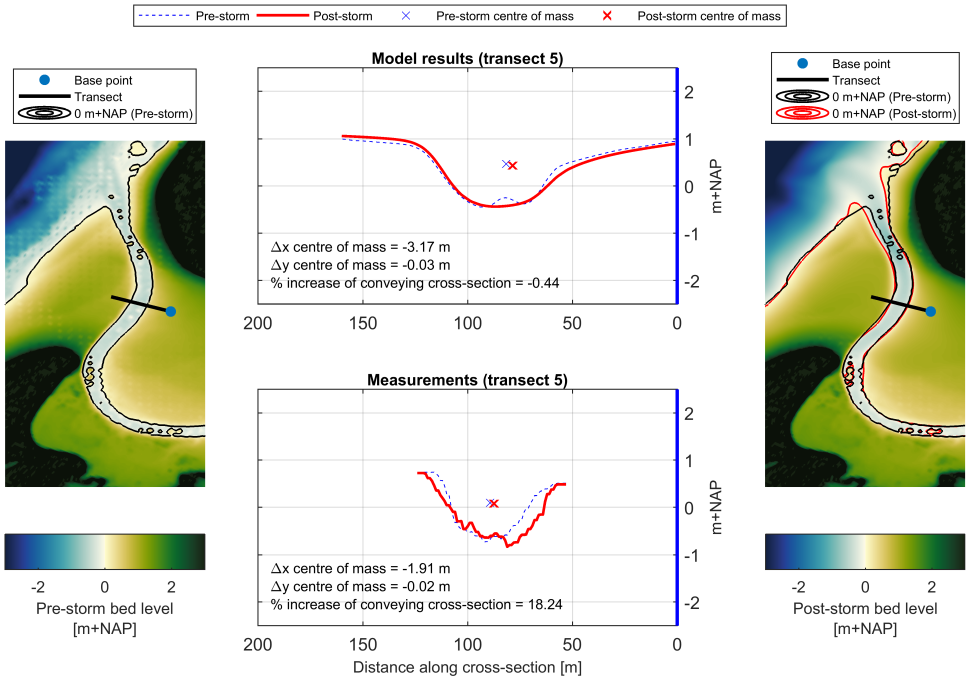

(a) *morfac = 1*

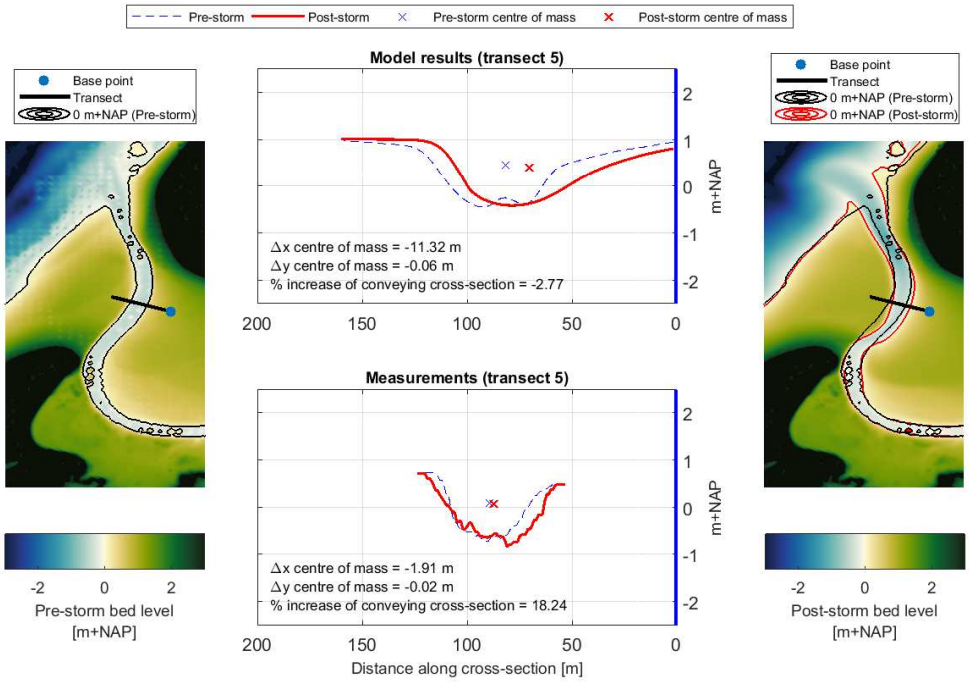

(b) *morfac = 2*

Figure F.7: Gully migration transect 5

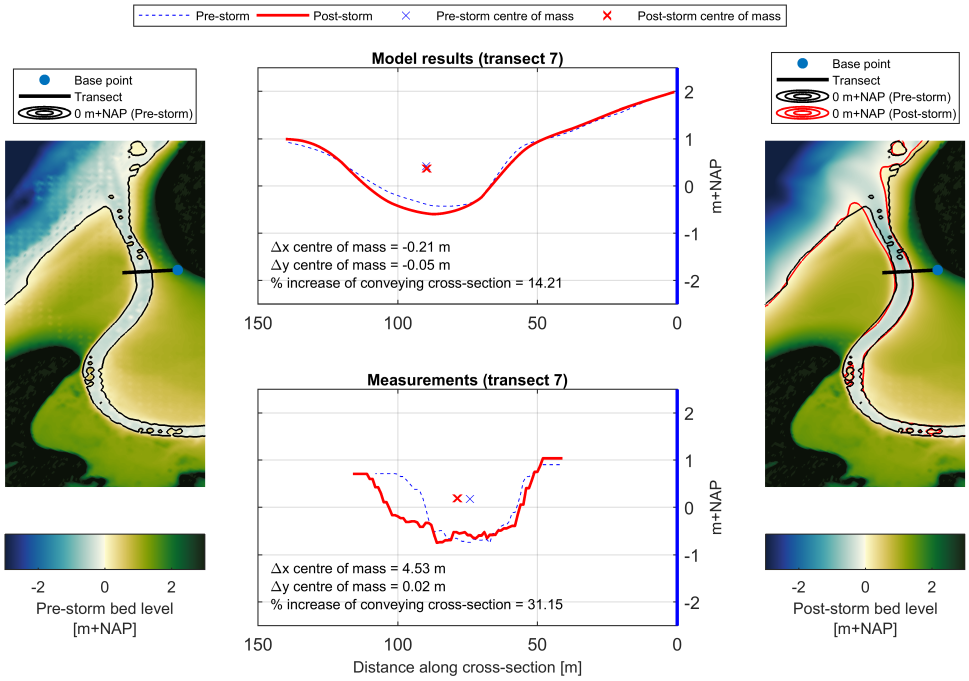

(a) *morfac = 1*

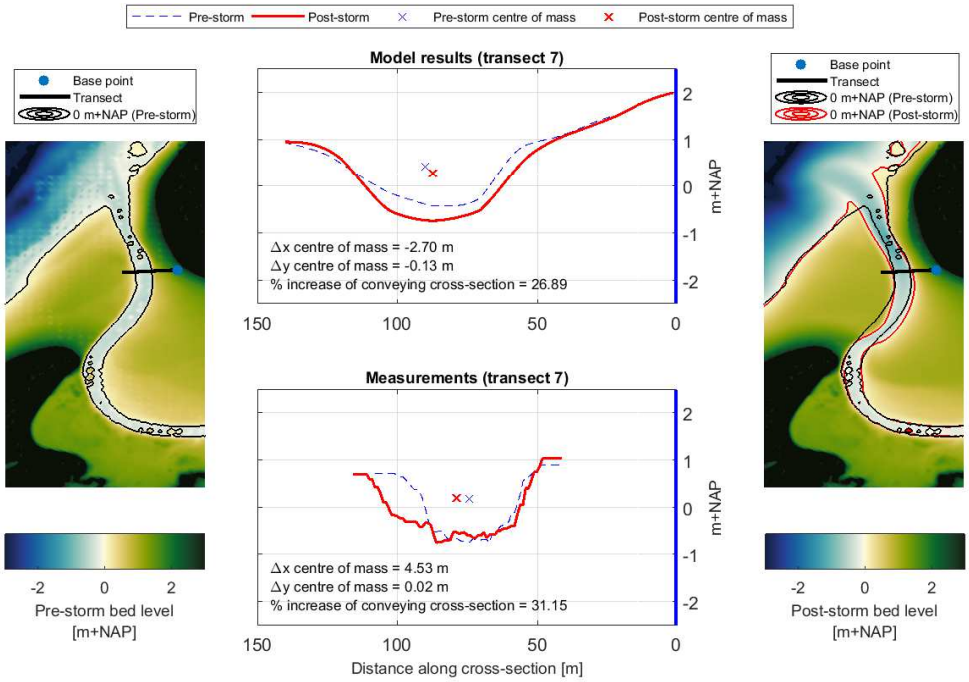

(b) *morfac = 2*

Figure E.8: Gully migration transect 7

F.3. Sediment transport formulation

The default sediment transport formulation in XBeach is the Van Thiel-Van Rijn equation (van Rijn, 2007; Van Thiel de Vries, 2009). The XBeach Kingsday version also gives the option to use the Soulsby-Van Rijn equation (Soulsby, 1997; van Rijn, 1984). Both formulations calculate the equilibrium sediment concentrations with equation F.1.

$$C_{eq} = max(min(C_{eq,b}, \frac{1}{2}C_{max}) + min(C_{eq,s}, \frac{1}{2}C_{max}), 0) \tag{F.1}$$

The formulations differ in how the bed load and suspended load components of the equilibrium sediment concentration are calculated:

Van Thiel-Van Rijn (XBeach default)

$$C_{eq,b} = \frac{A_{sb}}{h} * (\sqrt{v_{mg}^2 + 0.64 * u_{rms,2}^2} - U_{cr})^{1.5} \tag{F.2}$$

$$C_{eq,s} = \frac{A_{ss}}{h} * (\sqrt{v_{mg}^2 + 0.64 * u_{rms,2}^2} - U_{cr})^{2.4} \tag{F.3}$$

Soulsby-Van Rijn

$$C_{eq,b} = \frac{A_{sb}}{h} * (\sqrt{v_{mg}^2 + 0.018 * \frac{u_{rms,2}^2}{C_d}} - U_{cr})^{2.4} \tag{F.4}$$

$$C_{eq,s} = \frac{A_{ss}}{h} * (\sqrt{v_{mg}^2 + 0.018 * \frac{u_{rms,2}^2}{C_d}} - U_{cr})^{2.4} \tag{F.5}$$

The sensitivity of the model to the choice of sediment transport formula was analysed by comparing gully morphology and sedimentation and erosion in the slufter valley. Figure F.9 shows the results for both formulations concerning 2D sedimentation and erosion. Outside of De Slufter the sedimentation and erosion magnitudes are larger for the Soulsby-Van Rijn formula. Due to a lack of measured short-term bed level change data, it cannot be analysed which is more accurate. It is therefore chosen to use the default formulation. Inside De Slufter no significant difference between the two formulations can be distinguished.

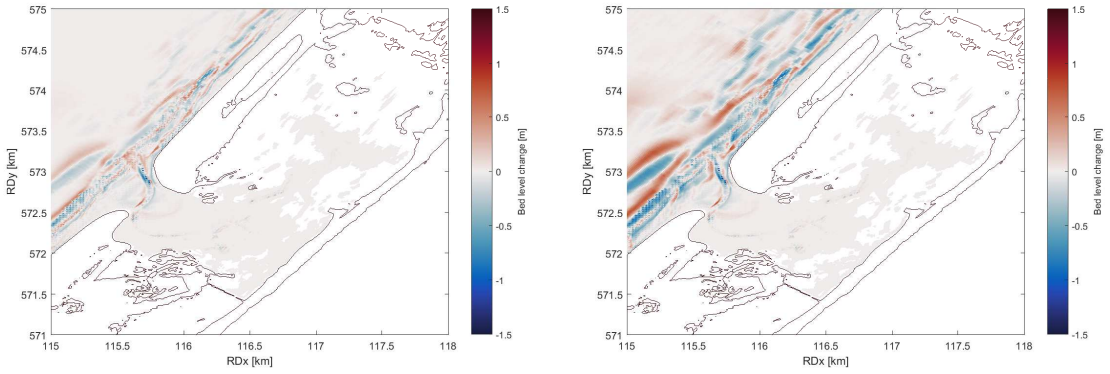

(a) Van Thiel-Van Rijn

(b) Soulsby-Van Rijn

Figure F.9: Sedimentation and erosion on the foreshore and in the valley of De Slufter for different sediment transport formulas.

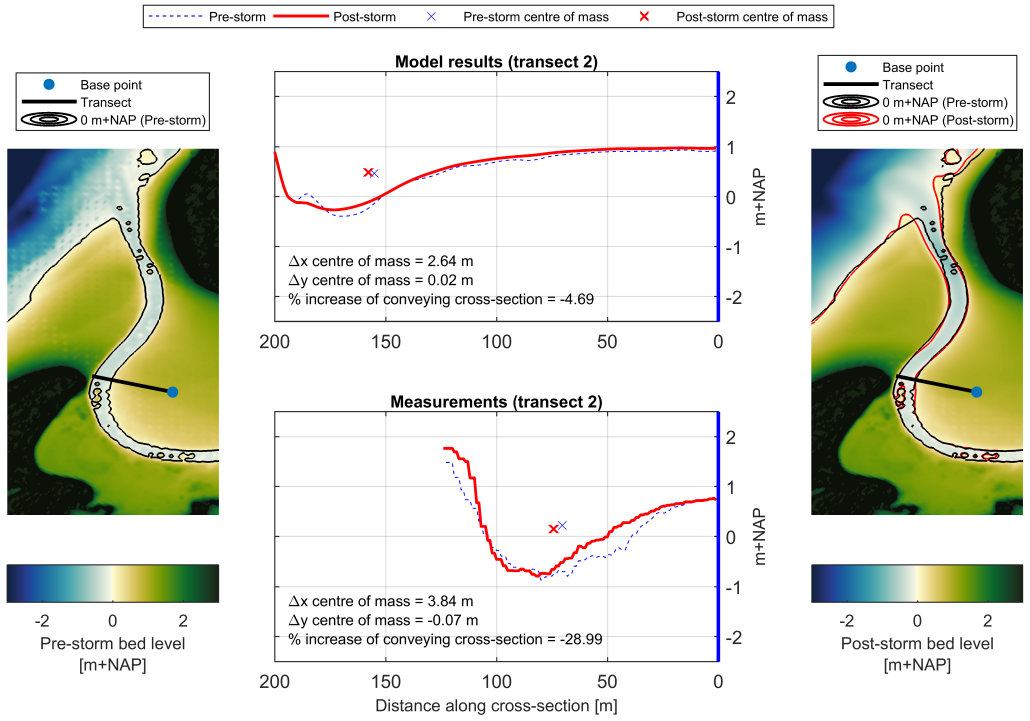

(a) Migration of gully transect 2.

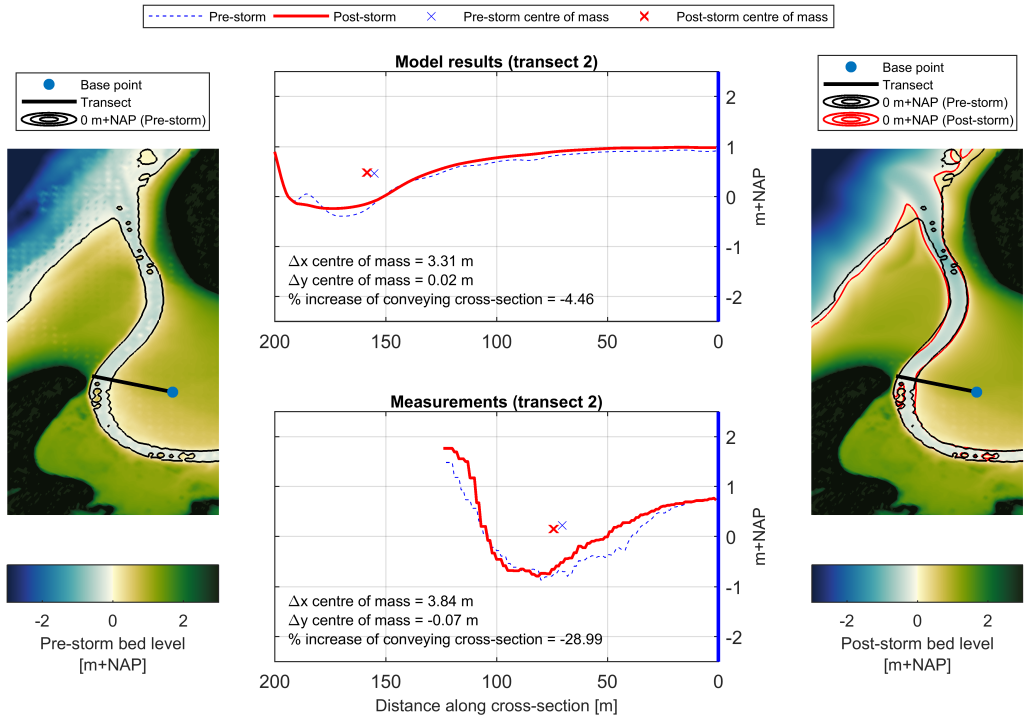

(b) Migration of gully transect 2.

Figure F.10: Gully migration transect 2 or the two different sediment transport formulations. The gully transect number refers to the transects in figure D.1.

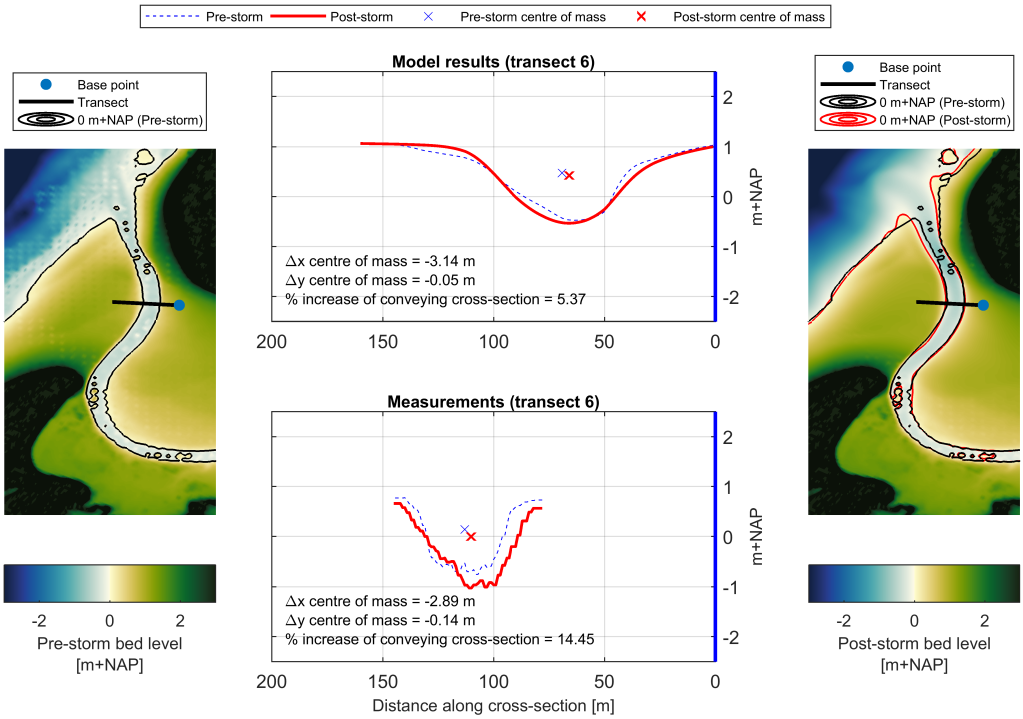

(a) Migration of gully transect 6.

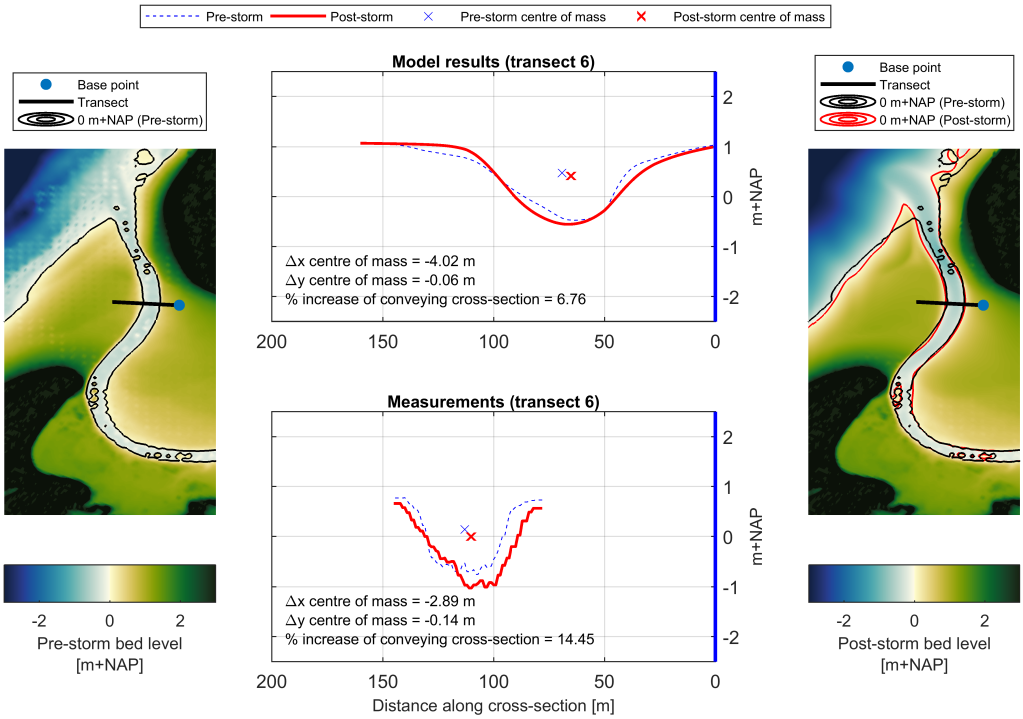

(b) Migration of gully transect 6.

Figure F.11: Gully migration transect 6 or the two different sediment transport formulations. The gully transect number refers to the transects in figure D.1.

From figures F.10 and F.11 it is concluded that inside De Slufter the choice for one of the two sediment transport formulations does not produce significantly different results.

F.4. Wave direction

The sensitivity analysis on wave direction was executed for 1/100 year storms. The reason behind choosing such a 'small' storm was because waves from the West cannot attain 1/3000 year wave heights.

F.4.1. Dune erosion

The obliquity of waves during a storm is an important parameter for the amount of dune erosion. The obliquity has two important consequences. First, obliquity leads to longshore transport. Longshore transport is generally maximum when the angle between wave and shoreline are 45°. Second, normally incident waves generally lead to more dune erosion than waves from an angle. It is therefore expected that waves with an obliquity of 0° – 45° lead to the highest dune erosion.

These expected processes are recognized in the alongshore distribution of dune erosion for different wave directions, shown in figure F.12. First, dune erosion of the dune row is generally largest for waves coming from the West, which have an obliquity of 33°. Furthermore, waves from the North, which have an obliquity of 57° show the least erosion. Waves from the Northwest or the West-Northwest, which have a smaller obliquity show smaller but similar erosion at the southern and northern dune.

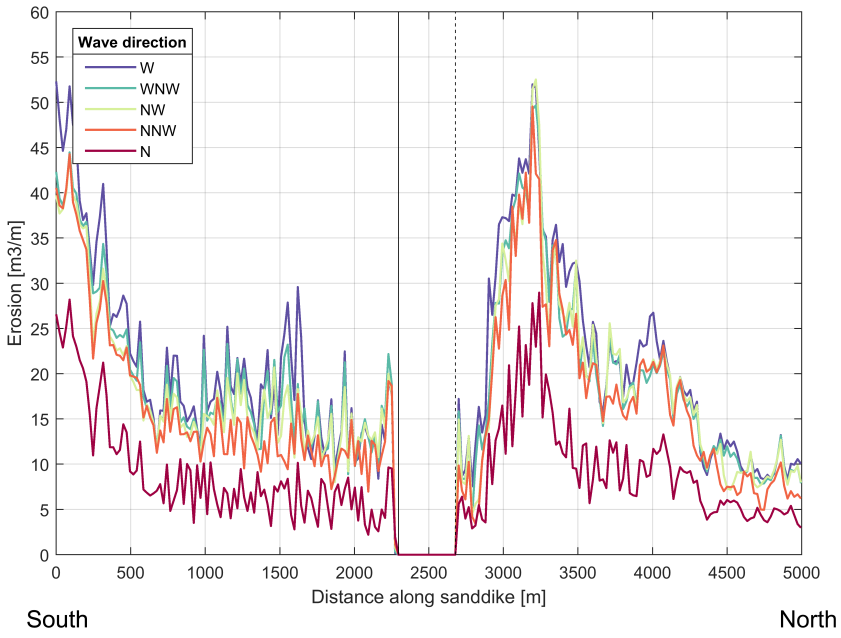

Figure F.12: Erosion of the front dune row for different mean wave directions during a 1/100 year storm.

Longshore transport for waves from the North is relatively low due to the high obliqueness (57°). This further explains why dune erosion for waves from the North is smallest. North-northwestern waves, which have an obliquity of 34°, lead to much higher erosion volumes than waves from the N, also due to obliqueness. The results show that when waves have a positive obliqueness (leading to northward transport), velocities are higher at the southern dune. When waves have a negative obliqueness, leading to southward transport, velocities are higher at the northern dune.

Because the southern valley is still in the process of filling up, alongshore velocities are directed towards the mouth. Wave-induced longshore velocities thus either increase or mitigate flow velocities. This behaviour is shown in figure F.13.

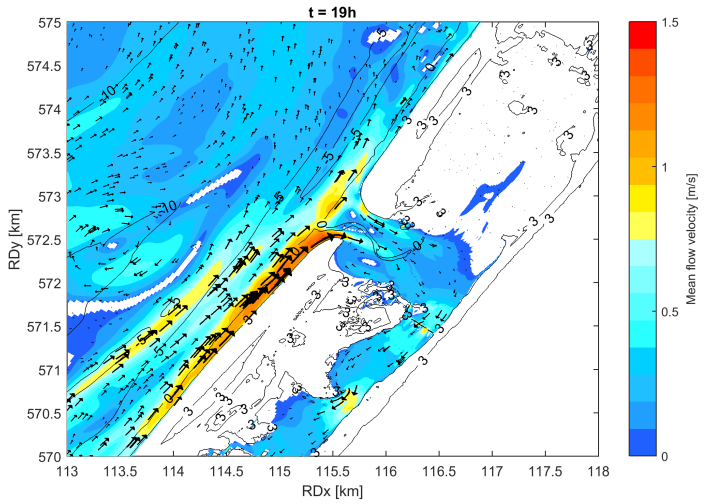

(a) W

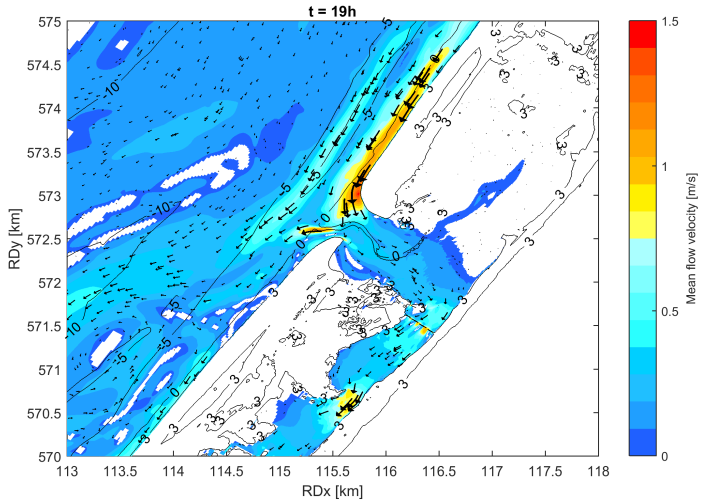

(b) NNW

Figure F.13: Mean horizontal flow velocity distribution during the peak of a 1/100 year storm for different wave directions.

F.4.2. Sand dike erosion

The distribution of sand dike erosion and the total erosion along the sand dike show that erosion is highest for waves coming from the Northwest. The erosion volumes are very small however. Differences between erosion for Western, West-northwestern and Northwestern waves are small. For waves from the NNW and N differences are significant however, with total erosion volumes two-thirds or even less compared to Northwestern waves. This is caused by the topography of De Slufter. Waves from the North and North-northwest are mainly directed towards higher ground. Due to the large spreading, a quite a lot of wave energy still propagates into the valley for Northern storms. For the Western storms, the area of the sand dike that is under attack is significantly larger though. This is clear from figure F.16.

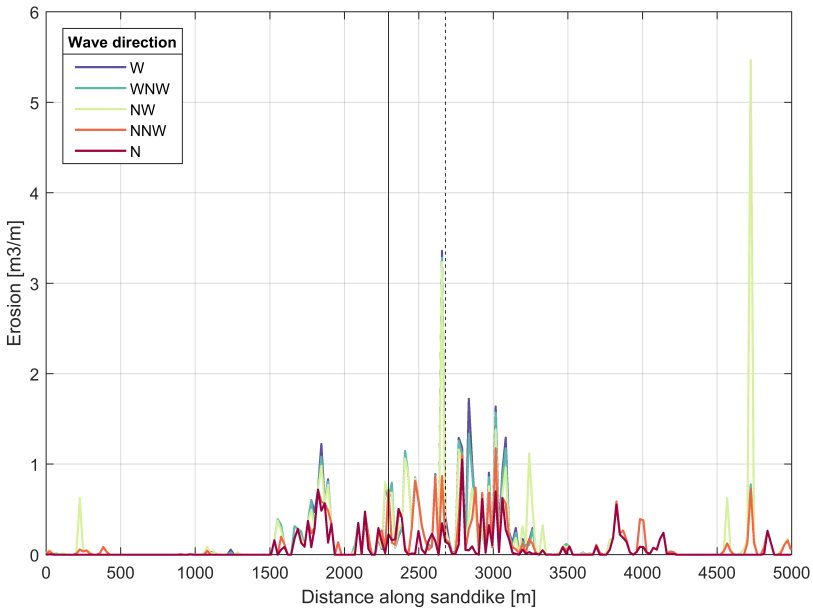

Figure F.14: Erosion of the sand dike for different mean wave directions during a 1/100 year storm.

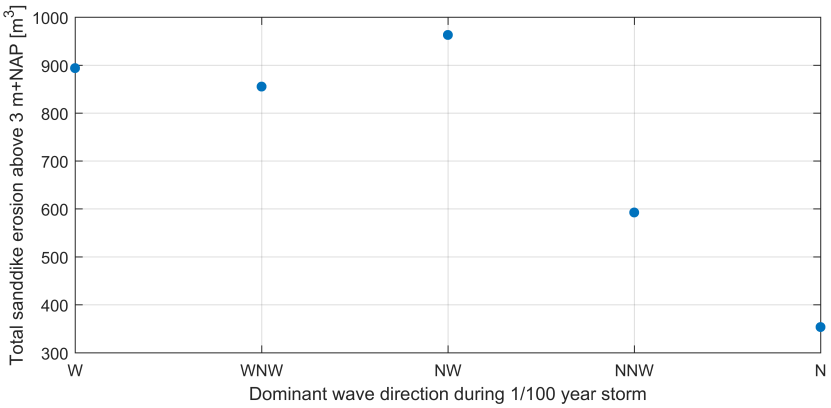

Figure F.15: Total sand dike erosion over dominant wave direction. All storms had a return period of 100 years and a duration of 36 hours.

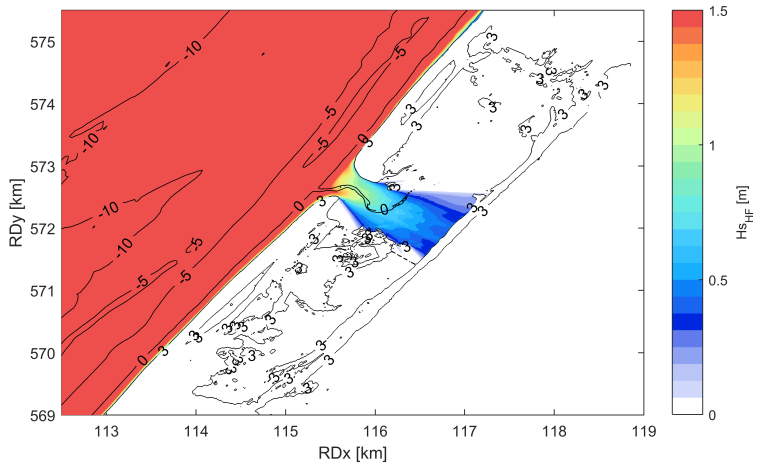

(a) N

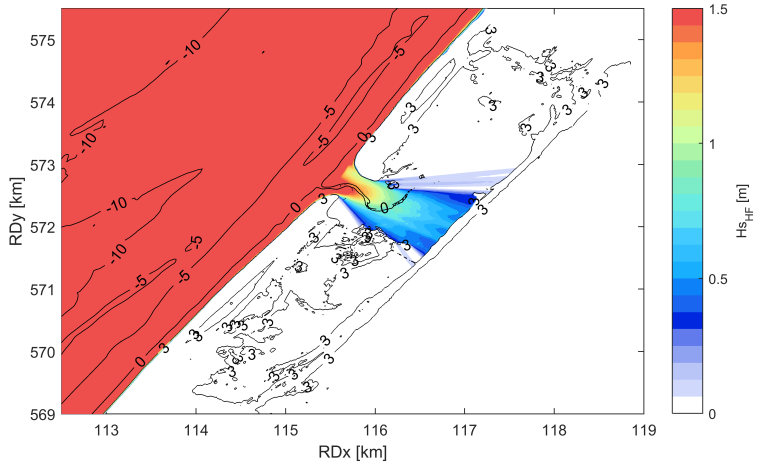

(b) W

Figure F.16: 2D short wave height distribution for Western and Northern 1/100 year storms.

F.5. Storm duration

The results for 4 storms with different lengths were analysed to assess the effect of storm duration on dune and sanddike erosion. Figure shows the imposed boundary conditions of these storms.

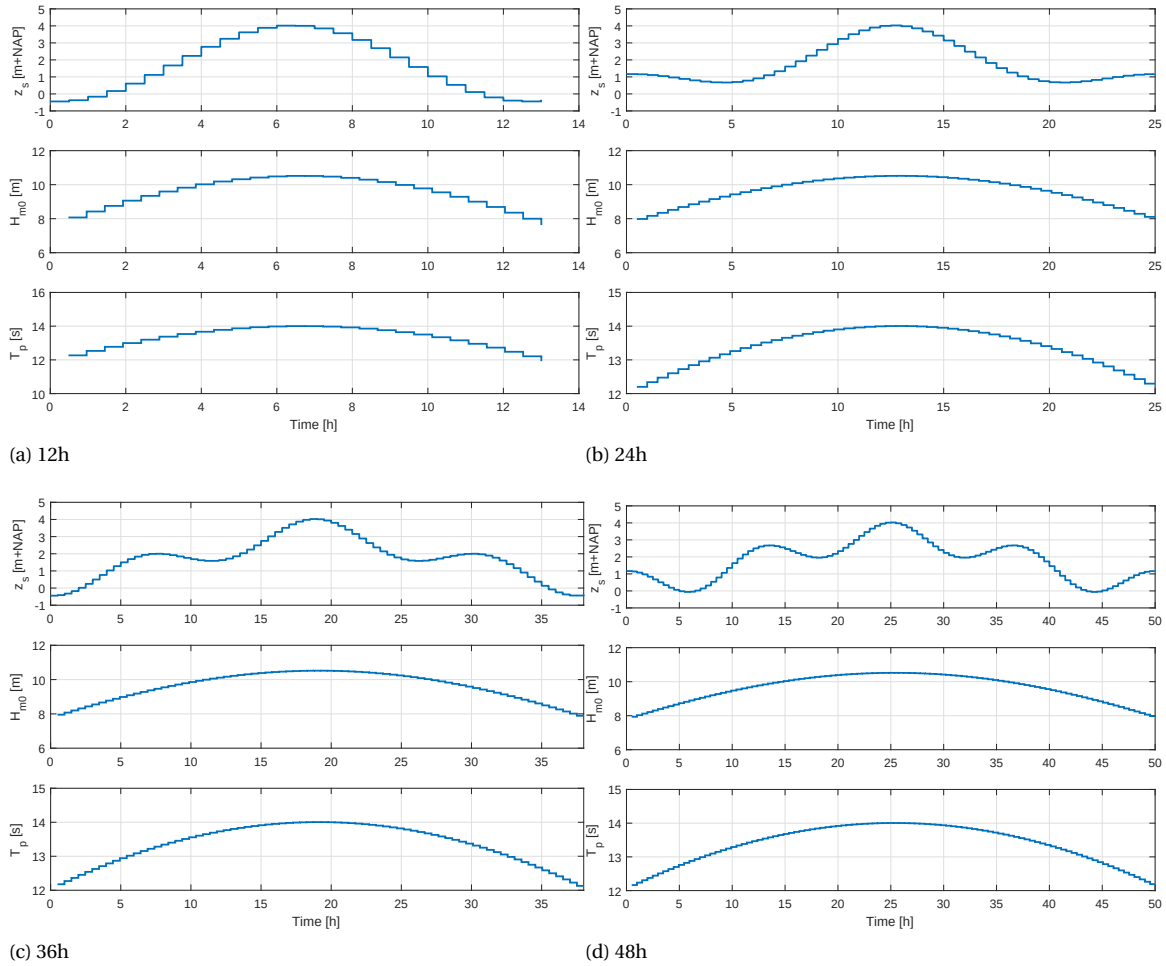

(a) 12h (b) 24h

(c) 36h (d) 48h

Figure F.17: Time-varying boundary conditions for storms with different durations. All storms have the same maximum offshore SSL, significant wave height and peak period.

Storm erosion along the sand dike is not significantly larger for 48h storms than for 12h storms, as is clear from figure F.18. This is a clear indication that sand dike erosion is governed by the maximum water level during a storm and not by duration of the forcing. The high dependence on maximum water level for morphological response is in accordance with findings by Van Der Vegt and Hoekstra (2012).

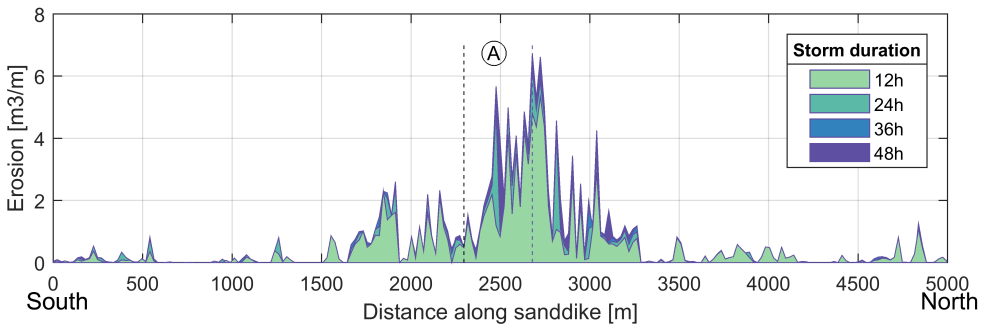

Figure F.18: Erosion along sand dike for different storm durations, see figure F.17.

The 12 hour storm leads to the most severe 2D erosion and sedimentation. Reason for this is that, due to the short duration in combination with equal SSL, the speed with which the water level increases is larger than for longer storms. This leads to higher velocities and thus to a higher sediment transport.

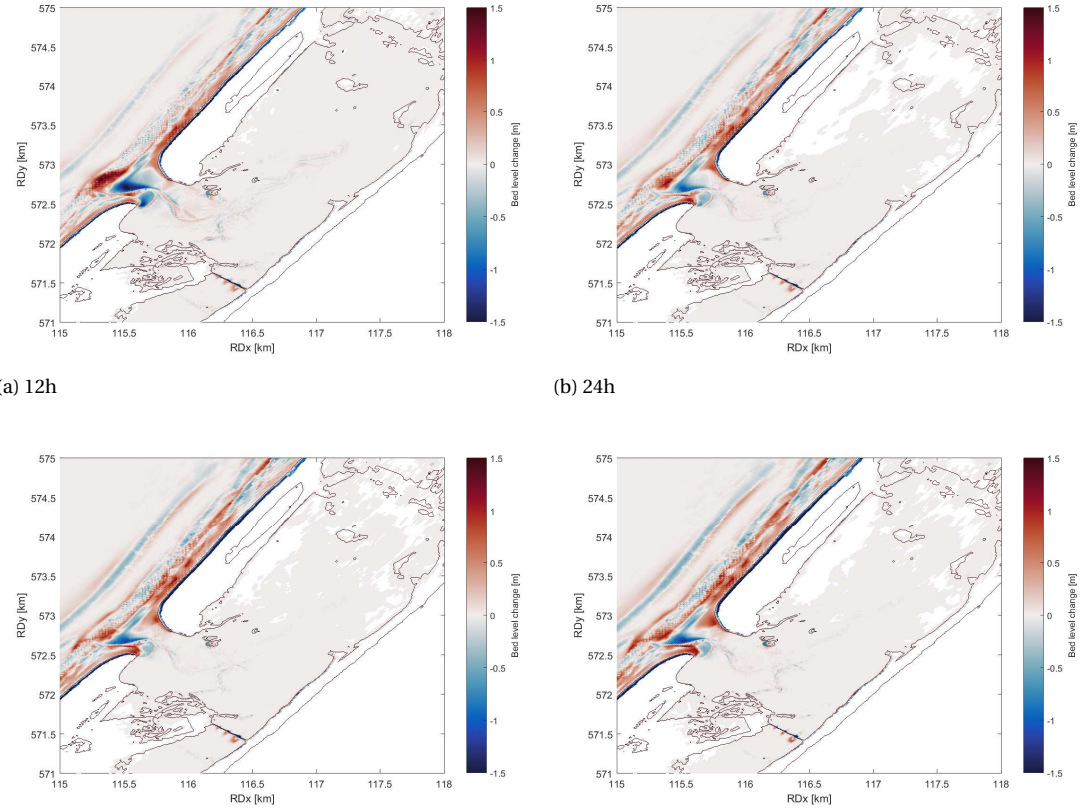

(a) 12h

(b) 24h

(c) 36h

(d) 48h

Figure F.19: 2D sedimentation and erosion for different storm durations

F.6. Wave directional spreading

In a late stage of this study, it was found that an unrealistically small value for the spreading parameter 's' was chosen, leading to an unrealistically large wave directional spreading. As it was too late to remodel all scenarios, a small selection of scenarios was remodelled with a more realistic value to assess the sensitivity of the results of this study to the spreading parameter. The realistic value for 's' is based on wave observations at 'Amelander Zeegat - Buoy 1-1 and 1-2' (AZB11 and AZB12, respectively) during 2007. The transformation of wave spreading observations to a wave spreading parameter in XBeach is not straightforward. Therefore, before the sensitivity of the model is discussed, the calculation of the wave spreading parameter from observations is explained.

Calculation of wave spreading parameter 's' The transformation of observed wave directional spreading at AZB11 and AZB12 is difficult due to the unclear and inconsistent use of the definition 'wave directional spreading' in different studies.

In XBeach, the wave directional spreading parameter is used to calculate a standard deviation 'σ' and, subsequently, a standard distribution (Deltares, 2017). The shape of the standard distribution determines the distribution of wave energy over different directions. The directional spreading in XBeach is thus symmetrical and it therefore represents a idealised situation.

For the observations, the definition is more complex. The directional spreading parameter is presented in data as 's0bh', which is defined as the 'average wave spreading in the spectral domain' (Zijdenbos, 2015),

which is a vague definition. Due to the limited measurement data, not all necessary information on the distribution of wave energy $S(f,\theta)$ is known. To estimate wave directional spreading, 4 moments are calculated from measurement data, (A1, B1, A2 and B2). These moments are interpreted as 'a measure for the width of the distribution of wave energy over all directions' (H. Peters, personal communication, November 2016). However, the actual spreading of wave energy is also dependent on the shape of the distribution, which can be complex (i.e. with two peaks). Therefore, it is difficult to translate the observations to a spreading parameter in XBeach.

The determination of a realistic spreading parameter 's' is thus a problem. However, with the help of an earlier study with SWAN on the the wave observations at AZB11 and AZB12 the spreading parameter can be approximated. In that study the same $s0bh$ input was used as in this thesis. By comparing the observations to the output in SWAN, for which a definition is known, the 'physical' meaning of s0bh is assumed. This comparison is shown in figure F.20. Based on this figure, it is concluded that the observed $s0bh$ at the wave buoys is similar to the DSPRDEGR parameter in the SWAN output. The DSPRDEGR can be interpreted as a standard deviation (Delft University of Technology, 2018). Consequently, the $s0bh$ parameter is also interpreted as a standard deviation.

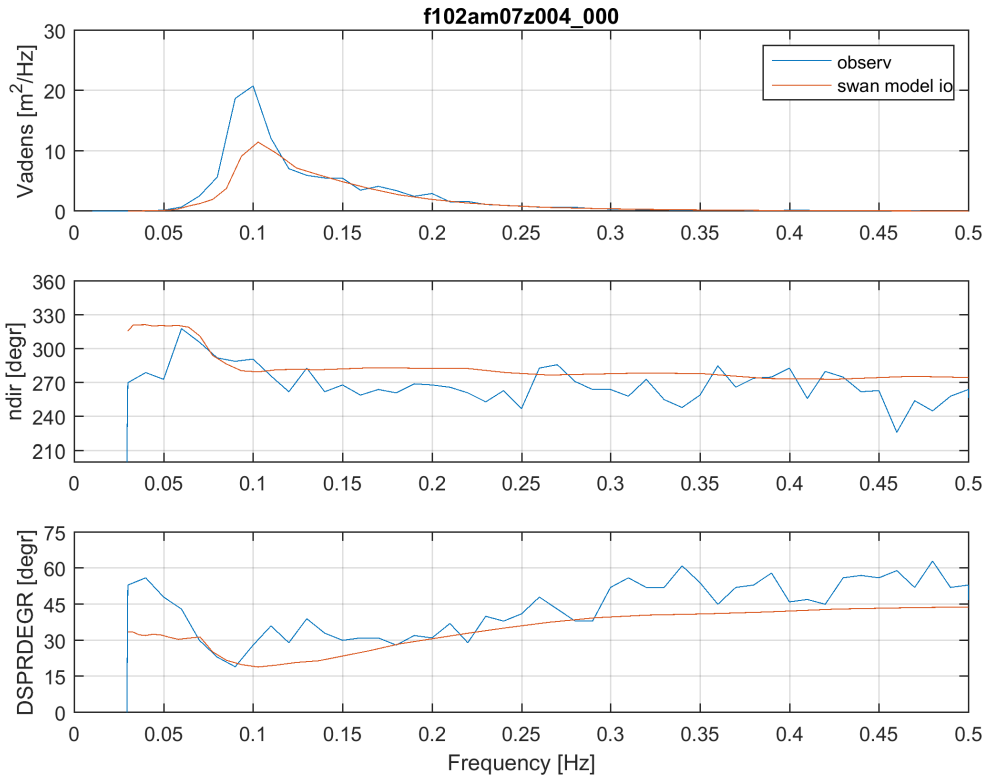

Figure F.20: Comparison of model input to resulting SWAN output of 2007 study. The data represents spectra, with observations in blue and model results in red. From the bottom panel it is concluded that the $s0bh$ parameter is similar to the SWAN DSPRDEGR parameter, which can be interpreted as a standard deviation (Delft University of Technology, 2018).

The observed $s0bh$ at AZB11 and AZB12 is thus interpreted as a standard deviation. The translation to the spreading parameter 's' in XBeach is then performed with equation F.6.

$$s = \frac{2}{(\sigma_{radians} * \frac{\pi}{180})^2} - 1 \tag{F.6}$$

First, the observations are analysed to find a representative $s0bh$-value for a 1/3000 year storm (i.e. $H_s = 11.2m$). Based on figure F.21, the representative $s0bh$ value for observed wave heights higher than 10 lies in

between 20°and 25°. To be on the conservative side it is assumed that $s0bh_{1/3000 year storm} = 20°$ (conservative because it is a narrower spreading). Using equation F.6, this leads to an XBeach spreading parameter $s = 15$.

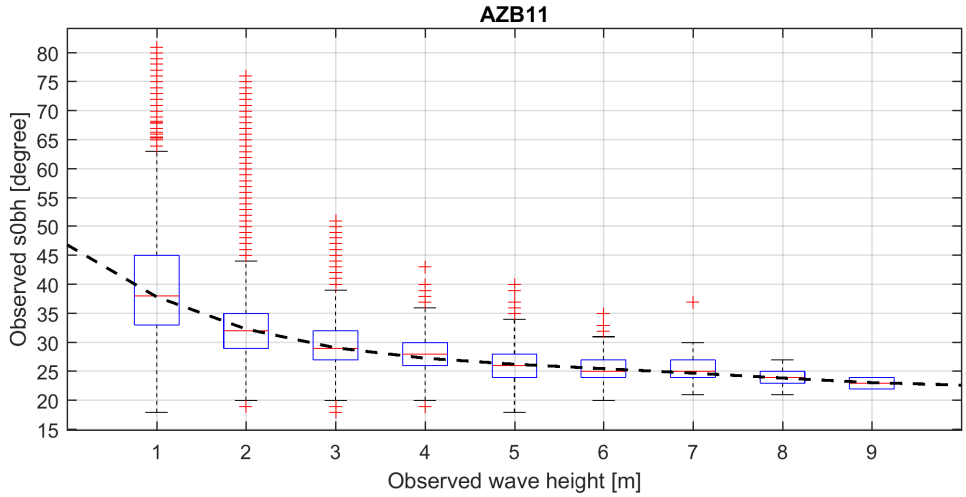

Figure F.21: Box plot of all *s0bh* observations at Amelander Zeegat buoy 1-1. The red lines represent the median. The blue boxes mark the 25th and 75th percentiles. The red plusses are outliers and the black striped line is the curved fit through the medians.

Sensitivity of results To assess the sensitivity of the model results to the spreading parameter, two present scenarios (Reference and 1500m wide mouth) and one future scenario (SLR = 1.95m) are rerun and analysed. Figures F.22 and F.23 show the short and long wave height, respectively, for the three scenarios with spreading parameters $s = 2$ and $s = 15$. Figures F.24 and F.25 show the alongshore dune and sand dike erosion, respectively, for the three scenarios with spreading parameters $s = 2$, $s = 15$ and $s = 40$.

The 2D distribution of short and long wave height shows that a more realistic spreading parameter leads slightly but not significantly larger wave heights at the sand dike. In all three scenarios, the narrower imposed wave directional spreading on the offshore boundary does lead to a narrower area of wave attack. This is due to the already discussed dissipation in the slufter valley. Wave heights do increase significantly outside De Slufter for a more realistic spreading parameter. However, inside De Slufter, wave height is (mostly) depth-limited. Higher wave heights outside De Slufter thus do not necessarily lead to higher wave heights inside De Slufter. Consequently, sand dike erosion does not increase significantly either.

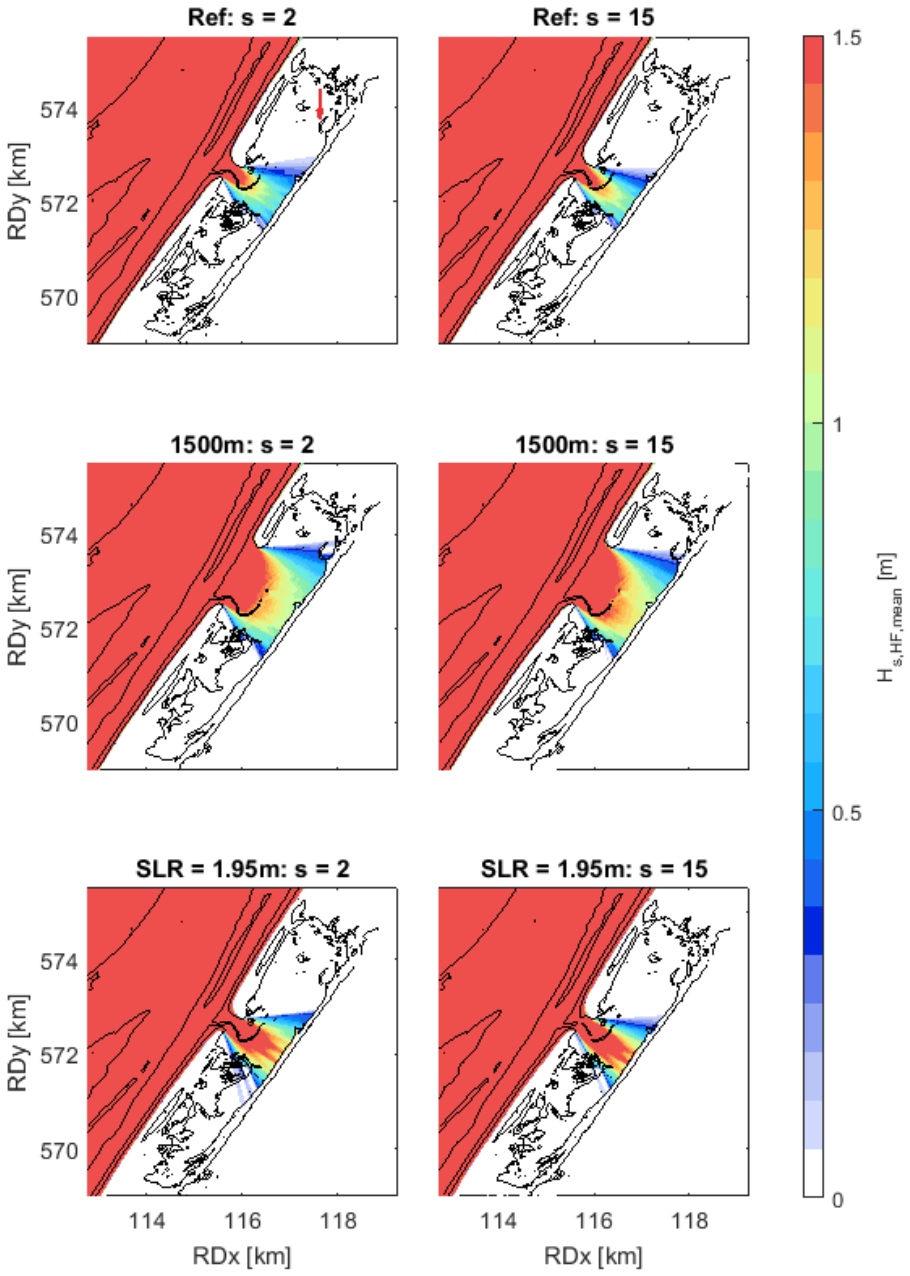

Figure F.22: 2D short wave height maps for different spreading parameters at the peak of the storm.

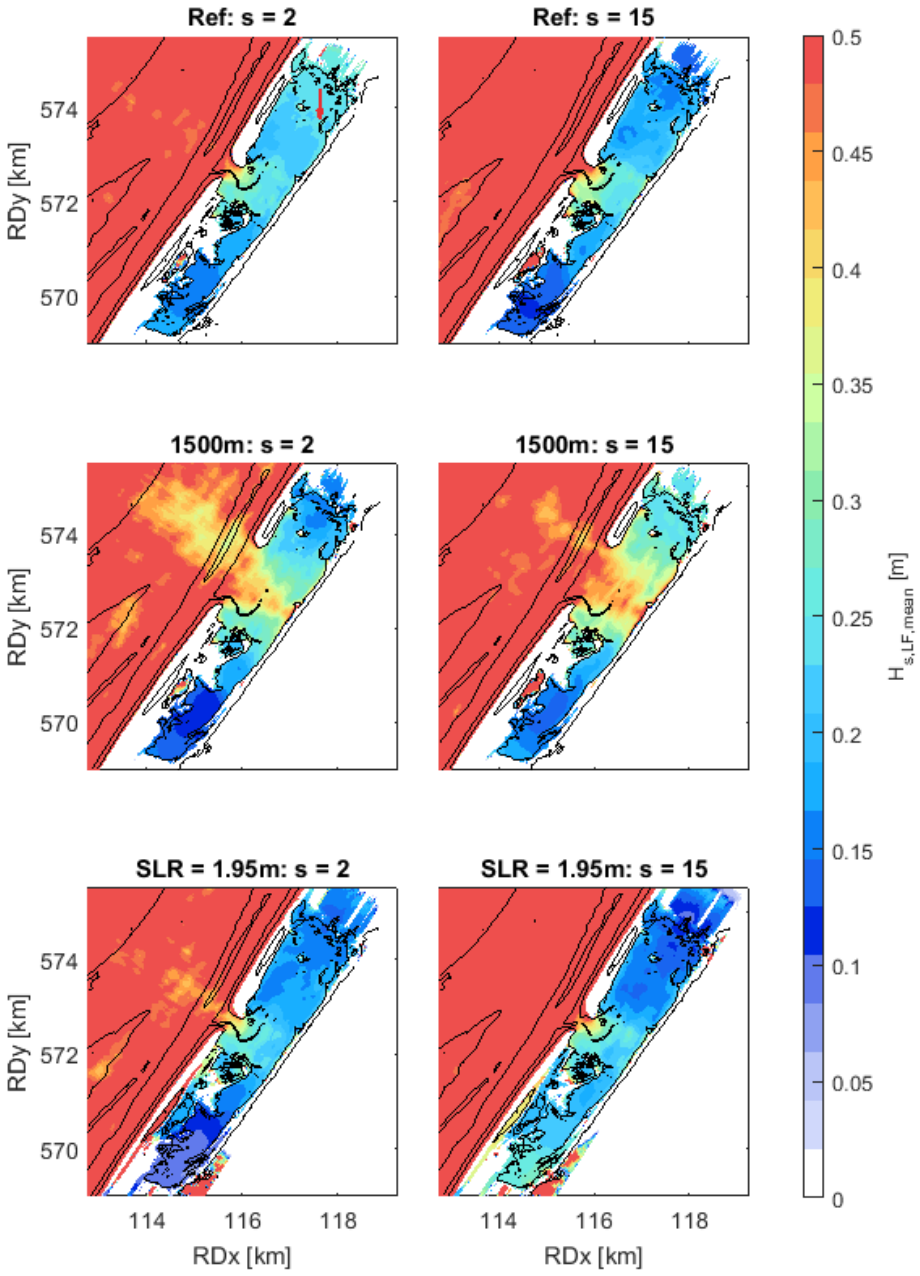

Figure F.23: 2D long wave height maps for different spreading parameters at the peak of the storm.

The wave directional spreading has a significant effect on the alongshore erosion of the front dune row. When the directional spreading becomes narrower, the dune erosion increases. This is a consequence of the fact that wave energy is focussed more, leading to higher short and long wave height at the shoreline. In figure F.24 this correlation is evident.

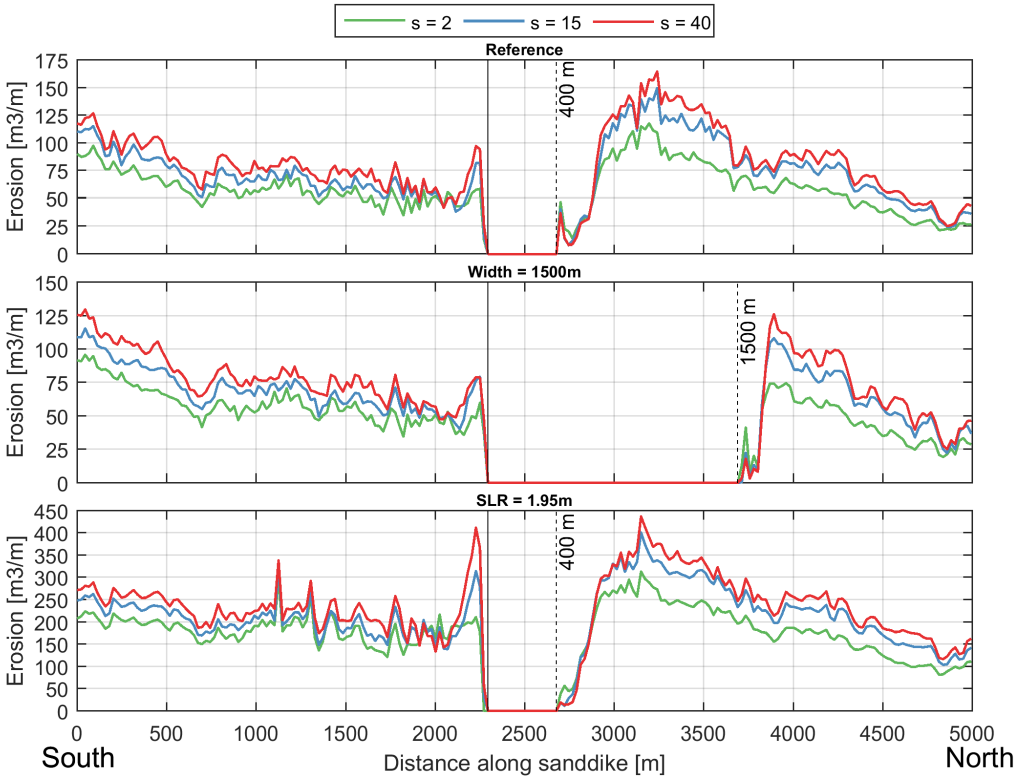

Figure F.24: Erosion along sand dike for different spreading parameters for 3 scenarios. The vertical continuous line indicates the location of the southern mouth edge and the vertical striped line the location of the northern edge.

For sand dike erosion, the influence of the more realistic spreading parameter is insignificant in the reference scenario. In the wider mouth scenario the sand dike erosion in front of the mouth is slightly higher. In the SLR = 1.95m scenario, sand dike erosion increases slightly in front of the mouth and in the southern valley ($x = 2000m$ to $x = 2700m$). The difference are small however, especially compared to the increase at the front dune row.

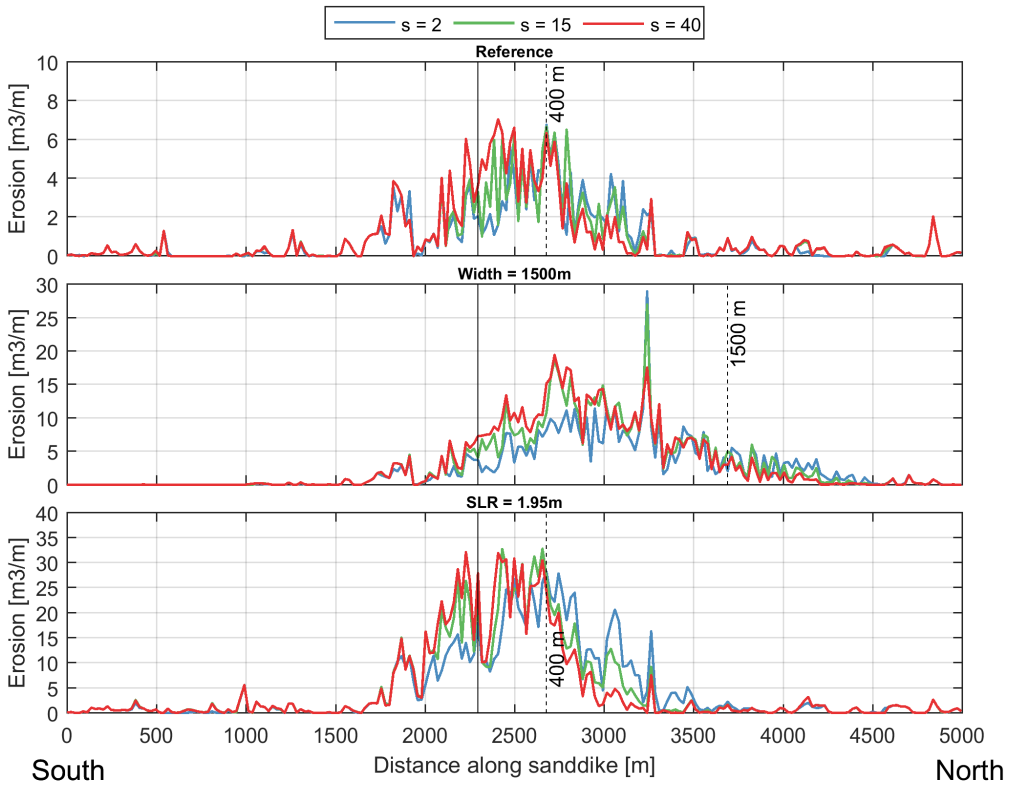

Figure F.25: Erosion along sand dike for different spreading parameters for 3 scenarios. The vertical continuous line indicates the location of the southern mouth edge and the vertical striped line the location of the northern edge.

F.7. Critical wet slope

One of the major differences between the previous study by Van Rooijen and Van Thiel de Vries (2014) and the present study is the choice of critical wet slope. This parameter determines the maximum bed level slope in x- and y-direction for inundated grid cells. In the previous study, this parameter was manually scaled down from 0.3 to 0.1. The sand dike erosion volumes in the previous study were much higher than in the present study. It is expected that this difference can largely be explained by the critical wet slope. Figure F.26 shows that the influence of the critical wet slope is significant, which means that it could indeed be a possible explanation between both studies. However, the erosion volumes in Van Rooijen and Van Thiel de Vries (2014) were still larger. This could be caused by the grid cell sizes. In this thesis, grid cell sizes near the dunes and near the sand dike were smaller than in the previous study. This means that erosion is resolved more accurately. A definitive explanation cannot be given. However, this was out of the scope of this study.

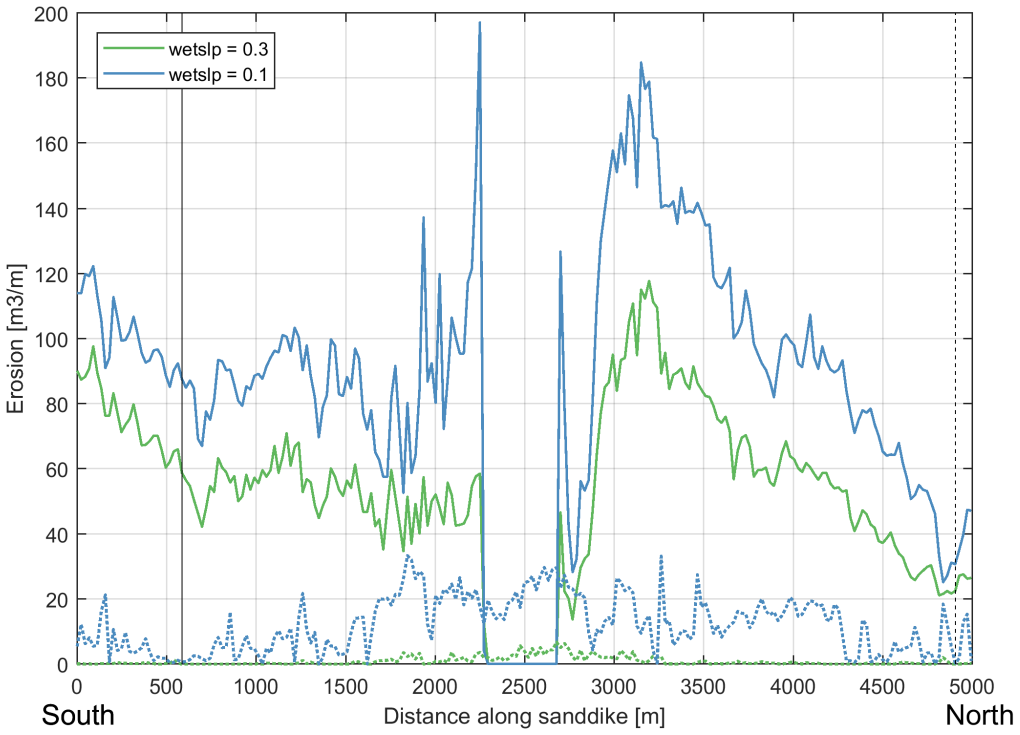

Figure F.26: Erosion along dune and sand dike for different critical wet slopes. The results show the significant influence of the critical wet slope on dune erosion. Continuous lines represent dune erosion. Dotted lines represent sand dike erosion.

F.8. Conclusion

The sensitivity analysis discussed the effect of certain assumptions and parameters on the results in this study. The effect of deviations from the chosen bed friction coefficient was shown to be negligible, as the resulting errors for values of 0.025 up to 0.065 were in the range of 0.068 to 0.09, which is very low.

Next, the effect of a higher morfac on the morphological changes inside the slufter valley were discussed by analyzing the gully migration. The results proved that using a *morfac*> 1 is not allowed as it leads to overestimations in gully migration. Due to a higher *morfac* the interaction between tidal forcing and wave-induced forcing is not well represented.

The analysis of the sediment transport formulations indicated that there were no signifcant morphological differences between the two formulations inside the valley. Offshore, the Soulsby-Van Rijn formulations resulted in higher morphological activity. However, as no short-term measurements of bed level change are available in the area, no conclusion could be drawn on which formulation was more accurate. Therefore, the default Van Thiel-Van Rijn formulation is deemed appropriate.

The effects of imposing different mean wave directions on the offshore boundary were also discussed. The results showed that Western waves lead to higher erosion rates of the front dune row. However, the differences are within an acceptable range. Also, the erosion of the dune is not of significant importance. The results for sand dike erosion show that, while differences are low, Northwestern waves generally lead to more erosion (although erosion rates were small for all directions).

Next, storm duration was assessed. The results showed that for a 12h storm, almost the same amount of erosion occurs as for a 48h storm. 2D sedimentation and erosion showed that 12 hour storms even lead to more morphological activity than longer storms. This is due to the higher water level gradients in the offshore forcing.

The analysis on wave directional spreading showed that a more realistic spreading parameter in XBeach does not necessarily lead to a significant increase in sand dike erosion. This is caused by the large amount of dissipation in the valley. Wave heights in De Slufter are thus depth-limited and not governed by offshore wave height. This is not the case near the front dune row. There, dune erosion increases significantly for narrower directional spreading.

Last, the model sensitivity to the critical wet slope was assessed with the goal of explaining the differences between this thesis and the previous study by Van Rooijen and Van Thiel de Vries (2014). For a smaller critical wet slope, the erosion volumes increase significantly at the sand dike and the front dune row. Erosion volumes in the previous study are still larger though. However, as the volumes are in the same order of magnitude, the choice of critical wet slope is considered a likely explanation for the large differences.